

REVEALING THE ORIGIN OF CHEMICAL WEAPONS



Mirjam de Bruin-Hoegée

Revealing the Origin of Chemical Weapons

Mirjam de Bruin-Hoegée

2024

Revealing the Origin of Chemical Weapons

PhD thesis, University of Amsterdam, The Netherlands

ISBN: 978-90-9038-333-0

Printing: Ridderprint | www.ridderprint.nl

Layout & Design: Mirjam de Bruin-Hoegée | www.forensicscientist.nl

Copyright © 2024 Mirjam de Bruin-Hoegée, Utrecht

Revealing the Origin of Chemical Weapons

ACADEMISCH PROEFSCHRIFT

ter verkrijging van de graad van doctor

aan de Universiteit van Amsterdam

op gezag van de Rector Magnificus

prof. dr. ir. P.P.C.C. Verbeek

ten overstaan van een door het College voor Promoties ingestelde commissie,

in het openbaar te verdedigen in de Aula der Universiteit

op woensdag 12 juni 2024, te 14:00 uur

door Janny Mirjam Hoegée

geboren te Nieuwegein

Promotiecommissie

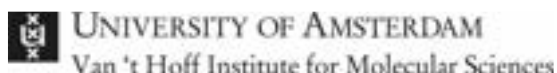
<i>Promotores:</i>	Prof. dr. A.C. van Asten Prof. dr. ir. P.J. Schoenmakers	Universiteit van Amsterdam Universiteit van Amsterdam
<i>Copromotores:</i>	Dr. D. Noort Dr. M.J. van der Schans	OPCW TNO
<i>Overige leden:</i>	Prof. dr. M.C.G. Aalders Dr. C. Åstot Prof. dr. G. Corthals Dr. A. Gargano Prof. dr. A.E.D.M. van der Heijden Prof. dr. K. Keune Prof. dr. A.M. Rijs	Universiteit van Amsterdam FOI Universiteit van Amsterdam Universiteit van Amsterdam TU Delft, TNO Universiteit van Amsterdam Vrije Universiteit Amsterdam

Faculteit der Natuurwetenschappen, Wiskunde en Informatica

The work in this thesis was part of the Forensic Attribution for CWA INtelliGence (FACING) project, a collaboration between the Van 't Hoff Institute for Molecular Sciences (HIMS) of the University of Amsterdam and TNO Defence, Safety & Security. The FACING project is financed by the DO-AIO fund of the Dutch Ministry of Defence.



Ministry of Defence



Research consortium partners:



Netherlands Forensic Institute
Ministry of Justice and Security



This work was performed in the context of the Centre for Analytical Sciences Amsterdam (CASA) and Co van Ledden Hulsebosch Center (CLHC).



*“Work with enthusiasm,
as though you were working for the Lord
rather than for people.”*

Paulus – New Living Translation Bible 1996, Ephesians 6:7

Table of contents

Chapter 1	Introduction	11
Forensic intelligence		
Chapter 2	Chemical attribution of fentanyl: The effect of human metabolism	49
Chapter 3	Post-metabolism impurity profiling of carfentanil, remifentanil, sufentanil, and benzylfentanyl	77
Profiling in biological samples		
Chapter 4	Elucidation of in vitro chlorinated tyrosine adducts in blood plasma as selective biomarkers of chlorine exposure	109
Chapter 5	On-site detection and laboratory verification of the presence of nerve agent biomarkers using dried blood spots	133
Chapter 6	Verification of exposure to chemical warfare agents through analysis of persistent biomarkers in plants	155
Chapter 7	Biomarker profiling in plants to distinguish between exposure to chlorine gas and bleach using LC-HRMS/MS and chemometrics	181

	Characterization of dispersion devices	
Chapter 8	A novel standard for forensic elemental profiling of polymers by LA-ICP-TOF-MS	203
Chapter 9	Evaluating the strength of evidence of elemental profiling of polymers with LA-ICP-MS	229
Chapter 10	Conclusions and future perspectives	257
	Summary & Samenvatting	
	Summary	275
	Samenvatting	281
	Additional information	
	Supplemental information	289
	List of abbreviations	290
	List of publications	295
	Overview of co-authors' contributions	298
	Acknowledgements	302



1

Introduction

Part of this introduction is in preparation for submission. Mirjam de Bruin-Hoegée and Daan Noort, Nerve agents. In Christopher Timperley *et al.*, The chemistry of chemical forensics and attribution of chemical weapons, *Chemical Reviews*.

1.1. The evolving threat from chemical weapons

Toxic chemicals have been used as a weapon since ancient times. There are numerous examples, including shooting poisoned arrows, contaminating water supplies, or polluting food with snake venom or toxic plants.^{1,2} Byzantine chronicles describe the use of ‘Greek fire’, an incendiary weapon with sulfur as a key ingredient, resulting in the production of toxic sulfur dioxide fumes.³ Throughout the Middle ages, arsenic smoke was used in battles and sieges in China, Serbia, and The Netherlands.^{4,5}

The first large-scale attack with a weapon of mass destruction was during the First World War. Tons of chlorine gas were released by the German Army in Belgium, killing and wounding thousands of French and Algerian soldiers.⁶ It was followed by the production and deployment of phosgene, cyanogen chloride, and sulfur mustard endangering many soldiers and civilians.⁷ Although stockpiling continued in the Second World War, along with development of new chemical weapons such as nitrogen mustard, tabun, and sarin, no chemical weapons were used on the battlefield.⁴ Despite this, large quantities of hydrogen cyanide, known as Zyklon B, were used as a method of mass extermination in German concentration camps.⁵ Figure 1.1 shows an overview of defining incidents with chemical warfare agents from 1914 up to 2020.

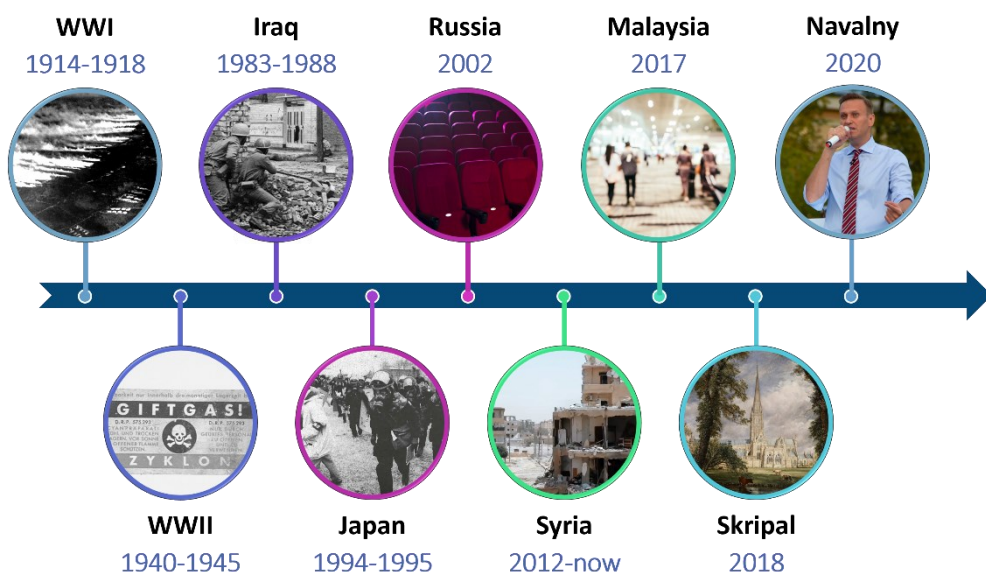


Figure 1.1. A timeline of defining incidents with chemical weapons from 1914 up to 2020.

The most extensive use of the newly developed nerve agents, such as tabun and sarin, was in the Iran-Iraq conflict from 1980-1988.^{7,8} It is estimated that the Iranian and Kurdish population suffered more than hundred thousand casualties as a result of



exposure to sulfur mustard and nerve agents.⁸ Several years later, sarin was unexpectedly used in a non-combat situation. Aum Shinrikyo terrorists released the nerve agent in Matsumoto City and the Tokyo subway.⁹ These horrifying incidents along with several other political events, accelerated negotiations for chemical disarmament. This worldwide effort finally led to the Chemical Weapons Convention (CWC) that came into force in 1997 and is currently signed by almost every country in the world.¹⁰ The Organisation for the Prohibition of Chemical Weapons (OPCW) is responsible for implementing this arms control treaty by monitoring compliance with disarmament and nonproliferation.

Tragically, the convention did not prevent the re-emergence of chemical weapons. Highly potent pharmaceutical-based agents were deployed by Russian special forces to end a Moscow theater hostage causing more than hundred deaths in 2002.¹¹ The treaty was again violated during the ongoing conflict in Syria, where sulfur mustard, sarin, and chlorine were repeatedly used in brutal bomb attacks.¹² More recently, nerve agents have also been used to assassinate individuals outside a battlefield. In 2017, VX was used to murder the half-brother of the North Korean leader Kim Jong Un at an airport in Malaysia.¹³ About a year later, a former Russian agent Sergei Skripal and his daughter were poisoned with a Novichok nerve agent in the United Kingdom.¹⁴ Once again, a chemical from the Novichok family was used in an assassination attempt, when the Russian opposition leader Alexi Navalny was poisoned in a plane in Russia.¹⁵

In response to these systematic violations, the international community granted the OPCW a new mandate to address the threat of chemical weapons use.¹⁶ After an alleged incident, attribution investigations can be requested to provide technical expertise to identify the perpetrators of chemical attacks in Syria and beyond.

1.2. Classification of chemical warfare agents

A wide range of toxic chemicals can potentially be employed as chemical warfare agents (CWAs). The Chemical Weapons Convention prohibits development, production, stockpiling, and utilization of any chemical intended to cause intentional death or harm through its toxic properties.¹⁷ Additionally, munitions, delivery systems, and related equipment designed to weaponize these chemicals are banned. To facilitate complete and verifiable destruction of chemical weapons, specific chemicals are listed in the convention. After long negotiations, it was decided to define three schedules not based on toxicity but on their application. Consequently, the first schedule prohibits chemicals that have been designed as a chemical weapon and have limited or no other peaceful applications. It also consists of key precursors and the highly potent toxins ricin and saxitoxin. The second schedule contains mainly precursors and chemicals traded in small quantities for legal purposes. Finally, the third schedule lists chemicals, such as

phosgene and hydrogen cyanide, that might be commercially produced in very large volumes. The purpose of these schedules is to identify chemicals for the application of verification measures. For example, the maximum quantities allowed for production or transportation vary among chemicals categorized under different schedules.

In the following subsections, important properties of four prominent types of chemical warfare agents are highlighted. The selection of these categories of toxic chemicals is based on their frequent use as chemical warfare agents in the past or the possible threat in the future. The first two groups of nerve and blister agents belong to Schedule 1. The third category of pharmaceutical-based agents is not explicitly mentioned in the Chemical Weapons Convention. Finally, the fourth category of toxic industrial chemicals is partially covered in Schedule 3. An overview of the main types of chemicals, degradation pathways, and human metabolism will be given.

1.2.1. Nerve agents

The first category of chemical warfare agents that will be discussed are nerve agents. This subsection covers general characteristics and main intoxication effects. Nerve agents are mostly organophosphorus compounds, with a characteristic leaving group, such as fluoride or cyanide. Their common toxicological mechanism of action is acetylcholinesterase (AChE) inhibition.¹⁸ Acetylcholine (ACh) transfers the signal from a nerve cell to receptors on a muscle cell, causing it to contract. Nerve agents prevent the normal breakdown of ACh by AChE. This results in the synaptic accumulation of ACh leading to over-stimulation of the cholinergic pathway giving rise to seizures and respiratory failure, finally leading to death.¹⁹ Conventional nerve agents are typically liquids at room temperature and can penetrate the body via inhalation or skin exposure. Many of these organophosphorus compounds are prohibited under the Chemical Weapons Convention and belong to Schedule 1. The group of nerve agents can be divided in five distinct classes: G-series, V-series, GV-series, Novichok agents, and (non-phosphorus) carbamates.²⁰ Figure 1.2 shows the basic structure of the various groups. The main representatives of the G-series are sarin (GB), soman (GD) and tabun (GA). After World War II, the V-series were developed, with VX as most lethal substance.² In addition, the third class of GV compounds contain the molecular structure of both G and V agents.²¹ The fourth and fifth group have recently been added to the list of prohibited chemicals of the CWC and are the first major changes since the treaty entered into force.²² Novichok agents, also called NVs or A-series, are listed as 1.A.13, 1.A.14, and 1.A.15 in CWC Schedule 1. The persistence of the V-series and Novichok agents is higher than the persistence of the G-series, which is relevant for the choice of detection techniques and sample collection for forensic purposes. The last family of carbamates (CWC Schedule 1, 1.A.16) are strictly no organophosphorus

compounds, but they are considered as nerve agents due to their similar toxicological method of action.²³

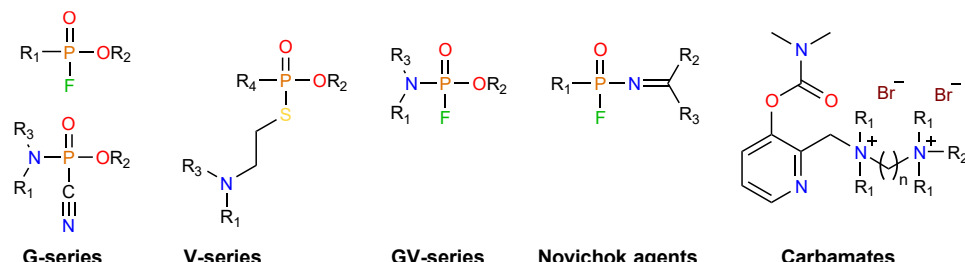


Figure 1.2. Overview of main structures of nerve agents. Various groups (R₁₋₄) can be connected to the main structure and the length (n) of the carbon chain can be changed. For the Novichok agents, R-groups include O-alkyl and N-alkyl groups.

1.2.1.1. Degradation pathways

Thermal degradation of chemical warfare agents can be encountered during a chemical attack or as a method of elimination. Traditionally, a chemical weapon consists of an explosive device with a chemical warfare agent payload. After detonation, the load of the explosive charge determines the amount of heat which is generated. If the explosive load is too high, the chemical warfare agents may degrade. Another cause of extensive heat may be the use of binary weapons, where two precursors are kept in separate compartments of the weapon system and are only being mixed inside the weapon on deployment to form the chemical agent by exothermic reactions.²⁴ In addition, various thermal destruction technologies have successfully been used to destroy chemical weapons. Some of them are prohibited by the OPCW because of the high ecological impact, such as open-pit burning, sea dumping, and land burial.²⁵ Other technologies are allowed, including plasma pyrolysis, incineration, and explosion chambers with off-gas treatment systems are frequently used.^{25,26}

The chemistry that is involved in these processes varies from partial combustion to full decomposition to ash, water, salts, and gaseous products. During destruction of sarin-filled rockets at Johnston Atoll no agent was detected in the exhaust, with a removal efficiency of more than 99.99%.²⁶ Figure 1.3 shows feasible degradation products of sarin, based on experiments and computational studies.²⁶⁻²⁹ The degradation of sarin via intramolecular H-transfer to the phosphorus oxoacid derivative and propene is kinetically and thermodynamically the most feasible.²⁷ Additionally, full combustion will lead to a product steam with O₂, CO₂, H₂O, and depending on the agent, HF, HCl, sulfur, or phosphorus oxides.

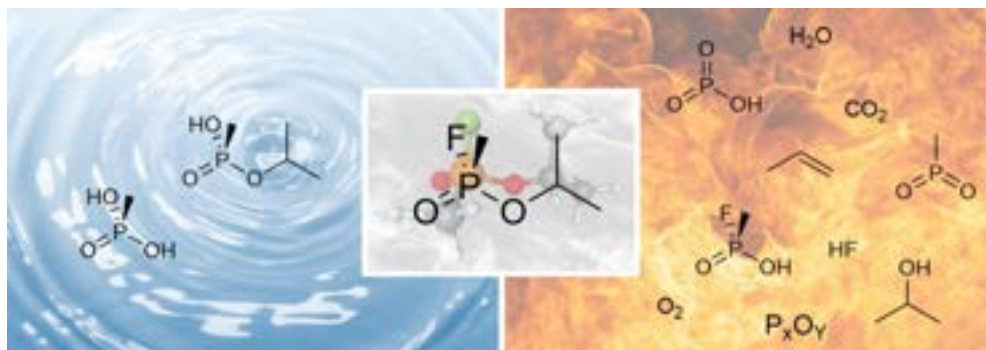


Figure 1.3. Degradation of sarin with primary hydrolysis pathway (left) and thermal degradation products identified based on experiments and computational studies (right).

In the presence of water, nerve agents can hydrolyze to isopropyl methylphosphonic acid (IMPA) and methylphosphonic acid (MPA) as presented in Figure 1.3.^{29,30} The hydrolysis reaction of sarin to IMPA is similar to the hydrolysis of soman and VX, where in the first step respectively pinacolyl methylphosphonic acid (PMPA) and ethyl methylphosphonic acid (EMPA) are formed. In the second step, MPA is formed as well. These hydrolysis products are often encountered in environmental and toxicological samples. Similar compounds are formed after neutralizing with aqueous NaOH, which is commonly used for the destruction of chemical agents.^{29–31} Such a concentrated base environment converts sarin to the sodium methyl phosphonate salt. The half-life in water ranges from a couple of days to a few weeks for G-series and V-series respectively.³² Besides these phosphorus hydrolysis products, more water reactants have been identified, including alcohols and thiol degradation products.^{29,33}

1.2.1.2. Human metabolism

Analysis of biomedical samples can be performed for several reasons, such as providing rapid chemical diagnostics to provide guidance for adequate medical treatment or to allow verification of chemical weapon use for forensic investigations.³⁴ Various samples can be obtained from surviving casualties, including blood, urine, and hair. During post-mortem examinations of deceased victims, tissues and body fluids can be collected. Chemical warfare agents can rarely be detected in unchanged form in living organisms.³⁵ Therefore, to find molecular evidence, other indicators of exposure to chemical warfare agents need to be found. For this purpose, either free metabolites or adducts to proteins and deoxyribose nucleic acid (DNA) are considered.³⁶ A distinct advantage of using biomedical samples is the possibility to find long-lasting biomarkers of exposure, which will increase the time window of opportunity for verification activities. For example, various biotransformation products were detected in the blood and tissue of victims, several weeks after an alleged exposure.^{31,37} Major biomarkers for nerve agents are albumin, butyrylcholinesterase (BChE), and AChE adducts and free

metabolites. Figure 1.4 shows the major metabolism products of VX. It is important to note that the attached group can degrade to the methylphosphonic acid adduct as shown in Figure 1.3. The adducts mainly bind to the amino acids serine, tyrosine and cysteine, but in albumin lysine can be metabolized as well.³⁸ Other potential biomarkers and novel targets are phosphorylated ubiquitin, disulfide adducts, and a large range of free metabolites.^{39–41} Typical analytical methods for human biological samples are liquid chromatography-mass spectrometry (LC-MS), gas chromatography-mass spectrometry (GC-MS), nuclear magnetic resonance (NMR), and immunological detection assays.^{31,34–36,42,43}

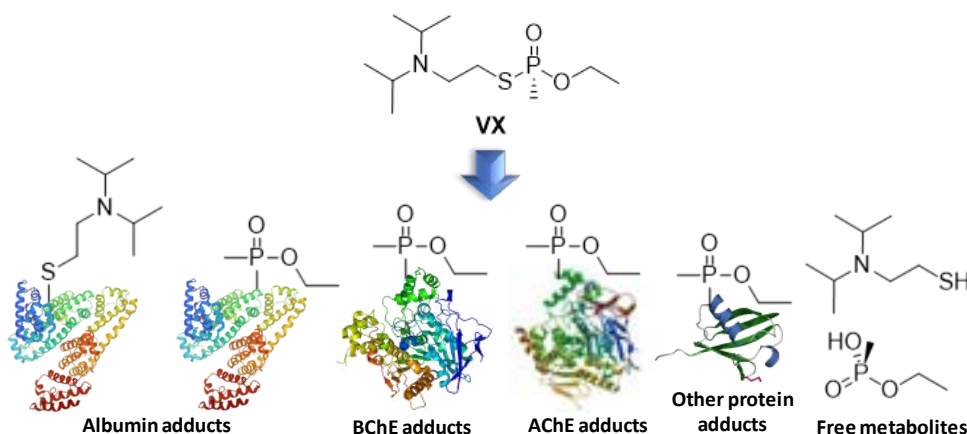


Figure 1.4. Major protein adducts and metabolites formed after metabolism of VX.

1.2.2. Blister agents

Blister agents or ‘vesicants’ are oily liquids with distinct odors which can be dispersed as liquid, aerosol or vapor.⁴⁴ Figure 1.5 shows the chemical structures of sulfur mustard (HD), nitrogen mustard, and lewisite, three well-established types of blister agents that have been developed as chemical weapons. Blister agents reduce the fighting capability of soldiers. Although they can be fatal after severe exposure, it mainly results in injured people.⁴⁵ Following exposure, there is a latent period before physical effects are noticed. After the delayed onset of several hours, dependent on the exposure concentration, eye burns and skin blistering occur.⁴⁶ Patients may vomit and suffer from temporary blindness. Moreover, significant respiratory tract damage and acute lung symptoms, including pulmonary edema, can develop, which may be fatal.⁴⁶ At the same time, indirect health effects occur, such as bone marrow depression and protein, DNA, and ribonucleic acid (RNA) damage.⁴⁷ Also, chronic physical effects and a higher risk for mental health disorders were observed in survivors of sulfur mustard exposure.^{48,49}

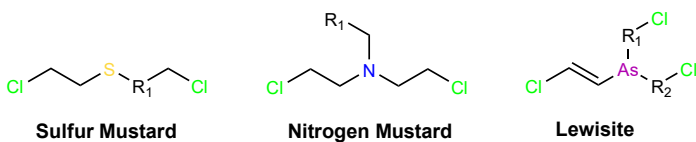


Figure 1.5. Overview of main structures of blister agents. Various groups (R₁₋₄) can be connected to the main structure.

After the release of chemical weapons, forensic analysis initially tries to establish the nature of the compound. This is especially important since these findings have considerable implications for maintaining the safety of first responders, administering suitable medical countermeasures, and applying the most effective decontamination approach. Due to the reactivity of these blister agents, it is often unfeasible to detect intact chemicals. In general, vesicants persist for a few days up to a few weeks, although large liquid droplets may persist for a longer period due to the formation of a protective layer.^{44,45} Consequently, analysis methods described in literature mainly focuses on measuring degradation products in environmental sources or metabolites and protein adducts in biomedical samples.

1.2.2.1. Degradation pathways

Various types of so-called environmental samples, such as soil,^{50,51} munition residue,⁵² concrete,⁵³⁻⁵⁵ paint, and rubber,^{56,57} have been collected and analyzed for evidence of chemical warfare agents by internationally validated methods.⁵⁸ GC-MS is one of the most applied methods for these types of samples. However, other laboratory methods such as LC-MS and NMR are also often utilized. Figure 1.6 shows the main degradation pathways of sulfur mustard.⁵⁹ The primary reaction in the environment is hydrolysis.⁵⁰ Sulfur mustard first transfers to mustard chlorohydrin and eventually it hydrolyzes to thiodiglycol. Notable products detected after thermal degradation were sesquimustard, 1,4-dithiane, and 1,4-dichloroethane.^{60,61} The products identified in concrete were particularly bis[2-(2-chloroethylthio)ethyl]ether, 2-chloroethyl vinyl sulfide, 2-hydroxyethyl vinyl sulfide.⁵⁴ Finally, oxidation can occur in the environment, e.g. on soil, or as a result of decontamination practices. It is important to note that most reactions can occur in different matrices, due to the presence of water, heat, or oxidizing catalysts.

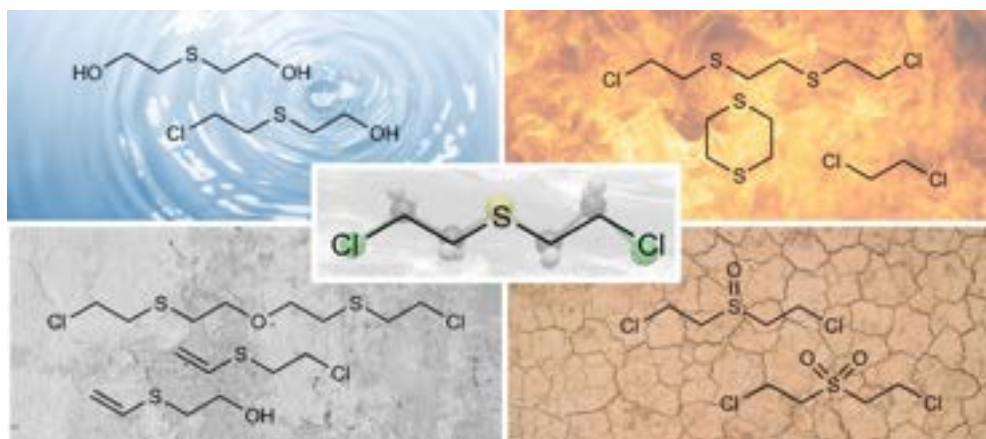


Figure 1.6. Degradation of sulfur mustard with primary hydrolysis pathway (upper left), thermal degradation (upper right), degradation on concrete (lower left), and oxidation (lower right).

1.2.2.2. Human metabolism

The metabolism of blister agents has been studied in detail by investigating in vivo, in vitro, and case studies. Due to the oxidation of sulfur and the presence of two electrophilic sites many biomarkers are formed after exposure.⁶² Figure 1.7 shows well established biomarkers for sulfur mustard. Short living metabolites are 1,1-sulfonylbis-[2-(methylsulfinyl)ethane] (SBMSE) and methylsulfinyl-2-[2-(methylthio)ethylsulfonyl]ethane (MSMTESE), which are metabolized through interaction with glutathione and rapidly excrete into urine.⁴² These biotransformation products were found until five days after poisoning with sulfur mustard.⁶³ Additionally, the hydrolysis product thioglycol (TDG) can be detected in urine and blood. This metabolite was also detected after induced release from blood protein adducts.⁶⁴ However, TDG can also be present in populations not exposed to blister agents. In contrast, protein and DNA adducts are specific long-living biomarkers. Stable adducts can be formed with the amino acids valine, histidine, cysteine, aspartic acid, glutamic acid, lysine, serine, and tyrosine.^{62,65-67} Two types of these protein adducts were detected in authentic cases. First, the albumin adducts formed at cysteine were still detectable after 29 days in people accidentally exposed to sulfur mustard.⁶³ Second, the valine adducts were found in samples from Iranian casualties taken up to 26 days after exposure.⁶⁸ In addition, DNA alkylation is assumed to be a major factor of the toxicity of mustard agents.⁵⁸ Various DNA adducts are formed with guanine and adenine, with N7-(2-hydroxyethylthioethyl)-2'-guanine (N7-HETE-G) as the major product. Also, this biomarker was found in Iranian victims up to 26 days after exposure.⁶⁸ The most applied analytical techniques are liquid chromatography(-high resolution) tandem mass spectrometry (LC-(HR)MS/MS). In addition, GC-MS has been

used after derivatization of the analyte of interest, or for analyzing free and reactivated metabolites.⁶⁹

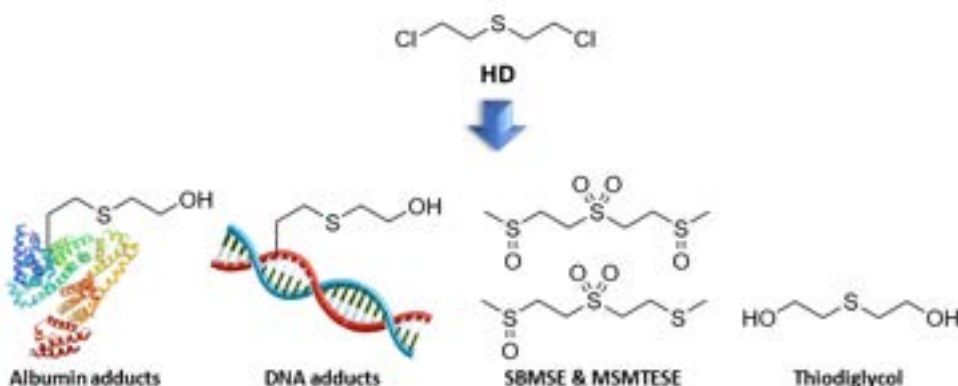


Figure 1.7. Major biomarkers formed after metabolism of sulfur mustard (HD).

1.2.3. Pharmaceutical-based agents

Synthetic opioids have originally been developed for medical purposes. Yet, they are not only applied under controlled medical conditions. Fentanyl and its analogues have also been used as illicit drug and are related to the dramatic number of overdose fatalities in the United States.⁷⁰ Recently, the OPCW adopted a decision that central nervous system (CNS)-acting chemicals, such as fentanyl, do not meet the definition of riot control agents which can be used for law enforcement purposes.⁷¹ The main reasoning was the low safety margin when delivered as an aerosol and the risk to cause permanent harm and death. Carfentanil, which is used as a tranquilizer for large mammals, is expected to be 10,000 more potent than morphine.⁷² Typical acute toxicological effects are reduced consciousness, respiratory depression, vomiting, pupillary constriction, shock, and respiratory failure which can lead to death.⁷³ Figure 1.8 shows the chemical structure of three potent pharmaceutical-based agents.

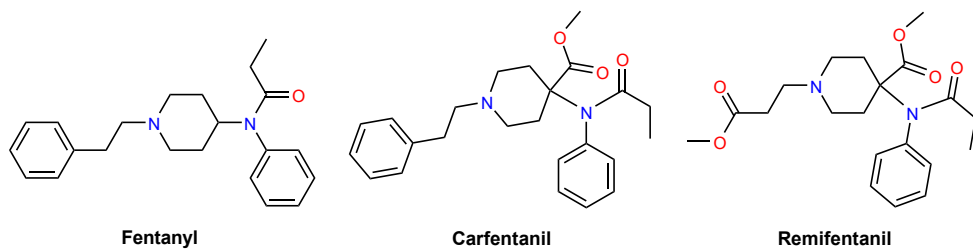


Figure 1.8. Examples of potent synthetic opioids: fentanyl, carfentanil, and remifentanil.

First responders can unintentionally be exposed to fentanyl and experience health effects. Predominantly, low doses will be encountered which do not lead to severe opioid toxicity.^{74,75} However, rapid portable detection of fentanyl would be beneficial to limit the exposure risk. Colorimetric swabs, lateral flow immunoassay test strips, Raman spectroscopy, (near-)infrared spectroscopy, ion mobility spectrometry, high-pressure mass spectrometry, GC-MS, and an on-site nano-liquid chromatography-electron ionization-mass spectrometer has been developed for field testing.^{76,77}

1.2.3.1. Degradation pathways

Fentanyl is stable for at least twelve weeks in soil and seven weeks in water.⁷⁸ An advantage of the persistence of fentanyl, is the possibility to find evidence of the location of a clandestine laboratory. A suitable detection method would be the application of GC-MS after extraction with ethyl acetate and aqueous ammonium hydroxide and subsequent derivatization.⁷⁹ Under the influence of more harsh conditions, fentanyl may eventually degrade (Figure 1.9). For example, styrene, pyridine, and N-phenylpropanamide were detected as potential markers of smoked fentanyl.^{80,81} In addition, fentanyl can be oxidized by aqueous solutions of peroxides and hypochlorites, which can be used to clean crime scenes. This yielded benzaldehyde, 1-phenethylpiperidine, N-(1-formylpiperidin-4-yl)-N-phenylpropionamide, 2-phenylacetaldehyde, and norfentanyl.⁸² Interestingly, the last two compounds are also human metabolism products.

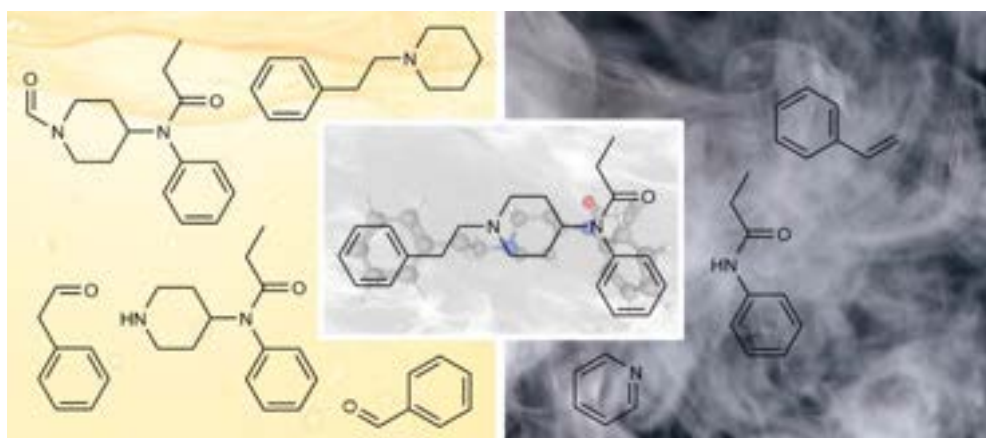


Figure 1.9. Degradation products of fentanyl after oxidizing (left) and smoking (right).

1.2.3.2. Human metabolism

Fentanyl metabolites are mainly detected in urine or blood plasma. Figure 1.10 shows the major metabolic pathways of fentanyl. The primary biotransformation occurs in the liver by phase 1 cytochrome-P450 (CYP) 3A enzymes, where fentanyl is metabolized into norfentanyl through oxidative N-dealkylation.⁸³⁻⁸⁵ Aside from this, other minor

biotransformation products can be detected. Fentanyl can undergo hydroxylation to form hydroxyfentanyl, β -hydroxyfentanyl, and 4-hydroxyfentanyl. Also, 4-anilino-N-phenethyl-piperidine (4-ANPP), which is also a precursor, was formed after hydrolysis.⁸⁵ The type and concentrations of biomarkers that are present depend largely on the circumstances. For example, post-mortem fentanyl concentrations in blood, collected within a day after therapeutic administration of fentanyl, were up to nine times higher than levels in living persons.⁸⁶ Additionally, fentanyl and 4-ANPP could be detected in the hair of non-medical opioid and heroin users.⁸⁷ LC-MS/MS was mostly applied as a sensitive, specific, and fast technique for the analysis of these substances.

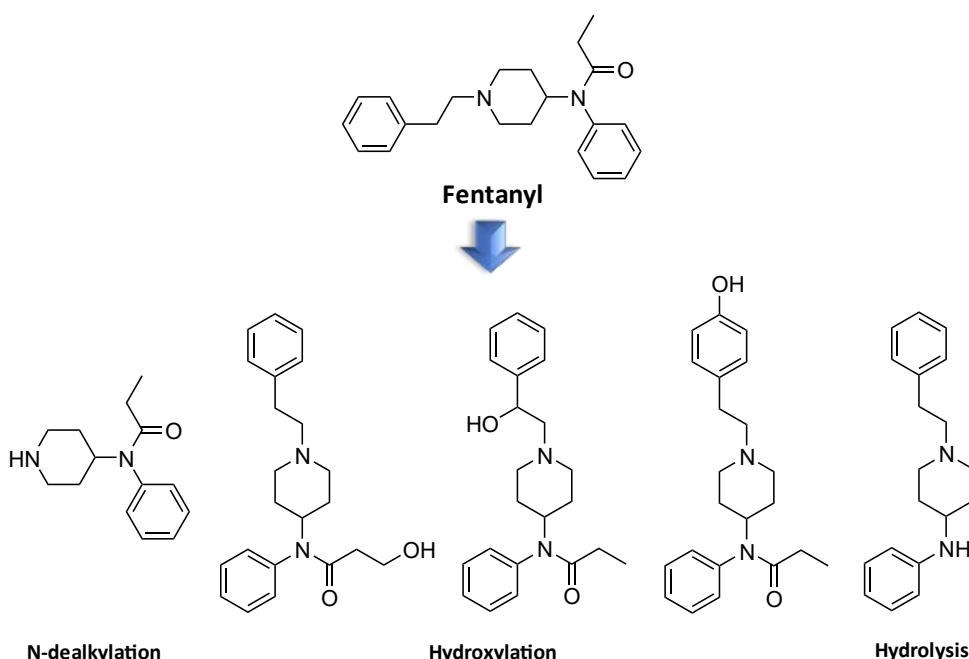


Figure 1.10. Major biomarkers formed after metabolism of fentanyl.

1.2.4. Toxic industrial chemicals

The final category of chemical threat agents that is discussed is the class of toxic industrial chemicals (TICs). This group contains a wide range of chemicals with diverse properties. TICs with a relatively low vapor pressure and a high dermal toxicity are for instance cyanides, allyl alcohol, and hydrazine. The median lethal doses (LD_{50}) are in the range of 10-100 mg/kg, which is considerably higher than the LD_{50} of VX for example, which is only 0.07 mg/kg.⁸⁸⁻⁹¹ In everyday life these chemicals are used for many applications. First, sodium and potassium cyanide are widely used in the mining industry for extracting gold from low-grade ore.⁹² Second, cyanide can be encountered in natural sources, such as plant seeds or volcanoes.⁹³ Severe concentrations result in



loss of consciousness, respiratory failure, and convulsions, which can lead to a cardiac arrest and death.^{92,94} Third, allyl alcohol is an important industrial precursor which is also applied as an herbicide in agriculture.⁹⁵ The metabolism of allyl alcohol to acrolein by alcohol dehydrogenase is responsible for the hepatotoxicity of allyl alcohol.⁹⁶ From a military point of view, hydrazines are particularly relevant since they are used as a fuel in heavy cargo carrier rockets.⁹⁷ The toxicological responses varied largely between species, with only limited evidence of carcinogenicity in humans.⁹⁸ However, hydrazine still poses a risk as a hepatotoxin and a potent contact sensitizer, which can also cause allergic contact eczema.⁹⁹

On the other hand, airborne chemicals with a high inhalation toxicity are typically chlorine and phosgene. The latter is also explicitly mentioned in schedule 3 of the chemical weapons convention, although it is commercially manufactured in large quantities. More than 12 million metric tons are produced annually.¹⁰⁰ It has main applications in the polymer industry, agriculture, and pharmaceuticals. After inhalation, respiratory tract and skin irritation are experienced. Soon afterwards, it might cause acute lung injury and pulmonary edema because of the accumulation of fluid in the lungs.¹⁰¹ Several cases of accidental industrial exposure have been reported. One exemplary case describes a man arriving at the hospital only suffering from mild throat irritation one hour after exposure to a high level of phosgene.¹⁰² Unfortunately, his symptoms deteriorated and 30 hours later he died of his injuries. This latent clinical effect is visible in more incidents with a short exposure to high concentrations of phosgene.

Alternatively, chlorine is not explicitly mentioned in the chemical weapons convention. When used properly, it can even support public health by disinfecting drinking water and improving water quality.¹⁰³ More applications, among other things, are paper bleaching, plastic manufacturing, development of pharmaceuticals, and pesticide production for agriculture.^{104,105} This broad spectrum of applications results in its ranking within the top ten chemicals manufactured in the United States.¹⁰⁶ However, accidental exposures are frequently encountered due to the extensive employment of chlorine gas for industrial and domestic purposes. Mostly, acute respiratory failure and irritation of eyes and throat were experienced.¹⁰⁷ The development of acute lung injury and pulmonary edema because of the accumulation of fluid in the lungs is rare. In the case of chemical warfare agent exposure, the fraction of deaths was slightly higher, most likely due to the longer exposure time to higher concentrations.^{12,107}

1.2.4.1. *Degradation pathways*

Since chlorine rapidly decomposes in the environment, it is challenging to verify its presence. Recently, markers have been detected in concrete as shown in Figure 1.11.

The most prominent chlorinated organic compounds were trichloromethylbenzene, trichlorophenol (TCP), and tetrachlorophenol (TeCP).¹⁰⁸ The latter was detected in paint chips collected from the walls of a room exposed to chlorine gas. The chlorinated phenol TCP was also found in wood together with bornyl chloride.¹⁰⁹ In water chlorine converts into hydrochloric acid, hypochlorous acid and chloride ions.¹⁰⁵ Additionally, some chlorinated markers have been found in soil and sewage sludge, although many contaminants might originate from chemical production factories. For instance, TCP, TeCP, and pentachlorophenol were observed in drinking water which was disinfected with chlorine dioxide.¹¹⁰ Various methods have been developed to identify these markers. For example, ion chromatography was applied to measure chloride concentrations in soil¹¹¹ More specific methods, such as gas chromatography(-high resolution) mass spectrometry (GC-(HR)MS), gas chromatography tandem mass spectrometry (GC-MS/MS), LC-MS/MS, and LC-HRMS/MS were applied to measure chlorophenols and other aromatic compounds.^{108,110}



Figure 1.11. Reaction products of chlorine in soil (upper left), concrete (upper right), water (lower left), paint (lower middle), and wood (lower right).

1.2.4.2. Human metabolism

Evidence of a chlorine attack can also be found in biomedical samples (Figure 1.12). The first biomarkers that were found were chlorinated amino acids 3-chlorotyrosine (Cl-Tyr) and 3,5-dichlorotyrosine (di-Cl-Tyr) in nasal tissue of rats.¹¹² The former was later detected in human autopsy samples as well.^{113,114} Second, the chlorinated fatty acids 2-chloropalmitaldehyde and 2-chlorostearaldehyde were found in lungs and plasma of mice and rats.¹¹⁵ In addition, phosphatidyl lipid chlorohydrins were measured in nasal and bronchoalveolar fluid.^{116–118} The fourth type of biomarker was 8-isoprostane, which was detected by a colorimetric enzyme-linked immunosorbent assay in the airways and blood following chlorine exposure in mice.¹¹⁹ Subsequently, chlorine exposed human nails could be distinguished from unchlorinated nails by Raman and Fourier-transform

infrared spectroscopy (FT-IR).¹²⁰ Lastly, hair could be a valuable source for forensic investigations. Cl-Tyr and di-Cl-Tyr could still be detected in hairs up to 10 months after exposure.^{121,122} The protein adducts, and chlorinated lipids were particularly detected by GC-MS, LC-MS/MS, and LR-HRMS.

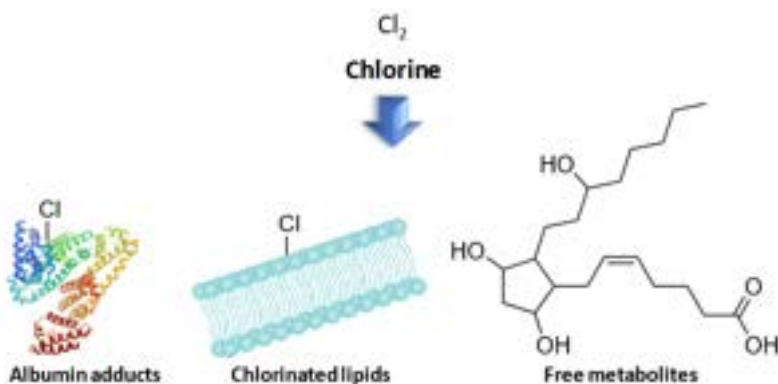


Figure 1.12. Major biomarkers formed after metabolism of chlorine.

1.3. Challenges for chemical forensic research

This section will address various challenges in the field of chemical forensics. It starts with a discussion on the growing need for sensitive and selective analytical techniques for qualification and quantification of trace levels in complex matrices. The subsequent sections describe recent developments and knowledge gaps in chemical profiling of chemical weapons for intelligence purposes. There will also be a focus on attribution in human biological samples and characterization of chemical dispersion devices. The last section ends with a brief discussion on chemometric models used in chemical attribution studies and the translation to the legal context.

1.3.1. Sensitive analysis in complex matrices

Constant innovation in analytical instruments advance the field of chemical forensics. Especially, the development of sensitive, selective, and rapid techniques would improve forensic analysis. As explained in Section 1.2, chemical warfare agents are highly reactive chemicals that rapidly degrade in the environment and metabolize in biological matrices. For this reason, it is often difficult to analyze the low levels of intact chemical that remain in the sample. Alternatively, transformed products might be less characteristic, emphasizing the importance of providing a reliable link with the original chemical threat agents. It should be investigated whether the markers can be distinguished from background concentrations and to examine the emergence because of other potential non-criminal activities. Another obstacle could be the efficiency of

the detection techniques which is often hampered by matrix interferences or co-eluting compounds. The application of appropriate sample preparation methods generally facilitates sensitive and selective analysis.

For the identification of unknown samples, the OPCW provides criteria for the chemical analysis.¹²³ Multiple techniques should be used, preferably including a high-resolution mass spectrometer for accurate mass measurements. Hyphenated techniques, where separation methods are coupled to spectral methods provide lower detection limits, shorter analysis time, better reproducibility, precision, and repeatability.¹²⁴ Therefore, these techniques are considered more valuable than other techniques and can be used as a primary identification method.

Multiple approaches are possible for the analysis of a questioned sample. The most general method is non-targeted screening which is the best method for identification of emerging chemicals. The chemical structure of compounds can be elucidated without any required prior information. Since, every year hundreds of new chemicals appear in the environment, it is important to be able to characterize these to limit the potential health risk.¹²⁵ Also, impurities might be detected in the sample which could provide valuable information for intelligence purposes, as will be discussed in the next subsection. However, it should be noted that each analytical technique only covers a part of the chemical space, limiting the range of chemicals that can be detected. On the other hand, targeted analytical methods can be used to search for specific chemicals. These compounds can be detected with high sensitivity and selectivity. A typical targeted method is LC-MS/MS with multiple reaction monitoring, where characteristic precursor and product ion transitions can provide rich information about the chemical structure. Ultimately, a combination of both approaches is applied to be able to identify and quantify a pre-selected group of chemicals without losing the ability to analyze the remainder of the sample for other relevant compounds.

1.3.2. Chemical profiling for forensic intelligence purposes

In addition to establishing the nature of the agent used, addressing the question of its origin is of equal if not greater importance to accurately reconstruct events and find the persons and institutions responsible. Valuable tactical information includes information on production, the route of synthesis, raw materials, and potential associations of materials. Figure 1.13 shows the history of a chemical, where each phase influences the appearance and chemical composition of a material. The current section mainly focusses on impurities related to the raw materials, production, and synthesis methods, whereas the topics discussed in the section 1.2 on the extent of degradation and hydrolysis may especially give information on the age, location, and storage method. The entire spectrum of information can assist national defense, law

enforcement, and the OPCW in solving crimes or preventing additional attacks with chemical weapons. Multi-analytical profiling strategies are required to use attribution studies of chemical warfare agents for forensic intelligence purposes.

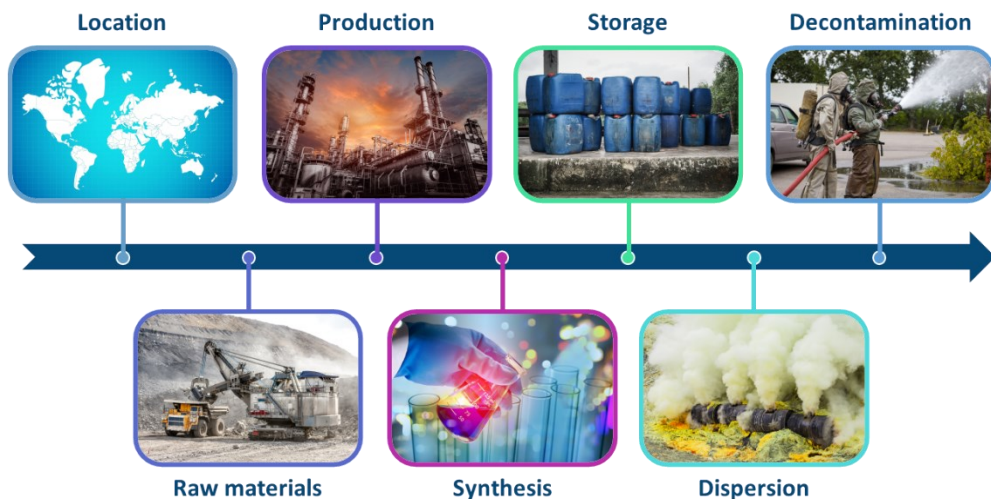


Figure 1.13. The history of a material influences the appearance and composition of a chemical weapon.

To date only a limited number of laboratory studies have been carried out to match chemical threat agents to its starting materials. This is partially due to the highly toxic nature of the chemicals, making the syntheses and analyses more demanding and dangerous. For this reason, many investigations are performed with simulants or precursors of chemical warfare agents. The next paragraphs summarize various chemical profiling studies of nerve agents and related compounds.

Table 1.1 shows the methods used and results obtained in chemical attribution studies of GA, GB, GD, Russian VX (VR), and VX. In addition, some related compounds were studied, such as the chemical weapon precursors methylphosphonic dichloride (DC), dimethyl methylphosphonate (DMMP) and N,N-dimethylphosphoramidic dichloride (DMPADC), and organophosphate (OP) pesticides. The analytical techniques often used for these studies, include GC-MS, comprehensive two-dimensional gas chromatography-mass spectrometry (GC x GC-MS), liquid chromatography quadrupole-time of flight mass spectrometry (LC-QTOF-MS), LC-MS/MS, elemental analyzer-isotope ratio mass spectrometry (EA-IRMS), NMR, and site-specific natural isotopic fractionation by nuclear magnetic resonance (SNIF-NMR). For data analysis, principal component analysis (PCA), hierarchical cluster analysis (HCA), partial least squares-discriminant analysis (PLS-DA), linear discriminant analysis (LDA) and random forest (RF) are most implemented.

Table 1.1. Overview of chemical profiling studies of nerve agents and related compounds.

Chemical	Samples	Matrix	Analytical techniques	Data analysis	Number of CAS	Ref.
GA	Products from 3 synthesis methods	n.a.	GCxGC-TOF-MS	PLS-DA	109	¹²⁶
GB	Hydrolyzed synthesis products from 2 DC stocks	n.a.	GC-MS	PCA, HCA	43	¹²⁷
GD	Hydrolyzed synthesis products from 3 pinacolyl alcohols	n.a.	NMR	n.a.	3	¹²⁸
VR	Products from 6 synthesis methods	n.a.	GC-MS-EI	PCA, PLS-DA	49	¹²⁹
VR	Products from 6 synthesis methods	Food	LC-MS/MS	PLS-DA	17	³²
VR	Products from 3 synthesis methods	Food	GC-MS, LC-MS	PLS-DA	31	¹³⁰
VX	Crude VX with DCC stabilizer	Burnt and decontaminated soil	GC-MS-dFPD, GCxGC-TOF-MS, LC-QTOF-MS	n.a.	32	¹³¹
VX	3 stocks with different ages	n.a.	NMR, GC-MS, LC-QTOF-MS	n.a.	44	¹³²
VX	10–15-year stored VX	n.a.	GC-MS, GC-FID	n.a.	24	¹³³
DC*	10 stocks from 4 suppliers	n.a.	LC-MS	XC-MS, HCA, KNN, PCA	34	¹³⁴
DC*	13 stocks from 4 suppliers	n.a.	EA-IRMS, NMR	HCA	1	¹³⁵
DC*	Products from 2 synthesis methods	n.a.	GC-MS	HCA, PCA	16	¹³⁶
DC*	Stocks from 6 suppliers	n.a.	SNIF-NMR	n.a.	6	¹³⁷
DMMP*	Stocks from 4 suppliers	Cotton, painted wall board, nylon coupons	GC x GC/MS	PCA, ANOVA	29	¹³⁸
DMMP*	Stocks from 6 suppliers	n.a.	GCxGC-TOF-MS	Pairwise Analysis, Matrix Factorization	29	¹³⁹
DMMP*	Products from 2 suppliers	Painted wall board	GC-MS	n.a.	14	¹⁴⁰
DMMP*	Stocks from 6 suppliers	Painted wall board	GCxGC-MS	n.a.	5	¹⁴¹
DMPADC*	Products from 3 synthesis methods	n.a.	GC-MS	PCA, PLS-DA, HCA	20	¹⁴²
OP Pesticides*	Stocks from 6 suppliers	Neat and formulated sources	GCxGC-TOF-MS	RF, PCA-LDA, PLS-LDA	1-200	¹⁴³

*Chemical weapon precursors or simulants

Besides these findings based on laboratory studies, chemical attribution signatures (CAS) were also found in case samples. For instance, four CAS were detected by GC-MS in sarin released during the terrorist attacks by Aum Shinrikyo in Matsumoto City in 1994 and Tokyo subway in 1995.⁹ In biomedical samples retrieved from a victim of an attack with nerve agents in the Syrian Arab Republic 2013, the synthesis by-product diisopropylmethylphosphonate (DIMP) was detected by LC-MS/MS and LC-QOF-MS, which could be used as potential CAS.³¹ Additionally, seven impurities were found in case samples from the assassination of Kim Jong-Nam in Malaysia.¹³ Furthermore, it was stated in a United States Government report that nerve agents obtained at various depots in Iraq, contained sarin and cyclosarin as well as a large number of impurities.¹⁴⁴ During the OPCW fact-finding mission in the Syrian Arab Republic regarding an alleged incident in Khan Shaykhun in 2017, various impurities and breakdown products related to sarin were found that could give information about the production route and raw materials.¹⁴⁵ On the contrary, no impurities other than hydrolysis products were found in samples retrieved from bomb craters and unexploded weapons in the Iran-Iraq conflict of 1987-1988.^{146,147} In addition, almost no impurities were found in the Novichok nerve agent found in Salisbury after the poisoning and hospitalization of three individuals.¹⁴

In the field of illicit drugs and chemical weapons, chemical attribution signatures are often based on synthesis impurities. Table 1.2 summarizes the precursors of some synthesis routes for sarin based on open literature.^{135,148-151} This information is relevant because the starting materials might be found as impurity in the final product which can be used for intelligence purposes. Phosphorus trichloride (A), triethyl phosphite (B), trimethyl phosphite (J) and thionyl chloride (K) are listed as OPCW Schedule 3B precursors.¹⁵² Diethyl methylphosphonate (C), methylphosphonic acid (D), methylphosphonic acid difluoride (F), methylphosphonic acid dichloride (DC) and DMMP are OPCW schedule 2B precursors.¹⁵³

Table 1.3 summarizes some synthesis routes for VX.^{129,131,132} Phosphorus trichloride (A) and DC and were also precursors of sarin. Methyldichlorophosphine (O), methylphosphonothioic dichloride (P), O,O'-diethyl methylphosphonothioate (Q), O-Ethyl methylphosphonothioic acid (R), 2-(N,N-diisopropylamino)ethyl chloride (T) and 2-(diethylamino)ethane-1-thiol (U) are listed as OPCW schedule 2B precursors.¹⁵³ Most of these starting materials were still identified as trace materials in VX product batches.^{13,129,131-133}

Table 1.2. Main precursors of various synthesis routes of sarin.

#	Precursors						
1	A	B	C	D	E	F	G
2				H	I		
3		J	DMMP	K			
4	M			N		L	

1

Table 1.3. Main precursors of various synthesis routes of VX.

#	Precursors			Product
1	DC		S	
2		Q	R	T
3	P			VX
4	O		U	



1.3.3. Attribution using biomedical samples

While chemical profiling and the feasibility of attribution by using bulk and environmental samples has been studied quite extensively, only limited literature is available when using biomedical samples for these purposes. Several reasons can be brought up for this. First of all, the chemicals of interest, including impurities and by-products might be present in extremely low concentrations, which complicates their unambiguous identification. This is especially the case for highly toxic chemicals like nerve agents or certain synthetic opioids. Often targeted mass spectrometry is used to achieve very low detection limits. However, if the identity of the impurities is not known, a full scan analysis is required which provides lower sensitivity and selectivity.^{34,154} Second, the impurity profile likely changes due to biochemical and toxicological processes. Third, it can be envisaged that the intact impurities are not present anymore, because they are excreted in the urine, either as such or after metabolism. Nonetheless, it is expected that the use of increasingly sensitive analytical techniques with high resolution options will improve the attribution possibilities in the future.

Until now, a few proof-of-principle studies and one case study have been performed on chemical profiling of biomedical samples. First, John et al. showed unequivocally that sarin had been used in the Syrian city of Saraqueb on April 29, 2013 by analyzing a variety of biotransformation products, including covalent protein adducts and the hydrolysis product IMPA.³¹ Interestingly, the synthesis by-product DIMP was also detected in the biomedical samples, which could potentially be used as a marker for attribution research.¹²⁷ In this case, however, the main purpose of the investigations was to assess unambiguous exposure to a nerve agent and no further attribution analysis was applied. Additionally, Blum et al. investigated the adducts of sesquimustard (Q), which is a common impurity in sulfur mustard mixtures and a degradation product in old munitions containing HD.¹⁵⁵ In-vitro studies of plasma incubated with Q and HD were performed. After sample preparation, dipeptide and tripeptide biomarkers were identified by LC-MS/MS and LC-HRMS/MS. The concentration of Q depends on the synthesis route, storage conditions and age.^{156,157} Therefore, its relative amount, as expressed in the relative levels of adducts of Q compared to adducts of HD, might be used to conduct source attribution. Another study by Hemme et al. also investigated biomarkers of exposure to a wide range of sulfur mustard analogues, all belonging to Schedule 1 of CWC.¹⁵⁸ Human plasma was exposed to five of these analogues, and subsequently tripeptide and histidine adducts were detected by LC-QTOF-MS and LC-MS/MS. The fragmentation pattern of the adducts was used for identification and assessed to discover valuable information for a potential chemical attribution signature. The second part of the research showed that adducts could still be identified in plasma samples at a 1% analogue level relative to

HD. Together these results provide important insights into the possibility of using sulfur mustard biomarkers for chemical provenancing in biomedical samples.

1.3.4. Characterization of dispersion devices

After the explosion or release of chemical, biological, radiological, and nuclear (CBRN) weapons it might be difficult to find traces of the intact chemical. In this case, determining the composition of the dispersion device could potentially provide leads for the forensic investigation. A chemical weapon is often associated with the toxic chemical itself, however also munition, devices, and other equipment used to inflict harm through the release of toxic chemicals are prohibited under the Chemical Weapons Convention.¹⁵⁹ Therefore, additional characterization and differentiation of these delivery systems could provide valuable intelligence information.

The most straightforward approach for characterization would be visual confirmation. Previously an analysis strategy was developed for differentiating flash bangers in pre- and post-explosive casework based on visual examination of plastic caps.¹⁶⁰ In addition, visual analysis of a cylinder found in Syria indicated that the cradle had the same design as previously used in other incidents where chlorine was used as a weapon.¹⁰⁹ The design and remnants of the chlorine cylinder could also distinguish between surface-to-surface weapons and air delivery. After the release of an aerial bomb containing sarin in Syria, the type of munition could be identified based on the investigation of the paint, material, and shape of metal fragments.¹⁶¹ Also, in the case of a sulfur mustard attack, examination of the artillery projectile provided some information on the military grade shell.¹⁶²

However, in the case of damaged munition, chemical analysis might provide more details about the type and origin of the delivery system. Pieces with chemical agent-resistant coatings are for instance more likely to be found as part of military objects than as fragments of improvised explosive devices. Furthermore, commercial gas cylinders are often coated in a color that identifies its contents. Also, the type of material could provide leads for tactical investigations. Military bombs are generally made of metal, while homemade explosives or chemical dispersion devices often consist of plastic materials. The highest degree of discrimination between flash bangers was obtained by combining visual examination with elemental profiling of the plastic caps.¹⁶³ Lastly, forensic comparisons have been applied to glass, tape, and paint evidence to discriminate between different sources and provide correct associations of pieces from the same origin.^{164,165}



1.3.5. Chemometrics in a legal context

Although chemical attribution signatures typically support law enforcement and assist tactical investigations, it can also provide important evidence in a court of law. Therefore, it is important to assess the evidential value of the attribution signature in forensic investigations. Traditionally, expert opinion was the guiding principle in court, for instance by manually comparing chromatograms for identification. However, development of databases and automated identification software eased this process. Database acceptance criteria of 800/1000 are generally applied for assuming an identification as positive.⁵⁸ In a chemical forensics study applied to CWA, a National Institute of Standards and Technology (NIST) database match of ≥ 950 and an automatic mass spectral deconvolution and identification system (AMDIS) net match of 70/100 were sufficient for matching impurities from different instruments and laboratories.¹³⁶ However, notable differences were observed between laboratories in the peak area, relative to the sum of all peak areas. This variation may have arisen due to differences in sample preparation recovery and analytical methods and instruments. Despite these visual differences it was possible to discriminate between two batches using multivariate techniques.

Various chemometric models can be applied to forensic evidence and used to discriminate between different samples. HCA was for instance applied to discriminate between two batches of a nerve agent precursor.¹³⁶ Additionally, the unsupervised method PCA and supervised methods such as PLS-DA or LDA are often utilized. One advantage of these methods is that they provide information about which variables contribute the most to the discrimination between groups. Consequently, these methods are often applied in profiling studies of chemical threat agents. On the other hand, match criteria, such as the standard deviation overlap method or Student's t-test, have been used to compare chemical attribution signatures of two or more samples.¹⁶⁶ A disadvantage of the match criterion approach is that slight differences can result in entirely opposing outcomes. A solution would be to use Bayesian statistics, where the degree of similarity is expressed using a likelihood ratio (LR). This expresses the ratio of the probability of observing the evidence when considering two opposing hypotheses. If a model with sufficient reference data is available, which is calibrated and validated, a quantitative expression of the evidential strength can be estimated. However, when this is not available, it is also possible that the expert estimates the probability of the evidence under the considered hypotheses using verbal statements.¹⁶⁷ The conclusion of the expert is written in a forensic report or stated in a court of law during the testimony. The Bayesian framework was for instance applied to chemical profiling of drugs¹⁶⁸ and explosives¹⁶⁹ using a score-based method with various similarity metrics. In the case of feature-based methods, profiles were modelled with a Gaussian distribution by a kernel density estimation. Although in principle a wide range of

machine learning algorithms can be applied, it is highly desirable to arrive at explainable models. This would prevent construction of models based on noise or random correlation.

1.4. Scope of the thesis

The main objective of the research in this thesis is to develop multi-analytical profiling strategies for chemical warfare agents and associated devices to support forensic intelligence purposes. Several challenges in chemical forensic research can be assessed as explained previously. To be able to address these knowledge gaps, this research will focus on three themes:

1. Forensic CWA intelligence
2. CWA profiling in biological samples
3. Characterization of CWA dispersion devices

1.4.1. Forensic intelligence

Chapters 2 and 3 explore the possibility of obtaining information about the synthesis route of chemical threat agents and subsequently linking a sample to other batches or starting materials. In addition to profiling of intact material, the potential of chemical attribution of synthetic drugs through the analysis of metabolic trace levels in human biological samples is investigated. **Chapter 2** focusses on the pharmaceutical agent fentanyl and **Chapter 3** examines various fentanyl analogues. Since, metabolized samples are investigated as well, the topic of these studies partially overlap with the second theme.

1.4.2. Profiling in biological samples

Chapter 4 introduces a high-resolution mass spectrometry method to identify selective biomarkers of chlorine exposure. The elucidation of site-specific chlorinated peptides is important as a more unambiguous indicator of exposure, since similar biomarkers exist for endogenous and exogenous exposure.

Chapter 5 elaborates on verification of exposure to nerve agents by portable detection and laboratory analysis of dried blood spots. The presence and stability of a wide range of nerve agent biomarkers is investigated using various analytical methods.

Chapter 6 presents a novel approach for analyzing protein adducts in vegetation as evidence of the release of chemical warfare agents. Liquid chromatography(-high resolution) tandem mass spectrometry methods are applied for the detection of nerve agent, blister agent, and chlorine gas biomarkers.



Chapter 7 expands the insights on the analysis of plant biomarkers using untargeted high resolution mass spectrometric analysis. The feasibility of forensic biomarker profiling in vegetation is investigated with the aim to distinguish between exposure to various chlorinating agents.

1.4.3. Characterization of dispersion devices

Chapters 8 and 9 describe the development of novel standards for forensic elemental profiling of polymer-based evidence by laser ablation-inductively coupled plasma time-of-flight mass spectrometry (LA-ICP-TOF-MS) and laser ablation-inductively coupled plasma-mass spectrometry (LA-ICP-MS). Additionally, the matrix-matched reference materials are applied to datasets of tapes, electrical wires, PVC tubing, and jerrycans. Several statistical models are applied to evaluate the evidential value of forensic classifications and comparisons.

Chapter 10 concludes the thesis and provides future research directions.

An overview of the research discussed in the various chapters of this thesis is schematically illustrated in Figure 1.14. In this figure, every circle is a distinct piece of evidence, which can be collected after an alleged attack to support forensic investigations. First, the forensic profile of the chemical threat agent itself is determined (Chapter 2 and 3). Second, if it is difficult to find traces of the intact chemical, it is valuable to assess the potential of chemical attribution in biomedical samples (Chapter 2 and 3). Third, human biological samples can also be used for identification of selective biomarkers (Chapter 4). Subsequently, a small volume of blood obtained by a finger-prick device and stored as dried blood spot is analyzed to obtain evidence of nerve agent exposure (Chapter 5). In addition, biomarkers of chemical warfare agents in plants are analyzed (Chapters 6 and 7). Finally, the potential of characterizing plastic parts of dispersion devices is explored (Chapters 8 and 9).

It should be noted that Chapters 2-9 of this thesis can be read independently, since these chapters are prepared for publication as scientific articles in peer-reviewed journals. Some overlap may occur in the introduction or discussion of these articles.



Figure 1.14. Illustration of various pieces of evidence that can be collected after a suspected attack with chemical weapons. The chapters in this thesis focus on revealing the origin of chemical weapons using the different types of evidence as indicated in the figure.



References

- (1) Salem, H.; Ternay, A. L.; Smart, J. K. Brief History and Use of Chemical Warfare Agents in Warfare and Terrorism. In *Chemical Warfare Agents: Chemistry, Pharmacology, Toxicology, and Therapeutics*; 2007; pp 27–46. <https://doi.org/10.1201/9781420046625-7>.
- (2) Szinicz, L. History of Chemical and Biological Warfare Agents. *Toxicology* **2005**, *214*, 167–181. <https://doi.org/10.1016/j.tox.2005.06.011>.
- (3) Turner, M. D.; Sapp, J. Fire and Brimstone: SO₂ as a Chemical Weapon in History. *Mil Med* **2023**, *188* (11–12), 286–288. <https://doi.org/10.1093/milmed/usad160>.
- (4) Smart, J. K. Chapter 2: History of Chemical and Biological Warfare: An American Perspective. In *Medical Aspects of Chemical and Biological Warfare*; 1997; pp 21–22.
- (5) Robinson, J. P.; Leitenberg, M. The Rise in CB Weapons. In *The Problem of Chemical and Biological Warfare*; Stockholm, 1971; Vol. 1.
- (6) Fitzgerald, G. J. Chemical Warfare and Medical Response During World War I. *Am J Public Health* **2008**, *98* (4), 611–625. <https://doi.org/10.2105/ajph.2007.11930>.
- (7) Chauhan, S.; Chauhan, S.; D'Cruz, R.; Faruqi, S.; Singh, K. K.; Varma, S.; Singh, M.; Karthik, V. Chemical Warfare Agents. *Environmental Toxicology and Pharmacology*. September 2008, pp 113–122. <https://doi.org/10.1016/j.etap.2008.03.003>.
- (8) Haines, D. D.; Fox, S. C. Acute and Long-Term Impact of Chemical Weapons: Lessons from the Iran-Iraq War. *Forensic Sci Rev* **2014**, *26* (2), 97–114.
- (9) Tu, A. T. Toxicological and Chemical Aspects of Sarin Terrorism in Japan in 1994 and 1995. *Toxin Reviews*. July 2007, pp 231–274. <https://doi.org/10.1080/15569540701496321>.
- (10) OPCW. *History*. <https://www.opcw.org/about-us/history> (accessed 2023-11-30).
- (11) Riches, J. R.; Read, R. W.; Black, R. M.; Cooper, N. J.; Timperley, C. M. Analysis of Clothing and Urine from Moscow Theatre Siege Casualties Reveals Carfentanil and Remifentanil Use. *J Anal Toxicol* **2012**, *36* (9), 647–656. <https://doi.org/10.1093/jat/bks078>.
- (12) Koblenz, G. D. Chemical-Weapon Use in Syria: Atrocities, Attribution, and Accountability. *Nonproliferation Review* **2019**, *26* (5–6), 575–598. <https://doi.org/10.1080/10736700.2019.1718336>.
- (13) Nakagawa, T.; Tu, A. T. Murders with VX: Aum Shinrikyo in Japan and the Assassination of Kim Jong-Nam in Malaysia. *Forensic Toxicol* **2018**, *36*, 542–544. <https://doi.org/10.1007/s11419-018-0426-9>.
- (14) OPCW. *Summary of the report on activities carried out in support of a request for technical assistance by the United Kingdom of Great Britain and Northern Ireland*. https://www.opcw.org/sites/default/files/documents/S_series/2018/en/s-1612-2018_e__1_.pdf (accessed 2023-02-06).
- (15) Dewey, K. Poisonous Affairs: Russia's Evolving Use of Poison in Covert Operations. *Nonproliferation Review* **2023**. <https://doi.org/10.1080/10736700.2023.2229691>.
- (16) OPCW. *CWC Conference of the States Parties Adopts Decision Addressing the Threat from Chemical Weapons Use*. <https://www.opcw.org/media-centre/news/2018/06/cwc-conference-states-parties-adopts-decision-addressing-threat-chemical> (accessed 2024-02-06).
- (17) Chemical Weapons Convention. *Convention on the Prohibition of the Development, Production, Stockpiling and Use of Chemical Weapons and on Their Destruction*. <https://www.opcw.org/chemical-weapons-convention> (accessed 2023-12-04).
- (18) Aroniadou-Anderjaska, V.; Apland, J. P.; Figueiredo, T. H.; De Araujo Furtado, M.; Braga, M. F. Acetylcholinesterase Inhibitors (Nerve Agents) as Weapons of Mass Destruction: History, Mechanisms of Action, and Medical Countermeasures. *Neuropharmacology* **2020**, *181*, 108298. <https://doi.org/10.1016/j.neuropharm.2020.108298>.
- (19) Black, R. M.; Read, R. W. Biological Markers of Exposure to Organophosphorus Nerve Agents. *Arch Toxicol* **2013**, *87*, 421–437. <https://doi.org/10.1007/s00204-012-1005-1>.
- (20) Castelvecchi, D. *Novichok nerve agents banned by chemical-weapons treaty*. *Nature*. <https://doi.org/10.1038/d41586-019-03686-y>.
- (21) Bajgar, J. Complex View on Poisoning with Nerve Agents and Organophosphates. *Acta Medica (Hradec Králové)* **2005**, *48* (1), 3–21. <https://doi.org/10.14712/18059694.2018.23>.

- (22) Noort, D.; Fidder, A.; Van Der Riet-Van Oeveren, D.; Busker, R.; Van Der Schans, M. J. Verification of Exposure to Novichok Nerve Agents Utilizing a Semitargeted Human Butyrylcholinesterase Nonapeptide Assay. *Chem Res Toxicol* **2021**, *34* (8), 1926–1932. <https://doi.org/10.1021/acs.chemrestox.1c00198>.
- (23) Costanzi, S.; Koblenz, G. D. *Updating the CWC: How We Got Here and What Is Next*. Arms Control Today. <https://www.armscontrol.org/act/2020-04/features/updating-cwc-we-got-here-what-next> (accessed 2024-02-05).
- (24) Palca, J. Binary Weapons in Trouble. *Nature* **1986**, *321* (June), 717.
- (25) OPCW. *Eliminating Chemical Weapons*. <https://www.opcw.org/work/eliminating-chemical-weapons> (accessed 2024-02-06).
- (26) Tedder, D. W.; Pohland, F. G. *Emerging Technologies in Hazardous Waste Management* 7; Springer Science+Business Media: New York, 1997; Vol. 1.
- (27) Ash, T.; Debnath, T.; Banu, T.; Das, A. K. Exploration of Unimolecular Gas-Phase Detoxication Pathways of Sarin and Soman: A Computational Study from the Perspective of Reaction Energetics and Kinetics. *Chem Res Toxicol* **2016**, *29*, 1439–1457. <https://doi.org/10.1021/acs.chemrestox.6b00132>.
- (28) Senyurt, E. I.; Schoenitz, M.; Dreizin, E. L. Rapid Destruction of Sarin Surrogates by Gas Phase Reactions with Focus on Diisopropyl Methylphosphonate (DIMP). *Defence Technology* **2021**, *17*, 703–714. <https://doi.org/10.1016/j.dt.2020.06.008>.
- (29) Kim, K.; Tsay, O. G.; Atwood, D. A.; Churchill, D. G. Destruction and Detection of Chemical Warfare Agents. *Chem Rev* **2011**, *111*, 5345–5403. <https://doi.org/dx.doi.org/10.1021/cr100193y>.
- (30) Jung, H.; Choi, S. VX Evaporation and Degradation from Urban Land Surfaces. *Environ Eng Sci* **2018**, *35* (6), 645–653. <https://doi.org/10.1089/ees.2017.0342>.
- (31) John, H.; Schans, M. J. van der; Koller, M.; Spruit, H. E. T.; Worek, F.; Thiermann, H.; Noort, D. Fatal Sarin Poisoning in Syria 2013: Forensic Verification within an International Laboratory Network. *Forensic Toxicol* **2018**, *36* (1), 61–71. <https://doi.org/10.1007/s11419-017-0376-7>.
- (32) Jansson, D.; Lindström, S. W.; Norlin, R.; Hok, S.; Valdez, C. A.; Williams, A. M.; Alcaraz, A.; Nilsson, C.; Åstot, C. Part 2: Forensic Attribution Profiling of Russian VX in Food Using Liquid Chromatography-Mass Spectrometry. *Talanta* **2018**, *186*, 597–606. <https://doi.org/10.1016/j.talanta.2018.02.103>.
- (33) Rohrbaugh, D. K. Characterization of Equimolar VX – Water Reaction Product by Gas Chromatography – Mass Spectrometry. *J Chromatogr A* **1998**, *809*, 131–139.
- (34) van der Schans, M. J. Laboratory Analysis of Chemical Warfare Agents, Adducts, and Metabolites in Biomedical Samples. *Handbook of Toxicology of Chemical Warfare Agents* **2020**, 969–981. <https://doi.org/10.1016/b978-0-12-819090-6.00056-8>.
- (35) Witkiewicz, Z.; Neffe, S. Chromatographic Analysis of Chemical Warfare Agents and Their Metabolites in Biological Samples. *TrAC - Trends in Analytical Chemistry* **2020**, *130*, 115960. <https://doi.org/10.1016/j.trac.2020.115960>.
- (36) Noort, D.; Schans, M. J.; Black, R. M. Methods for Retrospective Detection of Exposure to Toxic Scheduled Chemicals. Part B: Mass Spectrometric and Immunochemical Analysis of Covalent Adducts to Proteins and DNA. *Encyclopedia of Analytical Chemistry* **2020**, 1–21. <https://doi.org/10.1002/9780470027318.a9029.pub2>.
- (37) McGuire, J. M.; Taylor, J. T.; Byers, C. E.; Jakubowski, E. M.; Thomson, S. A. Determination of VX-G Analogue in Red Blood Cells via Gas Chromatography-Tandem Mass Spectrometry Following an Accidental Exposure to VX. *J Anal Toxicol* **2008**, *32*. <https://doi.org/10.1093/jat/32.1.73>.
- (38) Fu, F.; Gao, R.; Zhang, R.; Zhao, P.; Lu, X.; Li, L.; Wang, H.; Pei, C. Verification of Soman-Related Nerve Agents via Detection of Phosphonylated Adducts from Rabbit Albumin in Vitro and in Vivo. *Arch Toxicol* **2019**, *93*, 1853–1863. <https://doi.org/10.1007/s00204-019-02485-8>.
- (39) John, H.; Thiermann, H. Poisoning by Organophosphorus Nerve Agents and Pesticides: An Overview of the Principle Strategies and Current Progress of Mass Spectrometry-Based Procedures for Verification. *Journal of Mass Spectrometry and Advances in the Clinical Lab* **2021**, *19*, 20–31. <https://doi.org/10.1016/j.jmsacl.2021.01.002>.
- (40) Schmidt, C.; Breyer, F.; Blum, M. M.; Thiermann, H.; Worek, F.; John, H. V-Type Nerve Agents Phosphonylate Ubiquitin at Biologically Relevant Lysine Residues and Induce Intramolecular Cyclization



Chapter 1

- by an Isopeptide Bond. *Anal Bioanal Chem* **2014**, *406*, 5171–5185. <https://doi.org/10.1007/s00216-014-7706-y>.
- (41) Tsuchihashi, H.; Katagi, M.; Nishikawa, M.; Tatsuno, M. Identification of Metabolites of Nerve Agent VX in Serum Collected from a Victim. *J Anal Toxicol* **1998**, *22*, 383–388. <https://doi.org/10.1093/jat/22.5.383>.
- (42) Noort, D.; Benschop, H. P.; Black, R. M. Biomonitoring of Exposure to Chemical Warfare Agents: A Review. *Toxicol Appl Pharmacol* **2002**, *184* (2), 116–126. <https://doi.org/10.1006/taap.2002.9449>.
- (43) Røen, B. T.; Sellevag, S. R.; Lundanes, E. Quantification of Nerve Agent Biomarkers in Human Serum and Urine. *Anal Chem* **2014**, *86* (23), 11833–11840. <https://doi.org/10.1021/ac503408x>.
- (44) Nair, A.; Yadav, P.; Behl, A.; Sharma, R. K.; Kulshrestha, S.; Butola, B. S.; Sharma, N. Toxic Blister Agents: Chemistry, Mode of Their Action and Effective Treatment Strategies. *Chemico-Biological Interactions*. Elsevier Ireland Ltd December 1, 2021, p 109654. <https://doi.org/10.1016/j.cbi.2021.109654>.
- (45) Timperley, C. M.; Forman, J. E.; Abdollahi, M.; Al-Amri, A. S.; Baulig, A.; Benachour, D.; Borrett, V.; Cariño, F. A.; Curty, C.; Geist, M.; Gonzalez, D.; Kane, W.; Kovarik, Z.; Martínez-Álvarez, R.; Mourão, N. M. F.; Neffe, S.; Raza, S. K.; Rubaylo, V.; Suárez, A. G.; Takeuchi, K.; Tang, C.; Trifirò, F.; van Straten, F. M.; Vanninen, P. S.; Vučinić, S.; Zaitsev, V.; Zafar-Uz-Zaman, M.; Zina, M. S.; Holen, S.; Alwan, W. S.; Suri, V.; Hotchkiss, P. J.; Ghanei, M. Advice on Assistance and Protection Provided by the Scientific Advisory Board of the Organisation for the Prohibition of Chemical Weapons: Part 3. On Medical Care and Treatment of Injuries from Sulfur Mustard. *Toxicology*. Elsevier Ireland Ltd November 1, 2021, p 152967. <https://doi.org/10.1016/j.tox.2021.152967>.
- (46) Kehe, K.; Thiermann, H.; Balszuweit, F.; Eyer, F.; Steinritz, D.; Zilker, T. Acute Effects of Sulfur Mustard Injury-Munich Experiences. *Toxicology* **2009**, *263* (1), 3–8. <https://doi.org/10.1016/j.tox.2009.04.060>.
- (47) Rice, P. Sulphur Mustard. *Medicine* **2007**, *35* (10), 578–579. <https://doi.org/https://doi.org/10.1016/j.mpmed.2007.07.009>.
- (48) Rowell, M.; Kehe, K.; Balszuweit, F.; Thiermann, H. The Chronic Effects of Sulfur Mustard Exposure. *Toxicology* **2009**, *263* (1), 9–11. <https://doi.org/10.1016/j.tox.2009.05.015>.
- (49) Mousavi, B.; Khateri, S.; Soroush, M.; Ganjparvar, Z. Sulfur Mustard Exposure and Mental Health in Survivors of Iran-Iraq War with Severe Lung Injuries. *Toxin Rev* **2017**, *36* (4), 265–269. <https://doi.org/10.1080/15569543.2017.1303779>.
- (50) Popiel, S.; Sankowska, M. Determination of Chemical Warfare Agents and Related Compounds in Environmental Samples by Solid-Phase Microextraction with Gas Chromatography. *J Chromatogr A* **2011**, *1218* (47), 8457–8479. <https://doi.org/10.1016/j.chroma.2011.09.066>.
- (51) Terzic, O.; Gregg, H.; Voogt, P. De. Identification of Chemicals Relevant to the Chemical Weapons Convention Using the Novel Sample-Preparation Methods and Strategies of the Mobile Laboratory of the Organization for the Prohibition of Chemical Weapons. *Trends in Analytical Chemistry* **2015**, *65*, 151–166. <https://doi.org/10.1016/j.trac.2014.10.012>.
- (52) Black, R. M.; Clarke, R. J.; Cooper, D. B.; Read, R. W.; Utley, D. Application of Headspace Analysis, Solvent Extraction, Thermal Desorption and Gas Chromatography—Mass Spectrometry to the Analysis of Chemical Warfare Samples Containing Sulphur Mustard and Related Compounds. *J Chromatogr A* **1993**, *637* (1), 71–80. [https://doi.org/https://doi.org/10.1016/0021-9673\(93\)83100-7](https://doi.org/https://doi.org/10.1016/0021-9673(93)83100-7).
- (53) D'Agostino, P. A.; Provost, L. R. Capillary Column Electron Impact and Ammonia Chemical Ionization Gas Chromatographic-Mass Spectrometric and Gas Chromatographic-Tandem Mass Spectrometric Analysis of Mustard Hydrolysis Products. *Journal of Chromatography A* **1993**, *645* (2), 283–292. [https://doi.org/https://doi.org/10.1016/0021-9673\(93\)83388-9](https://doi.org/https://doi.org/10.1016/0021-9673(93)83388-9).
- (54) Brevett, C. A. S.; Sumpter, K. B.; Wagner, G. W.; Rice, J. S. Degradation of the Blister Agent Sulfur Mustard, Bis(2-Chloroethyl) Sulfide, on Concrete. *J Hazard Mater* **2007**, *140* (1–2), 353–360. <https://doi.org/10.1016/j.jhazmat.2006.09.067>.
- (55) Mizrahi, D. M.; Goldvaser, M.; Columbus, I. Long-Term Evaluation of the Fate of Sulfur Mustard on Dry and Humid Soils, Asphalt, and Concrete. *Environ Sci Technol* **2011**, *45* (8), 3466–3472. <https://doi.org/10.1021/es200023m>.

- (56) Wils, E. R. J.; Hulst, A. G.; de Jong, A. L. Determination of Mustard Gas and Related Vesicants in Rubber and Paint by Gas Chromatography—Mass Spectrometry. *J Chromatogr A* **1992**, *625* (2), 382–386. [https://doi.org/https://doi.org/10.1016/0021-9673\(92\)85226-J](https://doi.org/https://doi.org/10.1016/0021-9673(92)85226-J).
- (57) Mesilaakso, M.; Tolppa, E.-L. Detection of Trace Amounts of Chemical Warfare Agents and Related Compounds in Rubber, Paint, and Soil Samples by ^1H and ^{31}P (^1H) NMR Spectroscopy. *Anal Chem* **1996**, *68*, 2313–2318. <https://doi.org/https://doi.org/10.1021/ac960085f>.
- (58) Vanninen, P. *Recommended Operating Procedures for Analysis in the Verification of Chemical Disarmament*; University of Helsinki, 2023.
- (59) Munro, N. B.; Talmage, S. S.; Griffin, G. D.; Waters, L. C.; Watson, A. P.; King, J. F.; Hauschild, V. The Sources, Fate, and Toxicity of Chemical Warfare Agent Degradation Products. *Environ Health Perspectives* **1999**, *107* (12), 933–974. <https://doi.org/https://doi.org/10.1289/ehp.99107933>.
- (60) Bell, E. V.; Bennett, G. M.; Hock, A. L. The Decomposition of Some Halogenated Sulphides, and the Nature of the “Polymeric” Ethylene Sulphides. *Journal of Chemical Society* **1927**, *2*, 1803–1809.
- (61) Ashmore, M. H.; Nathanail, C. P. A Critical Evaluation of the Implications for Risk Based Land Management of the Environmental Chemistry of Sulphur Mustard. *Environment International*. Elsevier Ltd 2008, pp 1192–1203. <https://doi.org/10.1016/j.envint.2008.03.012>.
- (62) Noort, D.; Verheij, E. R.; Hulst, A. G.; De Jong, L. P. A.; Benschop, H. P. Characterization of Sulfur Mustard Induced Structural Modifications in Human Hemoglobin by Liquid Chromatography-Tandem Mass Spectrometry. *Chem Res Toxicol* **1996**, *9* (4), 781–787. <https://doi.org/https://doi.org.proxy.uba.uva.nl/10.1021/tx9502148>.
- (63) Steinritz, D.; Striepling, E.; Rudolf, K. D.; Schröder-Kraft, C.; Püschel, K.; Hullard-Pulstinger, A.; Koller, M.; Thiermann, H.; Gandor, F.; Gawlik, M.; John, H. Medical Documentation, Bioanalytical Evidence of an Accidental Human Exposure to Sulfur Mustard and General Therapy Recommendations. *Toxicol Lett* **2016**, *244*, 112–120. <https://doi.org/10.1016/j.toxlet.2015.08.1105>.
- (64) Capacio, B. R.; Smith, J. R.; Delion, M. T.; Anderson, D. R.; Graham, J. S.; Platoff, G. E.; Korte, W. D. Monitoring Sulfur Mustard Exposure by Gas Chromatography-Mass Spectrometry Analysis of Thiodiglycol Cleaved from Blood Proteins. *J Anal Toxicol* **2004**, *28* (5), 306–310. <https://doi.org/https://doi.org/10.1093/jat/28.5.306>.
- (65) Noort, D.; Hulst, A. G.; De Jong, L. P. A.; Benschop, H. P. Alkylation of Human Serum Albumin by Sulfur Mustard in Vitro and in Vivo: Mass Spectrometric Analysis of a Cysteine Adduct as a Sensitive Biomarker of Exposure. *Chem Res Toxicol* **1999**, *12* (8), 715–721. <https://doi.org/10.1021/tx9900369>.
- (66) Chen, B.; Ren, Z.; Zhang, T.; Yu, H.; Shu, Z. Bin; Liu, C.; Yang, Y.; Xu, P.; Liu, S. Simultaneous Quantification of Multiple Amino Acid Adducts from Sulfur Mustard-Modified Human Serum Albumin in Plasma at Trace Exposure Levels by Ultra-High Performance Liquid Chromatography—Triple Quadrupole Mass Spectrometry after Propionyl Derivatization. *J Chromatogr A* **2022**, *1678*, 463354. <https://doi.org/10.1016/j.chroma.2022.463354>.
- (67) Chen, B.; Zhang, Q.; Ren, Z.; Zhang, T.; Yu, H.; Liu, C.; Yang, Y.; Xu, P.; Liu, S. A Proteomics Strategy for the Identification of Multiple Sites in Sulfur Mustard-Modified HSA and Screening Potential Biomarkers for Retrospective Analysis of Exposed Human Plasma. *Anal Bioanal Chem* **2022**, *414*, 4179–4188. <https://doi.org/10.1007/s00216-022-04070-y>.
- (68) Benschop, H. P.; Van Der Schans, G. P.; Noort, D.; Fidder, A.; Mars-Groenendijk, R. H.; De Jong, L. P. A. Verification of Exposure to Sulfur Mustard in Two Casualties of the Iran-Iraq Conflict. *J Anal Toxicol* **1997**, *21*, 249–251. <https://doi.org/https://doi.org/10.1093/jat/21.4.249>.
- (69) John, H.; Koller, M.; Worek, F.; Thiermann, H.; Siegert, M. Forensic Evidence of Sulfur Mustard Exposure in Real Cases of Human Poisoning by Detection of Diverse Albumin-Derived Protein Adducts. *Arch Toxicol* **2019**, *93* (7), 1881–1891. <https://doi.org/10.1007/s00204-019-02461-2>.
- (70) Armenian, P.; Vo, K. T.; Barr-Walker, J.; Lynch, K. L. Fentanyl, Fentanyl Analogs and Novel Synthetic Opioids: A Comprehensive Review. *Neuropharmacology* **2018**, *134*, 121–132. <https://doi.org/10.1016/j.neuropharm.2017.10.016>.
- (71) OPCW. *Understanding Regarding the Aerosolised use of Central Nervous System-Acting Chemicals for Law Enforcement Purposes*.



Chapter 1

- <https://www.opcw.org/sites/default/files/documents/2021/12/c26dec10%28e%29.pdf> (accessed 2024-01-06).
- (72) Suzuki, J.; El-Haddad, S. A Review: Fentanyl and Non-Pharmaceutical Fentanyls. *Drug Alcohol Depend* **2017**, *171*, 107–116. <https://doi.org/10.1016/j.drugalcdep.2016.11.033>.
- (73) Frisoni, P.; Bacchio, E.; Bilel, S.; Talarico, A.; Gaudio, R. M.; Barbieri, M.; Neri, M.; Marti, M. Novel Synthetic Opioids: The Pathologist's Point of View. *Brain Sci* **2018**, *8* (9), 1–17. <https://doi.org/10.3390/brainsci8090170>.
- (74) Chiu, S. K.; Hornsby-Myers, J. L.; de Perio, M. A.; Shawder, J. E.; Wiegand, D. M.; Trout, D.; Howard, J. Health Effects from Unintentional Occupational Exposure to Opioids among Law Enforcement Officers: Two Case Investigations. *Am J Ind Med* **2019**, *62*, 439–447. <https://doi.org/10.1002/ajim.22967>.
- (75) Attaway, P. R.; Smiley-McDonald, H. M.; Davidson, P. J.; Kral, A. H. Perceived Occupational Risk of Fentanyl Exposure among Law Enforcement. *International Journal of Drug Policy* **2021**, *95*, 103303. <https://doi.org/10.1016/j.drugpo.2021.103303>.
- (76) Crocombe, R. A.; Giuntini, G.; Schiering, D. W.; Profeta, L. T. M.; Hargreaves, M. D.; Leary, P. E.; Brown, C. D.; Chmura, J. W. Field-Portable Detection of Fentanyl and Its Analogs: A Review. *J Forensic Sci* **2023**, *68*, 1570–1600. <https://doi.org/10.1111/1556-4029.15355>.
- (77) Abonamah, J. V.; Eckernrode, B. A.; Moini, M. On-Site Detection of Fentanyl and Its Derivatives by Field Portable Nano-Liquid Chromatography-Electron Ionization-Mass Spectrometry (NLC-EI-MS). *Forensic Chemistry* **2019**, *16*. <https://doi.org/10.1016/j.forc.2019.100180>.
- (78) Xega, R.; King, B. E.; Henderson, V.; Minyard, M. *Environmental Fate of Fentanyl in Soil and Relevant Waters*; Aberdeen Proving Ground, MD, 2020.
- (79) Valdez, C. A.; Rosales, J. A.; Vu, A. K.; Leif, R. N. Detection and Confirmation of Fentanyls in High Clay-Content Soil by Electron Ionization Gas Chromatography-Mass Spectrometry. *Journal of Forensic Sciences*. John Wiley and Sons Inc November 1, 2023, pp 2138–2152. <https://doi.org/10.1111/1556-4029.15354>.
- (80) Nishikawa, R. K.; Bell, S. C.; Kraner, J. C.; Callery, P. S. Potential Biomarkers of Smoked Fentanyl Utilizing Pyrolysis Gas Chromatography–Mass Spectrometry. *J Anal Toxicol* **2009**, *33*, 418–422. <https://doi.org/10.1093/jat/33.8.418>.
- (81) Fulton, A. C.; Forte, L.; Vaughan, S. R.; Holness, H. K.; Furton, K. G.; DeGreeff, L. E. Investigation of Volatile Organic Compounds from Trace Fentanyl Powder via Passive Degradation. *Forensic Chemistry* **2022**, *31*, 100456. <https://doi.org/10.1016/j.forc.2022.100456>.
- (82) Qi, L.; Cheng, Z.; Zuo, G.; Li, S.; Fan, Q. Oxidative Degradation of Fentanyl in Aqueous Solutions of Peroxides and Hypochlorites. *Def Sci J* **2011**, *61* (1), 30–35. <https://doi.org/10.14429/dsj.61.68>.
- (83) Tateishi, T.; Wood, A. J. J.; Guengerich, F. P.; Wood, M. Biotransformation of Tritiated Fentanyl in Human Liver Microsomes. Monitoring Metabolism Using Phenylacetic Acid and 2-Phenylethanol. *Biochem Pharmacol* **1995**, *50*, 1921–1924. [https://doi.org/10.1016/0006-2952\(95\)02088-8](https://doi.org/10.1016/0006-2952(95)02088-8).
- (84) Feierman, E.; Lasker, M. Metabolism of Fentanyl, a Synthetic Opioid Analgesic, by Human Liver Microsomes. *Drug metabolism and disposition* **1996**, *24* (9), 932–939.
- (85) Bird, H. E.; Huhn, A. S.; Dunn, K. E. Fentanyl Absorption, Distribution, Metabolism, and Excretion: Narrative Review and Clinical Significance Related to Illicitly Manufactured Fentanyl. *Journal of Addiction Medicine*. Lippincott Williams and Wilkins September 1, 2023, pp 503–508. <https://doi.org/10.1097/ADM.0000000000001185>.
- (86) Andresen, H.; Gullans, A.; Veselinovic, M.; Anders, S.; Schmoldt, A.; Iwersen-Bergmann, S.; Mueller, A. Fentanyl: Toxic or Therapeutic? Postmortem and Antemortem Blood Concentrations after Transdermal Fentanyl Application. *J Anal Toxicol* **2012**, *36*, 182–194. <https://doi.org/10.1093/jat/bks005>.
- (87) Salomone, A.; Palamar, J. J.; Bigiarini, R.; Gerace, E.; Corcia, D. Di; Vincenti, M. Detection of Fentanyl Analogs and Synthetic Opioids in Real Hair Samples. *J Anal Toxicol* **2019**, *43*, 259–265. <https://doi.org/10.1093/jat/bky093>.
- (88) Sciencelab. *MSDS - Allyl Alcohol*; Houston, Texas, 2017.
- (89) Sciencelab.com. *MSDS - Sodium Cyanide*; Houston, Texas, 2005.
- (90) Sciencelab.com. *MSDS - Hydrazine*; Houston, Texas, 2017.

- (91) National Research Council (US) Committee on Toxicology. *Review of Acute Human-Toxicity Estimates for Selected Chemical-Warfare Agents*; National Academies Press: Washington (DC), 1997. <https://doi.org/10.17226/5825>.
- (92) Abdalla, O. A. E.; Suliman, F. O.; Al-Ajmi, H.; Al-Hosni, T.; Rollinson, H. Cyanide from Gold Mining and Its Effect on Groundwater in Arid Areas, Yanqul Mine of Oman. *Environ Earth Sci* **2010**, *60*, 885–892. <https://doi.org/10.1007/s12665-009-0225-z>.
- (93) Logue, B. A.; Hinkens, D. M.; Baskin, S. I.; Rockwood, G. A. The Analysis of Cyanide and Its Breakdown Products in Biological Samples. *Crit Rev Anal Chem* **2010**, *40*, 122–147. <https://doi.org/10.1080/10408340903535315>.
- (94) Ikegaya, H.; Iwase, H.; Hatanaka, K.; Sakurada, K.; Yoshida, K.-I.; Takatori, T. Diagnosis of Cyanide Intoxication by Measurement of Cytochrome c Oxidase Activity. *Toxicol Lett* **2001**, *119*, 117–123. [https://doi.org/https://doi.org/10.1016/S0378-4274\(00\)00297-6](https://doi.org/https://doi.org/10.1016/S0378-4274(00)00297-6).
- (95) Toennes, S. W.; Schmidt, K.; Fandino, A. S.; Kauert, G. F. A Fatal Human Intoxication with the Herbicide Allyl Alcohol (2-Propen-1-Ol). *J Anal Toxicol* **2002**, *26* (1), 55–57. <https://doi.org/https://doi.org/10.1093/jat/26.1.55>.
- (96) Auerbach, S. S.; Mahler, J.; Travlos, G. S.; Irwin, R. D. A Comparative 90-Day Toxicity Study of Allyl Acetate, Allyl Alcohol and Acrolein. *Toxicology* **2008**, *253* (1–3), 79–88. <https://doi.org/10.1016/j.tox.2008.08.014>.
- (97) Kenessov, B. N.; Koziel, J. A.; Grotenhuis, T.; Carlsen, L. Screening of Transformation Products in Soils Contaminated with Unsymmetrical Dimethylhydrazine Using Headspace SPME and GC-MS. *Anal Chim Acta* **2010**, *674* (1), 32–39. <https://doi.org/10.1016/j.aca.2010.05.040>.
- (98) Santonen, T.; Kromhout, H.; Rietjens, I.; Tongeren, M. Van; Papameletiou, D.; Klein, C. L. *SCOEL/REC/164 Hydrazine*; Brussel, 2016.
- (99) Bolland, M. E.; Keun, H. C.; Beckonert, O.; Ebbels, T. M. D.; Antti, H.; Nicholls, A. W.; Shockcor, J. P.; Cantor, G. H.; Stevens, G.; Lindon, J. C.; Holmes, E.; Nicholson, J. K. Comparative Metabonomics of Differential Hydrazine Toxicity in the Rat and Mouse. *Toxicol Appl Pharmacol* **2005**, *204* (2), 135–151. <https://doi.org/10.1016/j.taap.2004.06.031>.
- (100) Voßnacker, P.; Wüst, A.; Keilhack, T.; Müller, C.; Steinhauer, S.; Beckers, H.; Yogendra, S.; Schiesser, Y.; Weber, R.; Reimann, M.; Müller, R.; Kaupp, M.; Riedel, S. Novel Synthetic Pathway for the Production of Phosgene. *Sci Adv* **2021**, *7*, 5186–5215. <https://doi.org/10.1126/sciadv.abj5186>.
- (101) Lu, Q.; Huang, S.; Meng, X.; Zhang, J.; Yu, S.; Li, J.; Shi, M.; Fan, H.; Zhao, Y. Mechanism of Phosgene-Induced Acute Lung Injury and Treatment Strategy. *International Journal of Molecular Sciences*. MDPI October 1, 2021, p 10933. <https://doi.org/10.3390/ijms222010933>.
- (102) Hardison, L. S.; Wright, E.; Pizon, A. F. Phosgene Exposure: A Case of Accidental Industrial Exposure. *Journal of Medical Toxicology* **2014**, *10*, 51–56. <https://doi.org/10.1007/s13181-013-0319-6>.
- (103) Onyutha, C.; Kwio-Tamale, J. C. Modelling Chlorine Residuals in Drinking Water: A Review. *International Journal of Environmental Science and Technology*. Institute for Ionics November 1, 2022, pp 11613–11630. <https://doi.org/10.1007/s13762-022-03924-3>.
- (104) The Chlorine Institute. *Chlorine*. <https://www.chlorineinstitute.org/chlorine> (accessed 2024-01-17).
- (105) Evans, R. B. Chlorine: State of the Art. *Lung* **2005**, *183* (3), 151–167. <https://doi.org/10.1007/s00408-004-2530-3>.
- (106) Achanta, S.; Jordt, S. E. Toxic Effects of Chlorine Gas and Potential Treatments: A Literature Review. *Toxicol Mech Methods* **2019**, *31* (4), 244–256. <https://doi.org/10.1080/15376516.2019.1669244>.
- (107) Govier, P.; Coulson, J. M. Civilian Exposure to Chlorine Gas: A Systematic Review. *Toxicol Lett* **2018**, *293*, 249–252. <https://doi.org/10.1016/j.toxlet.2018.01.014>.
- (108) Hamzah, N.; Höjer Holmgren, K.; Åstot, C.; van der Schans, M. J.; de Reuver, L.; Vanninen, P. Chlorinated Organic Compounds in Concrete as Specific Markers for Chlorine Gas Exposure. *J Hazard Mater* **2023**, *459*. <https://doi.org/10.1016/j.jhazmat.2023.132332>.
- (109) OPCW. *Third Report by the OPCW Investigation and Identification Team Pursuant to Paragraph 10 of Decision C-SS-4/DEC.3 “Addressing the Threat from Chemical Weapons Use” Douma (Syrian Arab Republic) – 7 APRIL 2018*. <https://www.opcw.org/sites/default/files/documents/2023/01/s-2125-2023%28e%29.pdf> (accessed 2023-04-28).



Chapter 1

- (110) Michałowicz, J.; Stufka-Olczyk, J.; Milczarek, A.; Michniewicz, M. Analysis of Annual Fluctuations in the Content of Phenol, Chlorophenols and Their Derivatives in Chlorinated Drinking Waters. *Environmental Science and Pollution Research* **2011**, *18*, 1174–1183. <https://doi.org/10.1007/s11356-011-0469-5>.
- (111) Hearn, J.; Eichler, J.; Hare, C.; Henley, M. Effect of Soil Moisture on Chlorine Deposition. *J Hazard Mater* **2014**, *267*, 81–87. <https://doi.org/10.1016/j.jhazmat.2013.12.044>.
- (112) Sochaski, M. A.; Jarabek, A. M.; Murphy, J.; Andersen, M. E. 3-Chlorotyrosine and 3,5-Dichlorotyrosine as Biomarkers of Respiratory Tract Exposure to Chlorine Gas. *J Anal Toxicol* **2008**, *32*, 99–105. <https://doi.org/10.1093/jat/32.1.99>.
- (113) Nishio, T.; Toukairin, Y.; Hoshi, T.; Arai, T.; Nogami, M. Determination of 3-Chloro-L-Tyrosine as a Novel Indicator of Chlorine Poisoning Utilizing Gas Chromatography-Mass Spectrometric Analysis. *Leg Med* **2020**, *47*, 101782. <https://doi.org/10.1016/j.legalmed.2020.101782>.
- (114) Nishio, T.; Toukairin, Y.; Hoshi, T.; Arai, T.; Nogami, M. Development of an LC–MS/MS Method for Quantification of 3-Chloro-L-Tyrosine as a Candidate Marker of Chlorine Poisoning. *Leg Med* **2021**, *53*, 101939. <https://doi.org/10.1016/j.legalmed.2021.101939>.
- (115) Ford, D. A.; Honavar, J.; Albert, C. J.; Duerr, M. A.; Oh, J. Y.; Doran, S.; Matalon, S.; Patel, R. P. Formation of Chlorinated Lipids Post-Chlorine Gas Exposure. *J Lipid Res* **2016**, *57*, 1529–1540. <https://doi.org/10.1194/jlr.M069005>.
- (116) Hemström, P.; Larsson, A.; Elfmark, L.; Åstot, C. L - α -Phosphatidylglycerol Chlorohydrins as Potential Biomarkers for Chlorine Gas Exposure. *Anal Chem* **2016**, *88* (20), 9972–9979. <https://doi.org/10.1021/acs.analchem.6b01896>.
- (117) Lindén, P.; Jonasson, S.; Hemström, P.; Ålander, L.; Larsson, A.; Ågren, L.; Elfmark, L.; Åstot, C. Nasal Lavage Fluid as a Biomedical Sample for Verification of Chlorine Exposure. *J Anal Toxicol* **2022**, *46*, 559–566. <https://doi.org/10.1093/jat/bkab069>.
- (118) Hemström, P.; Jugg, B.; Watkins, R.; Jonasson, S.; Elfmark, L.; Rutter, S.; Åstot, C.; Lindén, P. Phospholipid Chlorohydrins as Chlorine Exposure Biomarkers in a Large Animal Model. *Toxicol Lett* **2024**, *391*, 32–38. <https://doi.org/10.1016/j.toxlet.2023.11.008>.
- (119) Elfmark, L.; Ågren, L.; Akfur, C.; Bucht, A.; Jonasson, S. 8-Isoprostone Is an Early Biomarker for Oxidative Stress in Chlorine-Induced Acute Lung Injury. *Toxicol Lett* **2018**, *282*, 1–7. <https://doi.org/10.1016/j.toxlet.2017.10.007>.
- (120) Toprak, S.; Kahriman, F.; Dogan, Z.; Gokhan Ersoy; Can, E. Y.; Akpolat, M.; Can, M. The Potential of Raman and FT-IR Spectroscopic Methods for the Detection of Chlorine in Human Nail Samples. *Forensic Sci Med Pathol* **2020**, *16*, 633–640. <https://doi.org/10.1007/s12024-020-00313-5/Published>.
- (121) Pantazides, B. G.; Crow, B. S.; Quiñones-González, J.; Perez, J. W.; Harvilchuck, J. A.; Wallery, J. J.; Hu, T. C.; Thomas, J. D.; Johnson, R. C.; Blake, T. A. Development of a Clinical Assay to Measure Chlorinated Tyrosine in Hair and Tissue Samples Using a Mouse Chlorine Inhalation Exposure Model. *Anal Bioanal Chem* **2021**, *413* (6), 1765–1776. <https://doi.org/10.1007/s00216-020-03146-x>.
- (122) Martz, S. V.; Wittwer, M.; Tan-Lin, C. W.; Bochet, C. G.; Brackmann, M.; Curty, C. Influence of Chlorinating Agents on the Formation of Stable Biomarkers in Hair for the Retrospective Verification of Exposure. *Anal Chem* **2022**, *94*, 16579–16586. <https://doi.org/10.1021/acs.analchem.2c01867>.
- (123) OPCW Technical Secretariat. *Work Instruction for the Reporting of the Results of the OPCW Biomedical Proficiency Tests*; 2021.
- (124) Kumar, S.; Bogusz, M. J. Hyphenated Techniques in Liquid Chromatography and Their Applications in Forensic Toxicology: A Review. *Journal of Forensic Science and Medicine*. Wolters Kluwer Medknow Publications October 1, 2021, pp 123–136. https://doi.org/10.4103/jfsm.jfsm_65_21.
- (125) Guo, Z.; Huang, S.; Wang, J.; Feng, Y. L. Recent Advances in Non-Targeted Screening Analysis Using Liquid Chromatography - High Resolution Mass Spectrometry to Explore New Biomarkers for Human Exposure. *Talanta*. Elsevier B.V. November 1, 2020, p 121339. <https://doi.org/10.1016/j.talanta.2020.121339>.
- (126) Lu, X.; Zhu, X.; Gao, R.; Tang, H.; Pei, C.; Wang, H.; Xiao, J. Chemometrics-Assisted Analysis of Chemical Impurity Profiles of Tabun Nerve Agent Using Comprehensive Two-Dimensional Gas Chromatography-Time-of-Flight Mass Spectrometry. *J Chromatogr A* **2022**, *1685*, 463643. <https://doi.org/10.1016/j.chroma.2022.463643>.

- (127) Fraga, C. G.; Pérez Acosta, G. A.; Crenshaw, M. D.; Wallace, K.; Mong, G. M.; Colburn, H. A. Impurity Profiling to Match a Nerve Agent to Its Precursor Source for Chemical Forensics Applications. *Anal Chem* **2011**, *83* (24), 9564–9572. <https://doi.org/10.1021/ac202340u>.
- (128) Lindberg, S.; Engqvist, M.; Mörén, L.; Åstot, C.; Norlin, R. Source Attribution of the Chemical Warfare Agent Soman Using Position-Specific Isotope Analysis by ^2H NMR Spectroscopy: From Precursor to Degradation Product. *Anal Chem* **2021**, *93*, 12230–12236. <https://doi.org/10.1021/acs.analchem.1c01271>.
- (129) Holmgren, K. H.; Valdez, C. A.; Magnusson, R.; Vu, A. K.; Lindberg, S.; Williams, A. M.; Alcaraz, A.; Åstot, C.; Hok, S.; Norlin, R. Part 1: Tracing Russian VX to Its Synthetic Routes by Multivariate Statistics of Chemical Attribution Signatures. *Talanta* **2018**, *186*, 586–596. <https://doi.org/10.1016/j.talanta.2018.02.104>.
- (130) Williams, A. M.; Vu, A. K.; Mayer, B. P.; Hok, S.; Valdez, C. A.; Alcaraz, A. Part 3: Solid Phase Extraction of Russian VX and Its Chemical Attribution Signatures in Food Matrices and Their Detection by GC-MS and LC-MS. *Talanta* **2018**, *186*, 607–614. <https://doi.org/10.1016/j.talanta.2018.03.044>.
- (131) Gravett, M. R.; Hopkins, F. B.; Self, A. J.; Webb, A. J.; Timperley, C. M.; Riches, J. R. Fate of the Chemical Warfare Agent O-Ethyl S-2-Diisopropylaminoethyl Methylphosphonothiolate (VX) on Soil Following Accelerant-Based Fire and Liquid Decontamination. *Anal Bioanal Chem* **2014**, *406*, 5121–5135. <https://doi.org/10.1007/s00216-014-7963-9>.
- (132) Ovenden, S. P. B.; Webster, R. L.; Micich, E.; McDowall, L. J.; McGill, N. W.; Williams, J.; Zanatta, S. D. The Identification of Chemical Attribution Signatures of Stored VX Nerve Agents Using NMR, GC-MS, and LC-HRMS. *Talanta* **2020**, *211* (January), 120753. <https://doi.org/10.1016/j.talanta.2020.120753>.
- (133) D'Agostino, P. A.; Provost, L. R.; Visentini, J. Analysis of O-Ethyl S-[2-(Diisopropylamino)Ethyl] Methylphosphonothiolate (VX) by Capillary Column Gas Chromatography-Mass Spectrometry. *J Chromatogr A* **1987**, *402*, 221–232. [https://doi.org/10.1016/0021-9673\(87\)80020-1](https://doi.org/10.1016/0021-9673(87)80020-1).
- (134) Fraga, C. G.; Clowers, B. H.; Moore, R. J.; Zink, E. M. Signature-Discovery Approach for Sample Matching of a Nerve-Agent Precursor Using Liquid Chromatography-Mass Spectrometry, XCMS, and Chemometrics. *Anal Chem* **2010**, *82* (10), 4165–4173. <https://doi.org/10.1021/ac1003568>.
- (135) Moran, J. J.; Fraga, C. G.; Nims, M. K. Stable-Carbon Isotope Ratios for Sourcing the Nerve-Agent Precursor Methylphosphonic Dichloride and Its Products. *Talanta* **2018**, *186*, 678–683. <https://doi.org/https://doi.org/10.1016/j.talanta.2018.04.021>.
- (136) Holmgren, K. H.; Hakulinen, H.; Norlin, R.; de Bruin-Hoegée, M.; Spiandore, M.; See, S. Q. S.; Webster, R.; Jacques, K. L.; Mauravaara, L.; Ang, L. H.; Evans, C. P.; Ovenden, S.; Noort, D.; Delaporte, G.; Dahlén, J.; Fraga, C. G.; Vanninen, P.; Åstot, C. Interlaboratory Comparison Study of a Chemical Profiling Method for Methylphosphonic Dichloride, a Nerve Agent Precursor. *Forensic Chemistry* **2023**, *33*, 100473. <https://doi.org/10.1016/j.forc.2023.100473>.
- (137) Meier, U. C. Forensic Analysis of the Deuterium/Hydrogen Isotopic Ratios of the Nerve Agent Sarin, Its Reaction by-Product Diisopropyl Methylphosphonate and Their Precursors by ^2H SNIF-NMR. *Talanta* **2023**, *253*, 123890. <https://doi.org/10.1016/j.talanta.2022.123890>.
- (138) Fraga, C. G.; Sego, L. H.; Hoggard, J. C.; Acosta, G. A. P.; Viglino, E. A.; Wahl, J. H.; Synovec, R. E. Preliminary Effects of Real-World Factors on the Recovery and Exploitation of Forensic Impurity Profiles of a Nerve-Agent Simulant from Office Media. *J Chromatogr A* **2012**, *1270*, 269–282. <https://doi.org/10.1016/j.chroma.2012.10.053>.
- (139) Hoggard, J. C.; Wahl, J. H.; Synovec, R. E.; Mong, G. M.; Fraga, C. G. Impurity Profiling of a Chemical Weapon Precursor for Possible Forensic Signatures by Comprehensive Two-Dimensional Gas Chromatography/Mass Spectrometry and Chemometrics. *Anal Chem* **2010**, *82* (2), 689–698. <https://doi.org/10.1021/ac902247x>.
- (140) Mo, K. F.; Heredia-Langner, A.; Fraga, C. G. Evaluating and Modeling the Effects of Surface Sampling Factors on the Recovery of Organic Chemical Attribution Signatures Using the Accelerated Diffusion Sampler and Solvent Extraction. *Talanta* **2017**, *164*, 92–99. <https://doi.org/10.1016/j.talanta.2016.11.016>.



Chapter 1

- (141) Wahl, J. H.; Colburn, H. A. Extraction of Chemical Impurities for Forensic Investigations : A Case Study for Indoor Releases of a Sarin Surrogate. *Build Environ* **2010**, *45* (5), 1339–1345. <https://doi.org/10.1016/j.buildenv.2009.10.020>.
- (142) Lu, X.; Zhang, Z.; Liu, H.; Tang, H.; Gao, R.; Pei, C.; Wang, H.; Xiao, J. Forensic Signatures of a Chemical Weapon Precursor DMPADC for Determination of a Synthetic Route. *Talanta* **2021**, *232* (April), 122476. <https://doi.org/10.1016/j.talanta.2021.122476>.
- (143) Strozier, E. D.; Mooney, D. D.; Friedenberg, D. A.; Klupinski, T. P.; Triplett, C. A. Use of Comprehensive Two-Dimensional Gas Chromatography with Time-of-Flight Mass Spectrometric Detection and Random Forest Pattern Recognition Techniques for Classifying Chemical Threat Agents and Detecting Chemical Attribution Signatures. *Anal Chem* **2016**, *88*, 7068–7075. <https://doi.org/10.1021/acs.analchem.6b00725>.
- (144) Central Intelligence Agency (CIA) United States Government. *Comprehensive Report of the Special Advisor to the DCI on Iraq's WMD*; 2004; Vol. III.
- (145) OPCW. *Report of the OPCW Fact-Finding Mission in Syria Regarding an Alleged Incident in Khan Shaykhun, Syrian Arab Republic April 2017*. https://www.opcw.org/sites/default/files/documents/Fact_Finding_Mission/s-1510-2017_e_.pdf (accessed 2023-02-06).
- (146) Black, R. M.; Clarke, R. J.; Read, R. W.; Reid, M. T. J. Application of Gas Chromatography-Mass Spectrometry and Gas Chromatography-Tandem Mass Spectrometry to the Analysis of Chemical Warfare Samples, Found to Contain Residues of the Nerve Agent Sarin, Sulphur Mustard and Their Degradation Products. *J Chromatogr A* **1994**, *662*, 301–321. [https://doi.org/10.1016/0021-9673\(94\)80518-0](https://doi.org/10.1016/0021-9673(94)80518-0).
- (147) Black, R. M.; Read, R. W. Application of Liquid Chromatography-Atmospheric Pressure Chemical Ionisation Mass Spectrometry, and Tandem Mass Spectrometry, to the Analysis and Identification of Degradation Products of Chemical Warfare Agents. *J Chromatogr A* **1997**, *759*, 79–92. [https://doi.org/10.1016/S0021-9673\(96\)00763-7](https://doi.org/10.1016/S0021-9673(96)00763-7).
- (148) Wärme, R.; Juhlin, L. A New Microscale Method for the Conversion of Phosphorus Oxyacids to Their Fluorinated Analogues, Using Cyanuric Fluoride in Solution and on Solid Support. *Phosphorus Sulfur Silicon Relat Elem* **2010**, *185* (12), 2402–2408. <https://doi.org/10.1080/10426501003671445>.
- (149) Norlin, R.; Lindberg, G. Synthesis of [¹⁴C] Sarin. *J Labelled Comp Radiopharm* **2003**, *46*, 599–604. <https://doi.org/10.1002/jlcr.699>.
- (150) Muller, A. J. The Use of Organosilicon Esters for the Synthesis of Alkyl Phosphonofluorides. *Journal of Organic Chemistry* **1988**, *53*, 3364–3365. <https://doi.org/10.1021/jo00249a046>.
- (151) Dabkowski, W.; Michalski, J.; Wasik, J.; Cramer, F. New General Synthesis of Organophosphorus P-F Compounds via Reaction of Azolides of Phosphorus Acids with Acyl Fluorides: Novel Route to 2-Deoxynucleosidyl Phosphonofluorides and Phosphorodifluorides. *J. Chem. Soc. Perkin Trans. 1* **1994**, 817–820. <https://doi.org/10.1039/P19940000817>.
- (152) OPCW. Annex on Chemicals Schedule 3. <https://www.opcw.org/chemical-weapons-convention/annexes/annex-chemicals/schedule-3> (accessed 2022-07-06).
- (153) OPCW. Annex on Chemical Schedule 2. <https://www.opcw.org/chemical-weapons-convention/annexes/annex-chemicals/schedule-2> (accessed 2022-07-06).
- (154) Hamzah, N.; Kjellberg, M.; Vanninen, P. Optimized Method for Analysis of Ethanolamines, Hydrolysis Products of Nitrogen Mustards, from Urine Samples Using LC-MS/MS. *Journal of Chromatography B* **2021**, *1176* (March), 122762. <https://doi.org/10.1016/j.jchromb.2021.122762>.
- (155) Blum, M. M.; Richter, A.; Siegert, M.; Thiermann, H.; John, H. Adduct of the Blistering Warfare Agent Sesquimustard with Human Serum Albumin and Its Mass Spectrometric Identification for Biomedical Verification of Exposure. *Anal Bioanal Chem* **2020**, *412* (28), 7723–7737. <https://doi.org/10.1007/s00216-020-02917-w>.
- (156) Timperley, C. M.; Black, R. M.; Bird, M.; Holden, I.; Mundy, J. L.; Read, R. W. Hydrolysis and Oxidation Products of the Chemical Warfare Agents 1,2-Bis[(2-Chloroethyl)Thio]Ethane Q and 2,2'-Bis(2-Chloroethylthio) Diethyl Ether T. *Phosphorus Sulfur Silicon Relat Elem* **2003**, *178* (9), 2027–2046. <https://doi.org/10.1080/10426500390228710>.

- (157) National Research Council. *Interim Design Assessment for the Blue Grass Chemical Agent Destruction Pilot Plant*; The National Academies Press: Washington DC, 2005. <https://doi.org/10.17226/11213>.
- (158) Hemme, M.; Fidder, A.; van der Riet-van Oeveren, D.; van der Schans, M. J.; Noort, D. Mass Spectrometric Analysis of Adducts of Sulfur Mustard Analogues to Human Plasma Proteins: Approach towards Chemical Provenancing in Biomedical Samples. *Anal Bioanal Chem* **2021**, *413* (15), 4023–4036. <https://doi.org/10.1007/s00216-021-03354-z>.
- (159) Organisation for the Prohibition of Chemical Weapons. *Article II Definitions and Criteria*. Chemical Weapons Convention. <https://doi.org/10.1093/analyis/22.5.109>.
- (160) Bezemer, K.; Woortmeijer, R.; Koeberg, M.; Schoenmakers, P.; van Asten, A. Multicomponent Characterization and Differentiation of Flash Bangers — Part I: Sample Collection and Visual Examination. *Forensic Sci Int* **2018**, *290*, 327–335. <https://doi.org/10.1016/j.forsciint.2018.06.011>.
- (161) OPCW. *First Report by the OPCW Investigation and Identification Team (IIT) Pursuant to Paragraph 10 of Decision C-SS-4/Dec.3 “Addressing the Threat From Chemical Weapons Use” Ltamenah (Syrian Arab Republic) 24, 25, and 30 March 2017*. <https://www.opcw.org/sites/default/files/documents/2020/04/s-1867-2020%28e%29.pdf> (accessed 2023-02-06).
- (162) OPCW. *Report Of The OPCW Fact-Finding Mission In Syria Regarding The Incidents Of The Alleged Use Of Chemicals As A Weapon In Marea, Syrian Arab Republic, On 1 And 3 September 2015*. <https://www.opcw.org/sites/default/files/documents/2022/01/s-2017-2022%2B%28e%29.pdf> (accessed 2022-11-30).
- (163) Bezemer, K.; Woortmeijer, R.; Koeberg, M.; Wiarda, W.; Schoenmakers, P.; van Asten, A. Multicomponent Characterization and Differentiation of Flash Bangers — Part II: Elemental Profiling of Plastic Caps. *Forensic Sci Int* **2018**, *290*, 336–348. <https://doi.org/10.1016/j.forsciint.2018.06.012>.
- (164) Almirall, J. R.; Trejos, T. Applications of LA-ICP-MS to Forensic Science. *Elements* **2016**, *12* (5), 335–340. <https://doi.org/10.2113/gselements.12.5.335>.
- (165) Deconinck, I.; Latkoczy, C.; Günther, D.; Govaert, F.; Vanhaecke, F. Capabilities of Laser Ablation - Inductively Coupled Plasma Mass Spectrometry for (Trace) Element Analysis of Car Paints for Forensic Purposes. *J Anal At Spectrom* **2006**, *21*, 279–287. <https://doi.org/10.1039/b514007b>.
- (166) Weis, P.; Dücker, M.; Watzke, P.; Menges, S.; Becker, S. Establishing a Match Criterion in Forensic Comparison Analysis of Float Glass Using Laser Ablation Inductively Coupled Plasma Mass Spectrometry. In *Journal of Analytical Atomic Spectrometry*; 2011; Vol. 26, pp 1273–1284. <https://doi.org/10.1039/c0ja00168f>.
- (167) van Asten, A. *Chemical Analysis for Forensic Evidence*, 1st ed.; Elsevier: Amsterdam, 2022.
- (168) Bolck, A.; Ni, H.; Lopatka, M. Evaluating Score-and Feature-Based Likelihood Ratio Models for Multivariate Continuous Data: Applied to Forensic MDMA Comparison. *Law, Probability and Risk* **2014**, *14* (3), 243–266. <https://doi.org/10.1093/lpr/mgv009>.
- (169) Brust, H.; Willemse, S.; Zeng, T.; van Asten, A.; Koeberg, M.; van der Heijden, A.; Bolck, A.; Schoenmakers, P. Impurity Profiling of Trinitrotoluene Using Vacuum-Outlet Gas Chromatography-Mass Spectrometry. *J Chromatogr A* **2014**, *1374*, 224–230. <https://doi.org/10.1016/j.chroma.2014.11.055>.



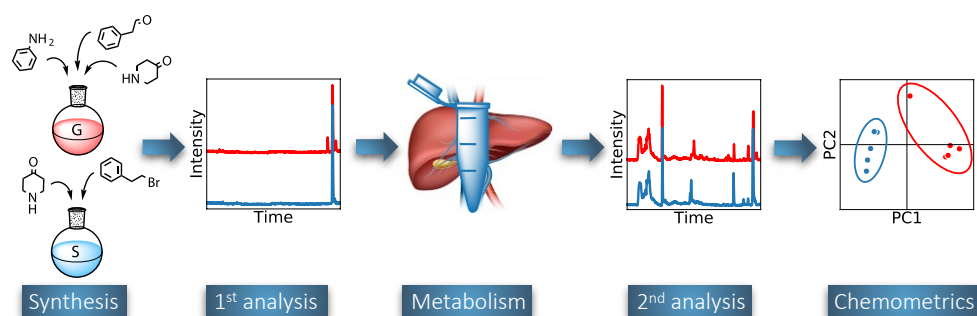
2

Chemical attribution of fentanyl: The effect of human metabolism

Mirjam de Bruin-Hoegée, Djarah Kleiweg, Daan Noort, Arian C. van Asten, Chemical attribution of fentanyl: The effect of human metabolism, *Forensic Chemistry* **2021**, 24, 100330.
DOI: [10.1016/j.forc.2021.100330](https://doi.org/10.1016/j.forc.2021.100330).

Abstract

Chemical attribution typically aims to establish a link between material found at a crime scene and a person, location or other evidence. In the field of illicit drugs, chemical attribution signatures are usually impurity profiles. Extending these to metabolized samples would create new possibilities in forensic investigations. The present study explores the effect of human metabolism on the impurity profile of fentanyl, as representative of synthetic opioids. Two different methods (Gupta and Siegfried) were used to synthesize fentanyl, after which the samples were incubated with liver microsomes to mimic human metabolism. The impurity profiles have been characterized with gas chromatography-mass spectrometry (GC-MS), gas chromatography with flame ionization detector (GC-FID), liquid chromatography quadrupole-time of flight mass spectrometry (LC-QTOF-MS) and liquid chromatography-high resolution tandem mass spectrometry (LC-HRMS/MS). It was found that GC-FID and LC-HRMS/MS can both be used to discriminate between the Gupta and Siegfried synthesis method. This holds both for the analyses performed before and after metabolism. In addition, principal component analysis (PCA) identified acetyl fentanyl as the most important marker compound. Associated detection limits are in the range of concentrations expected in case work. While acetyl fentanyl is not stable during metabolism, its discriminating potential is transferred to its metabolic product acetyl norfentanyl. In addition, the stable impurities phenylacetamide and 1-phenylethylpiperidin-4-ol were found to be significant classifiers. To implement the results in a forensic framework, linear discriminant analysis (LDA) was applied and used to establish likelihood ratios. To our knowledge, the present work demonstrates for the first time the possibility of chemical attribution of drugs through the analysis of metabolic trace levels in biological samples.



2.1. Introduction

An emerging category of chemical threat agents consists of the so-called pharmaceutical based agents (PBAs).¹ This includes the family of synthetic opioids like fentanyl, a compound which is estimated to be 50-100 times more potent than morphine.² Fentanyl has a lethal dose of only a few milligrams.³ Its analogues such as sufentanil and carfentanil are even more potent.⁴ Carfentanil was one of the components of the mixture of chemicals used to end the Moscow theater hostage crisis.⁵ Fentanyl is intended for analgesic use, but it is also illicitly used in pills or mixed with heroin or cocaine. The illicit use of fentanyl and its analogues has seen a rapid increase in the last decades, with a large outbreak starting in 2013 in the United States of America (USA) and Canada.⁶ In 2018, fentanyl and its analogues were the most common cause of overdose deaths in the USA.⁷ Its potency and wide availability make fentanyl attractive for misuse by criminals and terrorist groups. In this respect, chemical attribution typically aims to establish a link between material found at a crime scene and a person (usually a suspect), location or other evidence. Chemical attribution signatures, such as impurities, isotope ratios and other chemical or physical characteristics, are used to assess whether two different samples share a common origin. In the field of illicit drugs, chemical profiles are usually based on impurities related to production, processing and storage and are typically analyzed by analytical methods such as gas chromatography-mass spectrometry (GC-MS) and liquid chromatography-mass spectrometry (LC-MS).⁸ The potential of impurity profiling has been demonstrated for cannabis, heroin, cocaine, 3,4-methylenedioxymethamphetamine (MDMA), and amphetamine.⁹⁻¹³

It can be expected that the identity of the impurities heavily relies on the synthesis method applied. The first synthesis method of fentanyl was patented by Janssen and Gardocki in 1964.¹⁴ This method requires advanced skills in organic chemistry. Other methods, as developed by Siegfried¹⁵ and Gupta¹⁶ are more commonly used in clandestine laboratories.^{17,18} The Siegfried method is based on an internet recipe.¹⁵ The Gupta method is also referred to as 'One-Pot method', because the synthesis is carried out in a single reaction vessel.¹⁶ Compared to other illicit drugs, there is not much literature available on the chemical profiling of fentanyl. It is typically dosed at relatively low levels as additive to other psychoactive substances such as heroin. This makes chemical impurity profiling of fentanyl in case work samples very challenging. Lurie et al.¹⁹ developed a liquid chromatography-tandem mass spectrometry (LC-MS/MS) method to identify 40 preselected potential impurities of the Janssen or Siegfried synthesis method. Mayer et al.¹⁷ investigated chemical attribution signatures for the Siegfried, Valdez, and Gupta method and hybrid versions thereof. Multivariate statistical analysis was applied on the data obtained by GC-MS, liquid chromatography

quadrupole-time of flight mass spectrometry (LC-QTOF-MS) and induced coupled plasma-mass spectrometry (ICP-MS). Another study demonstrated the potential of direct-infusion electrospray ionization-mass spectrometry (ESI-MS) for profiling of fentanyl synthesized by the Siegfried method.²⁰ Most recently, Casale et al. used GC-MS and nuclear magnetic resonance (NMR) spectroscopy for the identification of three impurities characteristic to the Gupta synthesis method.²¹

After the (deliberate) release of a chemical threat agent, it is often difficult to find traces of the chemical that was used,^{22,23} either because of a lack of persistency, or due to the inability to enter the scene because of safety and security reasons. Under such circumstances the exposed people themselves might form a valuable source of information: biochemical indicators (biomarkers) of exposure can be found in human tissue for longer periods of time, depending on the nature of the chemical agent. Based on this concept a variety of methods have been developed over the last decades that allow retrospective analysis of signatures of chemical threat agents in biomedical samples, up to weeks after the actual exposure.²⁴ The general aim of the current study was to explore whether these two concepts, i.e. chemical profiling and retrospective biomarker analysis, could be combined into a novel concept of “chemical profiling in biomedical samples”. To this date, such studies have not yet been performed.

In the present study the effect of human metabolism on the impurity profile of fentanyl was investigated. Two different synthesis methods (Gupta and Siegfried) were used to synthesize small batches of fentanyl, which were subsequently analyzed in detail to assess their chemical profiles. The fentanyl samples were then incubated with human liver microsomes to mimic human metabolism. Oxidative N-dealkylation of fentanyl to norfentanyl is the predominant pathway in fentanyl metabolism,^{25,26} as illustrated in Figure 2.1. The other metabolic product phenylacetaldehyde can either be reduced to phenethyl alcohol or oxidized to phenylacetic acid. The impurity profiles (pre- and post-metabolism) were constructed with GC-MS, gas chromatography with flame ionization detection (GC-FID), liquid chromatography-quadrupole-time of flight mass spectrometry (LC-QTOF-MS) and LC-HRMS/MS. Multivariate data analysis was applied to the analytical data to identify potential marker compounds that indicate a specific fentanyl synthesis method. The current study demonstrates that analysis of biomedical samples for chemical provenance purposes might in principle form a valuable addition to the more classical chemical profiling approach based on analysis of bulk samples.

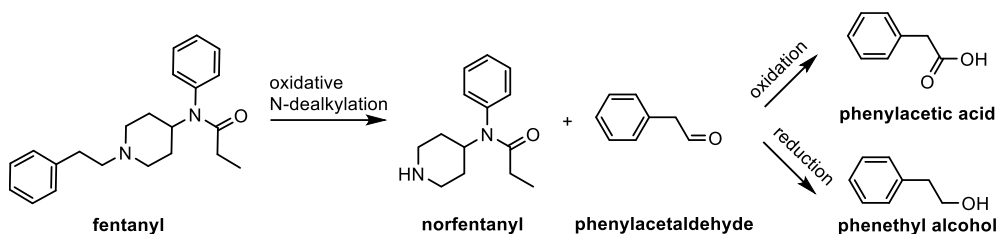


Figure 2.1. Reaction scheme of fentanyl metabolized to norfentanyl by oxidative N-dealkylation. Phenylacetaldehyde can either be reduced to phenethyl alcohol or oxidized to phenylacetic acid.

2.2. Materials and methods

2.2.1. Safety

Due to the extremely potent nature of fentanyl, samples and dilutions should be handled with care. Precautions were taken to prevent accidental exposure, including wearing gloves and eye protection. In case of exposure to opioids, the antidote naloxone could directly be administered to mitigate respiratory depression.

2.2.2. Chemicals

Fentanyl, benzylfentanyl and methyl 4-anilino-1-benzyl-4-piperidinecarboxylate were synthesized at TNO, Rijswijk. The chemicals used for the syntheses were obtained from Sigma Aldrich, except aniline which was obtained from Janssen Chimica. Norfentanyl (Sigma-Aldrich, ≥97%) and d₅-norfentanyl (Supelco, certified reference material) were used for the method optimization. The incubation protocol was optimized using fentanyl citrate (Spruyt Hillen). Pooled human liver microsomes (Sigma-Aldrich, CAS M0317, lot #SLCC0060 and lot #SLCC7022 and Xenotech, CAS H0610, lot #1610016) were used for the incubation. The NADPH-regenerating system consisted of NADP⁺ (Sigma-Aldrich, anhydrous), glucose-6-phosphate (Sigma-Aldrich, anhydrous), glucose-6-phosphate dehydrogenase (Sigma-Aldrich, lyophilized powder) and uridine 5'-diphosphoglucuronic acid (UDPGA, Sigma-Aldrich, trisodium salt, >98%). For LC analyses formic acid was obtained from Fluka (#06440) and acetonitrile was Optima LC-MS grade (Fisher #A955-1). Millipore water was used as a solvent (SimPak® 1). For GC analyses, stock solutions were made in dichloromethane (Biosolve, >99.9%).

2.2.3. Synthesis

The synthesis of fentanyl was performed in triplicate according to the open literature methods of Gupta¹⁶ and Siegfried.¹⁵ Figure 2.2 gives the overall synthetic strategy for the current study, similar to the scheme published by Mayer et al.¹⁷ Because of the nature of the compounds of interest, not all synthesis details are provided in the current work. So, briefly, in case of the Siegfried method the precursor N-Phenethyl-

Piperidone (NPP) was synthesized from piperidone and phenethyl-bromide. The obtained NPP further reacted with aniline giving the imine derivative which was reduced to the 4-Anilino-N-Phenethyl-Piperidine (4-ANPP). The latter was converted with propionyl chloride giving fentanyl hydrochloride. For the Siegfried method, each intermediate was purified before continuing with the next step, and the final product was obtained by crystallization. For the Gupta One-Pot method, no purification of intermediates was applied. Only the final product was obtained by crystallization, like the Siegfried method. Both syntheses were performed in triplicate and the products were stored as a powder at -20 °C. For two of the three samples of each synthesis method an aliquot of the reaction mixture was stored at room temperature (RT). All samples were analyzed in the current study.

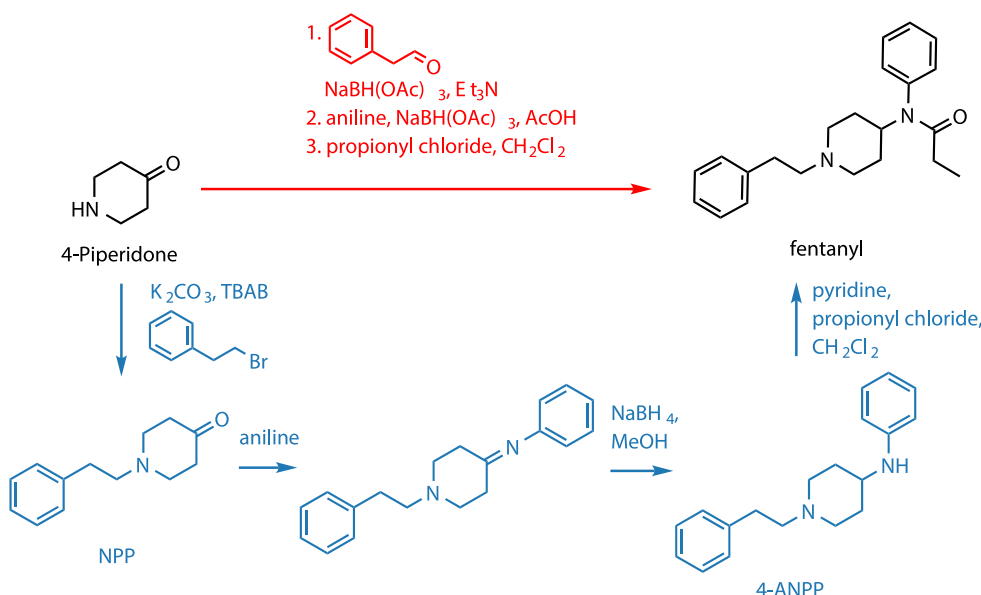


Figure 2.2. Reaction scheme of fentanyl synthesized by the One-Pot Gupta method (top, red) and the Siegfried method (bottom, blue).

2.2.4. Microsomal incubations and sample preparation

The liver is primarily responsible for the fentanyl metabolism.^{27–29} Liver microsomes can therefore be used to mimic human metabolism. This system is one of the most common *in vitro* models to study phase I metabolism and glucuronidation.³⁰ In this study, fentanyl was incubated according to earlier described methods.^{25–29} The conditions were optimized using fentanyl citrate with benzylfentanyl as internal standard to correct for varying instrument response. The following conditions were varied: concentration fentanyl, concentration microsomes and incubation time.

The fentanyl samples synthesized by the Gupta and Siegfried method were incubated in triplicate. The incubation method and sample preparation are described in detail in Figure 1 of the Supplementary information. First, 100 µL of 1 mg/mL fentanyl and 200 µL of 2.5 mg/mL human liver microsomes in 500 µL buffer were pre-incubated in a Grant-Bio PHMT Thermoshaker at 37 °C and were shaken at 300 rpm for 3 minutes. A 0.1 M potassium phosphate buffer with 2.5 mM MgCl₂ was used (pH = 7.4). Subsequently, the reaction was initiated by adding 200 µL of the NADPH-regenerating system. Concentrations were prepared of 1 mM NADP+, 5 mM glucose-6-phosphate, 1 U/mL glucose-6-phosphate dehydrogenase and 2 mM UDPGA. The samples were incubated for 72h (37 °C, 300 rpm). For each series of experiments a negative control was included, i.e. a blank experiment including all components except fentanyl. In addition, experiments were conducted without the addition of microsomes or the NADPH-regenerating system. A final control experiment assessed the stability of the fentanyl metabolites during incubation, by monitoring deuterated norfentanyl.

After incubation, the samples were divided into two fractions of 500 µL used for GC and LC analysis. For the sample work-up, 500 µL acetonitrile was added to the LC fraction to induce precipitation of the proteins. For the GC fraction, no acetonitrile was added before centrifuging, to avoid the presence of water in the sample afterwards. Both fractions were centrifuged for 10 minutes at 14,000 rpm (Eppendorf, 5417R). For the LC fraction, the supernatant was transferred to a glass vial and diluted five times in MilliQ, after which it was analyzed with LC-MS. For the GC fraction, the supernatant was transferred to a glass vial and 500 µL dichloromethane was added for liquid-liquid extraction. The dichloromethane fraction was then analyzed with GC-MS and GC-FID.

The efficiency of the sample preparation was determined using a known concentration of fentanyl and norfentanyl with benzylfentanyl as internal standard for LC-MS analyses and d5-norfentanyl as internal standard for GC-MS analyses. The incubation procedure was followed using the same chemicals and method, except for the 72 hours incubation time to avoid loss of fentanyl due to the metabolism.

2.2.5. Chemical analysis

2.2.5.1. GC-MS

The analyses were performed on an Agilent 7890B GC equipped with an Agilent VF-5ms column (5% phenylmethyl polysiloxane, 30 m x 0.25 mm x 0.25 µm). One microliter of sample was injected by an autosampler (Combi Pal, Ctc analytics). Helium was used as the carrier gas at a constant flow of 1 mL/min. The GC injector was operated in splitless mode at 275 °C. The oven temperature was maintained at 40°C for 1 min., then ramped at 10 °C/min. to 280 °C and held for 15 min. Detection was performed with an Agilent 5977A MS, which operated in electron ionization (EI) mode with an ionization potential

of 70 eV and a scan range of 25-550 mass units. Compounds were identified using Agilent ChemStation by spectral comparison to the National Institute of Standards and Technology (NIST) Mass Spectral Library. The results of the in vitro experiments were compared to a negative control, as described in section 2.2.4.

2.2.5.2. GC-FID

Additionally, the analyses were performed with an Agilent 7890A GC equipped with an Agilent VF-5ms column (5% phenylmethyl polysiloxane, 50 m x 0.32 mm x 0.40 µm). One microliter of sample was injected by an autosampler (Agilent 7683B injector) to the injector, which was operated in splitless injection mode at 275 °C. Helium was used as the carrier gas at a constant flow of 1 mL/min. The oven temperature was held at 40 °C for 1 min., then ramped at 10 °C/min. to 210 °C and held for 5 min., and finally ramped at 10 °C/min. to 280 °C and held for 30 min. Detection was performed with an FID at 250 °C, with a hydrogen flow of 40 mL/min. and an air flow of 450 mL/min. Data analysis was done by manual integration of peaks previously identified with GC-MS using Agilent ChemStation. The results of the in vitro experiments were compared to a negative control, as described in section 2.2.4.

2.2.5.3. LC-QTOF-MS

The first exploratory sample analyses were performed with a Thermo Ultimate 3000 UHPLC equipped with a Waters Acquity HSS T3 C18 column (1.8 µm, 1.0 x 150 mm). The column temperature was maintained at 35 °C and the flow rate was 100 µL/min. Eluent A was 0.2 v% formic acid in MilliQ water. Eluent B was 0.2 v% formic acid in acetonitrile. Gradient elution started at 100% eluent A, ramping to 80% eluent B in 30 minutes and holding for 5 minutes. Then equilibrating at 100% eluent A for 1 minute. The injection volume was 10 µL. The UHPLC was coupled to a Bruker Maxis Impact QTOF MS, which was set to a mass range of m/z 50-700 and operated in the positive electrospray ionization (ESI) mode. Data were acquired with full scan MS mode. The capillary voltage was 4500 V and the collision energy was 6 eV. The spectral acquisition rate was 1 Hz. The data were analyzed with MetaboliteDetect to search for compounds with DataAnalysis after subtraction of a negative control baseline signal. Peak areas of compounds were calculated by automatic integration of the extracted ion chromatogram of the identified compounds. After analysis, a target table was constructed and searched against all samples.

2.2.5.4. LC-HRMS/MS

After LC-QTOF-MS analyses, the samples were analyzed with a Thermo Ultimate 3000 UHPLC equipped with a Waters Acquity HSS T3 C18 column (1.8 µm, 2.1 x 100 mm). The column temperature was maintained at 30 °C and the flow rate was 100 µL/min. Eluent A was 0.2 v% formic acid in MilliQ water. Eluent B was 0.2 v% formic acid in acetonitrile.

Gradient elution started at 100% eluent A, ramping to 80% eluent B in 10 minutes and holding for 5 minutes. Then equilibrating at 100% eluent A for 1 minute. The injection volume was 10 μL . The UHPLC was coupled to a Thermo Scientific Q Exactive Plus Orbitrap MS, which was set to a mass range of m/z 50-750 and operated in positive ESI mode. The capillary voltage was set to 3.5 kV, and the source temperature was maintained at 320 °C, the relative sheath gas (nitrogen) flow was 35. The sensitivity of the method was assessed for fentanyl and its impurities. Data were first acquired with full scan MS mode. Based on the results obtained and the previously constructed target table with LC-QTOF-MS, an inclusion list was established using targeted MS/MS in parallel reaction monitoring (PRM) mode. The collision energy was 25 eV for all compounds. The data were analyzed with Xcalibur and Compound Discoverer. Peak areas were calculated by automatic integration of the extracted ion chromatogram of the identified compounds after subtraction of a negative control baseline signal. Compounds with a peak area lower than 10,000 were excluded. If peaks were only detected post metabolism, compounds with a peak area lower than 1,000,000 were excluded. Compounds that were present in the inclusion list and that were characteristic to a synthesis method were included.

2.2.5.5. LC-MS/MS

The optimization experiments were performed with a Waters Acquity ultra-high pressure liquid chromatography (UPLC) equipped with a Waters Acquity HSS T3 C18 column (1.8 μm , 2.1 x 100 mm). The mobile phase consisted of MilliQ water and acetonitrile both with 0.2% formic acid, using a gradient at a flow rate of 100 $\mu\text{L}/\text{min}$. Gradient elution started at 100% eluent A, ramping to 80% eluent B in 10 minutes and holding for 2 minutes. Then equilibrating at 100% eluent A for 3 minutes. The injection volume was 10 μL . The UPLC was coupled to a ThermoFisher TSQ Triple Quadrupole MS, which was operated in the positive ESI mode. The capillary voltage was set to 3.5 kV and the cone gas flow was 150 L/h. The cone voltage was 40 V and the collision energy was 30 eV for all compounds, with argon as collision gas set at a flow of 0.19 mL/min. Data was acquired with selected reaction monitoring (SRM) mode. The transitions monitored were m/z 337 → 188 and 337 → 105 for fentanyl, m/z 233 → 177 and 233 → 84 for norfentanyl and m/z 323 → 174 and 323 → 91 for the internal standard benzylfentanyl. A solvent delay of 3 minutes was used. Data analysis was performed with Xcalibur software.

2.2.6. Data analysis

Statistical analysis was performed with Python 3.8.2 using scikit-learn 0.22.1.31 Since these packages are open source, it is freely usable and distributable. The code written for this research is published under a GNU General Public License.³² The peak areas of the GC-FID were normalized to the sum of all peaks. The peak areas of the LC-HRMS/MS

were normalized to the internal standard methyl 4-anilino-1-benzyl-4-piperidinecarboxylate. The responses of the GC-FID for fentanyl and the found impurities were assumed to be uniform.³³ Two types of statistical analysis were performed. Principal component analysis (PCA) was used to reduce the dimensionality of the data and to confirm the discriminatory power of potential markers that were identified by visual inspection. The robustness of PCA was checked by leave-one-out validation. Supervised linear discriminant analysis (LDA) was used to maximize discrimination between the two synthesis methods. Kernel density estimations (KDEs) were constructed and used to express likelihood ratio (LR) values for the assignment of an unknown sample, in a similar way as Brust et al.³⁴ A match criterion approach offers a simple alternative to multivariate statistical analysis. This approach results in absolute statements accompanied by error rates. The statistical tool Student's t was applied to assess which impurities were characteristic for a specific synthesis route. An impurity was considered characteristic if there was less than 1% probability that the observation arises from random variation (beyond 99% confidence interval). Given the aim of the research the following hypothesis pair was considered:

H₁: The victim has been exposed to fentanyl produced with the Gupta method

H₂: The victim has been exposed to fentanyl produced with the Siegfried method

2.3. Results

2.3.1. Method optimization and validation

The GC-MS method was optimized for fentanyl citrate (t_r : 25.4 min.) and norfentanyl (t_r : 18.9 min.) with internal standard d_5 -norfentanyl (t_r : 18.9 min.), in order to determine the conversion of fentanyl to norfentanyl. Linear calibration curves were obtained for these standards in the range of 5 – 50 µg/mL with $R^2 = 0.9969 - 0.9984$ (Figure 2, Supplementary information). The mean values of the quality controls were within 23% for 5 µg/mL and within 10% relative standard deviation for 50 µg/mL ($n = 3$). The sample preparation efficiencies, determined by spiking a known concentration of fentanyl and norfentanyl into the microsomal incubation mixture, were respectively $129\% \pm 12\%$ and $22.3\% \pm 1.1\%$ (std., $n = 8$). Evaporation of the volatile organic phase is the most likely cause for obtaining recoveries exceeding 100%. The low recovery of norfentanyl is probably due to limited transfer from the polar phase to the organic phase. The most relevant impurities in the GC-FID chromatogram as presented in Figure 2.3 were identified with GC-MS as fentanyl (X, t_r : 45.7 min.), acetyl fentanyl (W, t_r : 43.9 min.), 4-ANPP (V, t_r : 38.1 min.) and N-phenylpropanamide (L, t_r : 20.4 min.). These impurities were clearly visible in the pre-incubation chromatogram. In the post-

incubation chromatogram, other compounds were observed, including the metabolism product phenethyl alcohol (H, t_r : 15.5 min.).

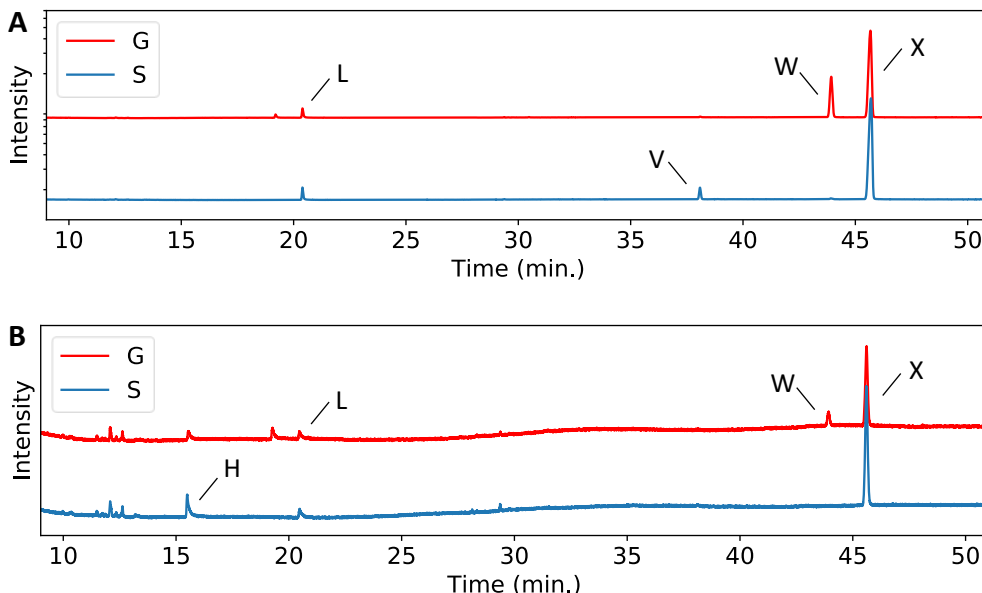


Figure 2.3. Representative GC-FID chromatograms of the Gupta (G) and Siegfried (S) samples. A) Pre-metabolism B) Post-metabolism. The following most relevant impurities have been highlighted: phenylethyl alcohol (H), N-phenylpropanamide (L), acetyl fentanyl (W) and fentanyl (X).

The LC-MS/MS method was optimized for fentanyl citrate (t_r : 7.49 min.) with internal standard benzylfentanyl (t_r : 7.32 min.) and for norfentanyl (t_r : 6.37 min.). Linear calibration curves were obtained in the range of 5 – 200 ng/mL with $R^2 = 0.9986 - 0.9996$. The mean values of the quality controls were within 25% for 5 ng/mL and within -7% relative standard deviation for 200 ng/mL ($n = 3$). The sample preparation efficiencies, determined by spiking a known concentration of fentanyl and norfentanyl into the microsomal incubation mixture, were respectively $105\% \pm 6\%$ and $107\% \pm 3\%$ (std., $n = 5$). Surprisingly, no losses due to protein precipitation were observed. This is probably due the simplified microsomal model system compared to sample preparation of more complex biological samples such as human whole blood. The following most relevant impurities were identified in the LC-HRMS/MS total ion chromatograms as presented in Figure 2.4: fentanyl (X, t_r : 10.9 min.), acetyl fentanyl (W, t_r : 10.5 min.) and N-phenylacetamide (J, t_r : 11.1 min.). In the post-incubation chromatogram, more peaks were visible, including the metabolic product norfentanyl (T, t_r : 9.4 min.).

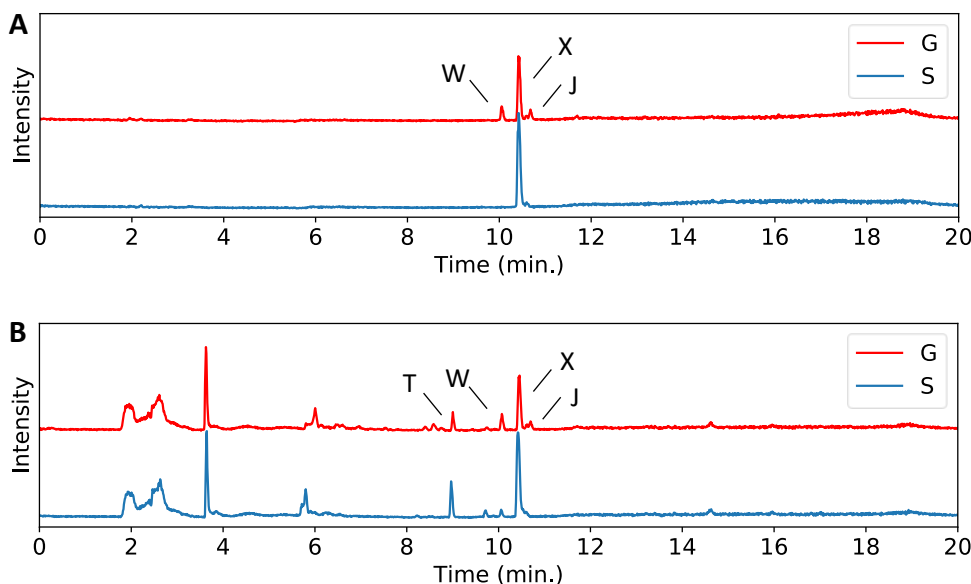


Figure 2.4. Representative LC-HRMS/MS total ion chromatograms of the Gupta (G) and Siegfried (S) samples. A) Pre-metabolism B) Post-metabolism. The following most relevant impurities have been highlighted: norfentanyl (T), acetyl fentanyl (W), fentanyl (X) and N-phenylacetamide (J).

2.3.2. Pre-metabolism impurity profiling

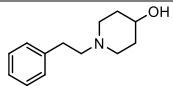
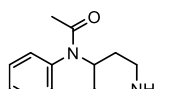
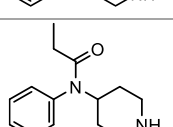
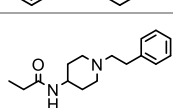
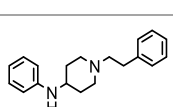
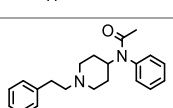
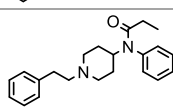
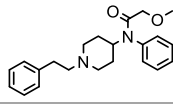
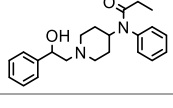
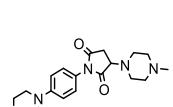
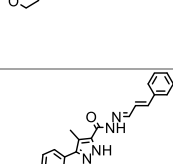
In the pre-metabolism fentanyl samples, a total of 24 impurities were identified. An overview of all the impurities found in this study is given in Table 2.1. The suggested tentative structures were based on the use of various methods and reference sources, as indicated in the table footnote. An example of a tentative identification of a compound by targeted MS/MS is given in Figure 3 of the Supplementary information. All the listed impurities were present in the samples prepared according to the Gupta synthesis method, whereas only 17 impurities were detected in the samples made by the Siegfried method. This difference can be explained by the purification steps performed after each intermediate synthesis step in the Siegfried method.

Table 2.1. Impurities detected by GC-FID and LC-HRMS/MS in samples synthesized by the Gupta or Siegfried method, obtained before and after metabolism. Chemicals are sorted by their mass.

Ref	Name	Mass (g/mol)	Formula	Synthesis method	Detected samples	Analysis	Tentative structure
A	Aniline*	93.1	C ₆ H ₇ N	Gupta, Siegfried	pre, post	LC	
B	4-piperidone*	99.1	C ₅ H ₉ NO	Gupta, Siegfried	pre, post	LC	
C	γ-Amino- butyric acid†	103.1	C ₄ H ₉ NO ₂	Gupta, Siegfried	pre, post	LC	
D	Muscimol†	114.1	C ₄ H ₆ N ₂ O ₂	Gupta, Siegfried	post	LC	
E	Tetramethyl- urea*	116.2	C ₅ H ₁₂ N ₂ O	Gupta, Siegfried	pre, post	LC	
F	Tris(hydroxy- methyl)- amino- methane*	121.1	C ₄ H ₁₁ NO ₃	Gupta, Siegfried	pre, post	LC	
G	N-Ethyl- aniline‡	121.2	C ₈ H ₁₁ N	Gupta, Siegfried	pre, post	GC	
H	phenylethyl alcohol‡	122.2	C ₈ H ₁₀ O	Gupta, Siegfried	post	GC	
I	N-BOC- hydroxyl- amine†	133.2	C ₅ H ₁₁ NO ₃	Gupta, Siegfried	pre	LC	
J	N-phenyl- acetamide*‡	135.2	C ₈ H ₉ NO	Gupta, Siegfried	pre, post	LC, GC	
K	Tri- methadione*	143.1	C ₆ H ₉ NO ₃	Gupta, Siegfried	post	LC	
L	N-phenyl- propanamide ^{17,19} ‡§	149.2	C ₉ H ₁₁ NO	Gupta, Siegfried	pre, post	LC, GC	
M	N-Butyl- aniline‡	149.2	C ₁₀ H ₁₅ N	Gupta	pre	GC	
N	phenylethyl acetate‡	164.2	C ₁₀ H ₁₂ O ₂	Gupta	pre	GC	
O	1-benzyl- piperazine†	176.3	C ₁₁ H ₁₆ N ₂	Gupta, Siegfried	pre, post	LC	
P	Phenethyl- propanamide ¹⁹ §	177.2	C ₁₁ H ₁₅ NO	Gupta, Siegfried	pre, post	LC	
Q	2,6- Diisopropyl- aniline†	177.3	C ₁₂ H ₁₉ N	Gupta	pre, post	LC	

2 Chapter 2

Table 2.1. (continued)

Ref	Name	Mass (g/mol)	Formula	Synthesis method	Detected samples	Analysis	Tentative structure
R	1-phenyl-ethylpiperidin-4-ol ^{17,19§}	205.3	C ₁₃ H ₁₉ NO	Gupta, Siegfried	pre, post	LC	
S	Acetyl norfentanyl ^{35§}	218.3	C ₁₃ H ₁₈ N ₂ O	Gupta, Siegfried	post	LC	
T	Norfentanyl*	232.3	C ₁₄ H ₂₀ N ₂ O	Gupta, Siegfried	post	LC	
U	N-(1-phenyl-ethylpiperidin-4-yl) propenamide*	260.4	C ₁₆ H ₂₄ N ₂ O	Gupta	pre, post	LC	
V	4-anilino-N-phenethyl-piperidine (4-ANPP)*‡	280.4	C ₁₉ H ₂₄ N ₂	Gupta, Siegfried	pre, post	LC, GC	
W	Acetyl fentanyl*‡	322.4	C ₂₁ H ₂₆ N ₂ O	Gupta, Siegfried	pre, post	LC, GC	
X	Fentanyl*‡	336.5	C ₂₂ H ₂₈ N ₂ O	Gupta, Siegfried	pre, post	LC, GC	
Y	Methoxy-acetyl fentanyl*	352.5	C ₂₂ H ₂₈ N ₂ O ₂	Gupta, Siegfried	pre, post	LC	
Z	β-Hydroxy-fentanyl*	352.5	C ₂₂ H ₂₈ N ₂ O ₂	Gupta, Siegfried	pre, post	LC	
AA	3-(4-Methyl-1-piperazinyl)-1-[4-(4-morpholinyl)-phenyl]-2,5-pyrroldinedione†	358.4	C ₁₉ H ₂₆ N ₄ O ₃	Gupta, Siegfried	pre, post	LC	
AB	MFCD-01916771†	374.4	C ₂₂ H ₂₂ N ₄ O ₂	Gupta, Siegfried	pre, post	LC	

*The compound was tentatively identified with targeted MS/MS. †Identification with Compound Discoverer.

‡Identification with spectral comparison to the NIST mass spectral library. §The tentative structure was determined by comparison with literature.

2.3.2.1. Match criterion using confidence intervals

A simple rule-of-thumb guideline was established in order to obtain information on the synthesis route involved. A match criterion approach was applied using confidence intervals. Consequently, three impurities were found to be significant classifiers for the synthesis method for the pre-metabolism samples. The impurities 1-phenylethylpiperidin-4-ol (R) and acetyl fentanyl (W) were characteristic for the Gupta synthesis route. The impurity 4-ANPP (V) was found to be indicative for the Siegfried synthesis route. Table 2.2 shows the characteristic relative levels of fentanyl impurities prior to metabolism. The responses were measured by GC-FID and LC-HRMS/MS for respectively the Gupta and Siegfried method. For example, if the relative response of impurity W is within 23 – 47% of the fentanyl peak area, as measured by LC-HRMS/MS, this indicates that fentanyl is produced with the Gupta method. The same holds when either acetyl fentanyl (W) or 4-ANPP (V) is detected with GC-FID. Not applicable (n.a.) is shown when the impurity is not detected by the analysis method. Another approach is to use a ratio of compounds as indicator for the synthesis method used. This ratio is often constant in various kinds of matrices. For LC-HRMS/MS the ratio of V/R was 1.7 ± 0.9 and 110 ± 84 ($\pm 95\%$ confidence interval), for respectively the Gupta and Siegfried method. Additionally, the ratio of W/V was 103 ± 60 for the Gupta and 0.4 ± 0.6 for the Siegfried method. Because no overlapping values were found, these ratios are interesting factors for a simple and straight forward assessment of the synthesis route involved.

Table 2.2. Characteristic relative responses of fentanyl impurities measured by GC-FID and LC-HRMS/MS for respectively the Gupta and Siegfried method. Samples were measured pre-metabolism. The relative responses of the impurities are given with the 95% confidence interval ($n = 5$) and represent the peak area relative to that of fentanyl.

Impurity	GC-FID		LC-HRMS/MS	
	Gupta (%)	Siegfried (%)	Gupta (%)	Siegfried (%)
R	n.a.	n.a.	0.12 – 0.42	0.011 – 0.045
V	0	0.4 – 2	0.09 – 0.79	0.3 – 5.1
W	14 – 22	0	23 – 47	0.2 – 1.4

2.3.2.2. PCA

In addition to the simple rule-of-thumb guideline, a chemometric analysis was applied to retrieve robust information on the synthesis route. To illustrate the chemical attribution signatures of the Gupta and Siegfried synthesis method, a PCA model was built for the impurities detected by LC-HRMS/MS. Since a limited number of impurities was detected by GC, chemometric analysis of the GC data provided little added value.

The score plot of the two first principal components (PCs) based on impurities detected by LC pre-metabolism, showed grouping of the samples according to their synthesis as

is illustrated in Figure 2.5. The first PC accounts for 96% of the variance and is predominantly composed of impurity acetyl fentanyl (W). The second PC accounts for 3% of the total variance and is mainly characterized by N-phenylacetamide (J), N-phenylpropanamide (L), 4-ANPP (V) and 3-(4-Methyl-1-piperazinyl)-1-[4-(4-morpholinyl)phenyl]-2,5-pyrrolidinedione (AA). N-Butylaniline (M) was only detected by GC and AA was only detected by LC. The performance of the unsupervised PCA models was tested with leave-one-out validation (Figure 4, Supplementary information). The PCA model showed good robustness, since leaving out one sample resulted in similar explained variance. In this study other impurities were found than described in previous studies.^{19,21} The first study focused on the Siegfried and Janssen synthesis routes and reported among others, N-phenylpropanamide (L), 1-phenylethylpiperidin-4-ol (R), 4-ANPP (V) and acetyl fentanyl (W) as markers common for both routes. In the current study 4-ANPP (V) was also found to be a Siegfried-specific marker, although the other compounds were identified as Gupta markers. The second study also characterized acetyl fentanyl (W) as a Gupta marker. Additional characteristic impurities in the current research included N-phenylacetamide (J), N-Butylaniline (M) and 3-(4-Methyl-1-piperazinyl)-1-[4-(4-morpholinyl)phenyl]-2,5-pyrrolidinedione (AA). Most of these impurities were also found by Mayer et al.,¹⁷ except for N-Butylaniline (M) which to our knowledge has not been previously reported.

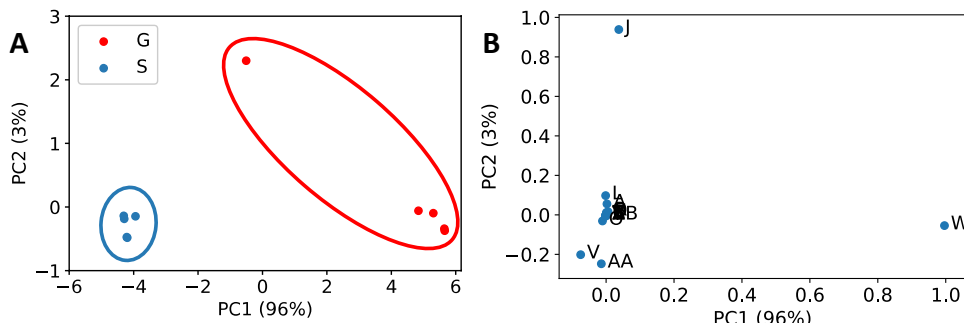


Figure 2.5. A) PCA-score plot based on 21 impurities detected by LC-HRMS/MS pre-metabolism showing good separation of the synthesis methods Gupta (G) or Siegfried (S). B) Corresponding PCA loadings. PC1 is responsible for 96% of the variance and is predominantly composed of impurity W. PC2 accounts for 3% of the total variance and is mainly characterized by J, L, V and AA.

2.3.2.3. LDA

To put the results in a forensic framework, LDA was used to find maximum discrimination between two groups. The LDA value is a linear combination of the original variables, i.e. normalized peak area. An advantage of this supervised pattern recognition method is that only one dimension (first canonical variate) is defined, when LDA is applied to two classes. In this study two classes were used, requiring only the

first canonical variate for the separation of the classes. A disadvantage of the supervised LDA technique is a higher probability of overfitting, which results in too optimistic model performance. To avoid this problem PCA can be applied in combination with LDA.³⁶ This is often performed when the number of features exceed the number of samples per category. PCA reduces the dimensionality as described in section 3.2.2. Figure 2.6 shows the KDE distributions for both synthesis methods obtained using LDA in combination with PCA. The distributions based on LC-HRMS/MS pre-metabolism data were highly discriminating. Because the GC results showed very good separation only based on a few impurities, no LDA was applied.

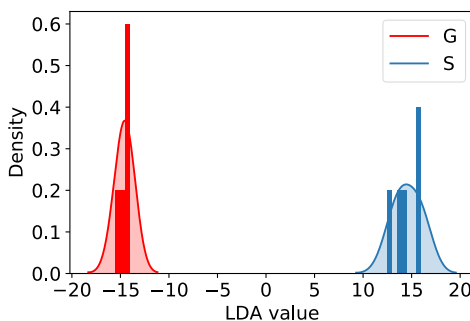


Figure 2.6. Distribution of LDA scores for Gupta (G) and Siegfried (S) samples detected by LC-HRMS/MS pre-metabolism. The bars represent the frequency of the individual measurements for a given LDA value adding up to 1. The shaded curve is the kernel density estimation with a bandwidth of 1 (G) and 1.2 (S).

2.3.3. Post-metabolism impurity profiling

2.2.3.1. Metabolism of fentanyl

Fentanyl was incubated using human liver microsomes. The conversion of fentanyl to norfentanyl was $31.8 \pm 1.5\%$ (std., $n = 4$), using a fentanyl concentration of 100 µg/mL fentanyl, 0.5 mg/mL microsomes and 72 hours incubation time. The reduction in fentanyl concentration statistically corresponded to the formation of norfentanyl. A decrease in the incubation time, the concentration of microsomes or an increase in the concentration of fentanyl resulted in a relatively lower conversion.

Several blank runs were conducted to ensure that the effects observed could be related to the metabolic processes occurring during the incubation process. A blank experiment including all components except fentanyl indicated that no disturbing matrix effects occurred for the analysis of fentanyl and the related metabolites. This blank run was also used to correct for the baseline signal in establishing the peak areas of the compounds of interest. Additionally, experiments were conducted without the addition of the microsomes or the NADPH-regenerating system. This resulted in no detectable formation of norfentanyl indicating that this compound is not a-priori present in the

fentanyl samples and is only formed as the result of the metabolism. A final control experiment demonstrated the stability of the fentanyl metabolites during the incubation by monitoring deuterated norfentanyl. These series of blank runs, in combination with the results obtained from the pre-metabolism experiments, provided convincing evidence that the formation of fentanyl metabolites can be exclusively attributed to liver microsome action.

2.2.3.2. Match criterion using confidence intervals

In the post-metabolism fentanyl samples, a total of 23 impurities were found. These chemicals are included in the overview given in Table 2.3. Five new compounds were found in the post-metabolism samples, including the two fentanyl metabolism products. All impurities were present in the samples made by the Gupta synthesis method and all except two were identified in the Siegfried samples.

The match criterion approach was also applied to the post-metabolism samples. Five impurities were found to be synthesis method specific on the basis of significant differences with respect to confidence intervals. The impurities 1-phenylethylpiperidin-4-ol (R), acetyl norfentanyl (S), N-(1-phenylethylpiperidin-4-yl) propanamide (U) and acetyl fentanyl (W) were found to be characteristic for the Gupta synthesis route. Acetyl norfentanyl (S) was only detected post-metabolism. For GC-FID the presence of acetyl fentanyl (W) was sufficient to confidently distinguish the two synthesis routes. Both synthesis routes showed a large peak for phenylethyl alcohol (H) which is a by-product of the metabolic conversion of fentanyl to norfentanyl. Despite the consistent presence of phenylethyl alcohol this compound can be used for differentiation because its concentration is much higher in Siegfried samples. This can be explained by the reduced level of impurities in these samples. However, it should be noted that phenylethyl alcohol is a frequently encountered impurity, which can have many other possible origins. Table 2.3. shows the characteristic relative responses of fentanyl impurities post metabolism. The responses were measured by GC-FID and LC-HRMS/MS for respectively the Gupta and Siegfried method. For example, if the relative response of impurity H is within 11 – 18% of the fentanyl peak area measured by GC-FID, the victim most likely has been exposed to fentanyl produced with the Siegfried method (assuming that the microsomes correctly mimic human metabolism). For LC-HRMS/MS the ratio of S/R was 10 ± 5 and 1.0 ± 1.3 ($\pm 95\%$ confidence interval), for respectively the Gupta or Siegfried method. The ratio of W/R was 84 ± 50 and 9 ± 11 . Because these intervals do not overlap, these ratios are interesting features for distinguishing between the synthesis routes post-metabolism.

Table 2.3. Characteristic relative responses of fentanyl impurities measured by GC-FID and LC-HRMS/MS for respectively the Gupta and Siegfried method. Samples were measured post-metabolism. The relative responses of the impurities are given with the 95% confidence interval ($n = 5$).

Impurity	GC-FID		LC-HRMS/MS	
	Gupta (%)	Siegfried (%)	Gupta (%)	Siegfried (%)
H	9.0 – 10.0	11 – 18	n.a.	n.a.
R	n.a.	n.a.	0.05 – 0.13	0.007 – 0.032
S	n.a.	n.a.	0.4 – 1.2	0.002 – 0.029
U	n.a.	n.a.	0.005 – 0.035	0
W	13 - 22	0	4 – 10	0.03 – 0.27

2.2.3.3. PCA

A PCA model was also built for the impurities detected by LC for the post-metabolism samples. The score plot of the two first PCs showed grouping of the samples according to synthesis route as illustrated in Figure 2.7. The first PC is responsible for 73% of the variance with dominant loadings for the impurities acetyl fentanyl (W), norfentanyl (T), β -hydroxyfentanyl (Z) and acetyl norfentanyl (S). The second PC accounts for 22% of the total variance and is mainly characterized by norfentanyl (T), acetyl fentanyl (W), β -hydroxyfentanyl (Z), muscimol (D) and N-phenylacetamide (J). The LC chromatogram showed a large response of norfentanyl which is the main product of the metabolism of fentanyl and hence is present in all post-metabolism samples. N-phenylacetamide (J) is mainly detected in the Gupta samples and is most likely the product of the reaction between aniline and acetic acid. The latter is only used in the Gupta synthesis method.

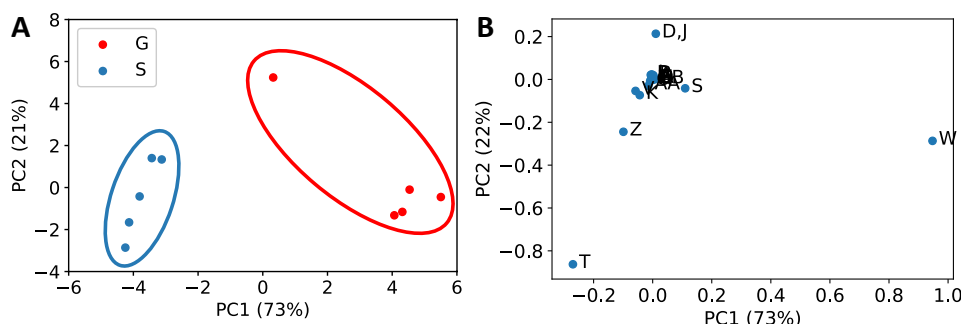


Figure 2.7. A) PCA-score plot based on 22 impurities detected by LC-HRMS/MS in the post-metabolism samples showing good separation of the synthesis methods Gupta (G) or Siegfried (S). B) Corresponding PCA loadings. PC1 is responsible for 73% of the variance and is predominantly composed of impurities W, T, S and Z. PC2 accounts for 22% of the total variance and is mainly characterized by compounds T, D, J, W and Z.

2.2.3.4. LDA

Like the pre-metabolism samples, PCA was used for dimensionality reduction before the application of LDA. Subsequently, LDA was applied to maximize the discrimination between the post-metabolism profiles for the two synthesis methods. Figure 2.8 shows the distributions of the LDA values for both synthesis methods. The distributions for the post-metabolism profiles as measured with LC-HRMS/MS show only a small overlap. The discussion in the next section elaborates on the transformation to LRs.

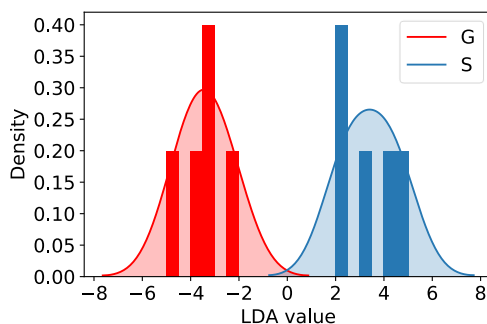


Figure 2.8. Distribution of LDA scores for Gupta (G) and Siegfried (S) samples detected by LC-HRMS/MS post-metabolism. The bars represent the frequency of the individual measurements for a given LDA value adding up to 1. The shaded curve is the kernel density estimation with a bandwidth of 1.

2.4. Discussion

Tippett plots were used to evaluate the performance of the LDA model for LR calculations.³⁷ In addition to LR calculations, Tippett plots can be used to provide information on the number of misclassifications.³⁴ Figure 2.9 shows the cumulative LR distributions for samples measured by LC-HRMS/MS. The Tippett plot shows the fraction of fentanyl samples that have a LR greater than the given value for samples produced with the Gupta (H_1) and Siegfried (H_2) method. The LRs were calculated for LDA values between respectively -20 to 20 and -8 to 8 for pre- and post-metabolism samples. This corresponds to the visual range of LDA values shown in Figure 2.6 and Figure 2.8. For pre-metabolism samples, LDA values above 3 were not used for the calculation, due to machine underflow. The LDA model for both pre- and post-metabolism samples yields well separated likelihood distributions and high evidential strength. If for an unknown sample a large positive LR is found the obtained profile is more probable when the victim has been exposed to fentanyl produced with the Gupta method (H_1) than when the victim has been exposed to fentanyl produced with the Siegfried method (H_2). Vice versa, for a large negative LR the evidence is more probable when H_2 is true than when H_1 is true. In over 50% of the pre-metabolism fentanyl samples, the LR exceeds very high minimum and maximum values of 10-300 and 1090. It is expected that after metabolism the impurity profile will contain less synthesis

method specific information due to marker loss, dilution and reactivity. The aim of this study was to investigate whether sufficient information would still be available to discern the fentanyl production route. Figure 2.9 shows that after liver microsome metabolism such information is indeed still available which is a very promising result. In over 50% of the fentanyl samples detected post-metabolism the LR will exceed minimum and maximum values of 10⁻⁸ and 10⁷. These plots also allow the study of misclassifications. For a method without misclassification, the pre- and post-metabolism graphs in Figure 2.9 would be perfectly separated at LR = 1 (dashed line). A perfect separation is visible for the pre-metabolism samples in the left plot. The post-metabolism distributions in the right plot show a small fraction of Siegfried samples with an LR > 1 and a small fraction of Gupta samples with an LR < 1. Consequently, for 0.4% of the Siegfried samples a false positive result is observed. Conversely, for 0.3% of the Gupta samples a false negative result is observed. The reason for this is the overlap in the KDEs shown in Figure 2.6 and Figure 2.8, which can be the result of the limited dataset. To improve the accuracy of the LR values, more data is required and a post-hoc calibration step is necessary.³⁸ Hence the LDA results and associated LR values presented in this study are of an indicative nature only.

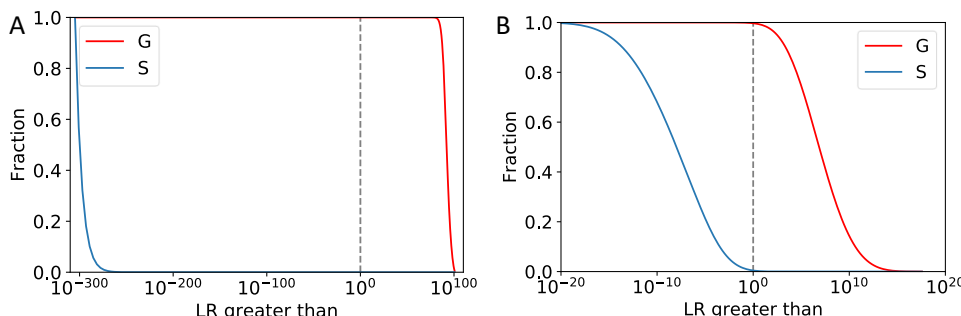


Figure 2.9. Tippett plots showing the cumulative likelihood ratio (LR) distributions calculated with LDA for fentanyl samples produced with the Gupta (G) and Siegfried (S) method, measured by LC-HRMS/MS. A) Pre-metabolism. B) Post-metabolism. The dashed lines show LR = 1.

The findings of the current study may be limited, because we had no access to real casework samples to verify the results. Having access to such samples is difficult as in many countries criminal law forbids the use of case work samples for forensic research. Furthermore, fentanyl induced overdose is currently still extremely rare in the Netherlands. However, in future investigations it is especially important to demonstrate the presence of the markers in real forensic toxicological samples, i.e. to demonstrate that the impurity profile can also be retrieved from whole blood samples from overdose victims. In addition, it might be valuable to use a separate training and test set, to see whether unknown samples are correctly classified. Due to the limited number of syntheses that were performed, such a robust validation could not be

conducted. Furthermore, samples synthesized by other laboratories or with chemicals from other suppliers could give different results. Surprisingly, Mayer et al. identified 4-ANPP (V) as a potential marker for the Gupta synthesis method, whereas it was identified as a Siegfried marker in the current study.¹⁷ A possible explanation for this contradictory result could be that Mayer et al. made some modifications to the Siegfried method, whereas in this study the synthesis was kept as close as possible to the original method as published by Siegfried. This suggests that small differences in synthesis method could have large consequences on the impurities present in fentanyl samples. An advantage however is that this would open possibilities to link a seized fentanyl sample to a specific laboratory. The prospect of linking a biomedical profile obtained from a victim to a given batch of material found at the home of a suspect could be very valuable in a forensic setting.

A concentration of 15 µg fentanyl per kg body mass is associated with health effects like chest wall rigidity, apnea and loss of consciousness.³⁹ Lethal doses are estimated to be a few milligrams, based on a lethal dose (LD50) of 30 µg/kg for non-human primates.³ Patches designed for analgesic use, deliver fentanyl in a rate of 12 – 100 µg/h. A specific case study describes a homicide attempt involving 120 µg/kg fentanyl (around 10 times the effective dose (ED50)), with a total dose of 6 mg. On arrival at the emergency department the young female victim was apneic with pinpoint pupils and had a decreased level of consciousness. She responded well to naloxone and was eventually discharged after nine days.⁴⁰ In the current study 100 µg was used for the microsomal incubations. This is a lower concentration than in the described examples, which might indicate that the sensitivity of the analysis methods applied in this work is sufficient for the levels relevant in forensic casework.

Because a model was used to mimic human metabolism, it is relevant to compare our post-metabolism results with fentanyl concentration in biomedical samples. It has been reported that fentanyl serum levels range from 0.3 to 2.5 ng/mL in patients that use fentanyl as a transdermal patch, and from 3.0 to 383 ng/mL in overdose victims.⁴¹ Similar concentrations have been reported in blood and urine of overdose victims.⁴² In this study, a higher fentanyl concentration was found after metabolism. A sensitivity analysis was applied in order to determine the lowest fentanyl level for which characteristic impurities can still be detected by the LC-HRMS/MS. These data must be interpreted with caution, because the lower concentration samples were dissolved in water thus not mimicking a complex biological matrix. To support these findings, the sensitivity analysis could be repeated with lower pre-metabolism concentrations and fentanyl samples spiked in biomedical matrices. For the impurities described in Table 2.3, acetyl norfentanyl (S) and N-(1-phenylethylpiperidin-4-yl) propanamide (U) were detected up to a fentanyl level of 90 ng/mL. This is in the range of levels found in victims

after an overdose. The impurities 1-phenylethylpiperidin-4-ol (R) and acetyl fentanyl (W) could even be detected up to a lower concentration of 0.9 ng/mL. This indicates that these impurities can also be detected in persons that receive a medical dose or experience mild poisoning symptoms. Qin et al. reported that acetyl norfentanyl (S) and acetyl fentanyl (W) could be detected up to a concentration of 2 pg/mg by UPLC-MS/MS.⁴³

Based on the match criterion method and PCA analysis, it can be concluded that N-phenylacetamide (J), 1-phenylethylpiperidin-4-ol (R) and acetyl fentanyl (W) are the most important markers for discrimination. However, acetyl fentanyl is not stable during metabolism, as it is metabolized to acetyl norfentanyl (S). In the present study 10% of acetyl norfentanyl was metabolized. Fortunately, enough acetyl fentanyl was left to discriminate between the synthesis methods. In the literature, contradictory results are reported regarding the extent of fentanyl metabolism. Some studies suggest that (almost) no intact fentanyl is left after exposure,^{44,45} while other authors state that norfentanyl often remains undetected in overdose cases.⁴⁶ In either case, impurities can be detected, so acetyl norfentanyl could be used as a potential marker if no acetyl fentanyl is left. It must be noted that acetyl (nor)fentanyl needs to be found in combination with (nor)fentanyl to be indicative of the Gupta synthesis method as acetyl fentanyl itself has also been classified as an illicit drug.^{6,47} There are two other impurities that show discriminative features pre- as well as post-metabolism. The first, phenylacetamide (J), can be formed from the starting materials aniline and acetic acid. The latter compound is only used for the Gupta synthesis, which is a probable explanation for the increased presence in these samples. The second impurity, 1-phenylethylpiperidin-4-ol (R), is a reduction product of the synthesis intermediate NPP. This compound is present at a slightly higher concentration in the Gupta samples, which is likely due to the presence of reducing agents and the lack of purification of intermediate reaction products. Therefore, phenylacetamide, 1-phenylethylpiperidin-4-ol, acetyl fentanyl and acetyl norfentanyl are the most important markers to discriminate between the Gupta and Siegfried synthesis method.

2.5. Conclusions

In the present study, the effect of human metabolism on the impurity profile of fentanyl was investigated with the use of human liver microsomes. The aim of the study was to identify marker compounds for a specific fentanyl synthesis method that could be detected post-metabolism, in order to evaluate the feasibility of using biomedical samples for chemical provenance purposes. In cases where only biomedical samples are available, the potential added value of the metabolism attribution method is obvious. In case where both biomedical samples and samples not subjected to

metabolism are available, combination of both methods would provide two complementary datasets. A total of 24 impurities were detected pre-metabolism and 23 impurities were identified post-metabolism. On the basis of a simple match criterion the fentanyl synthesis route could be established from the post-metabolism profile. Phenylethyl alcohol was found to be indicative of the Siegfried method, while acetyl norfentanyl, N-(1-phenylethylpiperidin-4-yl) propanamide, 1-phenylethylpiperidin-4-ol and acetyl fentanyl were indicative of the Gupta method. Classification of the synthesis method was also possible through the application of the PCA model. Eight relevant impurities were identified in the post-metabolism profiles using PCA, including three impurities which were also characteristic for the pre-metabolism profiles. Acetyl fentanyl and 1-phenylethylpiperidin-4-ol were characteristic both pre- and post-metabolism and could be detected up to levels that are realistic for forensic casework. GC-FID and LC-HRMS/MS can be used separately to discriminate between the Gupta and Siegfried synthesis method. Although it is valuable to use two different analysis methods, it is not necessary for obtaining appropriate discrimination. As one of the two methods is sufficient for the synthesis route attribution, almost every forensic (toxicological) laboratory will be able to implement post-metabolic fentanyl profiling. However, additional research is needed with respect to synthesis variations in a criminal setting and the preservation of the fentanyl marker profiles in whole blood samples of victims in forensic case work. Nonetheless, this work for the first time introduces a post-metabolic profiling concept that can be applied to biomedical samples for forensic casework and intelligence purposes.

2.6. Acknowledgements

We would like to thank Debora van der Riet-Van Oeveren and Ad L. de Jong (TNO Rijswijk) for their assistance with LC-QTOF-MS and LC-HRMS/MS analyses. We are also grateful to Gerrit-Jan de Bruin of Leiden University for fruitful discussions on multivariate statistics and critically reviewing the manuscript.

References

- (1) Heslop, D. J.; Blain, P. G. Threat Potential of Pharmaceutical Based Agents. *Intelligence and National Security* **2020**, *35* (4), 539–555. <https://doi.org/10.1080/02684527.2020.1750158>.
- (2) Stanley, T. H. The Fentanyl Story. *The Journal of Pain* **2014**, *15* (12), 1215–1226. <https://doi.org/10.1016/j.jpain.2014.08.010>.
- (3) Vardanyan, R. S.; Hruby, V. J. Future Prospects for Pharmaceutical Applications. *Future Medicinal Chemistry* **2014**, *6* (4), 385–412. <https://doi.org/10.4155/fmc.13.215.Fentanyl-related>.
- (4) Frisoni, P.; Bacchio, E.; Bilel, S.; Talarico, A.; Gaudio, R. M.; Barbieri, M.; Neri, M.; Marti, M. Novel Synthetic Opioids: The Pathologist's Point of View. *Brain Sciences* **2018**, *8* (9), 1–17. <https://doi.org/10.3390/brainsci8090170>.
- (5) Riches, J. R.; Read, R. W.; Black, R. M.; Cooper, N. J.; Timperley, C. M. Analysis of Clothing and Urine from Moscow Theatre Siege Casualties Reveals Carfentanil and Remifentanil Use. *Journal of Analytical Toxicology* **2012**, *36* (9), 647–656. <https://doi.org/10.1093/jat/bks078>.
- (6) Armenian, P.; Vo, K. T.; Barr-Walker, J.; Lynch, K. L. Fentanyl, Fentanyl Analogs and Novel Synthetic Opioids: A Comprehensive Review. *Neuropharmacology* **2018**, *134*, 121–132. <https://doi.org/10.1016/j.neuropharm.2017.10.016>.
- (7) National Institute on Drug Abuse. *Overdose Death Rates*. <https://www.drugabuse.gov/drug-topics/trends-statistics/overdose-death-rates> (accessed 2020-09-03).
- (8) Daéid, N. N.; Waddell, R. J. H. The Analytical and Chemometric Procedures Used to Profile Illicit Drug Seizures. *Talanta* **2005**, *67* (2), 280–285. <https://doi.org/10.1016/j.talanta.2005.05.018>.
- (9) Slosse, A.; Van Durme, F.; Samyn, N.; Mangelings, D.; Vander Heyden, Y. Evaluation of Data Preprocessings for the Comparison of GC–MS Chemical Profiles of Seized Cannabis Samples. *Forensic Science International* **2020**, *310*. <https://doi.org/10.1016/j.forsciint.2020.110228>.
- (10) Dams, R.; Benijts, T.; Lambert, W. E.; Massart, D. L.; De Leenheer, A. P. Heroin Impurity Profiling: Trends throughout a Decade of Experimenting. *Forensic Science International* **2001**, *123* (2–3), 81–88. [https://doi.org/10.1016/S0379-0738\(01\)00541-2](https://doi.org/10.1016/S0379-0738(01)00541-2).
- (11) Lociciro, S.; Hayoz, P.; Esseiva, P.; Dujourdy, L.; Besacier, F.; Margot, P. Cocaine Profiling for Strategic Intelligence Purposes, a Cross-Border Project between France and Switzerland. Part I. Optimisation and Harmonisation of the Profiling Method. *Forensic Science International* **2007**, *167* (2–3), 220–228. <https://doi.org/10.1016/j.forsciint.2006.06.052>.
- (12) Morelato, M.; Beavis, A.; Tahtouh, M.; Ribaux, O.; Kirkbride, P.; Roux, C. The Use of Organic and Inorganic Impurities Found in MDMA Police Seizures in a Drug Intelligence Perspective. *Science and Justice* **2014**, *54* (1), 32–41. <https://doi.org/10.1016/j.scijus.2013.08.006>.
- (13) Andersson, K.; Lock, E.; Jalava, K.; Huizer, H.; Jonson, S.; Kaa, E.; Lopes, A.; Poortman-van der Meer, A.; Sippola, E.; Dujourdy, L.; Dahlén, J. Development of a Harmonised Method for the Profiling of Amphetamines VI. Evaluation of Methods for Comparison of Amphetamine. *Forensic Science International* **2007**, *169* (1), 86–99. <https://doi.org/10.1016/j.forsciint.2006.10.020>.
- (14) Janssen, P. A.; Gardocki, J. F. Method for Producing Analgesia. U.S. Patent 3141823, 1964.
- (15) Siegfried. *Synthesis of Fentanyl*. <https://www.erowid.org/archive/rhodium/chemistry/fentanyl.html> (accessed 2020-10-28).
- (16) Gupta, P. K.; Ganesan, K.; Pande, A.; Malhotra, R. C. A Convenient One Pot Synthesis of Fentanyl. *Journal of Chemical Research* **2005**, No. 7, 452–453.
- (17) Mayer, B. P.; DeHope, A. J.; Mew, D. A.; Spackman, P. E.; Williams, A. M. Chemical Attribution of Fentanyl Using Multivariate Statistical Analysis of Orthogonal Mass Spectral Data. *Analytical Chemistry* **2016**, *88* (8), 4303–4310. <https://doi.org/10.1021/acs.analchem.5b04434>.
- (18) Mörén, L.; Qvarnström, J.; Engqvist, M.; Afshin-Sander, R.; Wu, X.; Dahlén, J.; Löfberg, C.; Larsson, A.; Östin, A. Attribution of Fentanyl Analogue Synthesis Routes by Multivariate Data Analysis of Orthogonal Mass Spectral Data. *Talanta* **2019**, *203* (April), 122–130. <https://doi.org/10.1016/j.talanta.2019.05.025>.
- (19) Lurie, I. S.; Berrier, A. L.; Casale, J. F.; Ito, R.; Bozenko, J. S. Profiling of Illicit Fentanyl Using UHPLC-MS/MS. *Forensic Science International* **2012**, *220* (1–3), 191–196. <https://doi.org/10.1016/j.forsciint.2012.02.024>.



Chapter 2

- (20) McBride, E. M.; Keller, R. E.; Verbeck, G. F. Direct-Infusion Electrospray Ionization-Mass Spectrometry Profiling of Fentanyl and Acetyl fentanyl Reaction Mixtures. *International Journal of Mass Spectrometry* **2018**, *428*, 55–61. <https://doi.org/10.1016/j.ijms.2018.03.004>.
- (21) Casale, J. F.; Hays, P. A.; Toske, S. G.; Mallette, J. R. Unique Bipiperidinyl Impurities Produced from the “One-Pot” Synthesis of Fentanyl. *Forensic Chemistry* **2020**, *17* (November 2019), 100203. <https://doi.org/10.1016/j.forc.2019.100203>.
- (22) van der Meer, J. A.; Trap, H. C.; Noort, D.; van der Schans, M. J. Comprehensive Gas Chromatography with Time of Flight MS and Large Volume Introduction for the Detection of Fluoride-Induced Regenerated Nerve Agent in Biological Samples. *Journal of Chromatography B* **2010**, *878* (17–18), 1320–1325. <https://doi.org/10.1016/j.jchromb.2010.02.019>.
- (23) OPCW. United Nations Mission to Investigate Allegations of the Use of Chemical Weapons in the Syrian Arab Republic. Final report. <https://unoda-web.s3.amazonaws.com/wp-content/uploads/%0A2013/12/report.pdf> (accessed 2020-10-06).
- (24) John, H.; Schans, M. J. Van Der; Koller, M.; Spruit, H. E. T.; Worek, F.; Thiermann, H.; Noort, D.; John, H. Fatal Sarin Poisoning in Syria 2013 : Forensic Verification within an International Laboratory Network. *Forensic Toxicology* **2018**, *36*, 61–71. <https://doi.org/10.1007/s11419-017-0376-7>.
- (25) Tateishi, T.; Wood, A. J. J.; Guengerich, F. P.; Wood, M. Biotransformation of Tritiated Fentanyl in Human Liver Microsomes. Monitoring Metabolism Using Phenylacetic Acid and 2-Phenylethanol. *Biochemical Pharmacology* **1995**, *50*, 1921–1924. [https://doi.org/10.1016/0006-2952\(95\)02088-8](https://doi.org/10.1016/0006-2952(95)02088-8).
- (26) Feierman, E.; Lasker, M. Metabolism of Fentanyl, a Synthetic Opioid Analgesic, by Human Liver Microsomes. *Drug metabolism and disposition* **1996**, *24* (9), 932–939.
- (27) Tateishi, T.; Krivoruk, Y.; Ueng, Y. F.; Wood, A. J. J.; Guengerich, F. P.; Wood, M. Identification of Human Liver Cytochrome P-450 3A4 as the Enzyme Responsible for Fentanyl and Sufentanil N-Dealkylation. *Anesthesia and Analgesia* **1996**, *82*, 167–172. <https://doi.org/10.1097/00000539-199601000-00031>.
- (28) Labroo, R. B.; Paine, M. F.; Thummel, K. E.; Kharasch, E. D. Fentanyl Metabolism by Human Hepatic and Intestinal Cytochrome P450 3A4: Implications for Interindividual Variability in Disposition, Efficacy, and Drug Interactions. *Drug Metabolism and Disposition* **1997**, *25* (9), 1072–1080.
- (29) Guittot, J.; Buronfosse, T.; Désage, M.; Lepape, A.; Brazier, J. L.; Beaune, P. Possible Involvement of Multiple Cytochrome P450s in Fentanyl and Sufentanil Metabolism as Opposed to Alfentanil. *Biochemical Pharmacology* **1997**, *53*, 1613–1619. [https://doi.org/10.1016/S0006-2952\(96\)00893-3](https://doi.org/10.1016/S0006-2952(96)00893-3).
- (30) Asha, S.; Vidyavathi, M. Role of Human Liver Microsomes in *In Vitro* Metabolism of Drugs-A Review. *Applied Biochemistry and Biotechnology* **2010**, *160*, 1699–1722. <https://doi.org/10.1007/s12010-009-8689-6>.
- (31) Pedregosa, F.; Varoquaux, G.; Gramfort, A.; Michel, V.; Thirion, B.; Grisel, O.; Blondel, M.; Prettenhofer, P.; Weiss, R.; Dubourg, V.; Vanderplas, J.; Passos, A.; Cournapeau, D.; Brucher, M.; Perrot, M.; Duchesnay, E. Scikit-Learn: Machine Learning in Python. *Journal of Machine Learning Research* **2011**, *12*, 2825–2830.
- (32) de Bruin-Hoegée, M.; de Bruin, G. J. Python Code for Chemical Attribution of Fentanyl. 2020. <https://doi.org/10.5281/zenodo.4276396>.
- (33) Scanlon, J. T.; Willis, D. E. Calculation of Flame Ionization Detector Relative Response Factors Using the Effective Carbon Number Concept. *Journal of Chromatographic Science* **1985**, *23*, 333–340.
- (34) Brust, H.; Koeberg, M.; Van Der Heijden, A.; Wiarda, W.; Mügler, I.; Schrader, M.; Vivo-Truyols, G.; Schoenmakers, P.; Van Asten, A. Isotopic and Elemental Profiling of Ammonium Nitrate in Forensic Explosives Investigations. *Forensic Science International* **2015**, *248*, 101–112. <https://doi.org/10.1016/j.forsciint.2014.11.024>.
- (35) Watanabe, S.; Vikingsson, S.; Roman, M.; Green, H.; Kronstrand, R.; Wohlfarth, A. In Vitro and In Vivo Metabolite Identification Studies for the New Synthetic Opioids Acetyl fentanyl, Acrylfentanyl, Furanyl fentanyl, and 4-Fluoro-Isobutyrylfentanyl. *AAPS Journal* **2017**, *19* (4), 1102–1122. <https://doi.org/10.1208/s12248-017-0070-z>.
- (36) Yang, J.; Yang, J. Y. Why Can LDA Be Performed in PCA Transformed Space? *Pattern Recognition* **2003**, *36* (2), 563–566. [https://doi.org/10.1016/S0031-3203\(02\)00048-1](https://doi.org/10.1016/S0031-3203(02)00048-1).

- (37) Evett, I. W.; Buckleton, J. S. Statistical Analysis of STR Data. In *Advances in Forensic Haemogenetics*; Carracedo, A., Brinkmann, B., Bär, W., Eds.; Springer: Heidelberg, 1996; pp 79–86. <https://doi.org/10.2169/naika.96.385>.
- (38) van Es, A.; Wiarda, W.; Hordijk, M.; Alberink, I.; Vergeer, P. Implementation and Assessment of a Likelihood Ratio Approach for the Evaluation of LA-ICP-MS Evidence in Forensic Glass Analysis. *Science and Justice* **2017**, *57*, 181–192. <https://doi.org/10.1016/j.scijus.2017.03.002>.
- (39) Streisand, J. B.; Bailey, P. L.; LeMaire, L.; Ashburn, M. A.; Tarver, S. D.; Varvel, J.; Stanley, T. H. Fentanyl-Induced Rigidity and Unconsciousness in Human Volunteers. *Clinical Investigations* **1993**, *78* (4), 629–634.
- (40) Lyttle, M. D.; Verma, S.; Isaac, R. Transdermal Fentanyl in Deliberate Overdose in Pediatrics. *Pediatric Emergency Care* **2012**, *28* (5), 463–464. <https://doi.org/10.1097/PEC.0b013e31825358b4>.
- (41) Suzuki, J.; El-Haddad, S. A Review: Fentanyl and Non-Pharmaceutical Fentanyls. *Drug and Alcohol Dependence* **2017**, *171*, 107–116. <https://doi.org/10.1016/j.drugalcdep.2016.11.033>.
- (42) Henderson, G. L. Fentanyl-Related Deaths: Demographics, Circumstances, and Toxicology of 112 Cases. *Journal of Forensic Sciences* **1991**, *36* (2), 422–433. <https://doi.org/10.1520/jfs13045j>.
- (43) Qin, N.; Shen, M.; Xiang, P.; Wen, D.; Shen, B.; Deng, H.; Qiang, H.; Song, F.; Shi, Y. Determination of 37 Fentanyl Analogues and Novel Synthetic Opioids in Hair by UHPLC-MS/MS and Its Application to Authentic Cases. *Scientific Reports* **2020**, *10* (1), 1–13. <https://doi.org/10.1038/s41598-020-68348-w>.
- (44) McClain, D. A.; Hug, C. C. Intravenous Fentanyl Kinetics. *Clinical Pharmacology & Therapeutics* **1980**, *28*, 106–114. <https://doi.org/10.1038/clpt.1980.138>.
- (45) Poklis, A. Fentanyl: A Review for Clinical and Analytical Toxicologists. *Clinical Toxicology* **1995**, *33* (5), 439–447. <https://doi.org/10.3109/15563659509013752>.
- (46) Burns, G.; Derienz, R. T.; Baker, D. D.; Casavant, M.; Spiller, H. A. Could Chest Wall Rigidity Be a Factor in Rapid Death from Illicit Fentanyl Abuse? *Clinical Toxicology* **2016**, *54* (5), 420–423. <https://doi.org/10.3109/15563650.2016.1157722>.
- (47) Wilde, M.; Pichini, S.; Pacifici, R.; Tagliabruni, A.; Busardò, F. P.; Auwärter, V.; Solimini, R. Metabolic Pathways and Potencies of New Fentanyl Analogs. *Frontiers in Pharmacology* **2019**, *10* (238), 1–16. <https://doi.org/10.3389/fphar.2019.00238>.



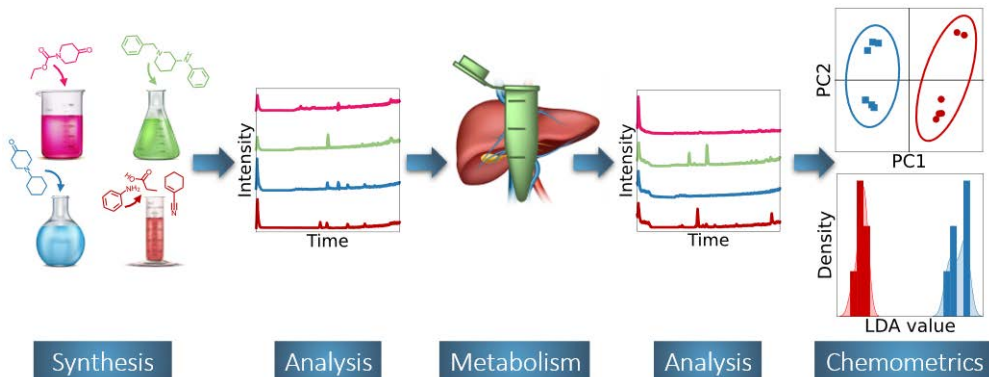
3

Post-metabolism impurity profiling of carfentanil, remifentanil, sufentanil, and benzylfentanyl

Daan Vangerven, Mirjam de Bruin-Hoegée, Fleur Kerstens, Meike Kerklaan, Rowdy P. T. Bross, Alex Fidder, Marcel van der Schans, Daan Noort, Arian C. Van Asten, Post-metabolism impurity profiling of carfentanil, remifentanil, sufentanil, and benzylfentanyl. *Forensic Chemistry* **2024**. Under Review. DOI: 10.2139/ssrn.4796215.

Abstract

Carfentanil, remifentanil, and sufentanil are potent fentanyl analogues that are regularly mixed with illicit drugs causing many overdose deaths. Chemical impurity profiling of these drugs is a well-established technique for linking evidence found at a crime scene to other seized samples. The current study aims to expand the application of impurity profiling to metabolized samples of carfentanil, remifentanil, sufentanil, and benzylfentanyl to find synthesis specific markers. This is particularly relevant when the drug has been consumed, and no intact material is present at a crime scene. A limited number of batches of carfentanil, remifentanil, and sufentanil were synthesized according to the Ugi or 7-step method and benzylfentanyl was produced using the Siegfried method. After in-vitro metabolism with human liver microsomes, the samples were analyzed by gas chromatography-mass spectrometry (GC-MS), liquid chromatography tandem mass spectrometry (LC-MS/MS), and liquid chromatography high resolution tandem mass spectrometry (LC-HRMS/MS). Characteristic markers were found by applying a match criterion approach and principal component analysis (PCA). The precursors 4-ANBP, aniline, and N-phenylacetamide were identified in pre- and post-metabolism samples, indicating that specific synthesis information is retained after in-vitro metabolism. Another important finding was the presence of several metabolites of the precursors after exposure. The detected levels were in line with concentrations reported in case work. In addition, LDA was applied to maximize discrimination between synthesis methods and to establish likelihood ratios (LRs). Corrected LR values with empirical lower and upper bounds (ELUB) were in the range of 0.083 to 16 with very low false positive and false negative error rates. In conclusion, the presented work demonstrates the possibility of combining chemical profiling and retrospective biomarker analysis to obtain information about the production method, which could be useful for reconstructions and attribution in forensic investigations.



3.1. Introduction

The misuse of so-called pharmaceutical based agents (PBAs) has increased significantly in the past decade. In particular, the synthetic opioid fentanyl and fentanyl analogues are a great threat to the overall public health, especially in the United States of America (USA).¹ Fentanyl is a full agonist at the mu-opioid receptor and was first synthesized in the late 1950s as an approximately 50-100 times more powerful analgesic than morphine.² Its analogues such as sufentanil, remifentanil, and carfentanil are even more potent.³ Although first intended to be used as a therapeutic, pain relief drug only, fentanyl analogues quickly emerged in the illicit drug market in the USA where they are regularly mixed with more traditional illicit drugs such as cocaine and heroin. This results in many overdose deaths in what is now known as the opioid crisis. In addition, the potential of fentanyl and fentanyl analogues to be used as a chemical weapon is of increasing concern to national security agencies.⁴ A mixture of aerosolized carfentanil and remifentanil was applied by Russian special forces as a riot control agent to end the Moscow theatre siege by Chechen militants in 2002.^{1,5}

In the field of illicit drugs, chemical impurity profiling is often used to establish a link between seized drugs and a suspect or to link material from different cases. These impurities are often related to the raw materials, the synthesis protocol, and the processing and storage conditions. The analyses are usually performed with liquid chromatography-mass spectrometry (LC-MS) and gas chromatography-mass spectrometry (GC-MS).⁶ In general, carfentanil and remifentanil share similar synthetic routes with comparable precursors. One of these routes is the Ugi synthesis and is often referred to as 'Ugi four-compound reaction'. This is a one-pot reaction containing an amine, a carbonyl compound, an isocyanide, and a carboxylic acid.⁷ It is relatively straightforward to produce a piperidine precursor with the Ugi reaction, allowing for a 2-step synthesis of car- and remifentanil.⁸ Other synthetic routes, such as Strecker⁹ and Bargellini^{10,11} require more advanced organic chemistry knowledge. Likewise, sufentanil is commonly produced by a multi-step synthesis and often shares similar steps with synthetic routes of other fentanyl analogues.^{12,13} Finally, benzylfentanyl, which closely resembles the structure of fentanyl, can be synthesized by the Gupta and Siegfried method, as applied for the production of fentanyl.¹⁴

The forensic use of impurity profiling has already been studied extensively for MDMA, amphetamine, methamphetamine, cocaine, and heroin.¹⁵⁻¹⁹ Similarly, three recent chemical impurity profiling studies of fentanyl and its analogues focused on discriminating between synthesis routes. Ovenden et al. established a chemical attribution signature (CAS) for fentanyl batches and identified ten impurities for the Janssen, and five for the Siegfried method.²⁰ Additionally, four impurities were identified for the fentanyl precursor 4-anilino-N-phenethyl-piperidine (4-ANPP),

synthesized according to the Valdez method. Multivariate statistical analysis was performed on liquid chromatography-high resolution mass spectrometry (LC-HRMS) data and successfully applied to differentiate production routes. Mayer et al. identified 160 synthesis-related organic impurities of 3-methylfentanyl using GC-MS and liquid chromatography time-of-flight mass spectrometry (LC-QTOF-MS).²¹ Furthermore, Mörén et al. identified 68 impurities corresponding to either the Strecker, Bargellini, or Ugi synthetic method.²² The impurities were detected with GC-MS and LC-HRMS and the chemical profiles were classified according to their synthesis route using multivariate statistical analysis.²²

After the release of a chemical warfare agent, samples from the crime scene are taken to serve as forensic evidence. Environmental samples can be collected, but also biological matrices such as blood and urine from victims can be used as evidence.²³ Especially in cases where no intact chemical is present, biological samples can provide important information. An advantage of biomarkers detected in human biological samples is stability. Biomarkers of the nerve agent sarin could for instance still be identified weeks after exposure in human tissue.²⁴ Additionally, traces of carfentanil metabolites were found in urine of victims, five days after exposure in the Moscow theatre siege.²⁵ In such situations, exposed individuals could serve as a valuable source of intelligence for forensic investigators.

In the present study the concepts of chemical profiling and retrospective biomarker analysis were combined to obtain information on the synthetic route after exposure. This study includes one to four batches of three production methods, which were all based on open literature. First, carfentanil, remifentanil, and sufentanil were synthesized according to the 7-step method. Additionally, carfentanil and remifentanil were produced by the Ugi synthesis method. Third, benzylfentanyl was produced from 4-anilino-1-benzylpiperidine (4-ANBP) using the last step of the Siegfried method, as previously illustrated for the production of fentanyl.¹⁴ The chemicals were subsequently metabolized in-vitro with human liver microsomes (HLM) to mimic the human metabolic process. GC-MS, liquid chromatography tandem mass spectrometry (LC-MS/MS), and liquid chromatography high resolution tandem mass spectrometry (LC-HRMS/MS) analyses of the pre- and post-metabolism samples were conducted to establish chemical impurity profiles. Possible route-specific markers were identified using both the unsupervised multivariate data analysis method principal component analysis (PCA) and the supervised method linear discriminant analysis (LDA). The present study demonstrates the potential of using biomedical samples for retrieving information about the synthesis route after exposure. This may constitute valuable information when investigating and reconstructing a chemical attack or an overdose case.

3.2. Materials and Methods

3.2.1. Safety

Due to the extreme potency of carfentanil, remifentanil, and sufentanil, these substances were synthesized by skilled organic chemists in a specially secured laboratory for the production and handling of highly toxic compounds. The antidote naloxone could be administered directly to mitigate respiratory depression in case of accidental exposure. Chemical analyses were conducted from solution only and low concentrations of psychoactive substances were applied.

3.2.2. Chemicals

Purities of the chemicals exceeded 97%. Pooled human liver microsomes (lot #1210097) were obtained from Xenotech (Kansas City, USA). Human plasma was purchased from Sanquin (Amsterdam, The Netherlands). Dichloromethane was purchased from Merck, aniline from Janssen Chimica, d₅-fentanyl from LGC standards, and 4-anilino-1-benzylpiperidine (4-ANBP) from ABCR GmbH. Ethyl-4-oxo-1-piperidinecarboxylate, 1-benzyl-4-piperidone, propionic acid, 4-piperidone monohydrate hydrochloride, glucose-6-phosphate sodium salt (G6P), glucose-6-phosphate dehydrogenase from Leuconostoc mesenteroides (G6P-d lyophilized powder, lot #0000194160), β-nicotinamide adenine dinucleotide phosphate hydrate (NAPD+, lot #SLCG6216), and uridine 5'-diphosphoglucuronic acid trisodium salt (UDPGA) were obtained from Sigma-Aldrich. For LC analysis, formic acid (Fluka), acetonitrile (Biosolve), and MilliQ (Millipak® Express 40) were used.

3.2.3. Synthesis

All fentanyl analogues were prepared in-house at TNO Rijswijk. The compounds were characterized by NMR, GC-MS, and LC-MS. Because of the labor-intensive methods, a limited number of batches were synthesized, as presented in Table 3.1. Carfentanil and remifentanil produced by the Ugi route were synthesized by two different scientists. In addition, two batches of carfentanil were produced at least one year apart from the two other carfentanil batches. The purity of the crude products was estimated to be around 50% and the purified batches had a purity of 82 – 98%.

Due to the sensitive nature of the production of these compounds, not all synthetic details are provided, but an outline is illustrated in Figure 3.1. Only the structures of the starting materials and the intermediate precursors identified in this study are shown. The purity was determined by quantitative NMR by measuring three samples from the same batch. Sufentanil, with a purity of 92.5% ± 0.4%, was made according to a 7-step synthetic route using ethyl-4-oxo-1-piperidinecarboxylate as starting material. Benzylfentanyl (purity = 98.3% ± 0.4%) was synthesized from 4-ANBP by the Siegfried

method. In addition, carfentanil (purity = $83.5\% \pm 0.5\%$) and remifentanil (purity = $82.0\% \pm 0.02\%$) were prepared from 1-benzyl-4-piperidone according to the 7-step synthetic route. Propionic acid, cyanocyclohexene, and aniline were used for the Ugi reaction, which was performed by different organic chemists (purity 50 - >90%). The structure of the fourth starting material depended on the desired chemical. N-phenethyl-4-piperidone (R1) was a precursor for carfentanil and methyl (4-oxocyclohexyl)acetate (R2) for remifentanil. Methyl 1-benzyl-4-(phenylamino)piperidine-4-carboxylate (EA6176, purity of $94.9\% \pm 0.4\%$), which is a simulant for carfentanil, was used as internal standard for benzylfentanyl analysis.

Table 3.1. Overview of applied synthesis methods for carfentanil, remifentanil, sufentanil, and benzylfentanyl.

Compound	Method	Total number of batches	Organic chemists	Product
Carfentanil	7-step	1	1	purified
Carfentanil	Ugi	4	2	crude and purified
Remifentanil	7-step	1	1	purified
Remifentanil	Ugi	2	2	crude
Sufentanil	7-step	1	1	purified
Benzylfentanyl	Siegfried	1	1	purified

3.2.4. Human liver microsome incubation

In this study, fentanyl analogues were incubated according to a method described in previous work.¹⁴ First, a 0.1 M potassium phosphate buffer with 2.5 mM MgCl₂ (pH=7.4) was prepared. For pre-incubation of remifentanil, sufentanil, and benzylfentanyl, 100 µL of a 1 mg/mL fentanyl analogues solution was used. A lower concentration of 100 µL of 10 µg/mL of carfentanil was applied for safety reasons, since carfentanil is estimated to be 5-50 times more potent than remifentanil and sufentanil.² The solution of fentanyl analogues was pre-incubated in a Grant-Bio PHMT Thermoshaker at 37°C and 300 rpm, with 200 µL of 2.5 mg/mL human liver microsomes and 500 µL of the buffer solution. NADPH-regenerating system (NRS) stock was prepared with a final concentration of 1 mM NADP+, 5mM glucose-6-phosphate, 1 U/mL glucose-6-phosphate dehydrogenase, and 2 mM UDPGA in buffer. The reaction was initiated by adding 200 µL NRS stock solution to the samples. This was then incubated for 72h at 37°C and 300 rpm.

Negative controls were prepared by adding 100 µL buffer instead of fentanyl analogue solutions. After incubation, the samples were divided into two fractions of 500 µL for LC and GC analysis. Subsequently, 500 µL acetonitrile was added to the LC fraction to induce protein precipitation. The fractions were centrifuged for 10 minutes at 14.000 rpm (Eppendorf, 5430R). A final theoretical concentration of 0.9 µg/mL in MilliQ + 0.1 v/v% formic acid with an internal standard concentration of 10 ng/mL was prepared for

LC analysis. For the GC fraction, the supernatant was transferred to a glass vial and 400 μL of dichloromethane was added for liquid-liquid extraction. The dichloromethane layer was analyzed with GC-MS.

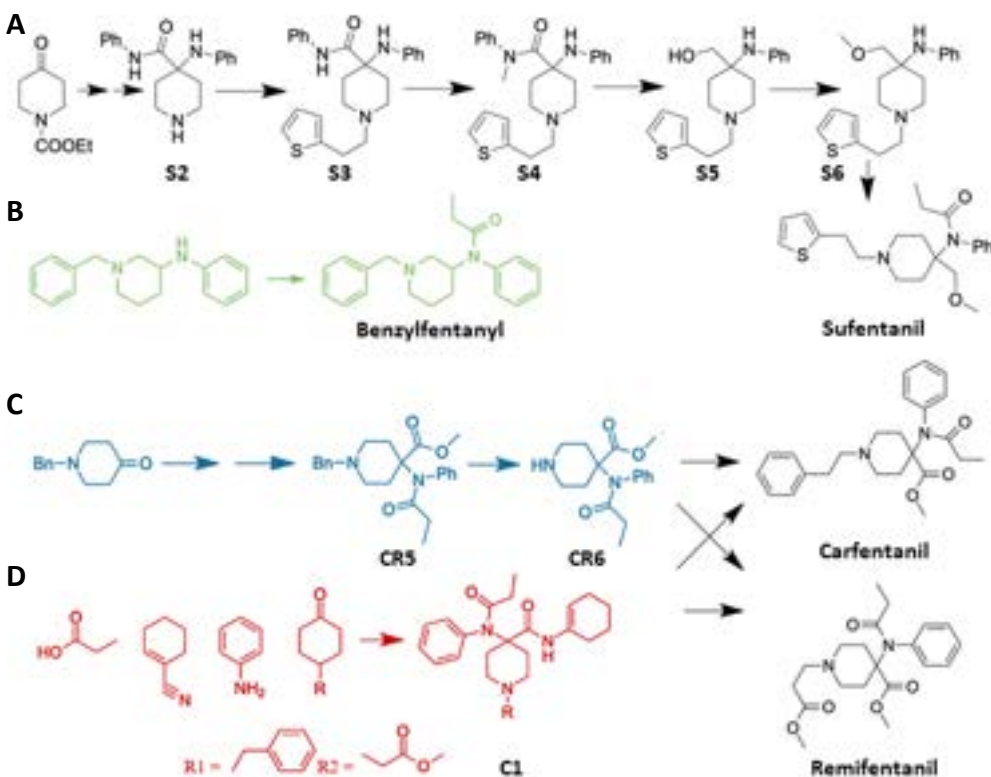


Figure 3.1. Reaction scheme of A) 7-step synthesis route of sufentanil (black), B) last step of Siegfried method for benzylfentanyl (green), C) 7-step synthesis route of carfentanil and remifentanil (blue), and D) Ugi-reaction for carfentanil and remifentanil (red).

3.2.5. Stability remifentanil in blood plasma

To evaluate the stability of remifentanil, 50 μL of 2 $\mu\text{g}/\text{mL}$ remifentanil was added to 200 μL blood plasma, which was preheated in a Grant-Bio PHMT Thermoshaker at 37 °C at 300 rpm for 10 minutes. After 0, 10, 30 min, and every hour until 8 hours, 250 μL 0.2 v/v% formic acid in acetonitrile was added to a selection of the samples to stop degradation. The samples were then prepared for analysis with LC-MS/MS. After brief vortexing, the samples were centrifuged for 10 minutes at 14.000 rpm. Subsequently, 250 μL of the supernatant was transferred to a 1.5 mL vial where 50 μL of a 10 ng/mL d₅-fentanyl solution and 200 μL 0.2 v/v% formic acid in MilliQ were added. A final concentration of 5 ng/mL was analyzed by LC-MS/MS.

3.2.6. Chemical analysis

3.2.6.1. GC-MS

Analyses were performed using an Agilent 7890B GC with an Agilent VF-5ms column (5% phenylmethyl polysiloxane, 30 m × 0.25 mm × 0.25 µm). The injection volume was 1 µL using an autosampler (Combi Pal, Ctc analytics). Helium was used as carrier gas at a constant flow of 1 mL/min. The GC was operated in splitless mode at 275 °C. The oven temperature was held for 1 min at 40 °C, then increased at 10 °C/min. to 280 °C and maintained at that temperature for 15 min. Detection was performed with an Agilent 5977A MS operating in electron ionization (EI) mode with an ionization potential of 70 eV and a scan range of 50-550 mass units. Compounds were identified with the National Institute of Standards and Technology Mass Spectral Library (NIST MS Search 2.0).

3.2.6.2. LC-MS/MS

Quantitative analyses were performed with a Waters ACQUITY ultra-high pressure liquid chromatography (UHPLC) system equipped with a Waters ACQUITY UPLC HSS T3 C18 column (1.8 µm, 2.1 x 100 mm). Mobile phase A consisted of MilliQ with 0.2 v/v% formic acid and mobile phase B consisted of acetonitrile with 0.2 v/v% formic acid, using a flow rate of 100 µL/min. Gradient elution started at 100% eluent A, ramping to 80% eluent B in 12 minutes, and holding that solvent composition for 2 minutes. Prior to the next analysis, the solvent composition was returned to 100% eluent A within 0.1 minutes and the system was equilibrated for 2 minutes. The injection volume was 5 µL. The chromatographic system was coupled to a Waters Xevo TQ-S triple-quadrupole MS detector. The MS operated in positive electrospray ionization (ESI) mode. The capillary voltage was set to 3.5 kV and the cone gas flow was 150 L/h. Data was acquired with selected reaction monitoring (SRM) mode using the transitions, collision energy, and cone energy as depicted in Table 3.2. Afterwards, the data was analyzed with MassLynx software.

Table 3.2. Mass spectrometric parameters for analytes and internal standards analyzed by LC-MS/MS.

Analyte	Precursor ion (m/z)	Product ion (m/z)	Collision energy (eV)	Cone energy (V)
Carfentanil	395.2	335.2, 279.3, 246.1, 133.9	20	17
Remifentanil	377.2	317.0, 228.1, 113.1	15	15
Sufentanil	387.2	335.2, 238.2, 111.0	20	20
Benzylfentanyl	323.1	230.9, 174.0, 90.8	15	10
d₅-fentanyl	342.1	105.0, 188.0	30	20
EA1672	325.1	232.0, 113.0	15	10
Norcarfentanil	291.0	259.1, 230.9, 142.0	10	10
Norfentanyl	233.0	177.1, 149.9	15	40
Remifentanil acid	363.0	303.0, 214.1, 113.1	15	15

3.2.6.3. LC-HRMS/MS

Pre-metabolism samples at 0.1-10 µg/mL and post-metabolism samples at 0.009-0.9 µg/mL were analyzed with a Thermo Scientific Ultimate 3000 UHPLC equipped with a Waters ACQUITY UPLC HSS T3 C18 column (1.7 µm, 1.0 x 100 mm). Mobile phase A consisted of MilliQ with 0.2 v/v% formic acid and mobile phase B consisted of acetonitrile with 0.2 v/v% formic acid, using a flow rate of 100 µL/min. Gradient elution started at 100% eluent A, ramping to 80% eluent B in 15 minutes and holding this composition for 7 minutes. The system was equilibrated for 7.9 minutes after returning to a 100% eluent A composition within 0.1 minute. The injection volume was 10 µL. The chromatographic system was connected to a Thermo Scientific Q Exactive Plus Orbitrap MS. The MS operated in positive ESI mode and the full mass range was set from 50 to 750 m/z. Capillary voltage was set to 3.5 kV and the source temperature was maintained at 320 °C. The relative sheath gas (nitrogen) flow was 35. Data was analyzed with Xcalibur software and Compound Discoverer (version 3.3.1.111) using Chemspider database for tentative identification. The accepted mass error for identification was 5 ppm.

3.2.7. Data analysis

Statistical analysis was performed with Python 3.11.1 using scikit-learn 1.3.0 and lir.^{26,27} The code used for this study is based on previous research.²⁸ The LC-HRMS/MS data was pre-processed by setting a minimum area threshold. For remifentanil samples the threshold was set at a million and for carfentanil samples the threshold was 100,000. In addition, samples were normalized to the area of the internal standard d₅-fentanyl. Before multivariate analysis, a match criterion approach was applied to calculate relative response ratios of selected impurities by dividing the area of an impurity against the area of the fentanyl analogue. Student's t-test was performed to calculate the 95% confidence interval. Subsequently, PCA and LDA were applied to carfentanil and remifentanil samples to reduce the dimensionality and highlight characteristic markers. Sufentanil and benzylfentanyl were not analyzed by multivariate analysis, since only one synthesis method was applied. The model was built using the area of the tentatively identified peaks of 3-12 repetitions of each batch measured by LC-HRMS/MS. The data was normalized using the StandardScaler function was applied, which subtracts the mean and scales the data to unit variance. After pre-processing, PCA was performed to reduce dimensionality of the dataset and to test the discriminating power of the selected impurities. The robustness was evaluated by leave-one-group-out validation. Additionally, LDA was applied as a data-dependent method to maximize discriminative power. Afterwards, Kernel Density Estimation (KDE) was applied to express the likelihood ratio (LR) for assigning unknown samples. The LR is defined as the probability of the evidence given H₁ divided by the probability of the

evidence given H₂. For classification of the synthesis route of either carfentanil or remifentanil, the following hypothesis pair was considered:

H₁: The victim has been exposed to carfentanil/remifentanil produced with the 7-step method

H₂: The victim has been exposed to carfentanil/remifentanil produced with the Ugi method

Tippett plots were constructed to assess the performance of the LDA model for LR calculations. To prevent extrapolation problems, the values of the LR were limited by imposing empirical lower and upper bounds (ELUB).²⁹

3.3. Results and discussion

3.3.1. Method optimization and validation

The LC-MS/MS method was optimized in terms of the separation and quantitative analysis of norfentanyl (t_r : 6.37 min), norcarfentanyl (t_r : 7.71 min), remifentanil (t_r : 8.30 min), benzylfentanyl (t_r : 8.72 min), d₅-fentanyl (t_r : 9.30 min), EA6176 (t_r : 9.33 min), carfentanil (t_r : 9.75 min), and sufentanil (t_r : 10.04 min). Linear calibration curves were obtained in order to determine the metabolic conversion of the analogues after incubation. These are in the range of 0.5-15 ng/mL for carfentanil, 5-100 ng/mL for remifentanil, 1-20 ng/mL for sufentanil, 0.1-5 ng/mL for norcarfentanyl, 0.5-50 ng/mL for benzylfentanyl, and 0.2-10 ng/mL for norfentanyl with R^2 between 0.9969-0.9999. The accuracy of the calibration curves was determined by analyzing quality controls at low, mid, and high concentrations (n=9-10). The mean values were within 15% of the actual value. The precisions were below 12% relative standard deviation (RSD). More details are provided in Section S.1 of the Supplementary information.

The metabolic conversion was assessed after incubation with human liver microsomes. Carfentanil concentration decreased with $85 \pm 15\%$ (stdv., n=22), sufentanil with $99.9 \pm 0.01\%$ (stdv., n=2), and benzylfentanyl with $72 \pm 11\%$ (stdv., n=3). The major metabolite norfentanyl was detected in all samples but at a low concentration of 14.2 ± 2.3 ng/mL (begin concentration of benzylfentanyl was 100 ng/mL). Also, a norcarfentanyl peak was present, but the concentration was below the detection limit preventing quantification. This is likely due to a low recovery because of limited transfer from the polar phase to the organic phase.¹⁴ Remarkably, remifentanil decreased below the detection limit and no main metabolite of remifentanil was observed after in-vitro metabolism. It was hypothesized that remifentanil degraded, therefore a separate stability study was conducted.

The stability of remifentanil was examined in blood plasma ($\text{pH}=7.4$) during an 8-hour time span. A decline in concentration was observed from $95.9 \pm 1.3 \text{ ng/mL}$ at 0 h to $19.5 \pm 1.0 \text{ ng/mL}$ at 8 h as can be seen in Figure 3.2A. Interestingly, the addition of 0.2 v/v% formic acid stopped the degradation. The unknown degradation product that was formed was identified as remifentanil acid. Figure 3.2B shows the increase of this metabolite from $0.15 \pm 0.004\%$ at 0 h to $2.09 \pm 0.08\%$ at 8 h, relative to the concentration of $d_5. This degradation product is in accordance with literature, which describes remifentanil acid as major metabolite due to non-specific metabolism in blood and to a lesser extent the formation of norcarfentanil because of liver metabolism.^{25,30,31} Since the degradation was already observed in an alkaline solution ($\text{pH} > 7$) without the presence of a biological matrix, it appears that the stability of remifentanil is more affected by the pH than by specific blood or tissue enzymes.^{32,33}$

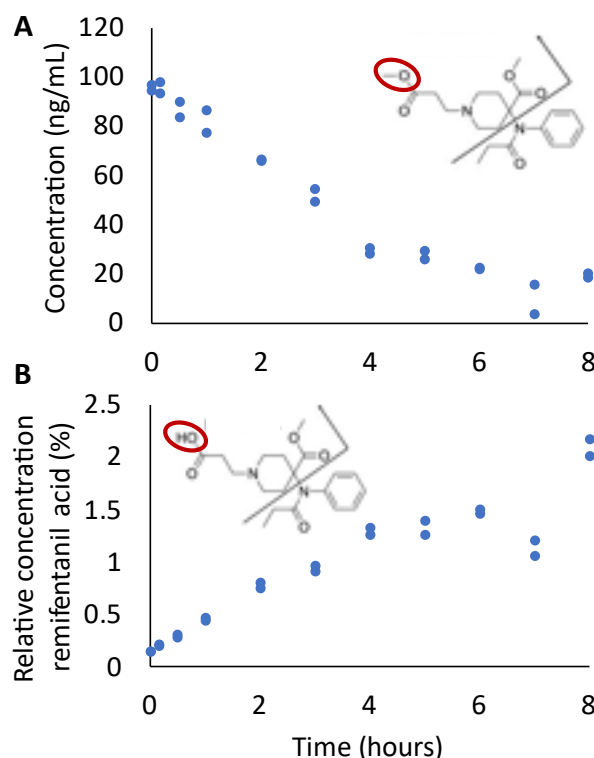


Figure 3.2. Stability remifentanil. A) Concentration remifentanil in blood plasma over time with molecular structure and transition fragment of remifentanil measured by LC-MS/MS. B) Ratio of remifentanil acid with internal standard $d_5 in blood plasma over time with molecular structure and transition fragment of remifentanil acid.$

Figure 3.3 shows representative LC-HRMS/MS total ion chromatograms for all fentanyl analogues synthesized with the Ugi and 7-step reaction. The parent compounds sufentanil (t_r : 8.16 min), benzylfentanyl (t_r : 6.80 min), carfentanil (t_r : 7.81 min), and remifentanil (t_r : 6.21 min) are clearly visible. Additionally, some impurities and metabolites are also highlighted: norfentanyl (t_r : 5.39 min), remifentanil acid (t_r : 5.98 min), $C_{17}H_{23}NO_3$ (R.R, t_r : 12.25 min), $C_{12}H_{27}NO_2$ (R.G, t_r : 6.77 min), and $C_{16}H_{35}NO_2$ (R.Q, t_r : 9.94 min). More details on the impurities are given in Section 3.3.2.

3.3.2. Impurity profiling

This section elaborates on the identified impurities in sufentanil, benzylfentanyl, remifentanil, and carfentanil samples detected by LC-HRMS/MS. Because of the low levels, no impurities could be identified by GC-MS and only the major compounds sufentanil, benzylfentanyl, and carfentanil were identified. Therefore, in the remainder of this study only the LC-HRMS/MS results are discussed. It should be emphasized that the results are based on a limited sample set and need to be verified by a larger data set in future research.

3.3.2.1. Sufentanil

Table 3.3 shows an overview of the most relevant impurities detected by LC-HRMS/MS in sufentanil samples synthesized according to the 7-step method. The impurities were present in all repeated measurements of only one synthesized batch. The tentative structures are based on comparison with reference databases or literature. In the pre-metabolism samples, a total of six impurities were identified. What stands out in the table is the presence of five precursors of the 7-step method in the pre-metabolism samples (S2-S6, also shown in Figure 3.1). In addition, the sixth impurity, thiofentanyl (S.G) is structurally similar to sufentanil and is most likely a synthesis by-product. Although only one synthesis route was examined, the presence of multiple precursors of the 7-step method is very characteristic and not expected in sufentanil synthesized using other precursors. However, to develop a full picture of possible impurities, additional studies will be needed that evaluate more synthesis methods.

In the post-metabolism samples, a total of nine impurities were identified, including two precursors. It is worth noting that precursor S5 could also be formed by metabolism of sufentanil via amide hydrolysis and demethylation. Interestingly, the other seven impurities are metabolites of the precursors S5 and S6. They can be formed because of N-dealkylation, (di)hydroxylation, or glucuronidation. These results indicate that characteristic synthesis information is retained after metabolism. This is a rather surprising outcome, since a batch with a high purity of 92.5% was examined.

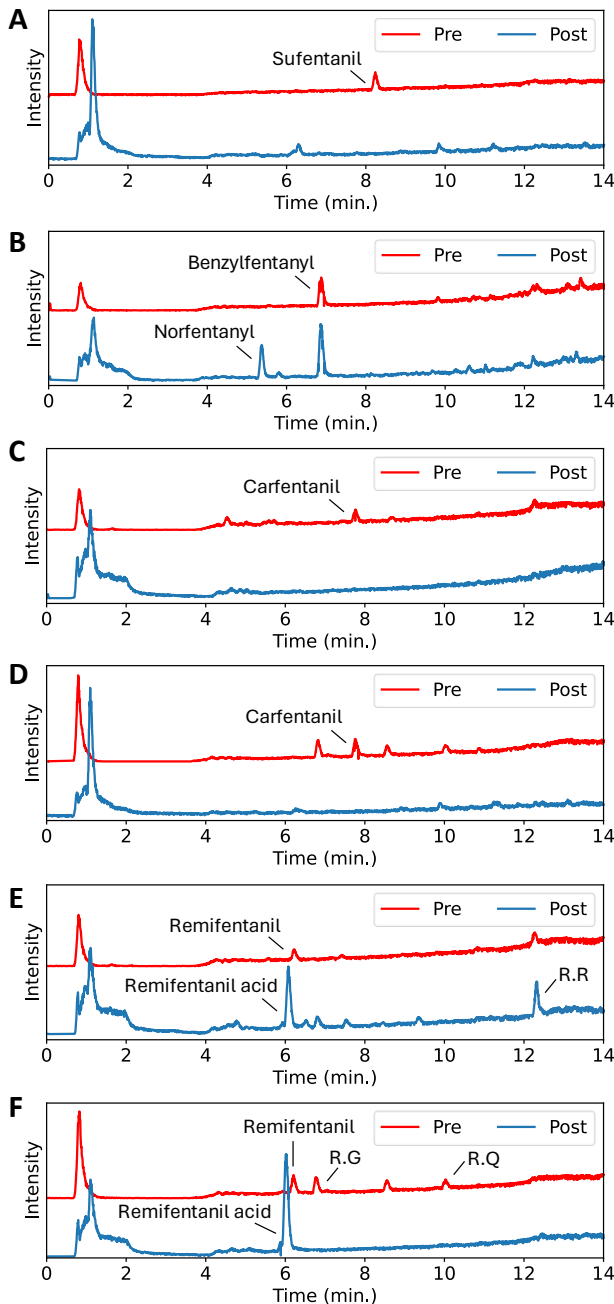


Figure 3.3. LC-HRMS/MS total ion chromatograms pre-metabolism (red) and post-metabolism (blue) for A) Sufentanil, B) Benzylfentanyl, C) Carfentanil synthesized with Ugi-reaction, D) Carfentanil synthesized with 7-step reaction, E) Remifentanil synthesized with Ugi-reaction, and F) Remifentanil synthesized with 7-step reaction. Visible impurities and metabolites have been highlighted: norfentanyl, remifentanil acid, C₁₇H₂₃NO₃ (R.R), C₁₂H₂₇NO₂ (R.G), and C₁₆H₃₅NO₂ (R.Q).

3 Chapter 3

Table 3.3. Pre- and post-metabolism impurities detected by LC-HRMS/MS for sufentanil synthesized according to the 7-step method. Chemicals are sorted by their mass.

Ref.	Name/ bio- transformation	Chemical formula	m/z	t _r (min)	Pre, post	Tentative structure
S.A	N-dealkylation S5†	C ₁₂ H ₁₈ N ₂ O	207.15	2.356	Post	
S.B	N-dealkylation of S6†	C ₁₃ H ₂₀ N ₂ O	221.165	4.754	Post	
S.C	S2†	C ₁₈ H ₂₁ N ₃ O	296.176	7.174	Pre, post	
S.D	S5†	C ₁₈ H ₂₄ N ₂ OS	317.168	6.264	Pre, post	
S.E	S6†	C ₁₉ H ₂₆ N ₂ OS	331.184	7.252	Pre	
S.F	Hydroxylation of S5†	C ₁₈ H ₂₄ N ₂ O ₂ S	333.164	5.63, 4.417	Post	
S.G	Thiofentanyl*	C ₂₀ H ₂₆ N ₂ OS	343.184	6.911	Pre	
S.H	Hydroxylation of S6†	C ₁₉ H ₂₆ N ₂ O ₂ S	347.179	5.882	Post	

S.I	Dihydroxylation of S5†	C ₁₈ H ₂₄ N ₂ O ₃ S	349.159	4.360, 4.261, 4.497	Post	
S.J	Sufentanil* GC	C ₂₂ H ₃₀ N ₂ O ₂ S	387.21	8.158	Pre, post	
S.K	S3†	C ₂₄ H ₂₇ N ₃ OS	406.195	8.797	Pre	
S.L	S4†	C ₂₅ H ₂₉ N ₃ OS	420.211	8.864	Pre	
S.M	N-dealkylation + glucuronidation of S5† OR N-dealkylation + demethylation + glucuronidation of sufentanil†	C ₂₁ H ₃₁ N ₂ O ₈	439.208	4.763	Post	
S.N	Hydroxylation + glucuronidation of S5†	C ₂₄ H ₃₂ N ₂ O ₇ S	493.201	5.928	Post	

*Identification with Compound Discoverer; †Identification and tentative structure determined by comparison with literature; ^{GC}Compound also detected using GC-MS

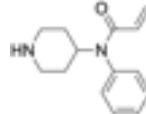
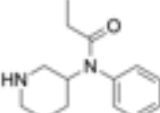
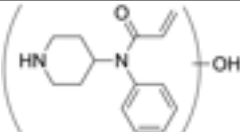
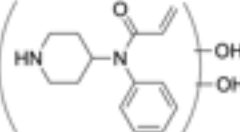
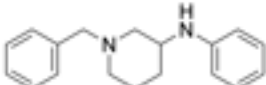
3.3.2.2. Benzylfentanyl

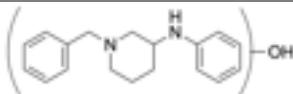
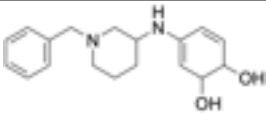
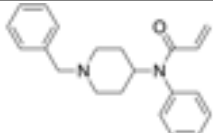
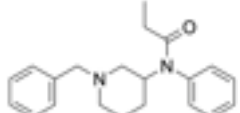
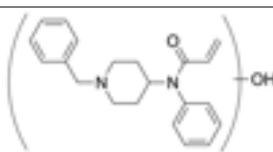
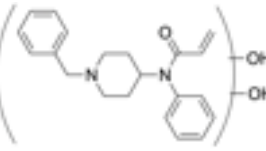
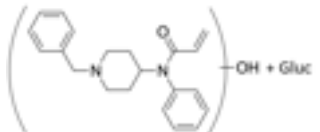
Table 3.4 lists the most important impurities detected by LC-HRMS/MS in benzylfentanyl samples synthesized using the Siegfried method. The impurities were present in all repeated measurements of only one synthesized batch. In the pre-metabolism samples, a total of three impurities were tentatively identified including the precursor 4-ANBP (B.F). The structurally similar marker 4-ANPP was also found to be indicative of fentanyl synthesized by the Siegfried method.¹⁴ The authors demonstrated that the marker was present in much higher amounts in the fentanyl samples synthesized by the Siegfried method compared to the Gupta method that produces fentanyl using a single reaction vessel. In addition, benzyl isobutyl ketone

(B.A) was identified as a marker. This compound has not been used for other industrial or pharmaceutical applications and may be specific for the synthesis of benzylfentanyl. Also, benzyl acrylfentanyl (B.I) was identified, which is structurally similar to benzylfentanyl.

As expected, norfentanyl was detected in post-metabolism samples. Furthermore, a total of eleven impurities were identified after in-vitro metabolism, including all markers that were detected in pre-metabolism samples. Of interest here is the presence of both the intact precursor 4-ANBP and its metabolites B.G and B.H. Likewise, benzyl acrylfentanyl (B.I) is also present as an intact marker in the post-metabolism samples and in its various metabolic forms. The remaining six impurities (B.B, B.D, B.E, B.K, B.L, and B.M) are (di)hydroxylation, glucuronidation, or N-dealkylation metabolites of benzyl acrylfentanyl (B.I). Similar to the results obtained for sufentanil, this data also show that characteristic synthesis information is potentially retained after metabolism. In this case the purity of the batch was even higher (98.3%).

Table 3.4. Pre- and post-metabolism impurities detected by LC-HRMS/MS for benzylfentanyl synthesized using the last step of the Siegfried method.

Ref.	Name / bio-transformation	Chemical formula	m/z	t _r (min)	Pre, post	Tentative structure
B.A	Benzyl isobutyl ketone*	C ₁₂ H ₁₆ O	177.128	6.853	Pre, post	
B.B	N-dealkylation of benzyl acrylfentanyl†	C ₁₄ H ₁₈ N ₂ O	231.150	5.247	Post	
B.C	Norfentanyl†	C ₁₄ H ₂₀ N ₂ O	233.165	5.394	Post	
B.D	N-dealkylation + hydroxylation of benzyl acrylfentanyl†	C ₁₄ H ₁₈ N ₂ O ₂	247.145	4.783, 6.905	Post	
B.E	N-dealkylation + dihydroxylation of benzyl acrylfentanyl†	C ₁₄ H ₁₈ N ₂ O ₃	263.14	5.251, 5.508	Post	
B.F	4-ANBP†	C ₁₈ H ₂₂ N ₂	267.186	6.393	Pre, post	

B.G	Hydroxylation of 4-ANBP†	C ₁₈ H ₅₅ N ₂ O	283.181	6.242	Post	
B.H	Dihydrodiol formation of 4-ANBP†	C ₁₈ H ₂₄ N ₂ O ₂	301.192	5.545	Post	
B.I	Benzyl acrylfentanyl*	C ₂₁ H ₂₄ N ₂ O	321.197	6.667	Pre, post	
B.J	Benzylfentanyl* GC	C ₂₁ H ₂₆ N ₂ O	323.212	6.798	Pre, post	
B.K	Hydroxylation of benzyl acrylfentanyl†B	C ₂₁ H ₂₄ N ₂ O ₂	337.192	5.99, 6.299	Post	
B.L	Dihydroxylation of benzyl acrylfentanyl†	C ₂₁ H ₂₄ N ₂ O ₃	353.189	6.076, 6.537	Post	
B.M	Hydroxylation + glucuronidation of benzyl acrylfentanyl†	C ₂₇ H ₃₂ N ₂ O ₇	513.224	5.756	Post	

*Identification with Compound Discoverer; †Identification and tentative structure determined by comparison with literature; ^{GC}Compound also detected using GC-MS

3.3.2.3. Remifentanil

Table 3.5 provides an overview of the most important impurities detected by LC-HRMS/MS in remifentanil samples synthesized by the 7-step and Ugi method. The impurities were present in all repeated measurements of two batches for the Ugi method synthesized by different scientists and one batch for the 7-step method. A more elaborate table with 18 additional markers is shown in Section S2 of the Supplementary data. For these additional impurities no tentative structure could be established, so only the chemical formula and mass are provided. As expected, norcarfentanil was detected in the post-metabolism samples and remifentanil acid was detected in all samples. In the pre-metabolism samples, a total of nine impurities were identified. Seven impurities were only detected in samples produced by the 7-step

synthetic route, while one marker was only detected in the samples synthesized by the Ugi-method, and one was present in both types of samples.

In post-metabolism samples, a total of thirteen impurities were identified. Four impurities were specific for the 7-step synthetic route, nine markers were only detected in the samples synthesized by the Ugi-method, and one was present in both types of samples. Only the precursor aniline could be tentatively identified in the post-metabolism samples as marker for the Ugi-reaction. It should be noted that this impurity is a commonly used precursor for a wide range of chemicals. However, it is toxic to humans therefore it is avoided in prescription drugs.^{34,35} Interestingly, this precursor was also detected in post-metabolism fentanyl samples synthesized by the Gupta and Siegfried method.¹⁴ Since most impurities could not be tentatively identified by comparison with databases, further work can focus on elucidating the structures by NMR analysis or comparison with reference standards.

Table 3.5. Pre- and post-metabolism impurities detected by LC-HRMS/MS for remifentanil synthesized according to the 7-step and Ugi-method.

Ref.	Name/ bio- transformation	Chemical formula	m/z	t _r (min)	Pre, post	Method	Tentative structure
R.A	Aniline	C ₆ H ₇ N	94.065	1.458	Post	Ugi	
R.B	Norcarfentanil (CR6)*	C ₁₆ H ₂₂ N ₂ O ₃	291.170	5.871	Post	7-step, Ugi	
R.C	Remifentanil acid†	C ₁₉ H ₂₆ N ₂ O ₅	363.191	5.975	Pre, post	7-step, Ugi	
R.D	Remifentanil*	C ₂₀ H ₂₈ N ₂ O ₅	377.207	6.206	Pre, post	7-step, Ugi	

*Identification with Compound Discoverer; †Identification and tentative structure determined by comparison with literature

3.3.2.4. Carfentanil

Table 3.6 provides an overview of the most important impurities detected by LC-HRMS/MS in carfentanil samples synthesized according to the 7-step and Ugi-method. The impurities were present in all repeated measurements of four batches for the Ugi method synthesized by different scientists and one batch for the 7-step method. A more elaborate table with 18 additional impurities without structural identification is

shown in Section S3 of the Supplementary data. In the pre-metabolism samples, a total of sixteen impurities were detected. In addition, norcarfentanil was detected which is not only a metabolite, but also a precursor in the 7-step synthesis method of carfentanil. Three impurities were specific for the 7-step synthetic route and thirteen markers were only detected in the samples synthesized by the Ugi-method. What is striking about these results is that different precursors were found for both synthetic methods, indicating the potential of attribution studies. The 7-step synthesis intermediate benzyl carfentanil (CR5, Ref. C.E) was only detected in the 7-step samples and the precursors of the Ugi-method aniline and C1 (C.G) were present in a considerable higher concentration in the Ugi-batches. Interestingly, eight other impurities with m/z 218.154, 222.149, 258.149, 290.176, 319.202, 324.208, 329.202, and 367.202 (C.H, C.I, C.L, C.M, C.P, C.Q, C.R, C.S, and C.W) indicative of the Ugi-method were also found by Mörén et al. as selective markers for this synthesis route.²²

A total of fifteen markers were found in the post-metabolism samples, including seven impurities that were also found in pre-metabolism samples. Five of these were also identified by Mörén et al.²² Remarkably, one of these impurities was only present in the post-metabolism samples in the current study. Probably this concentration was below the detection limit in the pre-metabolism samples. Two impurities were specific for the 7-step synthetic route and thirteen markers were only detected in the samples synthesized by the Ugi-method. Closer inspection of the table shows N-phenylacetamide (C.B) as post-metabolism marker of the Ugi-method, which was also identified in earlier studies as N-acetylation metabolite of the fentanyl precursor aniline.^{14,36} Similar to aniline itself, this compound is toxic due to interference with the oxygen transport by hemoglobin.³⁵ Although it has been used as an analgesic in the past, it has been replaced by the commonly used aniline derivative and pain killer acetaminophen (paracetamol). Therefore, it is not anticipated to find N-phenylacetamide in regular prescription drugs. Additionally, acetaminophen (C.C) was identified, which is a hydroxylation product of N-phenylacetamide.³⁵ This compound is often mixed with illicit drugs and is for this reason not a specific marker for carfentanil synthesis. Finally, (di)hydroxylation metabolites of pre-metabolism impurities were detected. For some impurities, the intact impurity and its metabolite were both detected in the post-metabolism impurity profile. Although a lower concentration was analyzed due to the potency of carfentanil, still a lot of characteristic impurities were detected in both crude and purified batches.

Table 3.6. Pre- and post-metabolism impurities detected by LC-HRMS/MS for carfentanil synthesized according to the 7-step and Ugi method.

Ref.	Name/ bio-transformation	Chemical formula	m/z	t _r (min)	Synthetic route	Pre, post	Tentative structure
C.A	Aniline*	C ₆ H ₇ N	94.065	6.85	Ugi	Pre	
C.B	N-phenylacetamide 14,36	C ₈ H ₉ NO	136.073	4.93	Ugi	Post	
C.C	Hydroxylation + N-acetylation of aniline ³⁶	C ₈ H ₉ NO ₂	152.071	7.57	Ugi	Post	
C.D	Norcarfentanil (CR6)	C ₁₆ H ₂₂ N ₂ O ₃	291.170	5.87	7-step, Ugi	Pre, post	
C.E	Benzyl carfentanil (CR5)	C ₂₃ H ₂₈ N ₂ O ₃	381.218	7.30	7-step	Pre	
C.F	Carfentanil* ^{GC}	C ₂₄ H ₃₀ N ₂ O ₃	395.233	7.81	7-step, Ugi	Pre, post	
C.G	C1*	C ₂₉ H ₃₇ N ₃ O ₂	460.296	13.03	Ugi	Pre	

*Identification with Compound Discoverer; †Identification and tentative structure determined by comparison with literature; ^{GC}Compound also detected using GC-MS.

3.3.3. Match criterion approach

Within forensic investigations it is often difficult to ascertain the exact exposure concentration. Since, the absolute amounts of the impurities are dependent on this level, normalization is required to correct for this. Table 3.7 shows the responses of three distinctive impurities after in-vitro metabolism of remifentanil relative to the response of remifentanil acid, due to the absence of remifentanil itself. The results are presented of six repeated measurements of one batch of remifentanil produced by the 7-step method and in total six measurements of two batches of remifentanil produced

by the Ugi method. The impurities aniline and R.H ($C_{12}H_{14}N_2O_2$, m/z 219.113) are characteristic for the Ugi synthesis method and R.G ($C_{12}H_{27}NO_2$, m/z 218.212) is distinctive to the 7-step method. It is apparent from this table that there are no overlapping ranges. A sensitive value is the ratio of R.H/R.G which is 33,000 times larger for the Ugi method compared to the 7-step method. Also, the ratio aniline/R.G gives a value that is 240 times higher for the Ugi method compared to the 7-step method. This approach can serve as a relatively straightforward tool to discriminate between synthetic routes, although more batches should be analyzed to verify these results.

Table 3.7. Characteristic relative responses of remifentanil impurities for the 7-step and Ugi-method. The 95% confidence interval is shown (n=6). Responses are relative to the peak area of remifentanil acid.

Impurity	7-step (%)	Ugi (%)
Aniline	0 - 1.01	16.1 - 17.8
R.G	0.012 - 0.037	0.0002 - 0.0077
R.H	0 - 0.01	17.3 - 30.6

Additionally, characteristic relative responses were found for carfentanil impurities, after in-vitro metabolism. Table 3.8 shows the 95% confidence intervals of six characteristic markers for the 7-step or Ugi method. The results are presented of nine repeated measurements of one batch of carfentanil produced by the 7-step method and in total 19 measurements of four batches of carfentanil produced by the Ugi method. The marker C.Y was characteristic for the 7-step method and all other markers were distinctive to the Ugi method. Some overlap was visible in responses of C.Y for the 7-step and the Ugi method. Nonetheless, a valuable ratio would be C.Y/C.T which is 88 times larger for the 7-step method compared to the Ugi method. The 95% confidence intervals of more impurities of remifentanil and carfentanil can be found in Section S4 of the Supplementary Information.

Table 3.8. Characteristic relative responses of carfentanil impurities for the 7-step (n=9) and Ugi-method (n=19). The 95% confidence interval is shown. Responses are relative to the peak area of carfentanil.

Impurity	7-step (%)	Ugi (%)
C.K	0.8 - 6.8	18.7 - 67.4
C.N	1.4 - 3.5	5.7 - 49.8
C.P	1.2 - 3.1	11.8 - 22.3
C.T	1.1 - 3.1	3.6 - 54.4
C.V	1.4 - 3.7	5.5 - 39.5
C.Y	34 - 315	0 - 57

3.3.4. Chemometric comparison

3.3.4.1. Remifentanil

Multivariate data analysis was applied to LC-HRMS/MS data to differentiate between the 7-step and Ugi synthetic route. First, PCA was applied to reduce the dimensionality and to identify discriminating impurities after in-vitro metabolism. Figure 3.4A shows the PCA score plot of the first two principal components (PCs) for post-metabolism remifentanil samples. The first PC accounts for 61% of the variance. Excellent separation of the two synthesis methods is visible, which is fully achieved by the first principal component and predominantly caused by impurities from the Ugi method (Figure 3.4B). Of interest here are the characteristic impurities R.G, R.H, and aniline (R.A) that were also considered for the match criterion approach. Likewise, good separation was observed for the pre-metabolism samples (section S5 in the Supplementary data). As expected, all impurities contribute to the separation, since most markers were either found in the Ugi batch or in the 7-step samples, without overlapping responses. The robustness of the PCA model was demonstrated by its consistent explained variance even when a sample was excluded. The leave-one-out validation plots are provided in Section S5 of the Supplementary information.

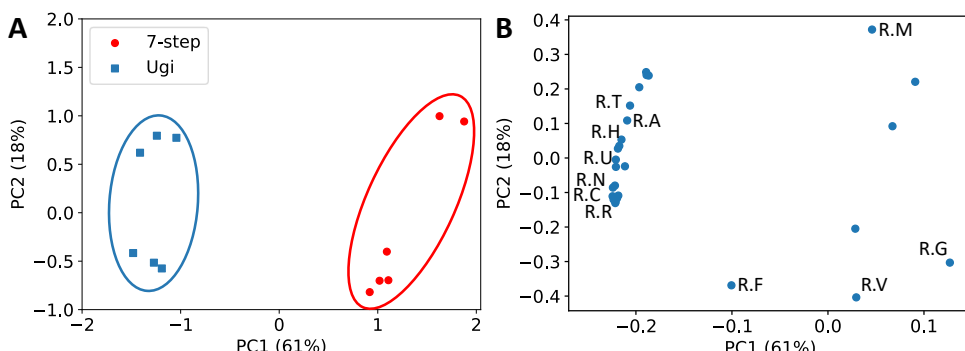


Figure 3.4. A) PCA-score plot of post-metabolism samples of remifentanil synthesized by the 7-step (red circle) and Ugi (blue square) method. B) Corresponding PCA loading plot with highlighted impurities.

Additionally, LDA was applied to achieve maximum discrimination between the two distinct groups. Since the number of impurities were in the same range as the number of samples, The first six principal components of PCA (94% of the variance) were used as input for the LDA.³⁷ Figure 3.5 shows the LDA scores and corresponding LRs with ELUB bounds for post-metabolism samples of remifentanil for both synthesis routes. Perfect separation was visible with false positive and false negative error rates near zero. The uncalibrated LR values without ELUB bounds were in the range of 10^{-200} to 10^{100} . Since, a limited number of samples were analyzed, the corrected LRs were much

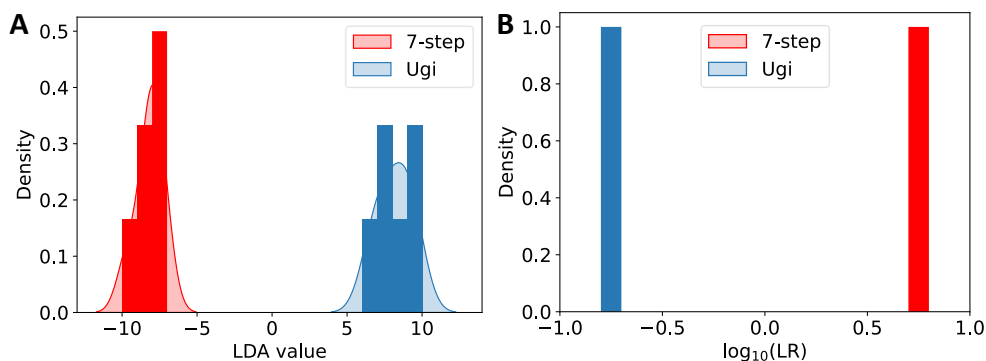


Figure 3.5. A) LDA score plot B) Corrected distribution of \log_{10} LRs with ELUB bounds, for remifentanil post-metabolism samples of 7-step synthesis (red) and Ugi method (blue), analyzed with LC-HRMS/MS. The bars show the frequency of the measurements, and the shaded curves represent the kernel density estimations.

3.3.4.2. Carfentanil

In accordance with the remifentanil results, the application of PCA to carfentanil samples after in-vitro metabolism also provided separation of the 7-step and Ugi synthesis methods. Figure 3.6 presents the PCA score plot with loadings of the first two PCs for post-metabolism carfentanil samples. The first PC accounts for only 34% of the variance and the second PC for 25%. It is worth noting that both components are required for separation, where the first PC is mostly dominated by C.P which is a characteristic marker for the Ugi method. The second component is predominantly composed of C.N, C.T, C.U, and C.V, which are also distinctive Ugi markers. The various batches are clearly distinguished. The Ugi samples in the top left are the purified samples, the samples in the left bottom are unpurified samples, and the samples in the right bottom are two other batches of unpurified samples synthesized by two different chemists. These results indicate that slight differences in purification can provide characteristic information. An advantage of this is that the impurity profiles can be used

to link a case sample to a specific production facility. Additionally, discrimination was observed for the pre-metabolism samples and the leave-one-out validation plots show robustness of the PCA model (Section S6 of the Supplementary information). Interestingly, consistent with the remifentanil results, aniline (C.A) is an important marker for the pre-metabolism carfentanil samples synthesized by the Ugi method. It is somewhat surprising that C.I ($C_{13}H_{19}NO$, m/z 222.149) and C.W ($C_{22}H_{26}N_2O_3$, m/z 367.202) were found to be discriminating markers for the second principal component. These markers were previously identified as indicative of the Ugi method but were found in similar levels in samples synthesized by the 7-step in this study. It may be possible that these markers are not specific for a synthesis route. An alternative explanation for this result is that the compounds are isomers since no structural identification is provided.

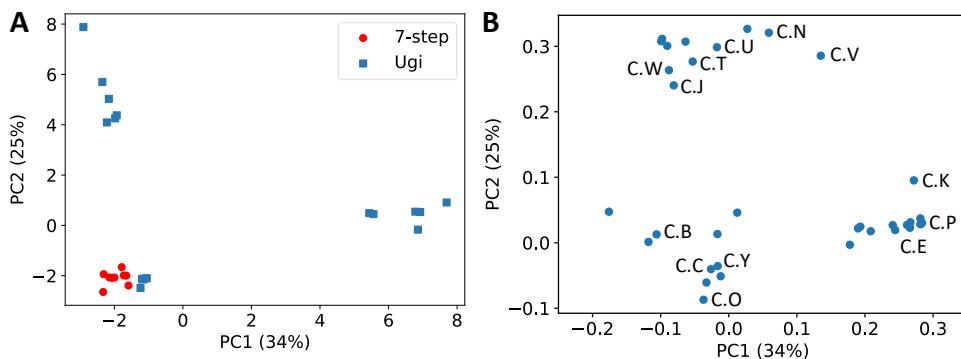


Figure 3.6. PCA-score plot of post-metabolism samples of carfentanil synthesized by the 7-step (red circle) and Ugi (blue square) method. B) Corresponding PCA loading plot with highlighted impurities.

To accomplish maximum separation, LDA was constructed using the first six PCs of the PCA (81% of the variance). Figure 3.7 illustrates the LDA distribution and corresponding LR scores with ELUB bounds for post-metabolism samples of carfentanil synthesized with the 7-step and Ugi method. The KDEs in the LDA plot show some overlap, meaning that a small fraction of the 7-step has an LR larger than 1 and a small fraction of the Ugi samples has an LR smaller than 1. Consequently, the rate of false negative results is 11% for the 7-step method and 8.6% for the Ugi synthesis method. No false positives and false negatives were found for the corrected ELUB LR distribution. Subsequently, the uncorrected LRs were in the range of 10^{-3} to 10^{45} . In comparison with the remifentanil results, the corrected ELUB LR values were slightly higher between 0.11 and 16. Section S6 of the Supplementary data presents the Tippett plots and pre-metabolism results. Extremely low error rates below 0.00013% were found for the uncorrected pre-metabolism distribution of carfentanil and no misleading evidence was calculated for the ELUB LR plot. The LR distribution without correction was between 10^{-100} and 10^{150} . These values were reduced to 0.083 to 13 after applying ELUB

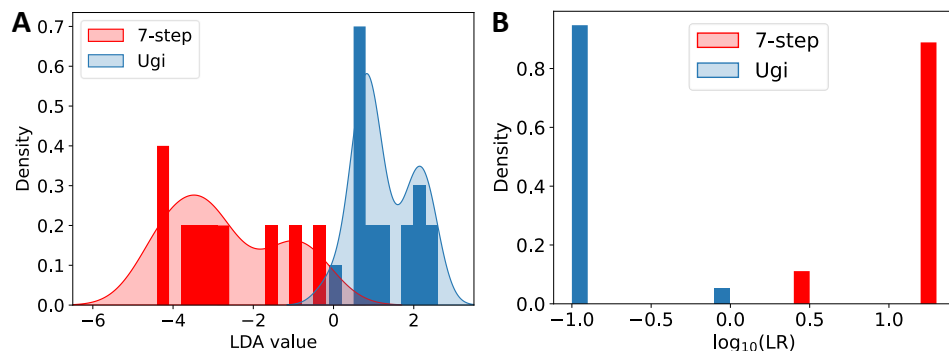


Figure 3.7. A) LDA score plot B) Corrected distribution of \log_{10} LRs with ELUB bounds, for carfentanil post-metabolism samples of 7-step synthesis (red) and Ugi method (blue), analyzed with LC-HRMS/MS. The bars show the frequency of the measurements, and the shaded curves represent the kernel density estimations.

3.3.5. Application in forensic casework

This section elaborates on the translation of the in-vitro impurity profiles to concentrations expected in forensic casework. Formin et al. reported carfentanil concentrations ranging from 2.7 – 10.4 ng/mL in urine samples of ten people and 0.2 – 9.3 ng/mL in blood samples of nine people that died from drug overdoses involving carfentanil.³⁸ In addition, Shanks and Behonick identified carfentanil in 262 postmortem toxicology casework samples in the range of 0.01 – 2 ng/mL.³⁹ It was hypothesized that carfentanil originated from contaminated street heroin. This was confirmed by several case studies where people were found dead after using heroin or other drugs. In most cases, the cause of death was confirmed as carfentanil intoxication or mixed drug intoxication. Concentrations associated with fatality from carfentanil were in the range of 0.01 – 0.6 ng/mL measured in femoral, iliac, cardiac, and subclavian blood.³⁹ In the current study, incubation was performed with a higher concentration of 1 µg/mL carfentanil, however the measured concentrations after metabolism were between 0.09 – 5.9 ng/mL. This is in the same range as established in the carfentanil case studies.

Several other studies investigated life-threatening remifentanil concentrations. Riches et al. analyzed a urine sample of a casualty who had survived the Moscow theatre

siege.²⁵ This siege was stopped by using aerosolized carfentanil and remifentanil. Traces of approximately 0.1 ng/mL norcarfentanil were found in urine five days after exposure, but it lacked traces of remifentanil (acid). Another study by Vanneste et al. discussed an acute remifentanil overdose where rapid intravenous injection of remifentanil occurred due to misuse of a syringe pump.⁴⁰ In this case, the calculated plasma concentration of 150 ng/mL remifentanil was considerably higher. In the present study, incubation was performed with a relatively high concentration of 100 µg/mL remifentanil. However, a much lower concentration below the detection limit of 5 ng/mL was measured after metabolism. Therefore, the detected concentration may be in the range expected in real overdose fatalities, but further research is required to establish the detection limits and to confirm casework concentrations. Currently, there are no post-mortem toxicological reports published for sufentanil. Since the lethal dose is comparable to remifentanil, it is expected that similar trace concentrations will be found.

Additionally, benzylfentanyl has been encountered in biomedical casework samples. Adamowicz et al. identified benzylfentanyl in two fatal cases along with fentanyl, norfentanyl, and other drugs.⁴¹ Concentrations of 67 – 110 ng/mL benzylfentanyl and 22 – 41 ng/mL norfentanyl were measured in postmortem blood samples. In the present study, a concentration of 100 µg/mL benzylfentanyl was applied. After incubation a concentration of 38 ng/mL benzylfentanyl and 14 ng/mL norfentanyl was detected. These concentrations are lower than encountered in the described casework samples. Therefore, the method is sensitive enough for potential impurity profiling in forensic casework.

Finally, it would be valuable if impurity profiling can be applied at the individual batch level. The current study mainly identified synthesis specific impurities. In this case, the impurity profile can be used to classify the synthesis method and gather intelligence information. The evidential value of the chemical attribution signature is then dependent on the rarity of the synthesis method. However, the present research also identified various markers for different batches. This suggests that it would be possible to link a sample to a specific laboratory. These variations can for example occur due to the application of different raw materials, concentrations, laboratory instruments, and purification methods. Additionally, the present study demonstrated that the same or related impurities were found in pre-metabolism batches compared to samples after metabolism. This indicates the potential of matching a profile of a blood sample of an exposed victim to a batch of intact material. It is therefore likely that post-metabolism impurity profiling can be applied to retrieve information about the production route and to link a casework sample to a specific laboratory. This should however be confirmed by analyzing biomedical case work samples from victims.

3.4. Conclusions

The present study was designed to investigate the effect of human metabolism on the impurity profile of synthetic opioids carfentanil, remifentanil, sufentanil, and benzylfentanyl. Characteristic impurities were identified in pre- and post-metabolism samples with LC-HRMS/MS. It is important to note that the results were based on a limited sample set and should be interpreted with caution. This study has highlighted 12-24 markers for each fentanyl analogue. A major finding was the presence of precursors of the 7-step, Ugi, and Siegfried synthesis method in the post-metabolism samples, indicating that specific synthesis information is retained after metabolism. Additionally, N-dealkylation, (di)hydroxylation, and glucuronidation metabolites of precursors S5 (m/z 317.168) and S6 (m/z 331.184) were detected in the sufentanil samples. Also, metabolites of 4-ANBP, aniline, and N-phenylacetamide were identified in post-metabolism samples of benzylfentanyl, remifentanil, and carfentanil, respectively. The match criterion approach for remifentanil has shown that the impurities aniline and R.H ($C_{12}H_{14}N_2O_2$, m/z 219.113) are characteristic markers for the Ugi synthesis method and R.G ($C_{12}H_{27}NO_2$, m/z 218.212) is distinctive to the 7-step method. For carfentanil C.T ($C_{18}H_{26}N_2O_4$, m/z 335.197) was identified as an important marker for the Ugi method and C.Y ($C_{26}H_{49}NO_9$, m/z 520.349) for the 7-step method. The importance of these markers was supported by PCA, used to classify the synthesis method. Subsequently, another distinct impurity, C.P ($C_{18}H_{26}N_2O_3$, m/z 319.202), emerged in pre- and post-metabolism samples of carfentanil. The method was found to be sensitive enough for potential impurity profiling in forensic casework. LDA was applied to maximize discriminative power and KDE was used to express likelihood ratios for assigning unknown samples. Separation between the synthesis routes was obtained. Corrected likelihood ratios with ELUB bounds were in the range of 0.083 to 16. Although the small LR range reflects the limited dataset, the findings show the potential of constructing likelihood ratio models for post-metabolism impurity profiling to facilitate forensic investigations. Future studies should investigate the syntheses variations encountered in forensic casework. In addition, further research needs to be done to validate the in-vitro model in real human biological samples. In conclusion, this work is consistent with the earlier observations of post-metabolism impurity profiling of fentanyl and demonstrates the potential of using biomedical samples for retrieving information about the production method of synthetic opioids after exposure.

References

- (1) Heslop, D. J.; Blain, P. G. Threat Potential of Pharmaceutical Based Agents. *Intelligence and National Security* **2020**, *35* (4), 539–555. <https://doi.org/10.1080/02684527.2020.1750158>.
- (2) Suzuki, J.; El-Haddad, S. A Review: Fentanyl and Non-Pharmaceutical Fentanyls. *Drug Alcohol Depend* **2017**, *171*, 107–116. <https://doi.org/10.1016/j.drugalcdep.2016.11.033>.
- (3) Kuczyńska, K.; Grzonkowski, P.; Kacprzak, Ł.; Zawińska, J. B. Abuse of Fentanyl: An Emerging Problem to Face. *Forensic Sci Int* **2018**, *289*, 207–214. <https://doi.org/10.1016/j.forsciint.2018.05.042>.
- (4) Tin, D.; Kallenborn, Z.; Hart, A.; Hertelendy, A. J.; Ciottone, G. R. Opioid Attack and the Implications for Counter-Terrorism Medicine. *Prehosp Disaster Med* **2021**, *36* (6), 661–663. <https://doi.org/10.1017/S1049023X21001059>.
- (5) Wax, P. M.; Becker, C. E.; Curry, S. C. Unexpected “Gas” Casualties in Moscow: A Medical Toxicology Perspective. *Ann Emerg Med* **2003**, *41* (5), 700–705. <https://doi.org/10.1067/mem.2003.148>.
- (6) Daéid, N. N.; Waddell, R. J. H. The Analytical and Chemometric Procedures Used to Profile Illicit Drug Seizures. *Talanta* **2005**, *67* (2), 280–285. <https://doi.org/10.1016/j.talanta.2005.05.018>.
- (7) Marcaccini, S.; Torroba, T. The Use of the Ugi Four-Component Condensation. *Nat Protoc* **2007**, *2*, 632–639. <https://doi.org/10.1038/nprot.2007.71>.
- (8) Malaquin, S.; Jida, M.; Gesquiere, J. C.; Deprez-Poulain, R.; Deprez, B.; Laconde, G. Ugi Reaction for the Synthesis of 4-Aminopiperidine-4-Carboxylic Acid Derivatives. Application to the Synthesis of Carfentanil and Remifentanil. *Tetrahedron Lett* **2010**, *51* (22), 2983–2985. <https://doi.org/10.1016/j.tetlet.2010.03.120>.
- (9) Cores, Á.; Clerigué, J.; Orocio-Rodríguez, E.; Menéndez, J. C. Multicomponent Reactions for the Synthesis of Active Pharmaceutical Ingredients. *Pharmaceutics* **2022**, *15* (8), 1009. <https://doi.org/10.3390/ph15081009>.
- (10) Butcher, K. J.; Hurst, J. Aromatic Amines as Nucleophiles in the Bargellini Reaction. *Tetrahedron Lett* **2009**, *50* (21), 2497–2500. <https://doi.org/10.1016/j.tetlet.2009.03.044>.
- (11) Serafini, M.; Murgia, I.; Giustiniano, M.; Pirali, T.; Tron, G. C. The 115 Year Old Multicomponent Bargellini Reaction: Perspectives and New Applications. *Molecules* **2021**, *26* (3), 558. <https://doi.org/10.3390/molecules26030558>.
- (12) Walz, A. J.; Hsu, F.-L. Synthesis of 4-Anilinopiperidine Methyl Esters, Intermediates in the Production of Carfentanil, Sufentanil, and Remifentanil. *Tetrahedron Lett* **2014**, *55* (2), 501–502. <https://doi.org/10.1016/j.tetlet.2013.11.058>.
- (13) Mathew, J.; Killgore, J. K. Methods for the Synthesis of Alfentanil, Sufentanil, and Remifentanil. US7208604B2, 2000.
- (14) de Bruin-Hoegée, M.; Kleiweg, D.; Noort, D.; van Asten, A. C. Chemical Attribution of Fentanyl: The Effect of Human Metabolism. *Forensic Chemistry* **2021**, *24*, 100330. <https://doi.org/10.1016/j.forc.2021.100330>.
- (15) Stojanovska, N.; Fu, S.; Tahtouh, M.; Kelly, T.; Beavis, A.; Kirkbride, K. P. A Review of Impurity Profiling and Synthetic Route of Manufacture of Methylamphetamine, 3,4-Methylenedioxymethylamphetamine, Amphetamine, Dimethylamphetamine and p-Methoxyamphetamine. *Forensic Sci Int* **2013**, *224* (1–3), 8–26. <https://doi.org/10.1016/j.forsciint.2012.10.040>.
- (16) Inoue, H.; Iwata, Y. T.; Kuwayama, K. Characterization and Profiling of Methamphetamine Seizures. *Journal of Health Science* **2008**, *54* (6), 615–622. <https://doi.org/10.1248/jhs.54.615>.
- (17) Onoka, I.; Banyika, A. T.; Banerjee, P. N.; Makangara, J. J.; Dujourdy, L. A Review of the Newly Identified Impurity Profiles in Methamphetamine Seizures. *Forensic Sci Int* **2020**, *2*, 194–205. <https://doi.org/10.1016/j.fsisyn.2020.06.004>.
- (18) Lociciro, S.; Hayoz, P.; Esseiva, P.; Dujourdy, L.; Besacier, F.; Margot, P. Cocaine Profiling for Strategic Intelligence Purposes, a Cross-Border Project between France and Switzerland. Part I. Optimisation and Harmonisation of the Profiling Method. *Forensic Sci Int* **2007**, *167* (2–3), 220–228. <https://doi.org/10.1016/j.forsciint.2006.06.052>.

- (19) Dams, R.; Benijts, T.; Lambert, W. E.; Massart, D. L.; De Leenheer, A. P. Heroin Impurity Profiling: Trends throughout a Decade of Experimenting. *Forensic Sci Int* **2001**, *123* (2–3), 81–88. [https://doi.org/10.1016/S0379-0738\(01\)00541-2](https://doi.org/10.1016/S0379-0738(01)00541-2).
- (20) Ovenden, S. P. B.; McDowall, L. J.; McKeown, H. E.; McGill, N. W.; Jones, O. A. H.; Pearson, J. R.; Petricevic, M.; Rogers, M. L.; Rook, T. J.; Williams, J.; Webster, R. L.; Zanatta, S. D. Investigating the Chemical Impurity Profiles of Fentanyl Preparations and Precursors to Identify Chemical Attribution Signatures for Synthetic Method Attribution. *Forensic Sci Int* **2021**, *321*, 110742. <https://doi.org/10.1016/j.forsciint.2021.110742>.
- (21) Mayer, B. P.; Valdez, C. A.; DeHope, A. J.; Spackman, P. E.; Williams, A. M. Statistical Analysis of the Chemical Attribution Signatures of 3-Methylfentanyl and Its Methods of Production. *Talanta* **2018**, *186*, 645–654. <https://doi.org/10.1016/j.talanta.2018.02.026>.
- (22) Mörén, L.; Lindén, P.; Qvarnström, J.; Engqvist, M.; Carlsson, M.; Afshin Sander, R.; Lindberg, S.; Larsson, A.; Östin, A. Classification of Carfentanil Synthesis Methods Based on Chemical Impurity Profile. *Forensic Chemistry* **2021**, *26*, 100355. <https://doi.org/10.1016/j.forc.2021.100355>.
- (23) van der Meer, J. A.; Trap, H. C.; Noort, D.; van der Schans, M. J. Comprehensive Gas Chromatography with Time of Flight MS and Large Volume Introduction for the Detection of Fluoride-Induced Regenerated Nerve Agent in Biological Samples. *Journal of Chromatography B* **2010**, *878* (17–18), 1320–1325. <https://doi.org/10.1016/j.jchromb.2010.02.019>.
- (24) John, H.; Schans, M. J. van der; Koller, M.; Spruit, H. E. T.; Worek, F.; Thiermann, H.; Noort, D.; John, H. Fatal Sarin Poisoning in Syria 2013: Forensic Verification within an International Laboratory Network. *Forensic Toxicol* **2018**, *36*, 61–71. <https://doi.org/10.1007/s11419-017-0376-7>.
- (25) Riches, J. R.; Read, R. W.; Black, R. M.; Cooper, N. J.; Timperley, C. M. Analysis of Clothing and Urine from Moscow Theatre Siege Casualties Reveals Carfentanil and Remifentanil Use. *J Anal Toxicol* **2012**, *36* (9), 647–656. <https://doi.org/10.1093/jat/bks078>.
- (26) Pedregosa, F.; Varoquaux, G.; Gramfort, A.; Michel, V.; Thirion, B.; Grisel, O.; Blondel, M.; Prettenhofer, P.; Weiss, R.; Dubourg, V.; Vanderplas, J.; Passos, A.; Cournapeau, D.; Brucher, M.; Perrot, M.; Duchesnay, E. Scikit-Learn: Machine Learning in Python. *Journal of Machine Learning Research* **2011**, *12*, 2825–2830. <https://doi.org/10.48550/arXiv.1201.0490>.
- (27) Netherlands Forensic Institute. LIR Python Likelihood Ratio Library. 2024. <https://github.com/NetherlandsForensicInstitute/lir> (accessed 2024-01-09).
- (28) de Bruin-Hoegée, M.; de Bruin, G. J. Python Code for Chemical Attribution of Fentanyl. 2020. <https://doi.org/10.5281/zenodo.4276396>.
- (29) Vergeer, P.; van Es, A.; de Jongh, A.; Alberink, I.; Stoel, R. Numerical Likelihood Ratios Outputted by LR Systems Are Often Based on Extrapolation: When to Stop Extrapolating? *Science and Justice* **2016**, *56* (6), 482–491. <https://doi.org/10.1016/j.scijus.2016.06.003>.
- (30) Egan, T. D. The Clinical Pharmacology of Remifentanil: A Brief Review. *J Anesth* **1998**, *12*, 195–204. <https://doi.org/https://doi.org/10.1007/BF02481730>.
- (31) Schüttler, J.; Schwilden, H. *Modern Anesthetics: Handbook of Experimental Pharmacology*; Starke, K., Ed.; Springer-Verlag: Berlin Heidelberg, 2008; Vol. 182.
- (32) Henkel, E.; Vella, R.; Behan, K.; Austin, D.; Kruger, P.; Fenning, A. The Effect of Concentration, Reconstitution Solution and PH on the Stability of a Remifentanil Hydrochloride and Propofol Admixture for Simultaneous Co-Infusion. *BMC Anesthesiol* **2020**, *20* (1), 283. <https://doi.org/10.1186/s12871-020-01194-5>.
- (33) Said, R.; Pohanka, A.; Andersson, M.; Beck, O.; Abdel-Rehim, M. Determination of Remifentanil in Human Plasma by Liquid Chromatography-Tandem Mass Spectrometry Utilizing Micro Extraction in Packed Syringe (MEPS) as Sample Preparation. *Journal of Chromatography B* **2011**, *879* (11–12), 815–818. <https://doi.org/10.1016/j.jchromb.2011.02.002>.
- (34) Iwersen-Bergmann, S.; Schmoldt, A. Acute Intoxication with Aniline: Detection of Acetaminophen as Aniline Metabolite. *Int J Legal Med* **2000**, *113*, 171–174.
- (35) Brune, K.; Renner, B.; Tiegs, G. Acetaminophen/Paracetamol: A History of Errors, Failures and False Decisions. *European Journal of Pain* **2015**, *19*, 953–965. <https://doi.org/10.1002/ejp.621>.



Chapter 3

- (36) Modick, H.; Weiss, T.; Dierkes, G.; Koslitz, S.; Käfferlein, H. U.; Brüning, T.; Koch, H. M. Human Metabolism and Excretion Kinetics of Aniline after a Single Oral Dose. *Arch Toxicol* **2016**, *90*, 1325–1333. <https://doi.org/10.1007/s00204-015-1566-x>.
- (37) Yang, J.; Yang, J. Why Can LDA Be Performed in PCA Transformed Space? *Pattern Recognit* **2003**, *36* (2), 563–566. [https://doi.org/10.1016/S0031-3203\(02\)00048-1](https://doi.org/10.1016/S0031-3203(02)00048-1).
- (38) Fomin, D.; Baranauskaite, V.; Usaviciene, E.; Sumkovskaja, A.; Laima, S.; Jasulaitis, A.; Minkuviene, Z. N.; Chmieliauskas, S.; Stasiuniene, J. Human Deaths from Drug Overdoses with Carfentanyl Involvement—New Rising Problem in Forensic Medicine A STROBE-Compliant Retrospective Study. *Medicine* **2018**, *97* (48), e13449. <https://doi.org/10.1097/MD.00000000000013449>.
- (39) Shanks, K. G.; Behonick, G. S. Detection of Carfentanil by LC-MS-MS and Reports of Associated Fatalities in the USA. *J Anal Toxicol* **2017**, *41*, 466–472. <https://doi.org/10.1093/jat/bkx042>.
- (40) Vanneste, B.; Van de Velde, M.; Struys, M.; Rex, S. Acute and Life-Threatening Remifentanil Overdose Resulting from the Misuse of a Syringe Pump. *Acta Anaesthesiol Belg* **2017**, *68* (2), 87–89.
- (41) Adamowicz, P.; Bakhmut, Z.; Mikolajczyk, A. Screening Procedure for 38 Fentanyl Analogues and Five Other New Opioids in Whole Blood by Liquid Chromatography-Tandem Mass Spectrometry. *Journal of Applied Toxicology* **2020**, *40*, 1033–1046. <https://doi.org/10.1002/jat.3962>.



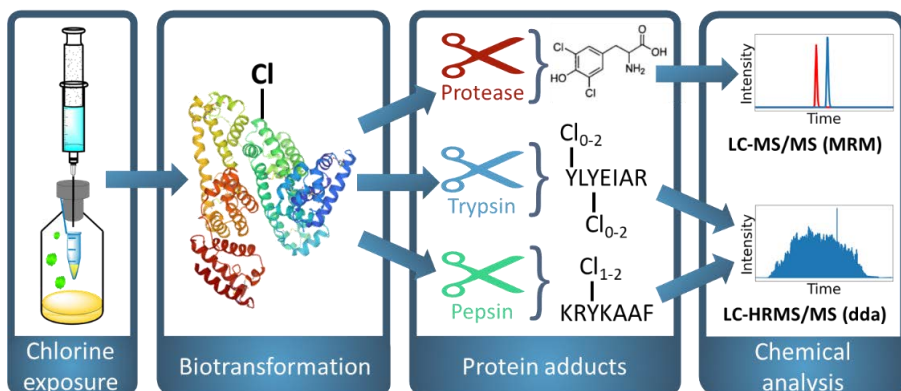
4

Elucidation of in vitro chlorinated tyrosine adducts in blood plasma as selective biomarkers of chlorine exposure

Mirjam de Bruin-Hoegée, Irene M. van Damme, Tomas van Groningen,
Debora van der Riet-Van Oeveren, Daan Noort, Arian C. van Asten,
Elucidation of in Vitro Chlorinated Tyrosine Adducts in Blood Plasma as
Selective Biomarkers of Chlorine Exposure. *Chemical Research in
Toxicology* **2022**, 35 (6), 1070–1079.
DOI: 10.1021/acs.chemrestox.2c00053.

Abstract

Chlorine is a widely available industrial chemical and involved in a substantial number of cases of poisoning. It has also been used as a chemical warfare agent in military conflicts. To enable forensic verification, the persistent biomarkers 3-chlorotyrosine and 3,5-dichlorotyrosine in biomedical samples could be detected. An important shortcoming of these biomarkers, however, is the relatively high incidence of elevated levels of chlorinated tyrosine residues in individuals with inflammatory diseases who have not been exposed to chlorine. Therefore, more reliable biomarkers are necessary to distinguish between endogenous formation and exogenous exposure. The present study aims to develop a novel diagnostic tool for identifying site-specific chlorinated peptides as a more unambiguous indicator of exogenous chlorine exposure. Human blood plasma was exposed *in vitro* to various chlorine concentrations and the plasma proteins were subsequently digested by pronase, trypsin or pepsin. After sample preparation, the digests were analyzed by liquid chromatography tandem mass spectrometry (LC-MS/MS) and liquid chromatography high resolution tandem mass spectrometry (LC-HRMS/MS). In line with other studies low levels of 3-chlorotyrosine and 3,5-dichlorotyrosine were found in blank plasma samples in this study. Therefore 50 site-specific biomarkers were identified that could be used as more unambiguous biomarkers for chlorine exposure. Chlorination of the peptides TY*ETTLEK, Y*KPGQTVK, Y*QQKPGQAPR, HY*EGSTVPEK and Y*LY*EIAR could already be detected at moderate *in vitro* chlorine exposure levels. In addition, the latter two peptides were found to have dichlorinated fragments. Especially, Y*LY*EIAR, with a distinct chlorination pattern in the MS spectra, could potentially be used to differentiate exogenous exposure from endogenous causes as other studies reported that this part of human serum albumin is nitrated rather than chlorinated under physiological conditions. In conclusion, trypsin digestion combined with high resolution MS analysis of chlorinated peptides could constitute a valuable technique for the forensic verification of exposure to chlorine.



4.1. Introduction

Chlorine (Cl_2), a highly reactive and toxic gas, is one of the most abundantly used industrial chemicals, with an annual production of multi-million tons.^{1,2} It has a wide variety of industrial applications, including the production of polymers and chlorinated solvents, separation of metals in mining, the disinfection of drinking water and use within the bleaching industry.³ It has been the cause of a significant number of cases of acute poisoning.^{4,5} Although known as a toxic dual-use chemical, it has not been scheduled by the Organisation for the Prohibition of Chemical Weapons (OPCW), mainly because the large scale of production and storage makes verification or inspections practically impossible.⁶ Notwithstanding, its use as a weapon is an obvious violation of the Chemical Weapons Convention (CWC). Chlorine gas was the first deployed chemical warfare agent during World War I, resulting in many victims.⁷ Recently, the OPCW published multiple reports stating that chlorine has been used in the ongoing conflict in the Syrian Arab Republic.⁸⁻¹³

Exposure to chlorine can cause severe acute and long-term health effects. Inhalation exposure to 1-3 ppm is already associated with mild irritation of mucous membranes.⁴ Based on this value the recommended exposure limit is 0.5 ppm for longer term exposure and the acceptable short term exposure limit is 1 ppm.¹⁴ Eye and throat irritation will develop at exposure levels between 5 and 15 ppm.⁴ Levels exceeding 15 ppm result in cough, chest pain and choking.¹⁵ From a concentration of 50 ppm, damage to the main airways and acute pulmonary edema occur.² In general, a dose above 400 ppm is lethal, as this high concentration will result in respiratory arrest, hemorrhage and acute burns of the upper and proximal lower airways.¹⁵ Long-term exposure can result in similar symptoms as short-term exposure below 50 ppm, where in 10% of the cases incomplete recovery after symptomatic treatment was reported.¹⁶

Especially in the case of major incidents with many affected individuals, methods for rapid triage and diagnosis of chlorine exposure are indispensable. Yet, detection of intact agents in biomedical samples is often not possible due to the reactivity of chemical threat agents. Furthermore, other traces of evidence of intentional release are usually difficult to obtain as well. For this purpose, biomarkers of exposure are used for verification purposes. Metabolic indicators for chlorine poisoning are the phospholipid L- α -phosphatidylglycerol¹⁷, chlorinated lipids such as 2-chloropalmitaldehyde and 2-chlorosearaldehyde¹⁸, 8-isoprostane (8-isoPGF_{2 α}) as a marker of lipid peroxidation¹⁹, and adducts to tyrosine, such as 3-chlorotyrosine (Cl-Tyr) and 3,5-dichlorotyrosine (di-Cl-Tyr)²⁰⁻²³. In particular tyrosine chlorination yields persistent biomarkers that can be found days after chlorine poisoning.²¹

During chlorine gas exposure, chlorine reacts in the body with aqueous mucus on epithelial tissue to form hydrochloric acid and hypochlorite.² Protein adducts can be formed when chlorine oxidizes tyrosine by electrophilic aromatic substitution.²¹ The aromatic ring in tyrosine is particularly reactive due to its electron-donating hydroxyl group. Figure 4.1 shows the reaction of tyrosine with chlorine, where substitution is directed towards the ortho position, leading to the formation Cl-Tyr and di-Cl-Tyr.²⁴



Figure 4.1. Reaction scheme of electrophilic aromatic substitution of tyrosine by chlorine, leading to the formation of 3-chlorotyrosine and 3,5-dichlorotyrosine.

An important shortfall of these biomarkers, however, is the relatively high incidence of elevated levels of chlorinated tyrosine residues in individuals who have not been exposed to chlorine. Chlorinated tyrosine biomarkers were found in people with inflammatory diseases^{21,25}, diabetes mellitus²⁶ and atherosclerotic vascular disease²⁷. For instance, Buss et al. reported that infants with respiratory distress had more than six times higher Cl-Tyr levels in tracheal aspirate proteins detected by GC-MS, compared to the control group without known diseases.²⁵ In addition, for patients with inflammatory disease, maximum levels of 20 ng/mL and 5 ng/mL blood have been analyzed by LC-MS/MS for Cl-Tyr and di-Cl-Tyr, respectively.²¹ Interestingly, in the referred study both the healthy and diseased group showed a relatively high Cl-Tyr level with a large variation, which makes verification even more difficult. In this respect, the di-Cl-Tyr adduct has been considered slightly more specific for exogenous chlorine exposure than the Cl-Tyr adduct.^{21,28} Nonetheless, verification of a chlorine attack based on these biomarkers is less reliable because of the potential presence of Cl-Tyr and di-Cl-Tyr in the blood plasma of non-exposed individuals. Therefore, more unambiguous biomarkers of chlorine exposure are necessary to differentiate exogenous exposure from endogenous processes.

A powerful tool to obtain sequence information for individual peptides is the use of liquid chromatography-high resolution tandem mass spectrometry (LC-HRMS/MS) for bottom-up proteomics. Data-dependent analysis in combination with database searching can be used to screen for peptides with post-translational modifications (PTMs). This strategy has successfully led to the identification of biomarkers for the exposure to other chemical threat agents.^{29,30} The validity of such an approach within the context of Cl-Tyr being a biomarker of inflammatory diseases has recently been reported by Nybo et al. in various publications.^{31–33} Detailed analysis of site-specific peptide modifications is expected to lead to improved differentiation of endogenous

reactions due to oxidative stress and exogeneous chlorine exposure, because the former will cause both chlorination and nitration of tyrosine whereas the latter will only result in chlorination.^{34,35}

Consequently, the current study aims to develop a diagnostic tool for identifying chlorine-tyrosine biomarkers as robust and specific indicators of exogeneous chlorine exposure. First, human blood plasma was exposed in vitro to various chlorine concentrations. Subsequently, the isolated plasma proteins were digested by pronase, trypsin or pepsin and analyzed by liquid chromatography tandem mass spectrometry (LC-MS/MS) and liquid chromatography high resolution tandem mass spectrometry (LC-HRMS/MS). The data was processed by Peaks® X+ software and manually interpreted to identify several chlorinated peptides of interest. The present work shows that such specific chlorinated peptides are indeed formed and, therefore, might serve as promising biomarkers for verification of human exposure to chlorine.

4

4.2. Experimental Procedures

4.2.1. Safety

Due to the potent nature of chlorine gas, all experiments were performed in a fume hood by trained personnel. Precautions were taken to prevent accidental exposure, including the use of gloves and eye protection.

4.2.2. Chemicals

Acetic acid, ammonium bicarbonate, calcium hypochlorite, 3-chloro-L-tyrosine, dithiothreitol (DTT), formic acid, pepsin from porcine gastric mucosa ($\geq 2,500$ units/mg protein), protease from *Streptomyces griseus* (pronase, ≥ 3.5 units/mg solid), sodium acetate trihydrate, sodium iodoacetate, trifluoroacetic acid, trypsin from bovine pancreas ($\geq 10,000$ BAEE units/mg protein) and urea were obtained from Sigma-Aldrich (Zwijndrecht, The Netherlands). Acetonitrile, acetone and methanol were purchased from Biosolve (Valkenswaard, The Netherlands). A peptide mixture of bovine serum albumin protein digest (BSA, LOT #UH285651) and hydrochloric acid were obtained from ThermoFisher Scientific (Landsmeer, The Netherlands). Additionally, water (MilliQ, SimPak® 1), 3,5-dichloro-L-tyrosine (BOC Sciences, London, UK) and $^{13}\text{C}_6$ -3-chloro-L-tyrosine (Cambridge Isotopic Laboratories, Andover MA, USA) were employed. The purities of the agents were higher than 97%. Human plasma was purchased from Sanquin (Amsterdam, The Netherlands).

4.2.3. In vitro chlorine exposure

The experimental setup is visualized in Figure 4.2. Human plasma (2 mL) was transferred to a 100 mL glass laboratory bottle. A 1.5 mL Eppendorf tube with 1, 10 and

50 mg calcium hypochlorite was placed in the bottle above the plasma sample. The reaction vial was sealed with a rubber septum and parafilm. A syringe was put through the septum and slowly, over a period of one minute, 1 mL of a 12M HCl solution was added to the calcium hypochlorite, after which 10, 100 or 500 ppm chlorine gas was generated in-situ for 2 hours. These concentrations will be described as low, medium, and high concentration, because the chlorine uptake in the plasma, the extent of adduct formation and the comparison between in vitro and in vivo exposure is unknown. Also, negative controls, i.e., blanks were included without HCl and calcium hypochlorite. The experiments were performed in triplicate for each concentration including the blanks.

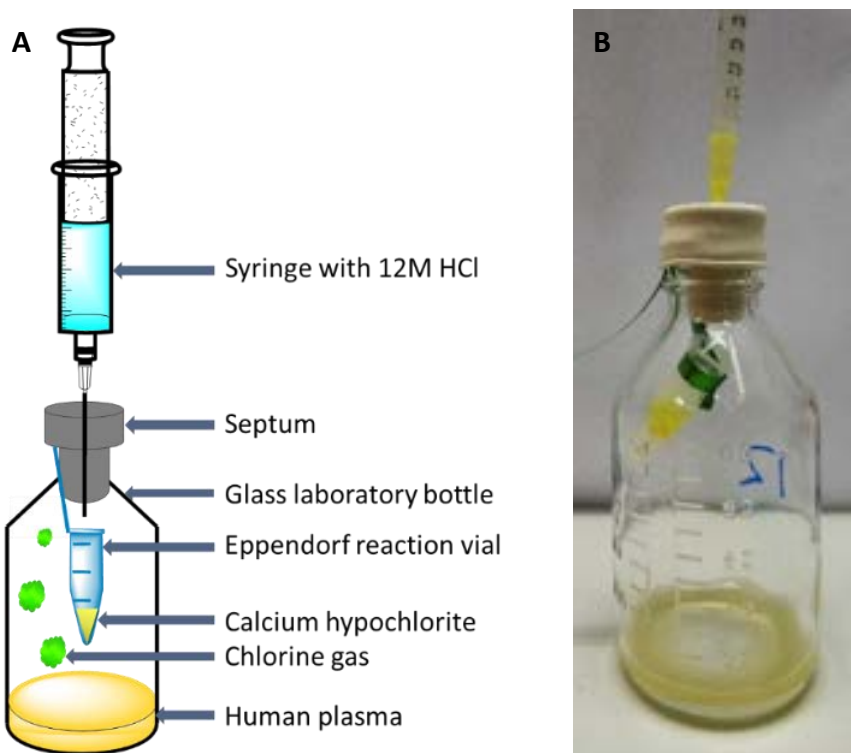


Figure 4.2. Experimental setup for in vitro exposure of human plasma to in-situ generated chlorine gas. A) Schematic view. B) Photo of the exposure system.

4.2.4. Protein precipitation and digestion

After chlorine exposure, all protein was precipitated by addition of 10 mL acetone, followed by centrifugation in a 15 mL Corning tube at 2000 rpm for 4 minutes (Heraeus Megafuge 1.0R). The acetone layer was discarded, and the steps were repeated. Afterwards, the protein precipitate was allowed to dry in the air at ambient temperature.

After precipitation, the isolated protein was digested by pronase, trypsin or pepsin. Pronase digests the protein up to individual amino acids, while trypsin only cleaves arginine (R) and lysine (K), resulting in longer peptides.³⁶ Pepsin is a nonspecific protease with phenylalanine (F), lysine (K), arginine (R) and proline (P) as favored residues.³⁷ Pepsin and trypsin allow analysis of specific chlorinated peptides. For pronase digestion, 3 mg of isolated protein was dissolved in 500 µL aqueous ammonium bicarbonate (ABC, 50 mM) and an aqueous solution of 100 µL pronase (10 mg/mL in 50 mM ABC). The samples were incubated overnight in a Thermoshaker (Grant-bio PHMT) at 37 °C and 800 rpm.

In addition, the protein was digested by trypsin. First, isolated protein was dissolved in 1 mL urea (8 M solution in 50 mM ABC), containing 5 µL of DTT (800 mM in water). The solution was incubated for 45 minutes at 37 °C and 800 rpm. After incubation, 100 µL sodium iodoacetate (150 mM in water) was added for carboxymethylation of reduced cysteine residues to prevent reformation of disulfide bonds. Subsequently, the solution was incubated for 30 minutes in the dark at 37 °C and 800 rpm. Afterwards, the sample was filtered through a 10 kDa Amicon ultra-centrifugal filter at 14.000 rpm for 10 minutes in an Eppendorf centrifuge (5417R). The residue was washed on the filter four times with 400 µL ABC buffer (50 mM) and then collected and dissolved in 400 µL water. Then, 30 µL trypsin solution (10 mg/mL in 50 mM acetate buffer, pH = 3.55) was added to the dissolved residue. The sample was incubated overnight at 37 °C and 800 rpm. In addition, the isolated protein was dissolved in 300 µL pepsin solution (62.5 µg/mL formic acid). The solution was incubated for 1.5 hours at 37 °C and 800 rpm.

4.2.5. Sample preparation

After pronase digestion, the sample was filtered through a 3 kDa Amicon ultra-centrifugal filter at 14.000 rpm for 10 minutes in an Eppendorf centrifuge. The filtrate was transferred to an LC-MS vial and analyzed as described in section 2.6. After trypsin and pepsin digestion, the samples were filtrated through a 10 kDa filter at 14.000 rpm for 10 minutes. To avoid pollution of the LC-Orbitrap-MS, the filtrates were purified with reversed phase solid phase extraction (SPE) using a C18 column (Bakerbond SPETM). To wet the sorbent bed and activate the nonpolar sorbents, 1 mL methanol was percolated through the column and 1 mL water was used to equilibrate the column. Afterwards, 100 µL of the filtrate was loaded onto the sorbent bed and washed with 1 mL water to desalt the peptides and remove other hydrophilic compounds from the sample matrix. The retained analytes were eluted with 1 mL 60% acetonitrile in water. Afterwards the sample was dried under nitrogen and dissolved in 1 mL water with 1% v/v formic acid. The final elute was transferred to an LC-MS vial and analyzed as described in section 2.6.

4.2.6. Chemical analysis

4.2.6.1. LC-MS/MS (SRM)

The pronase digests were diluted 10 to 1000-fold with water depending on the concentration prior to analysis on a Waters Acquity ultra-high pressure liquid chromatographic (UPLC) system equipped with a Waters Acquity HSS T3 C18 column (100 x 2.1 mm I.D., 1.8 µm). The blanks were not further diluted, except by the addition of the internal standard, resulting in a 1.1-fold dilution. The mobile phase consisted of water (Eluent A) and acetonitrile (Eluent B) both with 0.2% formic acid, using a gradient at a flow of 100 µL/min. Gradient elution started at 100% eluent A for one minute, followed by linear ramping to 80% eluent B in eight minutes and maintaining this composition for two minutes. After each analysis the system was equilibrated at 100% eluent A for three minutes. The injection volume was 5 µL at a temperature of 8 °C. The analysis was performed at room temperature. The UPLC system was coupled to a Waters (Milford, MA, USA) Xevo TQ-S triple-quadrupole mass Spectrometer, equipped with electrospray ionization, for quantification of the analytes in positive ionization mode. The capillary voltage was set to 3.5 kV with a nitrogen cone gas flow of 150 L/h, and a cone voltage of 10 V. The collision gas argon was set at a flow of 0.19 mL/min. Data was acquired with selected reaction monitoring (SRM) mode. The monitored transitions were m/z 216.2 → m/z 170.3 at a collision energy (CE) of 15 eV and m/z 216.2 → m/z 135.3 (CE = 25 eV) for Cl-Tyr, m/z 250.1 → m/z 204.0 (CE = 25 eV) and m/z 250.1 → m/z 169.0 (CE = 30 eV) for di-Cl-Tyr and m/z 222.0 → m/z 176.3 (CE = 15 eV) and m/z 222.0 → m/z 141.3 (CE = 25 eV) for the internal standard ¹³C₆-3-chloro-L-tyrosine.

4.2.6.2. LC-HRMS/MS (DDA)

The trypsin and pepsin digests were analyzed on an LC-HRMS/MS instrument consisting of an Ultimate 3000 RSLCnano system (Thermo Scientific Dionex Softron GmbH, Germany) coupled to an Orbitrap mass spectrometer (Q Exactive plus, Thermo Scientific, Bremen, Germany). First, 10 µL of the sample was injected onto an Acclaim PepMap 100 C18 µ-precolumn (5 mm x 300 µm I.D., 5 µm, 100 Å, Thermo Fisher Scientific) of 30 °C and washed with loading solvent (0.05% trifluoroacetic acid in water) at a flow of 30 µL/min for 3 minutes. Subsequently, the peptides were separated on an Acclaim PepMap C18 Analytical column (250 mm x 75 µm I.D., 2 µm, 100 Å, Thermo Fisher Scientific) at a constant flow of 300 nL/min at a temperature of 35 °C. Gradient elution started at 98% eluent A (0.1% v/v formic acid in water), followed by a linear increase to 25% eluent B (0.1% v/v formic acid in acetonitrile) in 10 minutes. After the analysis, eluent B was further increased to 80% in 5 minutes and this composition was maintained for 5 minutes. The column was returned to the initial conditions in 5 minutes and equilibrated for 23 minutes. The nanoLC system was coupled to the mass

spectrometer using an EASY-spray source. Positive electrospray ionization (ESI) analysis was performed with a spray voltage of 1.5 kV. The ion transfer capillary temperature was set at 250 °C. A full-scan range of m/z 300-2000 was applied at a resolution of 70.000. Subsequently, data dependent acquisition (DDA) was performed. Of each spectrum, the ten most abundant ions were selected for MS/MS analysis with a positive charge of 2-4 and a resolution of 17.500. The performance of the system was checked by measuring a quality control sample of a peptide mixture of 100 fmol BSA digest, where at least a coverage of 60% was required.

4.2.7. Data analysis

The raw LC-HRMS/MS data was analyzed using Peaks® X+ software (2019, Bioinformatics Solutions Inc., Waterloo, Canada). First a de novo search was performed that calculates all theoretically possible peptides. Afterwards a PEAKS DB Search was employed which compared all those peptides with the FASTA database, limiting the results to peptide sequences that were found in the database. The de novo algorithm interprets the tandem mass (MS/MS) spectrum of each peptide by calculating the mass differences between fragment ions and assigning those mass differences to specific amino acid residues. Three types of variable post-translational modifications (PTMs) were selected: single chlorination, dichlorination and nitration of tyrosine. The maximum allowed variable PTM per peptide was set to eight and the maximum missed cleavages was set to six. The error tolerance for the precursor mass and the fragment ion were set at 0.1 Da and 0.5 Da monoisotopic mass, respectively. Each amino acid in the de novo sequence was assigned a local confidence score. Default settings were used, while removing peptide sequences with an average local confidence (ALC) score below 50%. From each peptide, all amino acids with a local confidence higher than 30% were included in the de novo sequence tag of the peptides. This tag was used for the PEAKS DB search. The resulting peptides were exported and statistically analyzed by the open-source software Python 3.9.5 using difflib as part of the standard python package. The code written for this research is published under a GNU General Public License.³⁸ Because spectral interpretation was based on mass only, excluding the isotope pattern that is clearly discernable for chlorine, the MS/MS spectra of the most relevant peptides were also interpreted manually. Duplicate compounds, peptides with an area smaller than 10⁴ a.u. and peptides of non-human origin were removed. In addition, only peptides were selected for further research that were both present in the blank and highly exposed samples and with enhanced chlorination in the latter. The percentage of chlorinated tyrosine adducts (*PoC*) was calculated using Equation 4.1.

$$PoC = \left(1 - \frac{Area_0}{\sum_{i=0}^4 Area_i} \right) \times 100 \quad \text{Equation 4.1.}$$

Where Area_0 is the response of the unchlorinated peptide and $\sum_{i=0}^4 \text{Area}_i$ is the sum of the responses of the single, double, triple, and quadrupole chlorinated peptides, detected by the LC-HRMS/MS. The total number of observed chlorine atoms for each peptide did not exceed four. This calculation is based on the assumption of a uniform MS response between native and chlorinated species of a specific peptide.

4.3. Results & Discussion

4.3.1. Targeted LC-MS/MS analysis of 3-chlorotyrosine and 3,5-dichlorotyrosine

Before presenting the results of site-specific biomarkers, the overall Cl-Tyr and di-Cl-Tyr levels were established in a similar manner as reported by Crow et al.²¹ The results of the optimization and validation of the corresponding targeted LC-MS/MS method can be found in section S1 of the Supporting information. These levels can be used to indicate for which chlorinated tyrosine concentrations, site-specific peptides will be found, as explained in section 3.2. In addition, this section will clarify that these tyrosine biomarkers cannot always be used to distinguish between victims exposed to low chlorine levels and individuals who have not been exposed to chlorine at all.

Figure 4.3 shows the detected concentrations of Cl-Tyr and di-Cl-Tyr for the various chlorine exposure levels. The detected concentrations for the lowest exposure level were 0.15 ± 0.04 and 0.19 ± 0.06 nmol/mg protein for Cl-Tyr and di-Cl-Tyr respectively. The concentration of Cl-Tyr in this sample was only eight times higher than the concentration in the blank non-exposed sample. The Cl-Tyr values in the blank were above the limit of quantification (LOQ) of 0.9 pmol/mg protein and could easily be distinguished. The di-Cl-Tyr concentration in the blank was much lower and was consequently just below the LOQ of 0.7 pmol/mg protein. However, it had a signal-to-noise (S/N) ratio of at least 6 and the ion ratio deviated less than 6% from the reference standard, and could therefore be identified.³⁹ The overall ratio between Cl-Tyr/Tyr detected by LC-HRMS/MS as depicted in Tables S1 and S2 (Supporting information) show a similar tendency as the concentrations analyzed by LC-MS/MS, although the error range of the LC-HRMS/MS results was much larger, resulting in an overlap between medium and blank concentration.

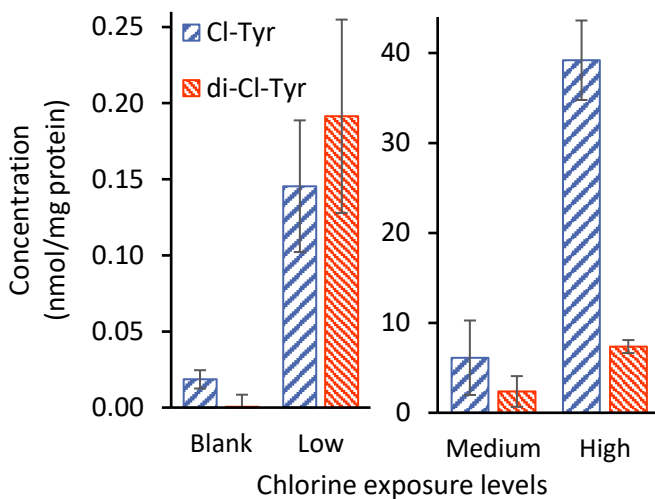


Figure 4.3. The effect of various chlorine gas exposure levels on 3-chlorotyrosine (Cl-Tyr) and 3,5-dichlorotyrosine (di-Cl-Tyr) concentrations. Error bars represent $\pm 1\text{SD}$ (standard deviation) for $n = 3$.

To evaluate how representative these chlorotyrosine levels are for concentrations found in the blood of exposed victims, the detected concentrations were compared to values reported in literature. Nishio et al. examined the Cl-Tyr levels in an autopsy sample of a person who possibly died of chlorine and drugs poisoning and reported a Cl-Tyr concentration of 60 ng/mL in left heart blood, analyzed by GC-MS.²² This is a lower concentration than observed for the blank and lowest exposure level in this study (0.15 and 1.2 $\mu\text{g}/\text{mL}$ blood, respectively) assuming that blood consists of 55% plasma and the amount of protein in human plasma is 70 mg/mL, as determined by the Bradford assay.⁴⁰ Nevertheless, many factors might influence the detected concentration, such as the moment of sampling after death, preservation of the samples and matrix effects. The Cl-Tyr levels that are analyzed by LC-MS/MS in rat and mouse models of chlorine exposure causing labored breathing and severe lung injury¹⁸ are slightly higher than the levels found by Nishio and are ten times lower than the concentrations observed at the lowest exposure level in this study.

These results show that chlorinated tyrosine levels in an exposed victim are not substantially higher than these values in healthy individuals. The difference is probably even smaller for diseased people with elevated chlorinated tyrosine levels. Being aware of the limitations of the chlorinated tyrosine adduct method, this study aims to identify more unambiguous biomarkers of chlorine exposure (section 3.2.) that can be more specifically linked to inhalation of chlorine gas.

4.3.2. Data dependent LC-HRMS/MS analysis of chlorinated peptides

4.3.2.1. Identification of chlorinated peptides

In this section the results will be described from analyzing peptide fragments containing chlorinated tyrosine residues, rather than focusing on the overall chlorinated tyrosine amino acid level after pronase digestion. In the trypsin digests, 42 peptides were identified with LC-HRMS/MS that could be used as potential biomarkers for chlorine exposure. Figure 4.4 shows peptides with the average percentage of chlorinated tyrosines at various exposure levels. A clear increase in chlorinated peptides with increasing chlorine exposure concentration is visible. Furthermore, only a limited number of peptides showed significant chlorination at medium chlorine exposure as chlorination of most peptides is only observed at the highest chlorine concentration. A vast majority of the peptides show either no modification or a single chlorination. Double chlorination was only observed for the peptides YQQKPGKAPK, YLYEiar and HYEGSTVPEK. The same trends are visible for the eight peptides that were identified as potential biomarkers after pepsin digestion (Figure S2 and Table S1, Supporting information). An extensive overview of the identified biomarkers with corresponding mass and retention time can be found in Table S3 of the Supporting information. Two chlorinated biomarkers were detected in both the trypsin and pepsin digests and that were chlorinated at the same tyrosine amino acid position. Additionally, not all biomarkers were detected in all repetitions at the highest concentration. This might be due to variation in the sample preparation efficacy and chlorine uptake of the plasma sample. The combination of various digestion methods enabled the identification of more peptides than with a single digestion method and consequently a larger part of the protein sequence was covered. The coverage of human serum album and haptoglobin was 56% and 33%, respectively (Figure S4, Supporting information.). It should be noted that a few chlorinated peptides were detected in the blank and low exposure level and not in higher chlorine exposure levels, although the blood plasma of the same donor was used. This unexpected finding was not investigated further as these peptides were not considered to be suitable markers for chlorine exposure.

Table 4.1 lists the most promising chlorinated peptides as biomarkers for exogeneous chlorine exposure. Because trypsin can cleave the protein on various amino acids and the efficiency is not 100%, the length of some chlorinated peptides varied slightly. The additional amino acids that were occasionally found are indicated with a dot notation of the chlorinated peptide sequence. All peptides were found to be unchlorinated in the blank samples and chlorinated at high chlorine exposure levels. The chlorinated variants of the peptides HY*EGSTVPEK, TY*ETTLEK, Y*KPGQTVK, Y*LY*EIAR and Y*QQKPGQAPR were detected in the medium chlorine exposure samples as well. This indicates that these peptides might even be used in case a lower concentration of

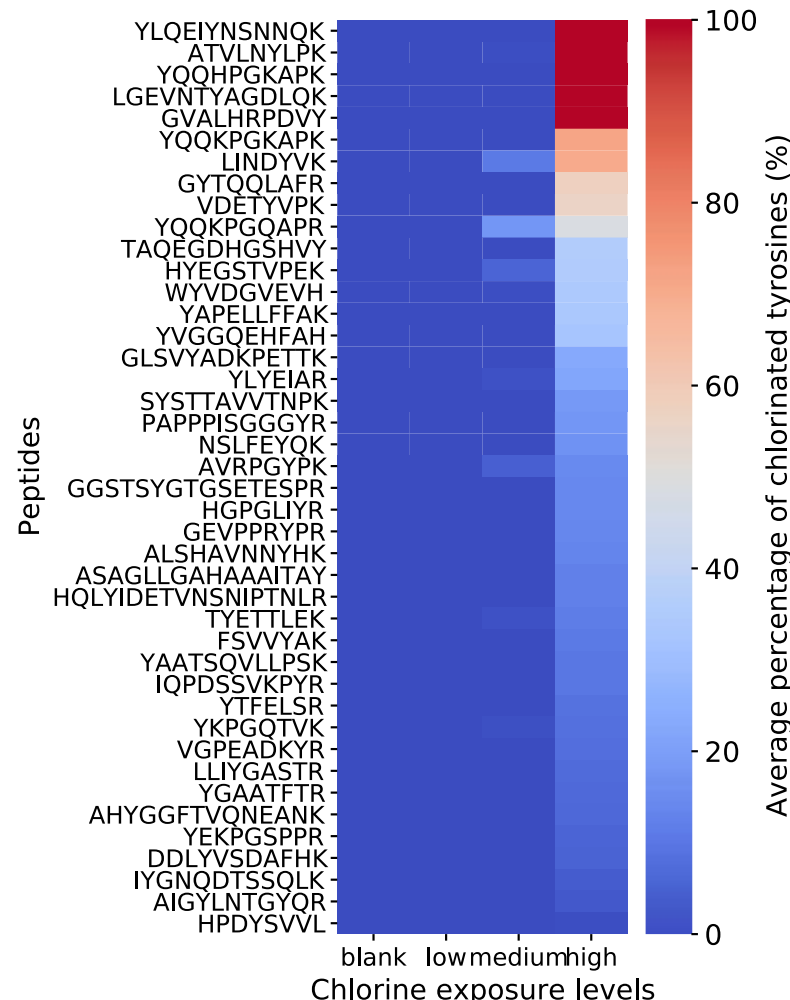


Figure 4.4. Heatmap of peptides identified with LC-HRMS/MS after trypsin digestion of human blood plasma, with corresponding average percentage of chlorinated tyrosines (PoC) for non-exposed, low, medium, and high chlorine exposure.

Table 4.1. Overview of peptides containing at least one chlorinated tyrosine residue, present in the precipitated proteins from human plasma exposed to various chlorine concentrations.

Blank peptide	Chlorinated peptide	Protein	Accession
HYEGSTVPEK	HY(Cl)EGSTVPEK.K	Haptoglobin	P00738 HPT_HUMAN
	HY(Cl ₂)EGSTVPEK.K	Haptoglobin	P00738 HPT_HUMAN
TYETTLEK	TY(Cl)ETTLEK	Albumin	P02768 ALBU_HUMAN
YKPGQTVK	SI.Y(Cl)KPGQTVK	Alpha-2-macroglobulin	P01023 A2MG_HUMAN
LYYEIAR	KK.Y(Cl)LYEIAR	Albumin	P02768 ALBU_HUMAN
	K.Y(Cl)LY(Cl)EIAR	Albumin	P02768 ALBU_HUMAN
	Y(Cl)LY(Cl ₂)EIAR	Albumin	P02768 ALBU_HUMAN
YQQKPGQAPR	Y(Cl)QQKPGQAPR	Immunoglobulin kappa variable 3-20	P01619 KV320_HUMAN

The Peaks® X+ software facilitated rapid analysis and evaluation of the many MS/MS spectra. Furthermore, interpreting each MS/MS spectrum according to the same fixed set of rules reduces human bias, which is important from a forensic point of view. Nevertheless, both the automated analysis and its results require critical human expert evaluation. Error tolerance thresholds for the parent- and fragment ion masses turned out to be of significant influence on the identified peptides and their modifications. Especially because only mass differences are used for identification of the chlorine PTMs, while other relevant information, such as isotope pattern is not incorporated as this can hamper protein identification rates.^{43,44} In addition, the isomers of Y(Cl)LYEIAR and Y(Cl)LY(Cl₂)EIAR were only found manually due to their trace level and the applied concentration threshold settings.

In future research, it would be interesting to examine potential differences between short-term exposure to a high concentration of chlorine gas and long-term low-level exposure. Because of the persistence of blood protein adducts, it is conceivable that the chlorination is cumulative, which may result in a higher concentration of chlorinated biomarkers for low-level long-term exposure than is expected based on a single exposure. Hence, the degree of mono-chlorination versus dichlorination and chlorination-to-nitration ratio of tyrosine residues might be useful to investigate exposure conditions.^{21,35}

Additionally, it should be emphasized that the *in vitro* chlorine gas exposure setup represents a simplified model in relation to actual human exposure and does not account for chemical and biological interactions that take place in the various parts of the human body. It is still under debate whether Cl₂ will be fully converted to HOCl and HCl in wet tissue before it reacts with biological molecules or that it will predominantly react with biological compounds before it can undergo hydrolysis. A comprehensive theoretical review by Squadrato et al. suggests that direct reaction of Cl₂ with biological molecules is kinetically favored.⁴⁵ However, other authors state, based on *in vitro* experiments, that hypochlorous acid (HOCl) reacts with amino acids and triggers an

inflammatory response in the lungs as a result of chlorine exposure.^{2,46,47} For this reason, verification of the chlorinated peptide biomarkers in samples of chlorine exposed victims is required to establish their value for forensic practice.

4.3.2.2. Mass spectrometric approach for assigning chlorinated peptides

The following section discusses the LC-HRMS/MS analysis of two of the chlorinated peptides, i.e., Y*LY*EIAR and HY*EGSTVPEK, in more detail. Figure 4.5 shows the extracted ion chromatograms (EICs) of the mono, di and tri-chlorinated peptide Y*LY*EIAR in plasma exposed to the highest chlorine concentration, with corresponding retention times (t_R). The results for the blanks and plasma exposed to other concentration are shown in the Supporting information (Figure S4). No chlorinated peptides were detected in the blank. Two peaks are visible at m/z 481.23 (one chlorine atom) and m/z 515.19 (three chlorine atoms), because either the first or the second tyrosine can exhibit (di-)chlorination.

4

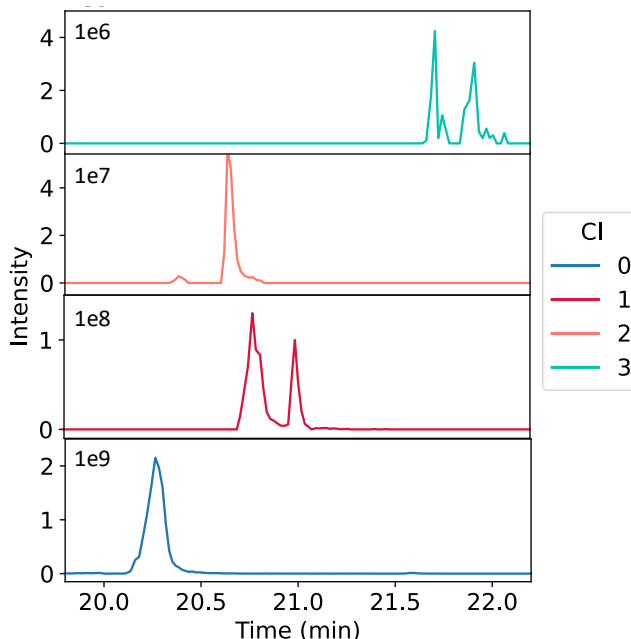


Figure 4.5. Extracted ion chromatograms of plasma exposed to the high chlorine exposure concentration analyzed by LC-HRMS/MS, with YLYEIAR at m/z 464.25 and t_R = 20.1-20.7 min (blue), Y(Cl)LYEIAR and YLY(Cl)EIAR at m/z 481.23 and t_R = 20.8-21.0 and 21.0-21.2 min (red), K.Y(Cl)LY(Cl)EIAR at m/z 562.26 and t_R = 20.6-20.8 min (orange), and Y(Cl)LY(Cl₂)EIAR and Y(Cl₂)LY(Cl)EIAR at m/z 515.19 and t_R = 21.7-21.9 and 21.9-22.0 min (green).

In the full scan MS spectrum of this doubly charged peptide, a distinct chlorine pattern is visible for single, double and triple chlorination (Figure 4.6B-D). The unchlorinated peptide showed a single peak as expected (Figure 4.6A). Table S4 in the Supporting information demonstrates the excellent correlation of the measured versus the theoretical isotope ratios for the acquired data. Figure 4.7 shows the MS/MS spectrum of the mono-chlorinated peptide Y(Cl)LYEiar. All y-ions were found, and their m/z ions are shown in the spectrum. The highest m/z 961.5 corresponds to the protonated ion [M+H⁺] of the peptide. The corresponding y-ions and the theoretical b-ions can be found in Table S5 of the Supporting information. The MS/MS spectra and corresponding fragmentation pattern of the di- and tri-chlorinated peptide YLYEiar are shown in Figure S5-S6 and Table S6-S7 of the Supporting information.

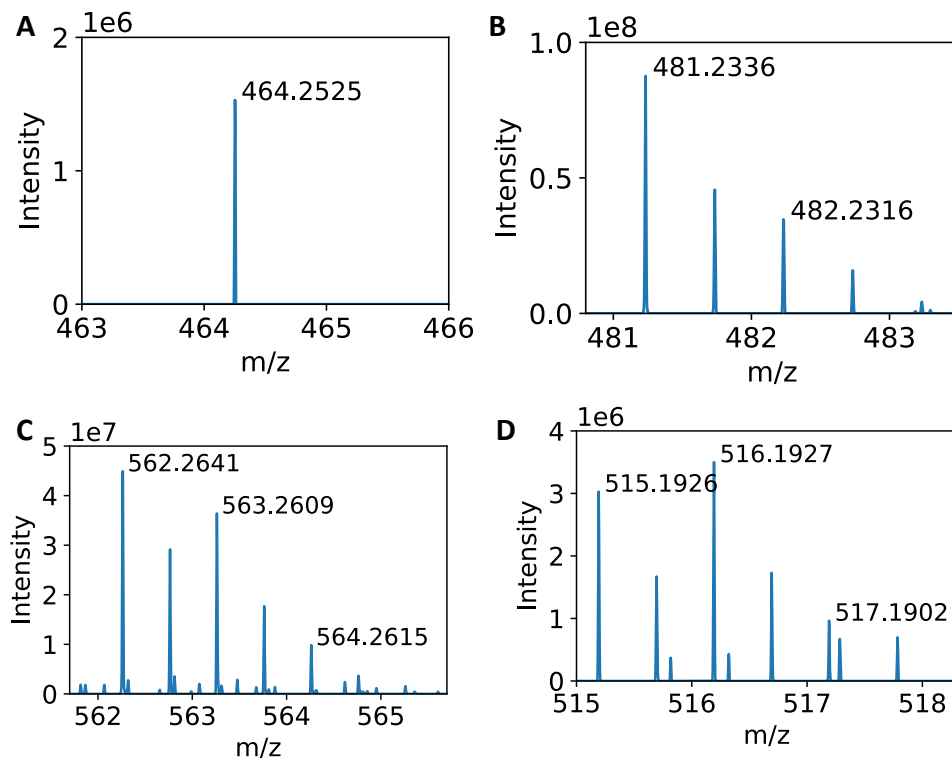


Figure 4.6. Full scan MS spectrum analyzed by LC-HRMS/MS of doubly charged chlorinated precursor Y*LY*EIAR showing the chlorine isotope pattern, A) no chlorination, B) single chlorination with an isotope ratio of around 2:1, C) double chlorination of K.Y*LY*EIAR with an isotope ratio of 5:4:1, and D) triple chlorination with an isotope ratio of 11:12:5:1.

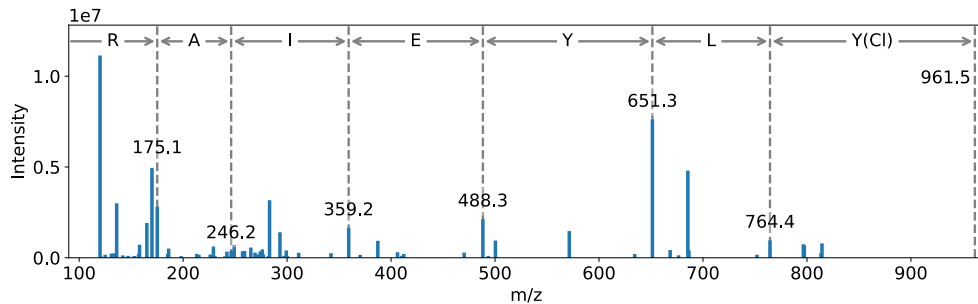


Figure 4.7. MS/MS spectrum of parent ion Y(Cl)LYEiar with an m/z 481.233 at an t_R of 20.76 min, present in the precipitated proteins from human plasma exposed to a medium and high concentration of chlorine gas. The m/z of the y-fragments and corresponding amino acids are shown.

The mono-chlorinated peptide HY*EGSTVPEKK showed the highest intensity compared to all chlorinated peptides in both the medium and highly exposed samples and is present as unchlorinated peptide in the blank. Because of its relevance, the EICs of the mono and di-chlorinated peptide HY*EGSTVPEKK in plasma exposed to the highest chlorine concentration is shown in Figure 4.8. The results for the blank samples and plasma exposed to other concentrations are presented in the Supporting information (Figure S7).

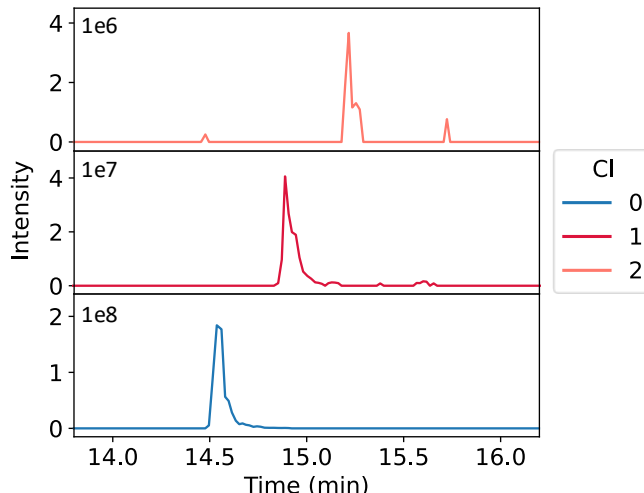


Figure 4.8. Extracted ion chromatograms of plasma exposed to the highest chlorine concentration analyzed by LC-HRMS/MS, with HYEGSTVPEKK at m/z 637.823 and t_R = 14.3-15.0 min (blue), HY(Cl)EGSTVPEKK at m/z 654.805 and t_R = 14.9-15.0 min (red), and HY(Cl₂)EGSTVPEKK at m/z 671.785 and t_R = 15.2-15.3 min (orange).

The MS/MS spectrum corresponding to HY(Cl)EGSTVPEKK is shown in Figure 9. All y-fragments and the $[M+H^+]$ precursor ion were found and depicted in Table S8 in the

Supporting information. Also, all except one of the b-fragments could be identified in the spectrum. The MS/MS spectrum and corresponding fragmentation pattern of the di-chlorinated peptide HY*EGSTVPEKK is shown in Figure S8 and Table S9 of the Supporting information.

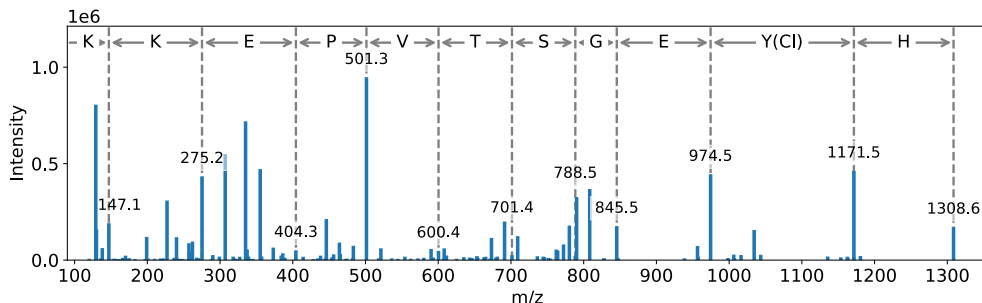


Figure 4.9. MS/MS spectrum of parent ion HY(Cl)EGSTVPEKK with an m/z 654.804 at an t_R of 14.88 min, detected in the trypsin digest of a plasma sample exposed to a medium and high concentration of chlorine gas. The m/z of the y-fragments and corresponding amino acids are shown.

4.3.3. Chlorinated sites in human serum albumin

To better understand the protein structure and interactions, the positions of the chlorinated tyrosine residues in human serum albumin were visualized in Figure 10. The locations of the identified chlorinated peptides are marked in Figure 10A. Figure 10B and C show a magnification of the Y138 and Y140 site of the single chlorinated peptides Y(Cl)LYEIAR and YLY(Cl)EIAR, respectively.

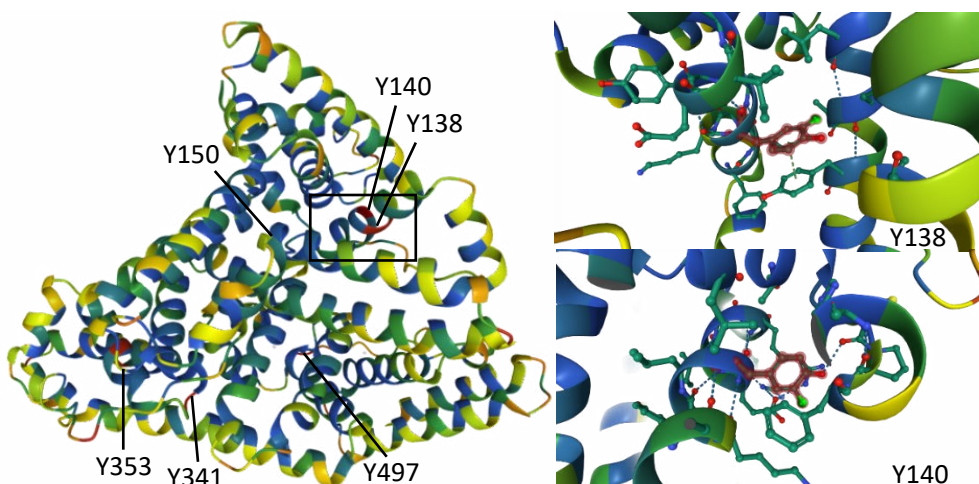


Figure 4.10. A) Positions of chlorinated tyrosine residues in human serum albumin. B) Chlorinated tyrosine residue Y138 of peptide sequence Y(Cl)LYEIAR. C) Chlorinated tyrosine residue Y140 of peptide sequence YLY(Cl)EIAR. Figure was created using uniprot.org © 2002 – 2022 UniProt Consortium.

4.4. Conclusions

In the current study, 50 chlorinated peptides have been identified after in vitro exposure of human plasma to chlorine. These peptides could potentially serve as biomarkers to verify exogenous chlorine exposure in humans. Within this set five chlorinated peptides were considered to be especially promising biomarkers due to their consistent presence in chlorine exposure samples, the occurrence of multiple degrees of chlorination and the presence of the unchlorinated peptide in the blank. These peptides HYEGSTVPEK, TYETTLEK, YKPGQTVK, YLYEIAR and YQQKPGQAPR have been detected in the medium exposure concentration samples as well and can be valuable when considering actual samples of potential chlorine exposure victims. Since most of these peptides are derived from proteins that are abundantly present in whole blood, forensic scientists might be able to assess alleged chlorine exposures in a relatively straightforward way. Because the current study works with a simplified in vitro exposure system, subsequent validation of these biomarkers in authentic biomedical samples is, however, pivotal. Nonetheless, the developed method allows for robust and specific analysis of chlorinated adducts formed in blood. Such biomarkers might be used to discriminate between endogenous and exogenous exposure, which is particularly relevant for forensic cases in which the context allows for multiple plausible explanations or suspected parties strongly deny the use of chlorine gas as a CWA.

4.5. Acknowledgements

We would like to thank Ad L. de Jong and Jelle C. de Koning (TNO Rijswijk) for their excellent technical assistance with LC-HRMS/MS analyses, and Gerrit-Jan de Bruin (Leiden University) for his valuable data analysis support.

References

- (1) United Nations Office for Disarmament Affairs. *Chemical Weapons*. <https://www.un.org/disarmament/wmd/chemical/> (accessed 2021-09-22).
- (2) Achanta, S.; Jordt, S. E. Toxic Effects of Chlorine Gas and Potential Treatments: A Literature Review. *Toxicology Mechanisms and Methods* **2019**, *31* (4), 244–256. <https://doi.org/10.1080/15376516.2019.1669244>.
- (3) American Chemistry Council (ACC). *2020 Guide to the Business of Chemistry*; 2020.
- (4) Winder, C. The Toxicology of Chlorine. *Environmental Research* **2001**, *85* (2), 105–114. <https://doi.org/10.1006/enrs.2000.4110>.
- (5) Morim, A.; Guldner, G. T. *Chlorine Gas Toxicity*. StatPearls. <https://www.ncbi.nlm.nih.gov/books/NBK537213/> (accessed 2022-02-08).
- (6) Organisation for the Prohibition of Chemical Weapons. *Annex on Chemicals*. <https://www.opcw.org/chemical-weapons-convention/annexes/annex-chemicals/annex-chemicals> (accessed 2021-09-22).
- (7) Sislin, J. D. Chemical Warfare in the Interwar Period: Insights for the Present? *Nonproliferation Review* **2018**, *25* (3–4), 185–202. <https://doi.org/10.1080/10736700.2018.1519343>.
- (8) OPCW Investigation and Identification Team (IIT). *First Report*; 2020.
- (9) OPCW Investigation and Identification Team (IIT). *Second Report*; 2021.
- (10) OPCW Fact-Finding Mission (FFM). Report of the Fact-Finding Mission Regarding the Incident of Alleged Use of Toxic Chemicals as a Weapon in Douma, Syrian Arab Republic, on 7 April 2018. <https://www.opcw.org/fact-finding-mission> (accessed 2021-07-27).
- (11) OPCW Fact-Finding Mission (FFM). Report of the OPCW Fact-Finding Mission in Syria Regarding the Incident in Aleppo, Syrian Arab Republic on 24 November 2018. <https://www.opcw.org/fact-finding-mission> (accessed 2021-08-02).
- (12) OPCW Fact-Finding Mission (FFM). Report of the OPCW Fact-Finding Mission in Syria Regarding the Incident of Alleged Use of Chemicals as a Weapon in Saraqib, Syrian Arab Republic, On 1 August 2016; 2020.
- (13) OPCW Fact-Finding Mission (FFM). Report of the OPCW Fact-Finding Mission in Syria Regarding the Incident of the Alleged Use of Chemicals as a Weapon in Kafr Zeita, Syrian Arab Republic 1 October 2016; 2022.
- (14) Centers for Disease Control and Prevention (CDC). *Chlorine*. <https://www.cdc.gov/niosh/npg/npgd0115.html> (accessed 2021-09-30).
- (15) White, C. W.; Martin, J. G. Chlorine Gas Inhalation: Human Clinical Evidence of Toxicity and Experience in Animal Models. *Proceedings of the American Thoracic Society* **2010**, *7* (4), 257–263. <https://doi.org/10.1513/pats.201001-0085M>.
- (16) Govier, P.; Coulson, J. M. Civilian Exposure to Chlorine Gas: A Systematic Review. *Toxicology Letters* **2018**, *293* (January), 249–252. <https://doi.org/10.1016/j.toxlet.2018.01.014>.
- (17) Hemström, P.; Larsson, A.; Elfmark, L.; Åstot, C. L -α-Phosphatidylglycerol Chlorohydrins as Potential Biomarkers for Chlorine Gas Exposure. *Analytical Chemistry* **2016**, *88* (20), 9972–9979. <https://doi.org/10.1021/acs.analchem.6b01896>.
- (18) Ford, D. A.; Honavar, J.; Albert, C. J.; Duerr, M. A.; Oh, J. Y.; Doran, S.; Matalon, S.; Patel, R. P. Formation of Chlorinated Lipids Post-Chlorine Gas Exposure. *Journal of Lipid Research* **2016**, *57*, 1529–1540. <https://doi.org/10.1194/jlr.M069005>.
- (19) Elfmark, L.; Ågren, L.; Akfur, C.; Bucht, A.; Jonasson, S. 8-Isoprostanate Is an Early Biomarker for Oxidative Stress in Chlorine-Induced Acute Lung Injury. *Toxicology Letters* **2018**, *282*, 1–7. <https://doi.org/10.1016/j.toxlet.2017.10.007>.
- (20) Sochaski, M. A.; Jarabek, A. M.; Murphy, J.; Andersen, M. E. 3-Chlorotyrosine and 3,5-Dichlorotyrosine as Biomarkers of Respiratory Tract Exposure to Chlorine Gas. *Journal of Analytical Toxicology* **2008**, *32*, 99–105. <https://doi.org/10.1093/jat/32.1.99>.
- (21) Crow, B. S.; Quiñones-González, J.; Pantazides, B. G.; Perez, J. W.; Winkeljohn, W. R.; Garton, J. W.; Thomas, J. D.; Blake, T. A.; Johnson, R. C. Simultaneous Measurement of 3-Chlorotyrosine and 3,5-

Elucidation of in vitro chlorinated tyrosine adducts

4

- Dichlorotyrosine in Whole Blood, Serum and Plasma by Isotope Dilution HPLC-MS-MS. *Journal of Analytical Toxicology* **2016**, *40* (4), 264–271. <https://doi.org/10.1093/jat/bkw011>.
- (22) Nishio, T.; Toukairin, Y.; Hoshi, T.; Arai, T.; Nogami, M. Determination of 3-Chloro-L-Tyrosine as a Novel Indicator of Chlorine Poisoning Utilizing Gas Chromatography-Mass Spectrometric Analysis. *Legal Medicine* **2020**, *47*, 101782. <https://doi.org/10.1016/j.legalmed.2020.101782>.
- (23) Nishio, T.; Toukairin, Y.; Hoshi, T.; Arai, T.; Nogami, M. Development of an LC-MS/MS Method for Quantification of 3-Chloro-L-Tyrosine as a Candidate Marker of Chlorine Poisoning. *Legal Medicine* **2021**, *53*, 101939. <https://doi.org/10.1016/j.legalmed.2021.101939>.
- (24) McMurry, J. *Organic Chemistry*, 8th ed.; Brooks/Cole, Cengage Learning, 2010.
- (25) Hendrikje Buss, I.; Senthilmohan, R.; Darlow, B. A.; Mogridge, N.; Kettle, A. J.; Winterbourn, C. C. 3-Chlorotyrosine as a Marker of Protein Damage by Myeloperoxidase in Tracheal Aspirates from Preterm Infants: Association with Adverse Respiratory Outcome. *Pediatric Research* **2003**, *53* (3), 455–462. <https://doi.org/10.1203/01.PDR.0000050655.25689.CE>.
- (26) Chen, H. J. C.; Yang, Y. F.; Lai, P. Y.; Chen, P. F. Analysis of Chlorination, Nitration, and Nitrosylation of Tyrosine and Oxidation of Methionine and Cysteine in Hemoglobin from Type 2 Diabetes Mellitus Patients by Nanoflow Liquid Chromatography Tandem Mass Spectrometry. *Analytical Chemistry* **2016**, *88* (18), 9276–9284. <https://doi.org/10.1021/acs.analchem.6b02663>.
- (27) Hazen, S. L.; Heinecke, J. W. 3-Chlorotyrosine, a Specific Marker of Myeloperoxidase-Catalyzed Oxidation, Is Markedly Elevated in Low Density Lipoprotein Isolated from Human Atherosclerotic Intima. *Journal of Clinical Investigation* **1997**, *99* (9), 2075–2081. <https://doi.org/10.1172/JCI119379>.
- (28) Chapman, A. L. P.; Senthilmohan, R.; Winterbourn, C. C.; Kettle, A. J. Comparison of Mono- and Dichlorinated Tyrosines with Carbonyls for Detection of Hypochlorous Acid Modified Proteins. *Archives of Biochemistry and Biophysics* **2000**, *377* (1), 95–100. <https://doi.org/10.1006/abbi.2000.1744>.
- (29) Fidder, A.; Hulst, A. G.; Noort, D.; de Ruiter, R.; van der Schans, M. J.; Benschop, H. P.; Langenberg, J. P. Retrospective Detection of Exposure to Organophosphorus Anti-Cholinesterases: Mass Spectrometric Analysis of Phosphylated Human Butyrylcholinesterase. *Chemical Research in Toxicology* **2002**, *15* (4), 582–590. <https://doi.org/10.1021/tx0101806>.
- (30) Dubrovskii, Y.; Murashko, E.; Chuprina, O.; Beltyukov, P.; Radilov, A.; Solovyev, N.; Babakov, V. Mass Spectrometry Based Proteomic Approach for the Screening of Butyrylcholinesterase Adduct Formation with Organophosphates. *Talanta* **2019**, *197* (January), 374–382. <https://doi.org/10.1016/j.talanta.2019.01.059>.
- (31) Nybo, T.; Cai, H.; Chuang, C. Y.; Gamon, L. F.; Rogowska-Wrzesinska, A.; Davies, M. J. Chlorination and Oxidation of Human Plasma Fibronectin by Myeloperoxidase-Derived Oxidants, and Its Consequences for Smooth Muscle Cell Function. *Redox Biology* **2018**, *19* (August), 388–400. <https://doi.org/10.1016/j.redox.2018.09.005>.
- (32) Nybo, T.; Dieterich, S.; Gamon, L. F.; Chuang, C. Y.; Hammer, A.; Hoefler, G.; Malle, E.; Rogowska-Wrzesinska, A.; Davies, M. J. Chlorination and Oxidation of the Extracellular Matrix Protein Laminin and Basement Membrane Extracts by Hypochlorous Acid and Myeloperoxidase. *Redox Biology* **2019**, *20*, 496–513. <https://doi.org/10.1016/j.redox.2018.10.022>.
- (33) Nybo, T.; Davies, M. J.; Rogowska-Wrzesinska, A. Analysis of Protein Chlorination by Mass Spectrometry. *Redox Biology* **2019**, *26*, 101236. <https://doi.org/10.1016/j.redox.2019.101236>.
- (34) Davies, M. J.; Fu, S.; Wang, H.; Dean, R. T. Stable Markers of Oxidant Damage to Proteins and Their Application in the Study of Human Disease. *Free Radical Biology and Medicine* **1999**, *27* (11–12), 1151–1163. [https://doi.org/10.1016/S0891-5849\(99\)00206-3](https://doi.org/10.1016/S0891-5849(99)00206-3).
- (35) Thomson, K. Investigating and Detecting Biomarkers for Oxidative Stress; 2011.
- (36) Berg, J. M.; Tymoczko, J. L.; Stryer, L.; Gatto, G. J. *Biochemistry*, 7th ed.; W. H. Freeman and Company: New York, 2012.
- (37) Zheng, J.; Strutzenberg, T. S.; Reich, A.; Dharmarajan, V.; Pascal, B. D.; Crynen, G. C.; Novick, S. J.; Garcia-Ordonez, R. D.; Griffin, P. R. Comparative Analysis of Cleavage Specificities of Immobilized Porcine Pepsin and Nepenthesin II under Hydrogen/Deuterium Exchange Conditions. *Analytical Chemistry* **2020**, *92*, 11018–11028. <https://doi.org/10.1021/acs.analchem.9b05694>.

- (38) de Bruin-Hoegée, M.; de Bruin, G. J. Python Code for Peptide Sequencing of Plasma after Chlorine Exposure. 2022. <https://doi.org/10.5281/zenodo.6040099>.
- (39) The commission of the European communities. Commission Decision of 12 August 2002 Implementing Council Directive 96/23/EC Concerning the Performance of Analytical Methods and the Interpretation of Results. *Official Journal of the European Communities* **2002**, *45* (L221), 8–36.
- (40) Sigma. *Technical Bulletin Bradford Reagent*. <https://intra.pasteur.uy/publico/bonilla/Protocolos/Cuantificacion sigma/b6916bul.pdf> (accessed 2022-01-31).
- (41) Van Eijk, H. M. H.; Deutz, N. E. P. Plasma Protein Synthesis Measurements Using a Proteomics Strategy. *Journal of Nutrition* **2003**, *133*, 2084–2089. <https://doi.org/10.1093/jn/133.6.2084s>.
- (42) Fu, F.; Liu, H.; Gao, R.; Zhao, P.; Lu, X.; Zhang, R.; Wang, L.; Wang, H.; Pei, C. Protein Adduct Binding Properties of Tabun-Subtype Nerve Agents after Exposure in Vitro and in Vivo. *Toxicology Letters* **2020**, *321*, 1–11. <https://doi.org/10.1016/j.toxlet.2019.12.014>.
- (43) Tran, N. H.; Rahman, M. Z.; He, L.; Xin, L.; Shan, B.; Li, M. Complete de Novo Assembly of Monoclonal Antibody Sequences. *Scientific Reports* **2016**, *6* (August), 1–10. <https://doi.org/10.1038/srep31730>.
- (44) Tay, A. P.; Liang, A.; Hamey, J. J.; Hart-Smith, G.; Wilkins, M. R. MS2-Deisotoper: A Tool for Deisotoping High-Resolution MS/MS Spectra in Normal and Heavy Isotope-Labelled Samples. *Proteomics* **2019**, *19* (17). <https://doi.org/10.1002/pmic.201800444>.
- (45) Squadrato, G. L.; Postlethwait, E. M.; Matalon, S. Elucidating Mechanisms of Chlorine Toxicity: Reaction Kinetics, Thermodynamics, and Physiological Implications. *American Journal of Physiology - Lung Cellular and Molecular Physiology* **2010**, *299*, 289–300. <https://doi.org/10.1152/ajplung.00077.2010>.
- (46) Evans, R. B. Chlorine: State of the Art. *Lung* **2005**, *183* (3), 151–167. <https://doi.org/10.1007/s00408-004-2530-3>.
- (47) Chauhan, S.; Chauhan, S.; D'Cruz, R.; Faruqi, S.; Singh, K. K.; Varma, S.; Singh, M.; Karthik, V. Chemical Warfare Agents. *Environmental Toxicology and Pharmacology* **2008**, *26*, 113–122. <https://doi.org/10.1016/j.etap.2008.03.003>.



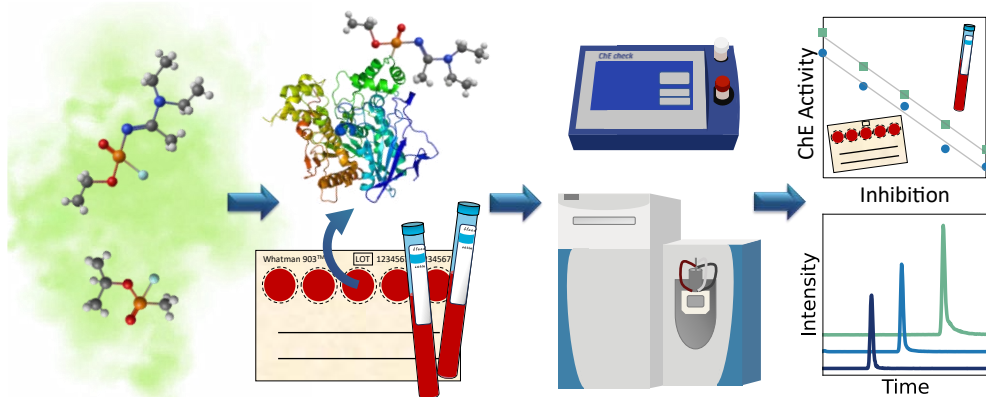
5

On-site detection and laboratory verification of the presence of nerve agent biomarkers using dried blood spots

Mirjam de Bruin-Hoegée, Alex Fidder, Tomas van Groningen, Marcel J. van der Schans, Daan Noort, Arian C. van Asten, On-Site Detection and Laboratory Verification of the Presence of Nerve Agent Biomarkers Using Dried Blood Spots. *Forensic Chemistry* **2023**, 35, 100526.
DOI: 10.1016/j.forc.2023.100526.

Abstract

The analysis of biomedical samples is important for the investigation of the alleged exposure to chemical warfare agents. The present study aims to use dried blood spots for portable detection and laboratory verification of organophosphate poisoning. After in-vitro incubation of blood with Novichok A-230, A-232 and A-234 and sarin, a volume of 25 and 50 µL was spotted on a protein saver card. Subsequently, the dried spots were extracted and analyzed by a mobile cholinesterase test kit. In addition, butyrylcholinesterase (BChE) was isolated and digested by pepsin followed by analysis with liquid chromatography tandem mass spectrometry (LC-MS/MS). The fluoride-activated samples were analyzed by gas chromatography tandem mass spectrometry (GC-MS/MS) and LC-MS/MS. It was found that the CWA induced cholinesterase inhibition was remarkably stable in dried blood spots. Even after at least one month storage under ambient conditions, the same linear reduction was visible as function of nerve agent exposure. Additionally, nonapeptide adducts were identified by LC-MS/MS one month after exposure. Also, intact Novichok nerve agents and regenerated sarin were observed by GC-MS/MS. In addition to the stability of the sample, important benefits of the proposed method include the less invasive sample collection and safer and easier shipping and storage conditions. In conclusion, this study shows the feasibility of using on-site detection and state-of-the-art laboratory analysis of dried blood spots for unambiguous verification of nerve agent exposure.



5.1. Introduction

Despite the efforts of the Organisation for the Prohibition of Chemical Weapons (OPCW) to achieve a world free of chemical weapons, there is still an ongoing threat of chemical warfare agent (CWA) use. For example, nerve agents have recently been used in large-scale attacks during the conflict in the Syrian Arab Republic,^{1–3} and to assassinate individuals in Malaysia,⁴ and the United Kingdom.^{5,6} In addition to evidence such as witness statements, video footage, and satellite imagery, chemical analysis is important for the investigation of the alleged use of toxic chemicals.

Nerve agents are mostly organophosphorus compounds and are prohibited under the Chemical Weapons Convention. Their toxicological mechanism of action is acetylcholinesterase inhibition, resulting in overstimulation of the cholinergic pathway.⁷ The nerve agent sarin (GB) is one of the most potent chemical weapons, affecting the nervous system.⁸ A 30-minutes exposure to 4 µg/m³ already gives mild effects, such as pinpoint pupils, blurred vision, runny nose and shortness of breath.⁹ An increased concentration of 0.19 mg/m³ is lethal or gives severe health effects, which can include muscular twitching, fluid accumulation within the airways and cessation of breathing. Besides, Novichoks, considered the fourth generation of CWAs, exert the same mechanism of action as other organophosphate nerve agents, although they are expected to be even more potent.^{10,11} Accordingly, the median lethal concentration (LC₅₀) is estimated to be eight times lower than it is for sarin.¹²

Since CWAs are highly reactive chemicals, the analysis is mainly focused on degradation products in environmental samples or metabolites and protein adducts in biomedical matrices. An overview of major pathways is given in Figure S1 and S2 in the Supplemental Information. Typical on-site detection techniques are based on ion mobility spectrometry, flame photometry, Raman and IR spectroscopy, and mass spectrometry.¹³ Most commonly applied laboratory techniques are gas and liquid chromatography combined with mass spectrometry.¹⁴

One of the remaining challenges for forensic examinations concerns the stability of the actual sample during collection, transportation, storage, and analysis.¹⁵ A possible way of preserving the CWA signature might be through drying of blood plasma or applying whole blood on filter paper. This fixation might maintain the reactive components into a more stable matrix and could potentially also slow down degradation of other relevant components. Advantages of using dried blood spots (DBS) include reduced sample volume, safer handling, and less stringent storage conditions.¹⁶ Also, less invasive sample collection is required since only a small amount of blood is obtained by a finger puncture instead of venous blood sampling which usually needs to be performed by a medical practitioner. For instance, sulfur mustard adducts of human

serum albumin can be detected in dried plasma samples weeks after drying.¹⁷ Also, nerve agents and simulants thereof have been detected in dried sample spots as free agent,^{18,19} hydrolysis product,^{20–22} tyrosine adduct,²³ and butyrylcholinesterase (BChE) adducts.^{15,24} Another category of chemical threat agents that have been studied through detection in dried blood spots are very powerful synthetic opioids like fentanyl.^{25–35} For all compounds, the most commonly applied analytical technique was liquid chromatography-tandem mass spectrometry (LC-MS/MS), but also paper spray mass spectrometry (PS-MS),^{22,26,29} various thermal desorption methods,^{19,35} online solid phase extraction (SPE) tandem mass spectrometry,^{30,32} and the Ellman assay²⁴ have been proven to be valuable methods.

Currently, sophisticated analytical methods have to be used to evaluate the DBS for organophosphate poisoning. Because of the life-threatening effects of a nerve agent intoxication, first responders or military personnel may need fast results which cannot easily be obtained by laboratory analysis. To overcome this limitation, on-site tests may be used, such as the user-friendly cholinesterase (ChE) mobile test kit, which was designed for whole blood.³⁶ The toxicological mechanism of organophosphate poisoning is acetylcholinesterase (AChE) and BChE inhibition,⁷ which is the basis of the detection principle used by the field kit. The application of the Ellman photometric assay produces a yellow color after reaction with AChE or BChE.^{37,38} It is expected that this portable technique is not only suitable for whole blood, but also for DBS analysis.

Chemical threat agents that have been scarcely studied are the Novichok nerve agents, which have only recently been added to Schedule 1 of the Chemical Weapons Convention (CWC). In 2021 two studies identified biomarkers for Novichok compounds in blood samples, based on mass spectrometric analysis of a nonapeptide adduct.^{39,40} In addition, human serum albumin protein modifications of Novichok A-234 in blood can be detected by LC-MS/MS^{41,42} while the intact or regenerated nerve agent can be identified by both GC-MS/MS and LC-MS/MS.⁴² Lastly, degradation products in urine could be found by LC-MS/MS after derivatization⁴³ or by hydrophilic interaction liquid chromatography-tandem mass spectrometry (HILIC-MS/MS).⁴⁴ Up to now, to our knowledge, no studies have been published concerning the detection of Novichok agents in dried blood spots or by using these samples for on-site point-of-care diagnosis by measuring the cholinesterase activity.

Therefore, the aim of this research is to explore whether dried blood spots can be used for both on-site and laboratory analysis of nerve agent biomarkers. A variety of analytical techniques were used for the identification of the specific agent (Figure 5.1). After incubation of blood with sarin (GB) and three types of Novichok nerve agents at various concentrations, dried blood spots were prepared and processed according to the procedure for the particular biomarkers. LC-MS/MS was used to analyze

phosphonylated tyrosine adducts, hydrolysis metabolites, and BChE adducts by applying the nonapeptide assay. Both LC-MS/MS and gas chromatography-tandem mass spectrometry (GC-MS/MS) were utilized for analyzing the intact nerve agent either present as free agent in the sample or as reactivated organophosphate after fluoride reactivation. In this article a toolbox is provided for the verification of exposure to nerve agents by combining a portable technique and state-of-the-art laboratory analysis to enable fast and reliable diagnosis after potential organophosphate intoxications.

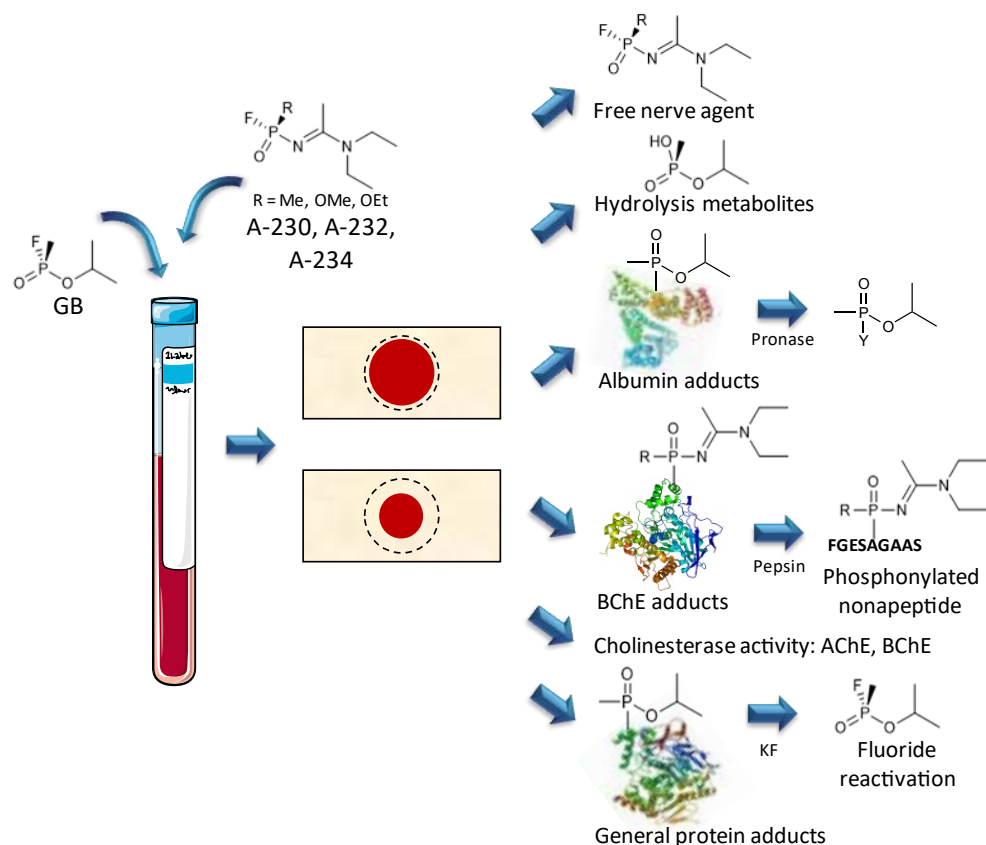


Figure 5.1. Method for biomarkers analysis in dried blood spots after nerve agent incubation of human whole blood. Blood was incubated with sarin (GB), Novichok A-230, A-232 or A-234. Subsequently, 25 and 50 µL blood was spotted on a protein saver card and dried. Various biomarkers could potentially be detected. 1) The nerve agents itself and its 2) hydrolysis metabolites; 3) tyrosine adducts in albumin; 4) nonapeptide with serine adduct in butyrylcholinesterase (BChE); 5) the acetylcholinesterase (AChE) or BChE activity; and finally, 6) the protein adducts can be reactivated by fluoride resulting in the original nerve agent.

5.2. Experimental

5.2.1. Safety

Due to the potent nature of nerve agents, all experiments were performed by trained personnel in the dedicated High-Tox facility at TNO (Rijswijk, The Netherlands), which is allowed under the Chemical Weapons Convention to synthesize and handle chemical warfare agents for research purposes. The chemicals were handled in solution and the concentrations were kept as low as possible to reduce the hazard. Precautions were taken to prevent accidental exposure, including the use of gloves and eye protection.

5.2.2. Chemicals

The nerve agents GB (o-Isopropyl methylphosphonofluoride, CAS: 107-44-8), Novichok A-230 (methyl-(1-(diethylamino)ethylidene)phosphonamidofluoride, CAS: 2387496-12-8), A-232 (Methyl (1-(diethylamino)ethylidene)phosphoramidofluoride, CAS: 2387496-04-8) and A-234 (Ethyl (1-(diethylamino)ethylidene)phosphoramidofluoride, CAS: 2387496-06-0) were synthesized in the high-tox facility of The Netherlands Organization for Applied Scientific Research (TNO, Rijswijk, The Netherlands). The purities of the synthesized compounds exceeded 95% as demonstrated by nuclear magnetic resonance (NMR), gas chromatography-mass spectrometry (GC-MS), and liquid chromatography-mass spectrometry (LC-MS). Butyrylcholinesterase monoclonal antibodies 3E8, diethyl ether, dynabeads protein G and hydrochloric acid were obtained from Thermo Scientific (Waltham, MA, USA). Acetic acid, ammonium bicarbonate (ABC), dimethyl pimelidate (DMP), ethyl acetate, formic acid, pepsin from porcine gastric mucosa ($\geq 2,500$ units/mg protein), phosphate buffered saline with 0.05% Tween-20 (PT buffer), phosphate buffered saline (PBS), potassium fluoride, protease from Streptomyces griseus (pronase, ≥ 3.5 units/mg solid), sodium bicarbonate, triethanolamine buffer (0.2M), and tris buffered saline, were obtained from Sigma-Aldrich (Zwijndrecht, The Netherlands). Additionally, dichloromethane (DCM, Biosolve), isopropanol (IPA, Acros Organics), and water (MilliQ, SimPak® 1) were employed. Acetone, acetonitrile, chloroform, and hexane were purchased from Biosolve (Valkenswaard, The Netherlands). The purities of the chemicals exceeded 97%. Human blood containing EDTA anticoagulant was obtained from Sanquin (Amsterdam, The Netherlands).

5.2.3. Preparation of dried blood spots

For each nerve agent two incubated samples were prepared with different concentrations. A solution of GB, A-230, A-232, or A-234 (100 μ L, 1 μ M) in IPA was added to 3 mL of human blood (final concentration 33 nM) to achieve an inhibition of 100% (assuming 3 nM AChE and 30-45 nM BChE in human whole blood). It should be

noted that a 100% inhibition is based on the average level of ChE in human blood. Because there is some variation between people, the inhibition can be lower than 100% or there can be a small excess of nerve agent that does not react. To make it more likely that all ChE has reacted, another sample was prepared with a large excess of nerve agent. In this case, either 100 µL of 13 µM or 40 µM nerve agent in IPA was added to 3 mL of blood (final concentration 0.4 µM or 1.3 µM). The samples were incubated overnight with gentle shaking at 50 rpm. Afterwards solutions of 25, 50, and 75% nerve agent inhibited samples were made, by mixing the blank and the 100% inhibited sample in various ratios. Five blood spots with a volume of 25 and 50 µL of each sample were spotted on Whatman 903TM protein saver cards and dried overnight under ambient conditions. Next the cards were stored for 3 days up to 3 months at 20–25°C and 50–70% relative humidity. The size of the DBS that was further processed was dependent on the analysis method. Either a 25 µL was cut in half (12.5 µL), a 25 or 50 µL spot was collected by using a small nail scissors.

5.2.4. On-site analysis of dried blood spots

For the portable assessment of cholinesterase inhibition, the ChE check mobile test kit was used, based on a reference method developed by Worek et al.³⁸ The suggested protocol was to use 10 µL whole blood, which could be obtained by using a finger-prick device. In this research initial experiments were performed with 10 µL liquid blood as well. This was later extended to the application of half a spot (12.5 µL) created from a volume of 25 µL whole blood, which was cut and brought into a vial with 2 mL buffer, that was provided with the ChE check mobile test kit. The DBS was extracted for one hour with gentle shaking. Afterwards, the cap was replaced for a reagent cap and either the AChE or BChE activity was measured by the ChE check mobile test kit (Securetec, Neubiberg, Germany).

5.2.5. Protein isolation and digestion from dried blood spots

5.2.5.1. Human butyrylcholinesterase adducts

The 25 µL spots, inhibited with an excess of 0.4 µM, were extracted in 0.5 mL PBS for 30 minutes with gentle shaking. A volume of 200 µL was added to the KingFisher magnetic particle processor (mL system, Thermo Fisher, Waltham, MA, USA) for isolation of human BChE using anti-HuBChE antibodies conjugated to magnetic beads according to the method as described by D. Noort et al.³⁹ After digestion with pepsin the nonapeptide adduct could be analyzed with LC-MS/MS as described in section 5.2.6.1.

5.2.5.2. Tyrosine adducts

In addition, samples were digested by pronase using a method designed for the analysis of tyrosine adducts after sarin exposure.³ A volume of 100 µL whole blood or a 50 µL-based dried blood spot extracted in 0.5 mL PBS was added to a 2 mL Eppendorf vial with 0.6 mL of acetone for protein precipitation. After centrifugation at 14000 rpm for 5 min (Eppendorf 5417R), the acetone layer was discarded, and the protein precipitate was allowed to dry in the air at ambient temperature for 30 minutes. Then, the isolated protein was dissolved in 400 µL of aqueous ABC buffer (50 mM) and an aqueous solution of 100 µL of pronase (10 mg/mL in 50 mM ABC). The samples were incubated for 90 minutes in a Thermoshaker (Grant-bio PHMT) at 50 °C and 500 rpm. Subsequently, the digest was purified using a reversed phase solid phase extraction (SPE) C18 column (Bakerbond SPE™).⁴⁵ After drying under nitrogen, the sample was dissolved in 50 µL water with 0.2% v/v formic acid and analyzed with LC-MS/MS as described in Section 5.2.6.1.

5.2.5.3. Phosphonic acid metabolites

Additionally, the samples were prepared for phosphonic acid analysis, based on sample preparation procedures for blood plasma. First 400 µL of the PBS extract of a 50 µL-based DBS and 100 µL 10 M HCl to protonate the phosphonic acids, were mixed in a 4 mL vial. Then, the sample was extracted four times with 2 mL diethyl ether/acetonitrile (85/15 %v/v). Finally, all extracts were combined and dried under nitrogen. Subsequently, the residue was dissolved in 50 µL water with 0.2% v/v formic acid and analyzed with LC-MS/MS as described in Section 5.2.6.1.

5.2.5.4. Intact agent analysis and fluoride-induced reactivation of protein adducts

For intact agent analysis, liquid extraction was performed with 300 µL DCM for 200 µL whole blood or a 50 µL DBS. The extract was subsequently analyzed by GC-MS as described in Section 5.2.6.2. For the fluoride reactivation^{3,42} a 4 mL vial was filled with 400 µL liquid blood or a 400 µL PBS extract of a 50 µL dried blood spot and 1.2 mL acetate buffer (0.2 M, pH=3.5), and placed in a water bath at 25 °C. After 10 minutes, 75 µL potassium fluoride solution (5.25 M) was added resulting in a final fluoride concentration of 250 mM. The vial was kept in the water bath for 15 additional minutes at 25 °C. Afterwards, the sample was loaded on the conditioned cartridge and washed with 0.5 mL, 0.8 M sodium bicarbonate solution. Then the sample was eluted with 2 mL chloroform and collected in a centrifugal tube. The water was frozen by holding the tube in dry ice mixed with acetone. The organic layer was collected and added to a 4 mL vial together with 150 µL ethyl acetate. The sample was concentrated under a gentle stream of nitrogen until a final volume of 100-150 µL was reached and subsequently analyzed by GC-MS/MS, as described in Section 5.2.6.3. Conditioning of the cartridge

was performed as follows: a NEXUS LRC cartridge (Agilent Technologies) with a bed mass of 60 mg and a volume of 10 mL was conditioned with subsequently 2 mL hexane, two times 4 mL ethyl acetate, two times 4 mL chloroform, and two times 5 mL water.

5.2.6. Instrumental analysis

5.2.6.1. LC-MS/MS

The nonapeptide and tyrosine adducts and the hydrolysis products of GB, Novichok A-230, A-232, and A-234 were analyzed on a Waters Acquity ultra-high pressure liquid chromatographic (UPLC) system equipped with a Waters Acquity HSS T3 C18 column (1.8 µm, 2.1 x 100 mm). Samples were kept at 8 °C in the autosampler and the injection volume was 5 µL. The analysis was performed at room temperature with a gradient flow of 100 µL/min. Eluent A was 0.2 v% formic acid in MilliQ water and eluent B was 0.2 v% formic acid in acetonitrile. The optimized gradient elution settings are specified in Section 2 of the Supplemental Information. The UPLC system was coupled to a Waters (Milford, MA, USA) Xevo TQ-S triple-quadrupole mass spectrometer, equipped with electrospray ionization for detection of the analytes in positive ionization mode. A capillary voltage of 3.5 kV was used with a nitrogen cone gas flow of 150 L/h and an argon collision gas flow of 0.19 mL/min. For each category of biomarkers, all nerve agents could be analyzed with a single chromatographic method³⁹. Data was first acquired in full scan mode and afterwards in multiple reaction monitoring (MRM) mode. The monitored mass transitions can be found in Section 2 of the Supplemental Information. Compounds were identified by comparison with reference standards, in accordance with OPCW guidelines for biomedical analysis.⁴⁶

5.2.6.2. GC-MS

The intact agent was analyzed on an Agilent 7890B GC equipped with an Agilent VF-5ms column (5% phenylmethyl polysiloxane, 30 m x 0.25 mm x 0.25 µm). One microliter sample was injected using an autosampler (Combi Pal, Ctc analytics). Helium was used as the carrier gas at a constant flow of 1 mL/min. The GC injector was operated in splitless mode at 275 °C. The split vent was opened at 0.5 min at 50 mL/min. The oven temperature was maintained at 90 °C for 1 min., then ramped at 10 °C/min. to 325 °C and held for 5 min. Detection was performed with an Agilent 5977A MS, which operated in electron ionization (EI) mode with an ionization potential of 70 eV and a scan range of 25–550 mass units. A solvent delay time of 2.6 minutes was applied. Compounds were identified by comparison with reference standards.

5.2.6.3. GC-MS/MS

The free nerve agent and the reactivated organophosphates after fluoride addition were also measured by an Agilent 8890 GC with an Agilent VF-5ms column (5% phenylmethyl polysiloxane, 30 m x 0.25 mm x 1 µm). A volume of 1 µL was injected with

a PAL RTC autosampler. A helium column flow of 1 mL/min was used. The GC injector was operated in splitless mode at 280 °C. The split vent was opened at 0.5 min with a flow of 50 mL/min. The oven temperature was maintained at 40 °C for 1 min, then ramped at 10 °C/min to 240 °C and then increased at 100 °C/min to 280 °C, which was maintained for 3 min. The GC system was coupled to an Agilent 7000D triple-quadrupole mass spectrometer, which operated in electron ionization (EI) mode. Nitrogen was used as a collision gas at 1.5 ml/min and a quench flow of 2.25 mL/min helium was applied. The solvent delay time was 3 minutes. Data were acquired in MRM mode. The monitored mass transitions and quantification method are described in Section 2 of the Supplemental Information. The method was in agreement with the OPCW guidelines for biomedical analysis.⁴⁶

5.3. Results & Discussion

5.3.1. On-site analysis of cholinesterase inhibition

Figure 5.2 shows the reduced cholinesterase activity after nerve agent inhibition of blood. As expected, a negative linear correlation was observed after exposure to GB or Novichok nerve agents. For GB, blood was exposed to an excess of nerve agent (1.3 μ M), to enable occupation of all accessible protein sites. It was expected that the remaining non-reacted GB would be hydrolyzed after one day and would be incapable of reacting with the non-exposed blood when mixing exposed and non-exposed blood in various ratios. For the Novichoks a 40 times lower concentration was applied (33 nM), because intact nerve agent remained in the sample, as described in section 5.3.3. This would otherwise react with the non-exposed blood when mixing in various ratios resulting in a lower ChE activity (Figure S4 in the Supplemental Information). For all Novichok variants tested the same degree of inhibition was observed, hence it was decided to present the average value for all variants in Figure 2. Because of the limited number of supplies for the ChE check mobile test kit, only three concentrations were evaluated for AChE inhibition of Novichok nerve agents. Figure 2 illustrates activities measured in dried blood spots one month after storage of the dried blood spots at ambient conditions. The activities shown for non-exposed blood correspond well with reference values for AChE and BChE activity of respectively 33 – 49 U/gHb and 1623 – 3861 U/L, reported by Worek et al based on blood analysis of 242 volunteers.³⁶

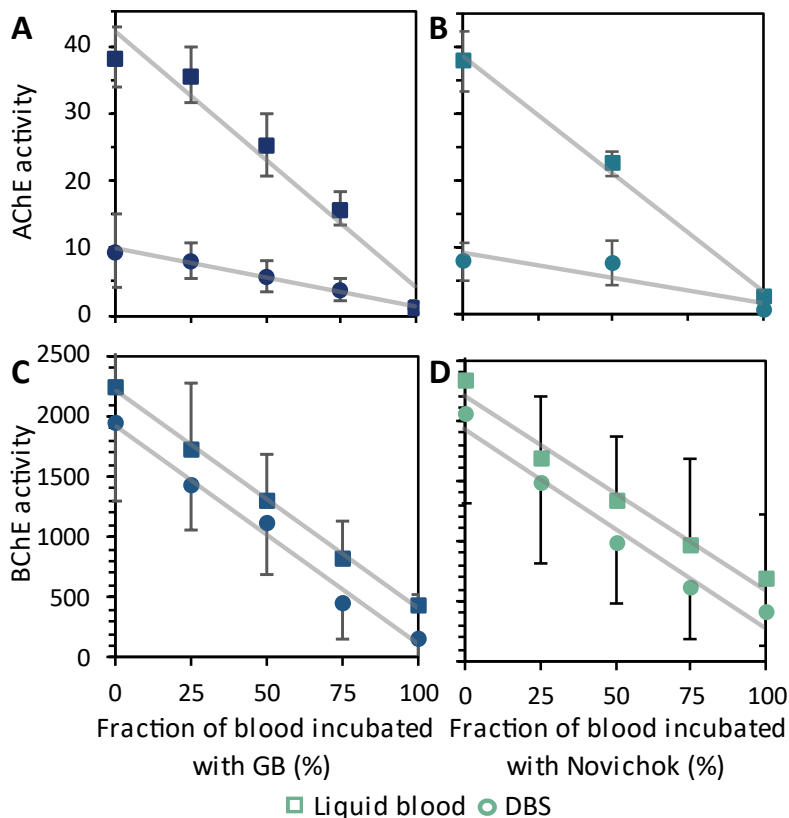


Figure 5.2. Cholinesterase activity of 10 µL liquid blood (□) and half a 25 µL-based DBS (12.5 µL) (○), one month after storage of the dried spots at ambient conditions. For GB an excess of 1.3 µM incubation was assumed to give 100% inhibition. For Novichok the fraction of blood incubated with 33 nM Novichok nerve agent is shown. A) AChE activity after GB inhibition (n=7), B) Average AChE activity after Novichok inhibition A-230, A-232, and A-234 (n=3), C) BChE activity after GB inhibition (n=8), D) Average BChE activity after Novichok A-230, A-232, and A-234 inhibition (n=9). Error bars represent ± 1 standard deviation (for clarity only positive error bars are shown for BChE activity of liquid blood and negative error bars for DBS).

For BChE similar behavior for liquid blood and dried blood spots is observed, although the dried blood spot consistently yields slightly lower activity. However, the AChE activity in dried blood spots was considerably lower than the activity in whole blood. This might be due to loss of AChE in vesicles that are generated during the concentration of red blood cells, which results in a reduced enzymatic activity.⁴⁷ Therefore, the AChE activity measurement of DBS does not provide a reliable indicator of CWA exposure. Interestingly, the activities measured in dried blood spots did not significantly change over a period of three months (Figure S5, Supplemental Information), which makes it a promising tool for retrospective nerve agent diagnosis.

5.3.2. Detection of BChE nonapeptide adducts by LC-MS/MS

A more specific method to verify nerve agent exposure and identify the agent is by utilizing a semi-targeted human butyrylcholinesterase nonapeptide assay. The nonapeptide adducts of sarin and Novichok nerve agents (incubation level 0.4 μM) were identified in dried blood spots, one month after storage of the dried spots at ambient conditions, as illustrated in Figure 5.3.

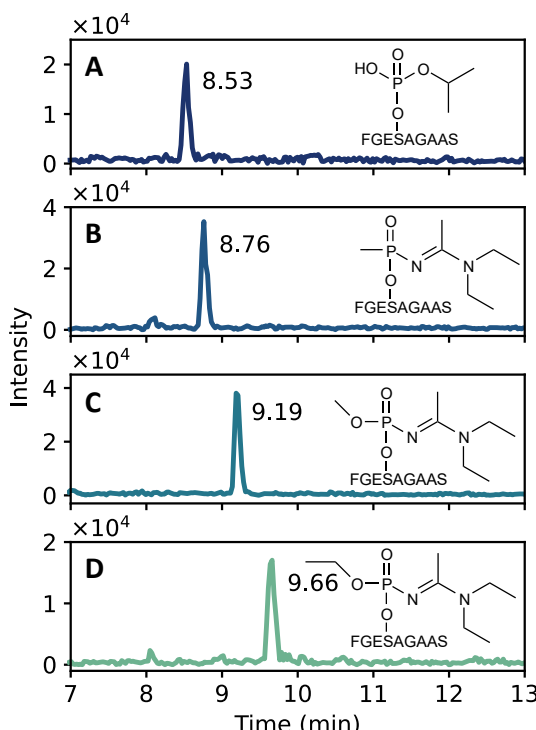


Figure 5.3. Extracted ion chromatograms of human BChE adducts measured in 100% inhibited dried blood spots (25 μl , 0.4 μM), one month after storage of the dried spots at ambient conditions. A) Sarin (m/z 916.3 \rightarrow 778.3), B) Novichok A-230 (m/z 970.4 \rightarrow 778/3), C) Novichok A-232 (m/z 986.4 \rightarrow 778/3), D) Novichok A-234 (m/z 1000.4 \rightarrow 778/3).

The biomarkers were verified with the use of references of Novichok spiked in plasma. Although the assessment of Novichok exposure in human plasma has been investigated before,³⁹ the current research demonstrated for the first time that these BChE adducts can also detected in dried blood spots. In addition, the sensitivity of the method was assessed. Figure 5.4 shows the extracted ion chromatograms of the nonapeptide adduct of A-234 for various percentages of inhibited blood. In a 25 μL dried blood spot with 50% inhibition, the biomarker could clearly be identified, while at 25% inhibition its presence is near the detection limit. The presence of the biomarker did not show a

linear trend, which is likely due to losses which occurred during the extensive sample preparation procedure.

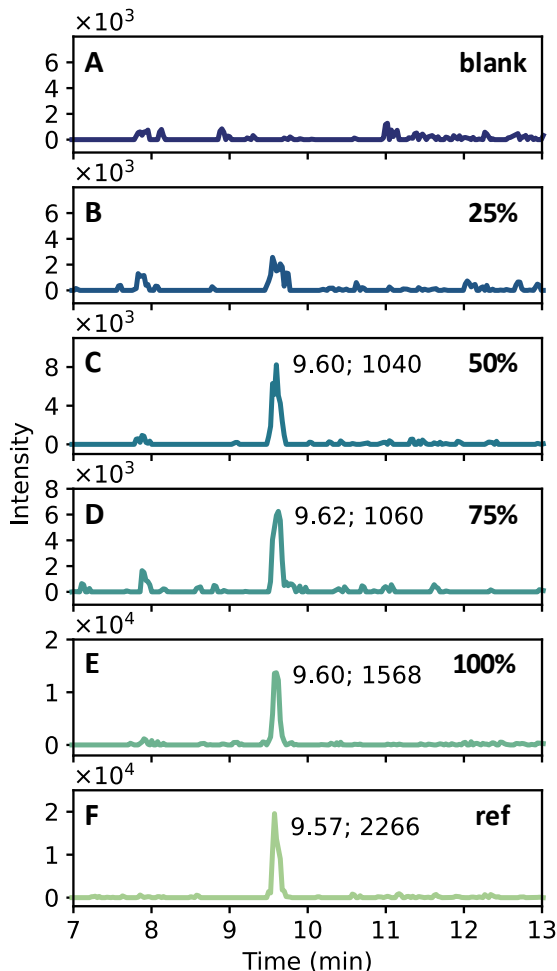


Figure 5.4. Extracted ion chromatograms of human BChE adducts of Novichok A-234 measured in 25 μL dried blood spots (excess exposure of 0.4 μM), one month after storage of the dried spots at ambient conditions (m/z 1000.4 \rightarrow 778/3). Corresponding retention times and peak areas are shown. A) sample preparation blank, B) 25%, C) 50%, D) 75%, E) 100% inhibited blood and F) Reference of Novichok A-234 spiked in 12.5 μL plasma (100% inhibition).

In future research, this might be resolved by using an internal standard, that could be added prior to the sample preparation. To give an indication how the DBS method relates to the direct detection of the nonapeptides in blood, a reference of Novichok A-234 was spiked in 12.5 μL plasma. The BChE was isolated with the same batch of magnetic beads and subsequently digested with the same pepsin solution. This should then in principle give a similar biomarker concentration as for the 25 μL DBS (assuming

55% of plasma in blood). As demonstrated in Figure 4E-4F, a 1.5-fold reduction in sensitivity is visible for DBS compared to plasma.

5.3.3. Analysis of free and regenerated nerve agent by GC-MS/MS and LC-MS/MS

The unambiguous verification of nerve agent exposure requires the identification of multiple biomarkers or the application of at least two analytical techniques.⁴⁶ A suitable supplementary method is the analysis of nerve agents after fluoride-induced reactivation by GC-MS/MS and LC-MS/MS. Earlier research demonstrates that very low concentrations, even below toxicologically relevant exposure levels, could be monitored in plasma and serum using this reactivation procedure.^{48,49} Therefore, the current study evaluates whether this method could be extended to dried blood spots as well. Figure 5.5 demonstrates that regenerated sarin was detected by GC-MS/MS using dried blood spots. The same result was found for liquid whole blood (Figure S6 in the Supplemental Information).

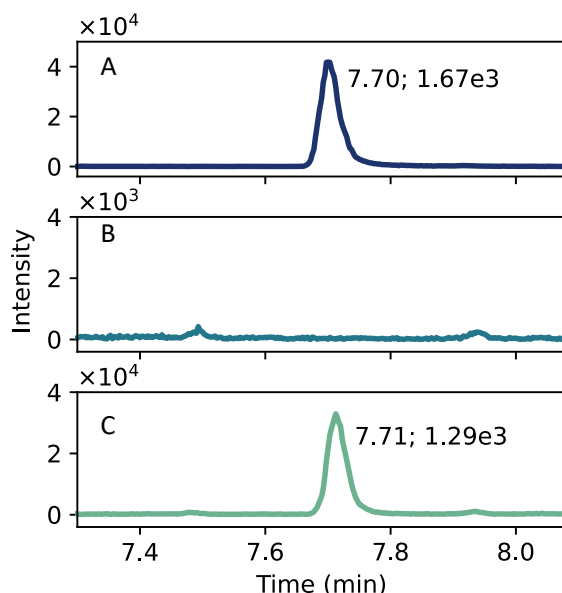


Figure 5.5. Extracted ion chromatograms of regenerated sarin in dried blood spots ($50 \mu\text{L}$, 33nM) after fluoride reactivation analyzed by GC-MS/MS, three days after storage of the dried spots at ambient conditions ($m/z 99 \rightarrow 81$). Corresponding retention times and peak areas are shown. A) Reference standard of sarin, B) Dried blood spots exposed to sarin without KF addition (control), C) DBS exposed to sarin with KF addition.

No intact sarin was detected in dried spots of human whole blood, exposed to this nerve agent, without KF addition. This confirms that the analyzed sarin is the result of regeneration after KF addition and hence was bound to the biomatrix. A concentration

of 5 ng/mL was established ($n=3$) after processing of a 50 μL dried blood spot. This is a higher level than expected based on the available ChE sites. A partial explanation would be the formation of other protein adducts besides ChE-adducts. In addition, it is likely that some solvent was evaporated during the sample preparation, resulting in a more concentrated sample.

The same procedure was applied to the Novichok nerve agents. Both GC-MS/MS and LC-MS/MS were employed, but the LC-MS/MS method appeared to be more sensitive since a 1 ng/mL sample was not detected by GC-MS/MS, while LC-MS/MS still showed a clearly visible peak. It should be noted that the current study mainly focuses on qualitative research, therefore future validation should verify this finding. Figure 5.6 shows the LC-MS/MS chromatograms of A-232 analyzed in dried blood spots without KF addition (control), and with KF addition (KF), compared to a reference standard. The peak areas of the nerve agents are similar or higher in the control samples than in the KF-regenerated samples. The same result was found for A-230 and A-234 in dried blood spots and for the Novichok nerve agents in liquid whole blood (Section S5 and S6 in the Supplemental Information).

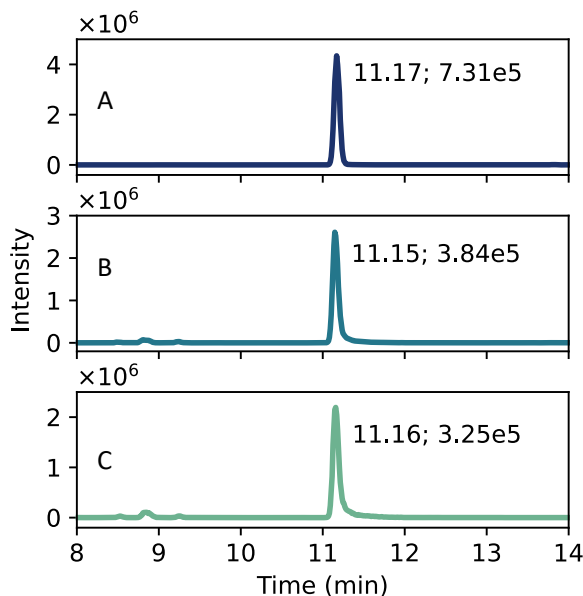


Figure 5.6. Extracted ion chromatograms of intact Novichok A-232 (211 → 73.8) in dried blood spots (50 μL , 33 nM) analyzed by LC-MS/MS, three days after storage of the dried spots at ambient conditions. Corresponding retention times and peak areas are shown. A) Reference standard, B) Dried blood spots exposed to nerve agent without KF addition (control), C) DBS exposed to nerve agent with KF addition.

No excess of Novichok agents (33 nM) was added during the in-vitro exposure, which suggests that not all available cholinesterase sites have been occupied and that the remaining chemical is not hydrolyzed. The latter is in accordance with previous research stating that the hydrolysis rate of Novichoks is considerably slower than for sarin.⁵⁰ Since intact nerve agent was detected at the same or higher level in both liquid whole blood and dried blood spots without KF addition compared to the samples with KF addition, it appears that no fluoride regeneration has occurred. This is a somewhat surprising observation, since the current study does not support the conclusions of Mirbabaei et al⁴². In this previous study no control samples without KF addition were shown. Although two methods were used for the removal of free A-234, this might have been ineffective. The observed A-234 in the KF samples could then originate from free agent instead of the regenerated agent, similar to the findings in the current study for both liquid and DBS samples of A-230, A-232 and A-234. Therefore, it is more relevant to use the intact Novichok nerve agent for retrospective analysis of Novichok nerve agent exposure in comparison with the fluoride reactivation method.

5.3.4. Limitations of dried blood spot analysis

In addition to phosphorylated serine adducts, tyrosine adducts in blood have also been used as marker to verify sarin poisoning, although lower concentrations were reported for this biomarker.³ Other studies confirm the presence of such adducts after the processing of a 400 µL dried blood spot.²³ However, in the current study no tyrosine adducts have been detected after the sample preparation of a 50 µL dried blood spot. Since the primary ChE targets will interact first and then the secondary albumin sites, experiments were also performed with blood incubated to an excess (1.3 µM) of chemical agent to make it more likely that all available protein adduct sites were occupied. However, after excess addition no albumin adducts were detected. This is most likely due to the limited sample volume handled with DBS, which results in an adduct concentration below the detection limit in the final extract.

The dried blood spots exposed to excess sarin (1.3 µM) were also screened for the hydrolysis products IMPA and MPA using LC-MS/MS. The latter was not detected and IMPA could not unambiguously be identified because only one mass transition was found at a low level (Figure S10 in the Supplemental information). Phosphonic or phosphoric acids of Novichok nerve agents were also not detected in the extracted ion chromatograms at m/z 193.1, 209.1, and 223.1. The subsequent hydrolysis products methyl phosphonic acid, monomethyl and monoethyl phosphate could also not be detected at m/z 97.0, 113.0, and 126.0, respectively. Shaner et al. demonstrated the possibility to analyze organophosphate hydrolysis products in dried blood spots by hydrophilic interaction liquid chromatography (HILIC).²⁰ Future research could focus on applying this method to dried blood spots exposed to Novichok nerve agents as well.

5.4. Conclusions

A toolbox of analytical techniques was developed for the retrospective analysis of nerve agent exposure using dried blood spots. We have demonstrated the possibility of on-site point-of-care diagnosis after sarin and Novichok nerve agent exposure using the ChE mobile test kit for BChE activity measurements. An advantage of using DBS compared to liquid whole blood is the less invasive sample collection and the possibility to store the sample under ambient conditions and conduct the analysis at a later stage. In addition, laboratory analysis of nonapeptide adducts with LC-MS/MS enabled a sensitive and selective manner to verify exposure and identify the agent involved. Additionally, the analysis of fluoride-induced regenerated sarin by GC-MS/MS provided a suitable supplementary method for verification purposes. For the first time the feasibility of detecting regenerated sarin in dried blood spots was demonstrated. For the Novichok nerve agents, no regenerated Novichok was detected. However, the intact chemical would be a valuable biomarker for unambiguous verification. This work shows that the corresponding nerve agent biomarkers in dried blood spots are very stable and can be detected at least one month after application on a protein saver card and storage under ambient conditions. Furthermore, the implementation in forensic practice is relatively straightforward due to the less invasive sample collection and safer and easier shipping and storage conditions. Future research should focus on the improvement of the sample preparation methods to further lower the detection limit and fully validate the quantitative method. In conclusion, the on-scene analysis of biomarkers in dried blood spots followed by laboratory verification is a promising analysis scheme to verify nerve agent exposure. This should however be confirmed in practice with regular and dried blood spot samples from an alleged exposure victim or animal model exposure studies. Fortunately, CWA exposure incidents are relatively rare which can hamper field validation.

References

- (1) OPCW. First Report by the OPCW Investigation and Identification Team (IIT) Pursuant to Paragraph 10 of Decision C-SS-4/Dec.3 "Addressing the Threat From Chemical Weapons Use" Ltamenah (Syrian Arab Republic) 24, 25, and 30 March 2017. <https://www.opcw.org/sites/default/files/documents/2020/04/s-1867-2020%28e%29.pdf> (accessed 2023-02-06).
- (2) OPCW. Report of the OPCW Fact-Finding Mission in Syria Regarding an Alleged Incident in Khan Shaykhun, Syrian Arab Republic April 2017. https://www.opcw.org/sites/default/files/documents/Fact_Finding_Mission/s-1510-2017_e_.pdf (accessed 2023-02-06).
- (3) John, H.; Schans, M. J. van der; Koller, M.; Spruit, H. E. T.; Worek, F.; Thiermann, H.; Noort, D.; John, H. Fatal Sarin Poisoning in Syria 2013: Forensic Verification within an International Laboratory Network. *Forensic Toxicol* **2018**, *36*, 61–71. <https://doi.org/10.1007/s11419-017-0376-7>.
- (4) Nakagawa, T.; Tu, A. T. Murders with VX: Aum Shinrikyo in Japan and the Assassination of Kim Jong-Nam in Malaysia. *Forensic Toxicol* **2018**, *36*, 542–544. <https://doi.org/10.1007/s11419-018-0426-9>.
- (5) OPCW. Summary of the report on activities carried out in support of a request for technical assistance by the United Kingdom of Great Britain and Northern Ireland. https://www.opcw.org/sites/default/files/documents/S_series/2018/en/s-1612-2018_e__1_.pdf (accessed 2023-02-06).
- (6) OPCW. *Summary of the report on activities carried out in support of a request for technical assistance by Germany*. <https://www.opcw.org/sites/default/files/documents/2020/10/s-1906-2020%28e%29.pdf> (accessed 2023-02-06).
- (7) Aroniadou-Anderjaska, V.; Apland, J. P.; Figueiredo, T. H.; De Araujo Furtado, M.; Braga, M. F. Acetylcholinesterase Inhibitors (Nerve Agents) as Weapons of Mass Destruction: History, Mechanisms of Action, and Medical Countermeasures. *Neuropharmacology* **2020**, *181*, 108298. <https://doi.org/10.1016/j.neuropharm.2020.108298>.
- (8) OPCW. *What is a Chemical Weapon*. <https://www.opcw.org/our-work/what-chemical-weapon> (accessed 2022-06-12).
- (9) The National Institute for Occupational Safety and Health (NIOSH). Sarin (GB): Nerve Agent. https://www.cdc.gov/niosh/ershdb/emergencyresponsecard_29750001.html (accessed 2022-06-12).
- (10) Costanzi, S.; Koblentz, G. D. Controlling Novichoks after Salisbury: Revising the Chemical Weapons Convention Schedules. *Nonproliferation Review* **2019**, *26* (5–6), 599–612. <https://doi.org/10.1080/10736700.2019.1662618>.
- (11) Steindl, D.; Boehmerle, W.; Körner, R.; Praeger, D.; Haug, M.; Nee, J.; Schreiber, A.; Scheibe, F.; Demin, K.; Jacoby, P.; Tauber, R.; Hartwig, S.; Endres, M.; Eckardt, K. U. Novichok Nerve Agent Poisoning. *The Lancet* **2021**, *397* (10270), 249–252. [https://doi.org/10.1016/S0140-6736\(20\)32644-1](https://doi.org/10.1016/S0140-6736(20)32644-1).
- (12) Franca, T. C. C.; Kitagawa, D. A. S.; Cavalcante, S. F. de A.; da Silva, J. A. V.; Nepovimova, E.; Kuca, K. Novichoks: The Dangerous Fourth Generation of Chemical Weapons. *Int J Mol Sci* **2019**, *20*, 1222. <https://doi.org/10.3390/ijms2005122>.
- (13) Plamboeck, A. H.; Stöven, S.; Duarte, R.; Fykse, E.; Griffiths, M.; Nieuwenhuizen, M.; Rivier, C.; Schans, M. Van Der. Trends in Analytical Chemistry Laboratory Analysis of CBRN-Substances : Stakeholder Networks as Clue to Higher CBRN Resilience in Europe. *Trends in Analytical Chemistry* **2016**, *85*, 2–9. <https://doi.org/10.1016/j.trac.2016.03.006>.
- (14) Witkiewicz, Z.; Neffe, S. Chromatographic Analysis of Chemical Warfare Agents and Their Metabolites in Biological Samples. *TrAC - Trends in Analytical Chemistry* **2020**, *130*, 115960. <https://doi.org/10.1016/j.trac.2020.115960>.
- (15) Hamelin, E. I.; Blake, T. A.; Perez, J. W.; Crow, B. S.; Shaner, R. L.; Coleman, R. M.; Johnson, R. C. Bridging the Gap between Sample Collection and Laboratory Analysis: Using Dried Blood Spots to Identify Human Exposure to Chemical Agents. *Proc. SPIE 9863, Smart Biomedical and Physiological Sensor Technology XIII* **2016**, *9863P*. <https://doi.org/10.1117/12.2223796>.

Detection of nerve agent biomarkers in dried blood spots

5

- (16) Ackermans, M. T.; de Kleijne, V.; Martens, F.; Heijboer, A. C. Hematocrit and Standardization in DBS Analysis: A Practical Approach for Hormones Mainly Present in the Plasma Fraction. *Clinica Chimica Acta* **2021**, *520* (January), 179–185. <https://doi.org/10.1016/j.cca.2021.06.014>.
- (17) John, H.; Willoh, S.; Hörmann, P.; Siegert, M.; Vondran, A.; Thiermann, H. Procedures for Analysis of Dried Plasma Using Microsampling Devices to Detect Sulfur Mustard-Albumin Adducts for Verification of Poisoning. *Anal Chem* **2016**, *88*, 8787–8794. <https://doi.org/10.1021/acs.analchem.6b02199>.
- (18) Yishai Aviram, L.; Loewenthal, D.; Weissberg, A.; Marder, D.; Gura, S.; Chapman, S.; Gez, R.; Lazar, S.; Dagan, S. Determination of Free G-Type Nerve Agents in Blood: In Situ Derivatization on a Dried Blood Spot (DBS) Paper Followed by LC–MS/MS Analysis. *Forensic Toxicol* **2020**, *38* (2), 327–339. <https://doi.org/10.1007/s11419-019-00516-8>.
- (19) Marder, D.; Dagan, S.; Yishai-Aviram, L.; Loewenthal, D.; Chapman, S.; Adani, R.; Lazar, S.; Weissberg, A.; Gura, S. Instantaneous Monitoring of Free Sarin in Whole Blood by Dry Blood Spot–Thermal Desorption–GC–FPD/MS Analysis. *Journal of Chromatography B* **2020**, *1136*, 121911. <https://doi.org/10.1016/j.jchromb.2019.121911>.
- (20) Shaner, R. L.; Coleman, R. M.; Schulze, N.; Platanitis, K.; Brown, A. A.; Seymour, C.; Kaplan, P.; Perez, J.; Hamelin, E. I.; Johnson, R. C. Investigation of Dried Blood Sampling with Liquid Chromatography Tandem Mass Spectrometry to Confirm Human Exposure to Nerve Agents. *Anal Chim Acta* **2018**, *1033*, 100–107. <https://doi.org/10.1016/j.aca.2018.06.049>.
- (21) Yishai Aviram, L.; Magen, M.; Chapman, S.; Neufeld Cohen, A.; Lazar, S.; Dagan, S. Dry Blood Spot Sample Collection for Post-Exposure Monitoring of Chemical Warfare Agents – In Vivo Determination of Phosphonic Acids Using LC–MS/MS. *Journal of Chromatography B* **2018**, *1093–1094*, 60–65. <https://doi.org/10.1016/j.jchromb.2018.06.035>.
- (22) McKenna, J.; Dhummakupt, E. S.; Connell, T.; Demond, P. S.; Miller, D. B.; Michael Nilles, J.; Manicke, N. E.; Glaros, T. Detection of Chemical Warfare Agent Simulants and Hydrolysis Products in Biological Samples by Paper Spray Mass Spectrometry. *Analyst* **2017**, *142*, 1442–1451. <https://doi.org/10.1039/c7an00144d>.
- (23) Koryagina, N. L.; Aliushina, T. I.; Karakashev, G. V.; Savel'eva, E. I.; Khlebnikova, N. S.; Radilov, A. S. Determination of Phosphonylated Tyrosine as a Marker of Exposure to Nerve Agents in Dried Blood Plasma Spots by HPLC–HRMS/MS. *Journal of Analytical Chemistry* **2019**, *74* (13), 1341–1348. <https://doi.org/10.1134/S1061934819130070>.
- (24) Perez, J. W.; Pantazides, B. G.; Watson, C. M.; Thomas, J. D.; Blake, T. A.; Johnson, R. C. Enhanced Stability of Blood Matrices Using a Dried Sample Spot Assay to Measure Human Butyrylcholinesterase Activity and Nerve Agent Adducts. *Anal Chem* **2015**, *87*, 5723–5729. <https://doi.org/10.1021/acs.analchem.5b00893>.
- (25) Massano, M.; Incardona, C.; Gerace, E.; Negri, P.; Alladio, E.; Salomone, A.; Vincenti, M. Development and Validation of a UHPLC–HRMS–QTOF Method for the Detection of 132 New Psychoactive Substances and Synthetic Opioids, Including Fentanyl, in Dried Blood Spots. *Talanta* **2022**, *241*, 123265. <https://doi.org/https://doi.org/10.1016/j.talanta.2022.123265>.
- (26) Skaggs, C.; Kirkpatrick, L.; Nguyen, C.; Dowling, S.; Zimmerman, H.; Ren, G.; Manicke, N. Simultaneous Optimization of Paper Spray Substrates and Solvents for Hydrophilic and Hydrophobic Molecules. *Int J Mass Spectrom* **2021**, *470*, 116705. <https://doi.org/10.1016/j.ijms.2021.116705>.
- (27) Rocca, L. M.; L'episcopo, N.; Gordiani, A.; Vitali, M.; Staderini, A. A ‘Dilute and Shoot’ Liquid Chromatography–Mass Spectrometry Method for Multiclass Drug Analysis in Pre-Cut Dried Blood Spots. *Int J Environ Res Public Health* **2021**, *18*, 1–20. <https://doi.org/10.3390/ijerph18063068>.
- (28) Seymour, C.; Shaner, R. L.; Feyereisen, M. C.; Wharton, R. E.; Kaplan, P.; Hamelin, E. I.; Johnson, R. C. Determination of Fentanyl Analog Exposure Using Dried Blood Spots with LC–MS–MS. *J Anal Toxicol* **2019**, *43*, 266–276. <https://doi.org/10.1093/jat/bky096>.
- (29) McKenna, J.; Jett, R.; Shanks, K.; Manicke, N. E. Toxicological Drug Screening Using Paper Spray High-Resolution Tandem Mass Spectrometry (HR-MS/MS). *J Anal Toxicol* **2018**, *42*, 300–310. <https://doi.org/10.1093/jat/bky001>.
- (30) Shaner, R. L.; Schulze, N. D.; Seymour, C.; Hamelin, E. I.; Thomas, J. D.; Johnson, R. C. Quantitation of Fentanyl Analogs in Dried Blood Spots by Flow-through Desorption Coupled to Online Solid Phase

5

Chapter 5

- Extraction Tandem Mass Spectrometry. *Analytical Methods* **2017**, *9*, 3876–3883. <https://doi.org/10.1039/c7ay00532f>.
- (31) Chepyala, D.; Tsai, I. L.; Liao, H. W.; Chen, G. Y.; Chao, H. C.; Kuo, C. H. Sensitive Screening of Abused Drugs in Dried Blood Samples Using Ultra-High-Performance Liquid Chromatography-Ion Booster-Quadrupole Time-of-Flight Mass Spectrometry. *J Chromatogr A* **2017**, *1491*, 57–66. <https://doi.org/10.1016/j.chroma.2017.02.037>.
- (32) Verplaetse, R.; Henion, J. Quantitative Determination of Opioids in Whole Blood Using Fully Automated Dried Blood Spot Desorption Coupled to On-Line SPE-LC-MS/MS. *Drug Test Anal* **2016**, *8*, 30–38. <https://doi.org/10.1002/dta.1927>.
- (33) Odoardi, S.; Anzillotti, L.; Strano-Rossi, S. Simplifying Sample Pretreatment: Application of Dried Blood Spot (DBS) Method to Blood Samples, Including Postmortem, for UHPLC-MS/MS Analysis of Drugs of Abuse. *Forensic Sci Int* **2014**, *243*, 61–67. <https://doi.org/10.1016/j.forsciint.2014.04.015>.
- (34) Clavijo, C. F.; Thomas, J. J.; Cromie, M.; Schniedewind, B.; Hoffman, K. L.; Christians, U.; Galinkin, J. L. A Low Blood Volume LC-MS/MS Assay for the Quantification of Fentanyl and Its Major Metabolites Norfentanyl and Despropionyl Fentanyl in Children. *J Sep Sci* **2011**, *34*, 3568–3577. <https://doi.org/10.1002/jssc.201100422>.
- (35) Li, D.; Li, Z.; Xu, B.; Chen, J.; Xue, J.; Hu, S.; Wen, L.; Guo, L.; Xie, J.; Jiang, G. Thermal Desorption Bridged the Gap between Dielectric Barrier Discharge Ionization and Dried Plasma Spot Samples for Sensitive and Rapid Detection of Fentanyl Analogs in Mass Spectrometry. *Analyst* **2022**, *147*, 4187–4196. <https://doi.org/10.1039/d2an00946c>.
- (36) Worek, F.; Schilha, M.; Neumaier, K.; Aurbek, N.; Wille, T.; Thiermann, H.; Kehe, K. On-Site Analysis of Acetylcholinesterase and Butyrylcholinesterase Activity with the ChE Check Mobile Test Kit-Determination of Reference Values and Their Relevance for Diagnosis of Exposure to Organophosphorus Compounds. *Toxicol Lett* **2016**, *249*, 22–28. <https://doi.org/10.1016/j.toxlet.2016.03.007>.
- (37) Ellman, G. L.; Courtney, K. D.; Andres, V.; Featherstone, R. M. A New and Rapid Colorimetric Determination of Acetylcholinesterase Activity. *Biochem Pharmacol* **1961**, *7* (2). [https://doi.org/10.1016/0006-2952\(61\)90145-9](https://doi.org/10.1016/0006-2952(61)90145-9).
- (38) Worek, F.; Mast, U.; Kiderlen, D.; Diepold, C.; Eyer, P. *Improved Determination of Acetylcholinesterase Activity in Human Whole Blood*; 1999; Vol. 288. www.elsevier.com/locate/clinchim.
- (39) Noort, D.; Fidder, A.; Van Der Riet-Van Oeveren, D.; Busker, R.; Van Der Schans, M. J. Verification of Exposure to Novichok Nerve Agents Utilizing a Semitargeted Human Butyrylcholinesterase Nonapeptide Assay. *Chem Res Toxicol* **2021**, *34* (8), 1926–1932. <https://doi.org/10.1021/acs.chemrestox.1c00198>.
- (40) Jeong, W. H.; Lee, J. Y.; Lim, K. C.; Kim, H. S. Identification and Study of Biomarkers from Novichok-Inhibited Butyrylcholinesterase in Human Plasma. *Molecules* **2021**, *26* (13). <https://doi.org/10.3390/molecules26133810>.
- (41) Lee, J. H.; Jang, W. E.; Park, J. H.; Mohammad, H. B.; Lee, J.-Y.; Jeong, W.-H.; Kim, M.-S. Identification of Organophosphate Modifications by High-Resolution Mass Spectrometry. *Bull Korean Chem Soc* **2022**, *43* (3), 444–449. <https://doi.org/10.1002/bkcs.12478>.
- (42) Mirbabaei, F.; Mohammad-Khah, A.; Naseri, M. T.; Babri, M.; Faraz, S. M.; Hosseini, S. E.; Ashrafi, D. Unambiguous Identification and Determination of A234-Novichok Nerve Agent Biomarkers in Biological Fluids Using GC-MS/MS and LC-MS/MS. *Anal Bioanal Chem* **2022**, *414* (11), 3429–3442. <https://doi.org/10.1007/s00216-022-03964-1>.
- (43) Yamaguchi, A.; Miyaguchi, H.; Tokeshi, M. Dimethoxytriadinylation LC-MS/MS of Novichok A-Series Degradation Products in Human Urine. *Anal Chem* **2022**, *94* (11), 4658–4665. <https://doi.org/10.1021/acs.analchem.1c04634>.
- (44) Otsuka, M.; Yamaguchi, A.; Miyaguchi, H. Analysis of Degradation Products of Novichok Agents in Human Urine by Hydrophilic Interaction Liquid Chromatography–Tandem Mass Spectrometry. *Forensic Toxicol* **2022**. <https://doi.org/10.1007/s11419-022-00656-4>.
- (45) de Bruin-Hoegée, M.; Lamriti, L.; Langenberg, J. P.; Olivier, R. C. M.; Chau, L. F.; van der Schans, M. J.; Noort, D.; van Asten, A. C. Verification of Exposure to Chemical Warfare Agents through Analysis of Persistent Biomarkers in Plants. *Analytical Methods* **2023**, *15*, 142–153. <https://doi.org/10.1039/d2ay01650h>.

Detection of nerve agent biomarkers in dried blood spots

- (46) OPCW Technical Secretariat. Work Instruction for the Reporting of the Results of the OPCW Biomedical Proficiency Tests; 2021.
- (47) Leal, J. K. F.; Adjobo-Hermans, M. J. W.; Brock, R.; Bosman, G. J. C. G. M. Acetylcholinesterase Provides New Insights into Red Blood Cell Ageing in Vivo and in Vitro. *Blood Transfusion* **2017**, *15* (3), 232–238. <https://doi.org/10.2450/2017.0370-16>.
- (48) Degenhardt, C. E. A. M.; Pleijsier, K.; Van Der Schans, M. J.; Langenberg, J. P.; Preston, K. E.; Solano, M. I.; Maggio, V. L.; Barr, J. R. Improvements of the Fluoride Reactivation Method for the Verification of Nerve Agent Exposure. *J Anal Toxicol* **2004**, *28*. <https://doi.org/10.1093/jat/28.5.364>.
- (49) Holland, K. E.; Solano, M. I.; Johnson, R. C.; Maggio, V. L.; Barr, J. R. Modifications to the Organophosphorus Nerve Agent-Protein Adduct Refluoridation Method for Retrospective Analysis of Nerve Agent Exposures. *J Anal Toxicol* **2008**, *32*. <https://doi.org/10.1093/jat/32.1.116>.
- (50) Noga, M.; Jurowski, K. What Do We Currently Know about Novichoks? The State of the Art. *Archives of Toxicology*. Springer Science and Business Media Deutschland GmbH March 1, 2023, pp 651–661. <https://doi.org/10.1007/s00204-022-03437-5>.



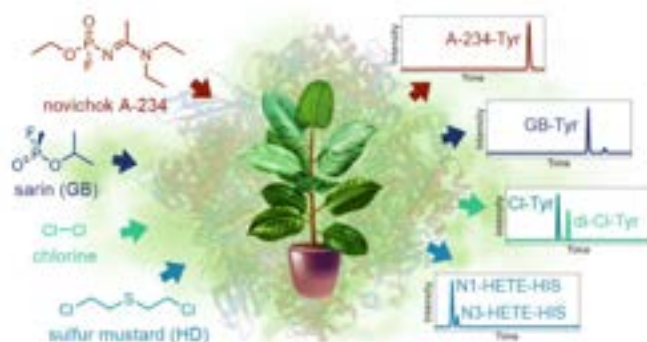
6

Verification of exposure to chemical warfare agents through analysis of persistent biomarkers in plants

Mirjam de Bruin-Hoegée, Latifa Lamriti, Jan Langenberg, René C. M. Olivier, Lai Fun Chau, Marcel J. van der Schans, Daan Noort, Arian C. van Asten, Verification of Exposure to Chemical Warfare Agents through Analysis of Persistent Biomarkers in Plants. *Analytical Methods* **2023**, *15*, 142–153. DOI: 10.1039/d2ay01650h.

Abstract

The continuing threats of military conflicts and terrorism may involve the misuse of chemical weapons. The present study aims to use environmental samples to find evidence of the release of such agents at an incident scene. A novel approach was developed for identifying protein adducts in plants. Basil (*Ocimum basilicum*), bay laurel leaf (*Laurus nobilis*) and stinging nettle (*Urtica dioica*) were exposed to 2.5 to 150 mg/m³ sulfur mustard, 2.5 to 250 mg/m³ sarin, and 0.5 to 25 g/m³ chlorine gas. The vapors of the selected chemicals were generated under controlled conditions in a dedicated set-up. After sample preparation and digestion, the samples were analyzed by liquid chromatography tandem mass spectrometry (LC-MS/MS) and liquid chromatography high resolution tandem mass spectrometry (LC-HRMS/MS), respectively. In case of chlorine exposure, it was found that 3-chloro- and 3,5-dichlorotyrosine adducts were formed. As a result of sarin exposure, the o-isopropyl methylphosphonic acid adduct to tyrosine could be analyzed, and after sulfur mustard exposure the N1- and N3-HETE-histidine adducts were identified. The lowest vapor exposure levels for which these plant adducts could be detected, were 2.5 mg/m³ for sarin, 50 mg/m³ for chlorine and 12.5 mg/m³ for sulfur mustard. Additionally, protein adducts following a liquid exposure of only 2 nmol Novichock A-234, 0.4 nmol sarin and 0.2 nmol sulfur mustard could still be observed. For both vapor and liquid exposure, the amount of adduct formed increased with the level of exposure. In all cases synthetic reference standards were used for unambiguous identification. The window of opportunity for investigation of agent exposure through the analysis of plant material was found to be remarkably long. Even three months after the actual exposure, the biomarkers could still be detected in the living plants, as well as in dried leaves. An important benefit of the current method is that a relatively simple and generic sample work-up procedure can be applied for all agents studied. In conclusion, the presented work clearly demonstrates the possibility of analyzing chemical warfare agent biomarkers in plants, which is useful for forensic reconstructions, including the investigation into alleged use in conflict areas.



6.1. Introduction

The importance of the Chemical Weapons Convention is highlighted by recent concerns of potential chemical attacks in Ukraine.¹ Over the last ten years, violations of the convention have taken place in the ongoing conflict in the Syrian Arab Republic, where the Organisation for the Prohibition of Chemical Weapons (OPCW) verified multiple attacks with sulfur mustard, sarin, and the toxic dual-use chemical chlorine.^{2–6} More recently, Alexei Navalny, Sergei Skripal and four other individuals were poisoned by different nerve agents belonging to the group of Novichocks.^{7,8} These chemical warfare agents (CWAs) exert the same mechanism of action as other organophosphate nerve agents, although they are expected to be even more potent.^{9,10} These incidents emphasize that there is a continued risk of the use of CWAs in both large-scale attacks as well as small scale deployment. Because of the high impact of these events, often extensive international investigations are being conducted to verify the use of chemical weapons.

Analytical methods for the detection of chemical threat agents in matrices such as organic solvents, air samples,^{11–13} soil,^{14,15} wipe,^{16,17} and other solid materials have been broadly investigated.¹⁸ However, detection of intact agents is often not possible due to the relatively high volatility and reactivity of these chemicals.¹⁹ In such cases, biomedical samples may provide evidence for a longer period of time, where persistent biomarkers can be used for verification.^{20,21} Nonetheless, it may be problematic to get access to human biological samples because of ethical, cultural and safety reasons. In addition, it might be difficult to link the victims to the actual exposure area. In contrast, environmental samples such as plant leaves are abundant, easy to collect and transport, and not subject to informed consent or ethic regulations as is the case with human biomedical samples. The use of plant evidence has been scarcely examined for the presence of the intact CWAs or associated degradation products.^{22–26} In addition, a news article reported that researchers at Lawrence Livermore National Laboratory identified small chlorine biomarkers and protein adducts in grass.²⁷ However, to our knowledge, no research article has been published that specifically targets plant protein adducts to demonstrate CWA exposure. We hypothesize that combining the analysis of environmental samples with methods applied to biomedical samples could provide powerful new options to investigate CWA exposure at an incident site long after the alleged release of the agent.

Most CWAs and toxic industrial chemicals can form covalent, long-lasting adducts with proteins.²⁸ This principle has formed the basis for analyzing biomedical samples for verification of exposure to such chemicals. Previous studies have shown that in case of human exposure to sulfur mustard, histidine protein adducts are formed.²⁹ After exposure to nerve agents, such as sarin and Novichok A-234, phosphorylated serines or

tyrosines are formed as specific biomarkers.^{30–32} Likewise, mono- and dichlorinated tyrosine adducts are the major protein markers for the presence of chlorine.^{33,34}

Also, plants also contain a lot of proteins, with ribulose-1,5-bisphosphate carboxylase-oxygenase (rubisco) being the most abundant protein on earth.³⁵ As a result, plant proteins could serve as potential scavengers for chemical threat agents and might form protein adducts in a similar way as unraveled for humans. Abundantly occurring plants, representing a wide range of vegetation, are bay laurel leaf (*Laurus nobilis*), basil (*Ocimum basilicum*) and stinging nettle (*Urtica dioica*), depicted in Figure 6.1. Stinging nettle is a rapidly growing weed with a high protein content and is originally native to Europe.^{36,37} In contrast, basil thrives in tropical and subtropical climates and is an aromatic herb and medicinal plant.³⁸ Bay laurel leaf is used as a herb used in many traditional practices and recipes, originating from the Mediterranean region, Asia, South and North America, and the Balkans.³⁹ It is expected that these species will be sufficiently representative to study CWA biomarker occurrence in plants in general. This will allow the use of the presented methodology for any type of vegetation encountered on the incident scene.

Consequently, the aim of the current study was to explore whether persistent biomarkers of various CWAs could be detected in plants after vapor and liquid exposure. A novel approach was developed for analyzing modified protein adducts in vegetation, a strategy that to our knowledge has not been reported in literature before. The model plants used in this study were exposed to sulfur mustard, sarin, chlorine or Novichok nerve agent A-234. After exposure, leaves were collected, cut into small pieces, and washed to remove excess of intact CWA. The plant material was dried, then digested by pronase or trypsin followed by analysis with liquid chromatography tandem mass spectrometry (LC-MS/MS) and liquid chromatography–high-resolution tandem mass spectrometry (LC–HRMS/MS). The present work demonstrates for the first time that plant biomarkers are promising indicators of CWA exposure that can be used for forensic reconstruction long after the alleged agent release.



Figure 6.1. Photo of leaves of selected plants. A) Bay laurel leaf (*Laurus nobilis*), B) Basil (*Ocimum basilicum*), C) Stinging nettle (*Urtica dioica*).

6.2. Experimental

6.2.1. Safety

The organophosphate nerve agents Novichok A-234 and sarin (GB) and the blister agent sulfur mustard (HD) are highly toxic chemicals. All experiments were performed by trained personnel in the dedicated High-Tox facility at TNO Rijswijk, which is allowed under the Chemical Weapons Convention to synthesize and handle chemical warfare agents. The experiments, including chlorine gas exposure, were performed in a fume hood by trained personnel. The chemicals were handled in a leak-tight containment and personal protection measures, such as lab coats, gloves and safety glasses were worn. In case of accidental exposure, an autoinjector with atropine sulphate and obidoxime as well as a diazepam preparation were readily available for administration by a specialized first aid team, to reduce the symptoms of intoxication.

6.2.2. Chemicals and materials

The chemicals A-234, GB, HD, o-isopropyl methylphosphonic acid adduct to tyrosine (GB-Tyr), N1-HETE-Histidine (N1-HETE-His), N3-HETE-Histidine (N3-HETE-His), A-234-Tyr and methylphosphonic acid (MPA)-Tyr were synthesized in the High-Tox facility at TNO, Rijswijk. The compounds were characterized by NMR, GC-MS and LC-MS. Purities of the synthesized agents, except for A-234-Tyr and MPA-Tyr which were only used for qualitative analysis, exceeded 95% (determined by NMR). 3,5-dichloro-L-tyrosine (di-Cl-Tyr) was purchased from BOC Sciences (London, UK) and $^{13}\text{C}_6$ -3-chloro-L-tyrosine was obtained from Cambridge Isotopic Laboratories (Andover MA, USA) Purities of the agents exceeded 97%. Acetic acid, ammonium bicarbonate (ABC), calcium hypochlorite, 3-chloro-L-tyrosine, dithiothreitol (DTT), formic acid, protease from Streptomyces griseus (pronase, ≥ 3.5 units/mg solid), sodium acetate trihydrate, sodium iodoacetate, trypsin from bovine pancreas ($\geq 10,000$ BAEE units/mg protein) and urea were obtained from Sigma-Aldrich (Zwijndrecht, The Netherlands). Acetonitrile (ACN), acetone, ethanol and methanol (MeOH) were purchased from Biosolve (Valkenswaard, The Netherlands). Hydrochloric acid (HCl) was obtained from ThermoFisher Scientific (Landsmeer, The Netherlands). Additionally, MilliQ water (SimPak® 1) was used. Laurel (*Prunus Lusitanica Angustifolia*, Intratuin), Ocimum Basilicum (Aldi) and Nettle (local plant, Rijswijk) originated from the Netherlands.

6.2.3. Exposure of the plants

6.2.3.1. Liquid exposure

Laurel, basil, and stinging nettle were exposed to various concentrations of Novichok A-234, sarin or sulfur mustard. First, a single leaf was exposed in duplicate to a blank of ACN or 100 μL (in small drops of approximately 5 μL) of 0.02, 0.4 and 4 mmol/L of A-

234, 0.004, 0.05 and 0.1 mmol/L of sarin or 0.02, 0.1, 1 and 10 mmol/L of sulfur mustard dissolved in ACN. The leaves had a total dry mass of about 30 mg and were left for 24 hours in a closed petri dish. Afterwards, the samples were prepared for analysis as described in section 6.2.4.

6.2.3.2. Vapor and gas exposure

Additionally, the plants were placed in a 2 L glass vessel and exposed to vapors of sarin or sulfur mustard in a dedicated set-up (Figure 6.2). First, vapors at a concentration of 2, 5, 25 or 250 mg/m³ sarin or 2.5, 12.5, 50 or 150 mg/m³ sulfur mustard were generated. The temperature was maintained at 20-22 °C. A syringe pump (Hamilton 1801N, 10-100 µL) delivered the agent at constant flow rate (10-250 nL/min) in a dry air stream (1 L/min) in a heated evaporation chamber at 140 °C. The incoming vapor flow entered the vessel at the bottom, while the outgoing flow exited at the top to promote a homogenous distribution. The exiting flow was led through a charcoal filter to trap and convert the threat agents. After a 30-minute exposure, the valves could be switched without opening the setup to clean the vessel by air flow for approximately 30 minutes. This was verified at the sampling spots with a handheld CWA detector (LCD 3.3, Smiths Detection).

For chlorine exposure, the plants were placed in a closed 2 or 20 L vessel and chlorine was generated by the reaction of calcium hypochlorite and HCl, similar to the method applied by de Bruin-Hoegée et al.²¹ A 1.5 mL Eppendorf tube with 1, 10 and 50 mg calcium hypochlorite was placed in the vessel above the plant. A syringe was put through a septum and slowly, over a period of one minute, 1 mL of a 12M HCl solution was added to the calcium hypochlorite, after which 50 mg/m³, 500 mg/m³, 5 g/m³ or 25 g/m³ chlorine gas was generated. The plants were left for 30 minutes in the closed vessel.

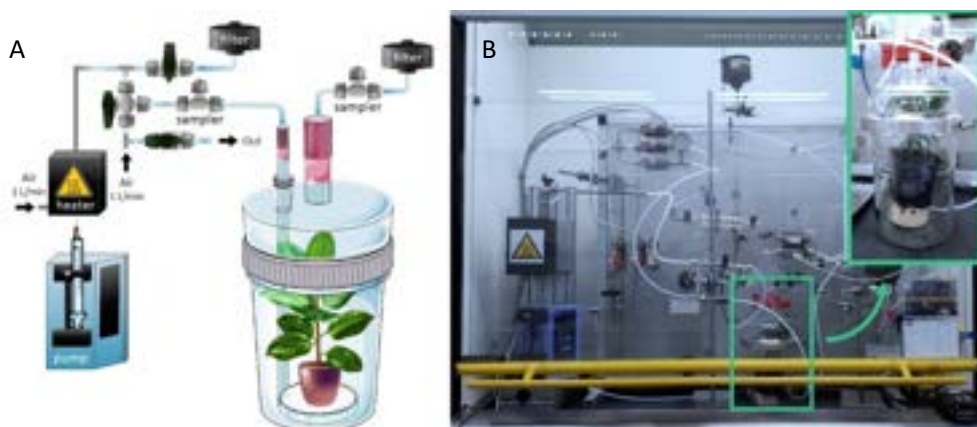


Figure 6.2. Dedicated vapor generation set-up for controlled exposure of plants to chemical warfare agents. A) Schematic view. B) Photo of vapor generation set-up.

6.2.4. Protein precipitation and digestion

Figure 6.3 summarizes the sample preparation steps. After exposure, two leaves of each plant species were collected and washed with methanol to remove potential intact CWAs. Also, two unexposed leaves were included. Subsequently, the leaf was placed in a 2 mL vial and cut into minuscule homogenous pieces using a small nail scissors. The sample was then transferred into a 15 mL centrifuge tube and washed with 10 mL acetone by centrifuging at 4000 rpm for 10 minutes (Megafuge 1.0R centrifuge). The washing step was included to dehydrate and clean the sample, because the aim of the study was to find protein adducts. It should be noted that potential other, small molecule biomarkers could have been removed during this procedure. This was repeated three times for HD and chlorine. Subsequently, the plant material was dried overnight at ambient temperature. It should be noted that drying is not required if only qualitative analysis is necessary, since digestion can be performed with wet leaves as well.

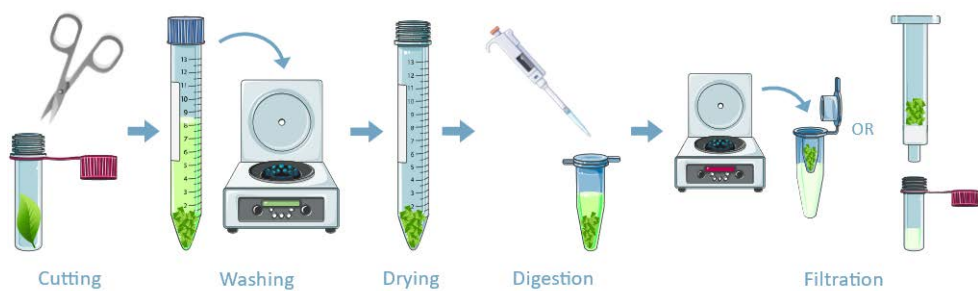


Figure 6.3. Schematic overview of the sample preparation steps. Figures adapted from smart.servier.com, CC BY 3.0.

Afterwards, the samples were digested. The applied method was adapted from protocols originally described for the detection of CWAs in biomedical samples.^{4,21,40} For pronase digestion, 400 µL ABC buffer (50 mM) and 100 µL pronase (10 mg/mL in 50 mM ABC) were added to 10 mg of dried leaf. The digests after HD and chlorine exposure were incubated overnight at 37 °C and a rotational speed of 800 rpm. Subsequently, the samples were filtered through a 10 kDa Amicon ultra-centrifugal filter at 14,000 rpm for 10 minutes in an Eppendorf centrifuge. The samples after sarin exposure were incubated with pronase for 90 minutes in a Thermoshaker (Grant-bio PHMT) at 50 °C and 500 rpm. It turned out that both digestion methods, for either sulfur mustard and chlorine and the procedure for sarin, provided similar results and could be used interchangeably.

The filtrates were purified with reversed phase solid phase extraction (SPE) using a C18 column (Bakerbond SPETM). To wet the sorbent bed and activate the nonpolar sorbents,

1 mL MeOH was percolated through the column and 1 mL water was used to equilibrate the column. Afterwards, the sample was loaded on the column and washed with 10% MeOH in water. The retained analytes were eluted with 1.5 mL MeOH and dried under nitrogen. The dried sample was then dissolved in 50 μ L water with 0.2% v/v formic acid and analyzed as described in section 6.2.5.

For trypsin digestion, 1 mL urea (8 M solution in 50 mM ABC) containing 5 μ L of DTT (800 mM in water) was added to 10 mg of plant material. Subsequently, the sample was incubated for 45 minutes at 37 °C and 800 rpm. After the incubation, 100 μ L sodium iodoacetate (150 mM in water) was added. Next, the sample was incubated for 30 minutes in the dark at 37 °C and 800 rpm. Thereafter, the sample was filtered through a 10 kDa Amicon ultra-centrifugal filter at 14,000 rpm for 10 minutes in an Eppendorf centrifuge (5417R). The residue was washed on the filter four times with 400 μ L ABC buffer (50 mM) and afterwards 400 μ L water and 30 μ L trypsin solution (10 mg/mL in 50 mmol/L acetate buffer, pH = 3.55) were added. The sample was incubated overnight at 37 °C and 800 rpm. After digestion, the samples were filtrated through a 10 kDa filter at 14,000 rpm for 10 minutes and analyzed as described in section 6.2.5.

6.2.5. Chemical analysis

6.2.5.1. Targeted analysis by LC-MS/MS

Prior to analysis, the pronase digests were diluted up to 100-fold by water with 0.2% v/v formic acid depending on the exposure concentration. The samples were analyzed by a Waters Acquity ultra-high-pressure liquid chromatographic (UPLC) system equipped with a Waters Acquity HSS T3 C18 column (100 x 2.1 mm I.D., 1.8 μ m). Samples were kept in the autosampler at 8 °C and a volume of 5 μ L was injected, after which the analysis was performed at room temperature with a gradient flow of 100 μ L/min. All compounds could be analyzed with a single chromatographic method. The optimized gradient elution settings can be found in Table A.1. of the Supporting Information. The UPLC system was coupled to a Waters (Milford, MA, USA) Xevo TQ-S triple-quadrupole mass Spectrometer, equipped with electrospray ionization. Analytes were quantified in positive ionization mode with a capillary voltage of 3.5 kV. The nitrogen cone gas flow was set to 150 L/h and the argon collision gas flow was set to 0.19 mL/min. Cone voltages of 40 V for A-234 and GB, 10 V for chlorine and 14 V for HD exposure were used. Data was acquired in selected reaction monitoring (SRM) mode.

The collision energy was optimized for each compound. Table 6.1 shows the chromatographic and mass spectrometric parameters for the protein adducts and metabolites which were analyzed by LC-MS/MS. The identification of the adducts was confirmed by comparing their retention times, precursor ion and characteristic fragment ion m/z values with synthetic reference standards. GB-Tyr, Cl-Tyr, di-Cl-Tyr,

Verification of exposure through analysis of biomarkers in plants

N1-HETE-His, N3-HETE-His and $^{13}\text{C}_6\text{-Cl-Tyr}$ were quantitatively analyzed, while A-234-Tyr and MPA-Tyr were only utilized for qualitative analysis. For the limit of detection (LOD) a signal-to-noise (S/N) ratio of at least 5 was required. Further results of the optimization and validation of the corresponding targeted LC-MS/MS method can be found in Section S1 of the Supporting Information.

Table 6.1. Chromatographic and mass spectrometric parameters for analytes and internal standards analyzed by LC-MS/MS.

Analyte	Precursor ion (m/z)	Retention time (min)	Product ion (m/z)	Collision energy (eV)	Linearity range (ng/mL)	Chemical structure
N1-HETE-His	260.0	3.7	105.0 81.8 61.0	11 25 25	1-100	
N3-HETE-His	260.0	4.2	105.0 81.8 61.0	11 25 25	1-100	
MPA-Tyr	260.1	5.1	214.1 197.1	13 13	n.a.	
$^{13}\text{C}_6\text{-Cl-Tyr}$	222.0	6.3	176.3 141.3	15 25	1-100	
Cl-Tyr	216.2	6.3	170.3 135.3	15 25	1-100	
di-Cl-Tyr	250.1	6.7	204.0 169.0	15 30	1-100	
GB-Tyr	302.1	8.1	260.1 214.1	13 13	0.05-20	
A-234-Tyr	386.2	9.3	313.0 285.0 244.1 74.1	15 15 15 15	n.a.	

6.2.5.2. *Data-dependent acquisition by LC-HRMS/MS*

The trypsin digests were analyzed on an LC-HRMS/MS instrument based on a previously published method.²¹ An Ultimate 3000 RSLCnano system (Thermo Scientific Dionex Softron GmbH, Germany) coupled to an Orbitrap mass spectrometer (Q Exactive plus, Thermo Scientific, Bremen, Germany) was used. A volume of 10 µL was injected onto an Acclaim PepMap 100 C18 µ-precolumn (5 mm x 300 µm I.D., 5 µm, 100 Å, Thermo Fisher Scientific) and subsequently separated on an Acclaim PepMap C18 Analytical column (250 mm x 75 µm I.D., 2 µm, 100 Å, Thermo Fisher Scientific). Afterwards, the raw data was analyzed using Peaks® X+ software (2019, Bioinformatics Solutions Inc., Waterloo, Canada) to identify the peptides that were present in the sample. A peaks database search was employed which compared all theoretically possible peptides with the FASTA database. Also, a de novo search was applied. The error tolerance for the precursor mass and the fragment ion were set at 10 Da and 0.5 Da monoisotopic mass, respectively.

6.3. Results & discussion

6.3.1. Visual examination of vegetation

Any discoloration or other physical changes of the leaves were monitored to assess potential visual cues for plant and leave collection in the field. After chlorine exposure, typical yellow staining was immediately observed (Figure 6.4B). Alternatively, leaves exposed to sulfur mustard (Figure 6.4D), A-234 or sarin showed discoloration, turning the leaf from green to a brown color. However, this was only visible for relatively high vapor concentrations, whereas lower concentrations (<25 mg/m³) did not result in immediate physical changes. More pictures are included in section S2 of the Supporting Information. Further knowledge of the physical state of the plant might be obtained by applying fluorescence detection before sample selection.⁴¹

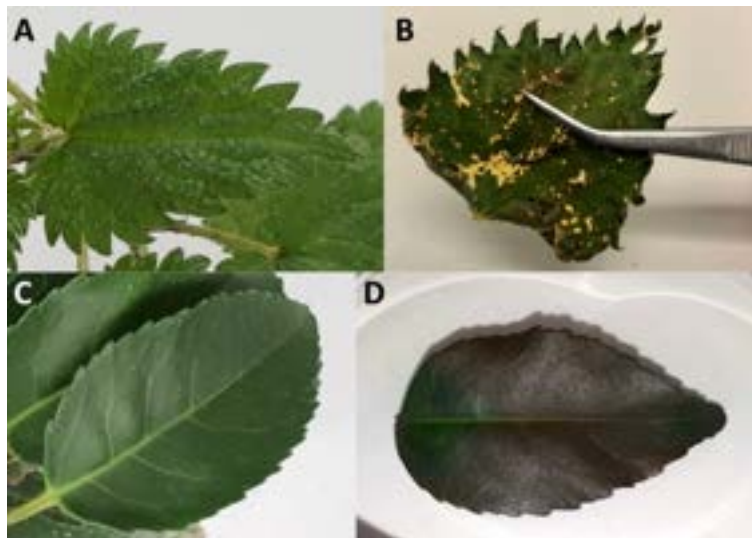


Figure 6.4. Physical state of nettle leaf upon chlorine gas exposure and laurel upon sulfur mustard exposure. A) Nettle leaf before exposure, B) Nettle leaf after 25 g/m³ chlorine exposure, C) Laurel before exposure, D) Laurel leaf after 20 µmol liquid sulfur mustard exposure.

6.3.2. Liquid exposure

Protein adducts were formed in plants after exposure to various chemical threat agents. To the best of our knowledge, this is the first time that these biomarkers are detected in plants. After liquid exposure to A-234, phosphorylated tyrosine adducts were found. Figure 6.5 shows representative extracted ion chromatograms of the sample preparation blank, a standard of tyrosine exposed to A-234, and nettle exposed to A-234. The retention time (t_R) and fragmentation pattern of the unknown sample correspond to the standard. No peaks were visible in the blank runs even after a 10-fold expansion of the base line signal. In Figure 6.6 the HRMS/MS spectrum of A-234-Tyr is presented with a mass error of only 0.22 ppm compared to the theoretical m/z value. The cleavage products with m/z 313.0949, 285.0635, 244.0734 and 74.0964 were clearly visible, which were only reported by one other study for the A-234 tyrosine adduct in biological fluids.⁴² This is the first study to identify the A-234 tyrosine adduct by comparing it to a synthetic reference standard. The lowest m/z of the adduct moiety diethylamine was observed in other studies for the nonapeptide fragmentation pattern as well.³² An increasing exposure concentration resulted in higher adduct formation in leaves exposed to liquid drops (Figure 6.7A), with a limit of detection of 2 nmol (448 ng).

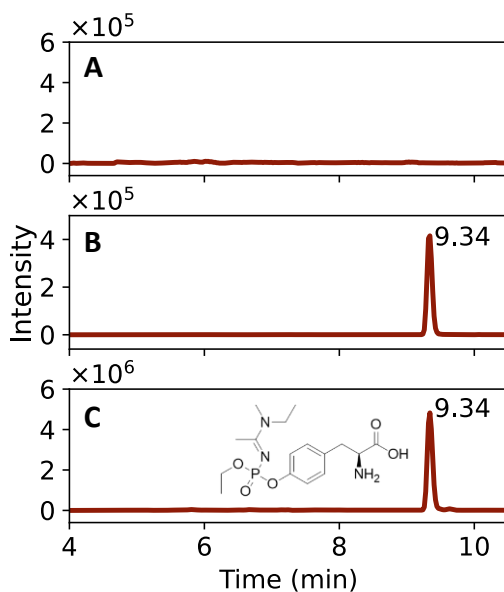


Figure 6.5. Extracted ion chromatograms (m/z 386.2 → 74.1) of phosphorylated tyrosine adduct with t_R = 9.34 min, after liquid exposure to A-234. A) Sample preparation blank. B) Standard A-234-Tyr. C) A-234-Tyr adducts measured in nettle plant after exposure to 40 nmol A-234.

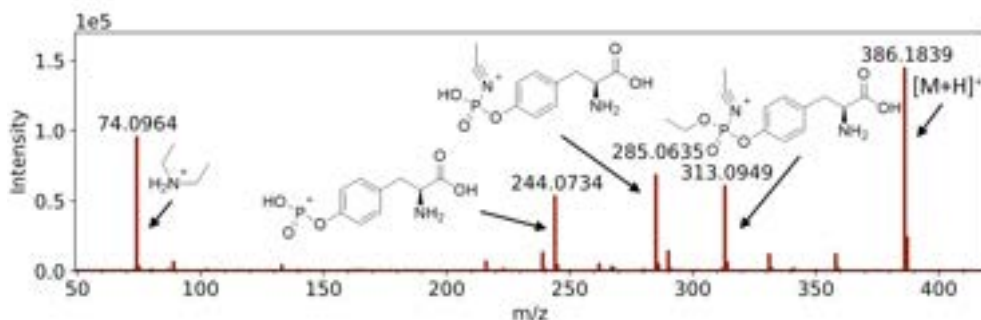


Figure 6.6. HRMS/MS spectrum with fragmentation pattern of the tyrosine adduct of Novichock A-234 (m/z 386.1839).

Furthermore, the o-isopropyl methylphosphonic acid adduct to tyrosine was also detected in vegetation after liquid exposure to sarin, confirmed by a reference standard. The MPA-Tyr adduct was not detected, indicating no aging of the adduct. A liquid exposure of 0.4 nmol sarin (56 ng) could still be observed in nettle leaves. When the exposure level was increased, a higher concentration of biomarkers was measured (Figure 6.7B).

Third, the N1- and N3-HETE-His adducts were detected after liquid exposure of leaves to sulfur mustard. An exposure of a single nettle leaf to 0.2 nmol HD (32 ng) could still

be detected. Both adducts were formed to a similar extent at each sulfur mustard concentration (Figure 6.7C). The next section will describe the results of the exposure of plants to GB and HD vapor including the chromatograms.

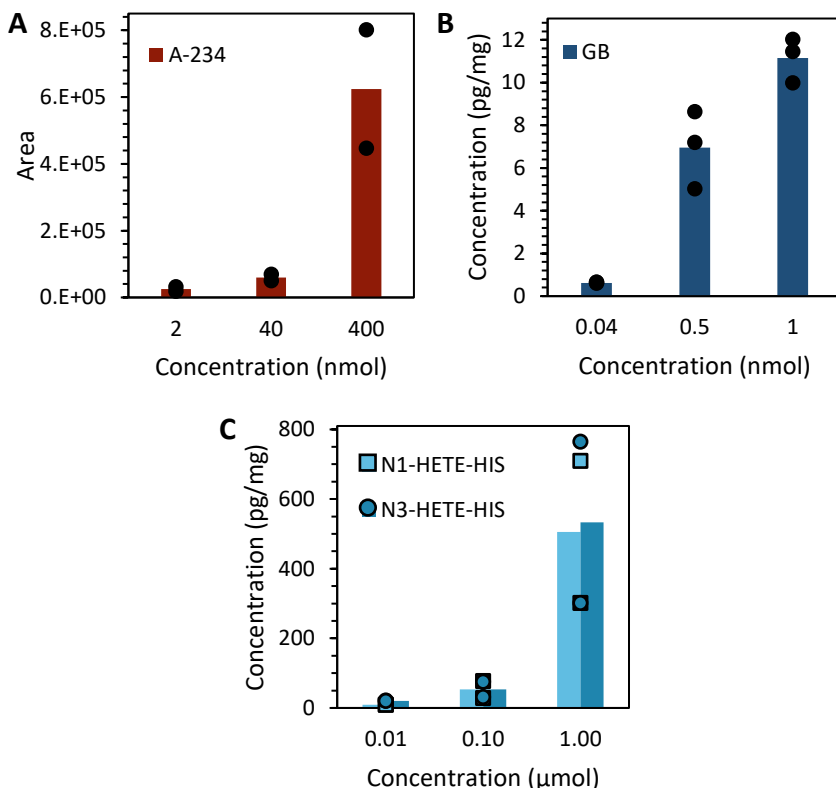


Figure 6.7. Effect of concentration of A-234, GB and HD of added droplets on the average adduct formation in nettle plant per mg dried leaf.

6.3.3. Vapor and gas exposure

6.3.3.1. Analysis of phosphorylated tyrosine adducts after sarin exposure

Similar to the liquid exposure results, the o-isopropyl methylphosphonic acid adduct to tyrosine was also detected in living plants after vapor exposure to sarin as confirmed by a reference standard (Figure 6.8). The same product was observed for all investigated plant species. The lowest observable exposure limit in basil was 2.5 mg/m^3 and in laurel and nettle 25 mg/m^3 after full plant exposure. This concentration is higher than the lethal dose for humans of 0.19 mg/m^3 for a 30-minute exposure⁴³. It can be expected that in real cases, the exposure pattern of plants is completely different compared to humans, because exposed people will leave the incident scene as soon as possible, while the vegetation can be exposed for a longer duration. This will then result

in a higher adduct concentration. Besides, vegetation might also be found very close to the center of the release and thus be exposed to much higher concentrations.

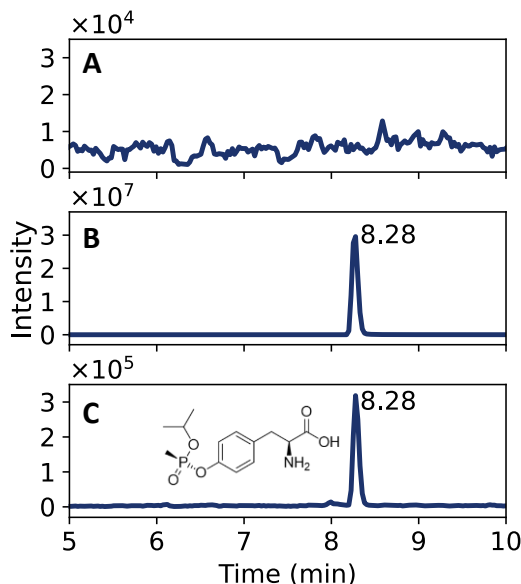


Figure 6.8. Extracted ion chromatograms of phosphorylated tyrosine adduct with $t_R = 8.28$ after sarin vapor exposure. A) Sample preparation blank. B) Standard GB-Tyr. C) GB-Tyr measured after plant exposure to 250 mg/m^3 sarin.

The persistence of the protein adducts was remarkable, GB-Tyr could still be detected in living plants, as well as in dried leaves, up to three months after the actual exposure. The extracted ion chromatograms analyzed three months after exposure, are presented in section S3 of the Supporting Information. Dried leaves did not require storage at reduced temperatures. This would facilitate the transport and storage of plant-based evidence during investigations of alleged use of chemical weapons. It is expected that the detection window could be extended even further, because the concentration of the adduct in the leaves did not significantly drop after three months, and for a high exposure experiment the MS response still exceeded the limit of quantification by a factor of 10.000.

6.3.3.2. Analysis of chlorotyrosine adducts

In case of exposure to the toxic industrial chemical chlorine, the 3-chloro- and 3,5-dichlorotyrosine adducts were identified in vegetation in line with studies involving biomedical samples (Figure 6.9). The lowest observable exposure limit was 500 mg/m^3 after full plant exposure of laurel and nettle, whereas for the experiments with basil, chlorine contact could be established from a concentration of 5 g/m^3 . The LOD was lowered when a single leaf was exposed to the same chlorine concentration, resulting

in a LOD of 50 mg/m³ after exposure of nettle. This is slightly below the lethal dose for humans, since a severe 30-minute exposure at 81 mg/m³ can result in cell death, pulmonary edema, or a sudden death due to narrowing of the airways.⁴⁴ Additionally, an increasing chlorine concentration resulted in an increased formation of di-Cl-Tyr adduct compared to Cl-Tyr. Interestingly, the observed persistence of the chlorine biomarkers was similar to the findings for the A-234 and sarin experiments. Each protein adduct could still be detected three months after the exposure experiment at a concentration significantly higher than the LLOQ (section S3 of the Supporting Information).

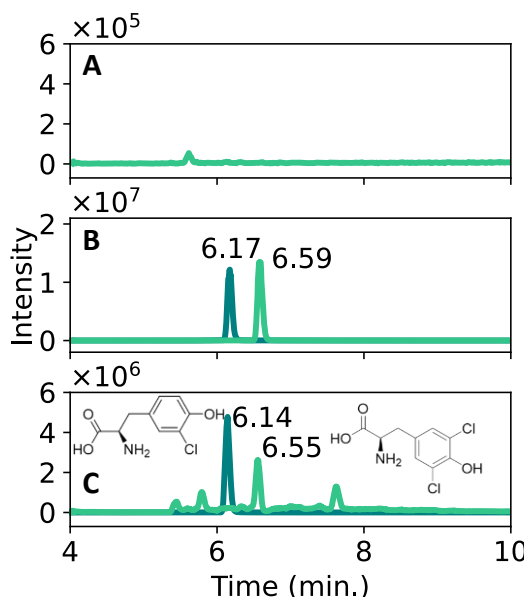


Figure 6.9. Extracted ion chromatograms of chlorinated tyrosine adducts after chlorine gas exposure. A) Sample preparation blank. B) Standard Cl-Tyr with $t_R = 6.17$ min and di-Cl-Tyr with $t_R = 6.59$ min. C) Cl-Tyr and di-Cl-Tyr, diluted 100 times, measured after 5 g/m³ plant exposure.

It should be noted that these tyrosine adducts do not immediately relate to a targeted attack with chlorine gas. Similar reactions can also occur when plants are exposed to accidental chlorine exposure, for instance after contact with household bleach. Further research should be conducted to investigate whether it would be possible to differentiate between various exposure scenarios and the chemicals involved through detailed analysis of plant biomarkers. Possibly this will require the analysis of chlorinated peptides as was recently demonstrated for human biological samples.²¹ However, the context of a given case and the conditions at the incident scene might also provide insight into the nature of the chlorine source.

6.3.3.3. Analysis of histidine adducts after sulfur mustard exposure

Figure 6.10 shows the N1- and N3-HETE-His adducts that were detected after exposure of plants to sulfur mustard. LC gradient separation was satisfactory to differentiate between these two isomers ($\Delta t_r > 0.4$ min). Both adducts could be detected in laurel at a vapor concentration as low as 12.5 mg/m^3 . In nettle the N1-HETE-His adduct was detected at the same exposure level, while the N3-HETE-His adduct was only visible after a higher exposure of 50 mg/m^3 . The biomarkers in basil could only be detected after an exposure of 150 mg/m^3 . In line with the other chemical warfare agents, the biomarkers of sulfur mustard could still be observed three months after exposure at a concentration significantly exceeding the LLOQ (section S3 of the Supporting Information). Life-threatening effects in humans already occur after a 30-minute exposure to 2.7 mg/m^3 .⁴⁵

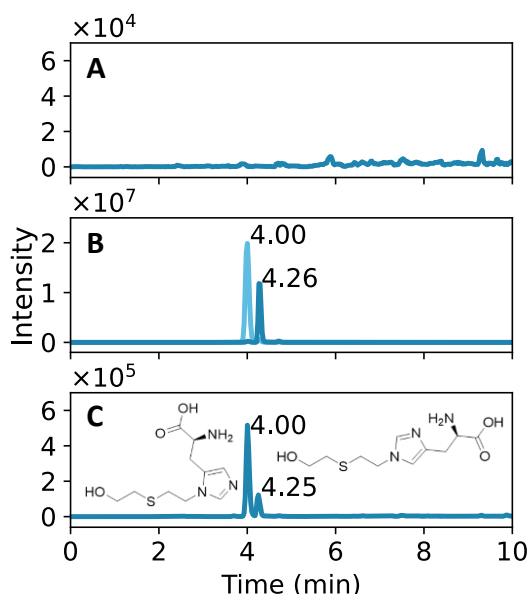


Figure 6.10. Extracted ion chromatograms of N1-HETE-His and N3-HETE-His adducts after sulfur mustard vapor exposure. A) Sample preparation blank. B) Standard N1-HETE-His with $t_R = 4.00$ min and N3-HETE-His with $t_R = 4.26$ min. C) N1-HETE-His and N3-HETE-His measured after 150 mg/m^3 plant exposure.

Further improvements in limit of detection might be obtained by processing more plant material. In this study only 10 mg of dried plant material was prepared for analysis, which was often less than the mass of a single leaf. Especially after large scale attacks, it is expected that much more vegetation has come into contact with the chemical agents and could hence be collected and processed for forensic investigations. Another potential advancement in sensitivity, which has remarkably decreased the detection

limit for the analysis of nerve agents in biomedical samples, might be realized by isolating specific proteins using antibodies.⁴⁶

Over time a slight increase in adduct concentration in the living plant was observed after sarin, chlorine, and sulfur mustard exposure, which might be due to accumulation in the soil or plant as is observed for free metabolites as well²⁵. However, given the small sample size, the results must be interpreted with caution as the variation in concentration observed in individual leaves was substantial, which might be due to the position relative to the vapor flow or the growth phase of the leaf.

6.3.4. Influence of plant exposure conditions

The conditions of the leaves were varied to mimic different weather conditions. Freshly picked leaves were compared with wetted, frozen, and dried leaves. After chlorine exposure, the concentration of Cl-Tyr and di-Cl-Tyr in the frozen and dried leaves was significantly lower than the adduct concentration detected in fresh leaves as shown in Figure 6.11. Nevertheless, as described before, it was still possible to identify protein adducts in dried leaves after three months. The di-Cl-Tyr concentration of the wetted leaves was also slightly reduced, while the Cl-Tyr concentration did not show a significant difference. Additionally, during sarin and sulfur mustard exposure, the humidity in the vapor generation setup was increased from dry air to 60% relative humidity. However, the adduct concentration was not affected by these conditions. Finally, a doubled exposure time with GB and HD resulted in more adduct formation as expected. At even higher exposure levels and durations, the biomarker formation is expected to level out when all available amino acid sites have reacted with the CWA. However, such a high exposure concentration was not applied due to safety reasons.

The observed biomarker concentration was considerably affected by the exposure area of the plant. An increase in biomarker formation with a factor of four was observed for a single leaf compared to a whole plant exposed to 5 or 25 g/m³ chlorine gas. This suggests that all the available chlorine fully reacts with an excess of biomaterial and that hence the biomarker formation is distributed over the various leaves of a full plant. As a result, the size of the plant and its surface area vs mass are indirectly affects the formed adducts. To improve the exposure design in future studies, it is recommended to precisely select the plant size and number of leaves to limit experimental variation. However, in real-life incidents CWA exposure will be uncontrolled and will vary greatly depending on the exposure conditions and the location of the vegetation at the scene.

In this study, no consistent differences in adduct concentration were observed for the various plant species. The variation within the individual experiments of one plant species was similar to the variation between different plant species. Nevertheless, all chemical warfare agent adducts were visible in all investigated plant species. A

plausible explanation for this might be that green plants in general contain a lot of similar proteins consisting of amino acids that are accessible to chemical threat agents, as will be discussed in more detail in section 3.5. It is therefore expected that these findings can be extrapolated to other vegetation as well.

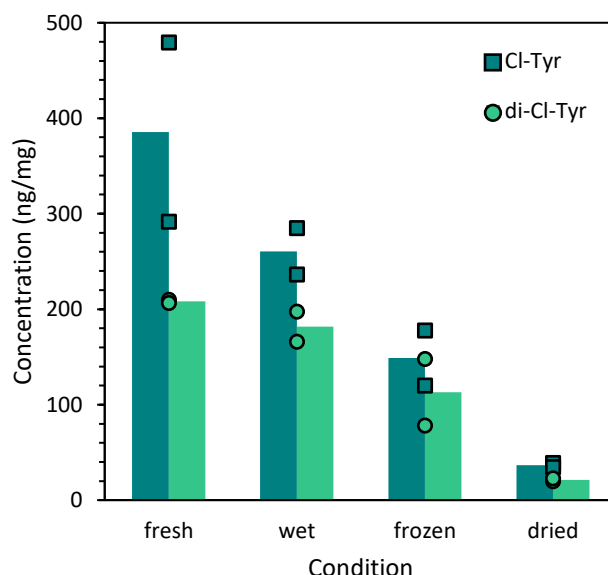


Figure 6.11. Influence of nettle leaf conditions on the average adduct concentration.

6.3.5. Protein identification with high resolution mass spectrometry

To provide more insight in which plant proteins react with the threat agents, peptide identification was performed by LC-HRMS/MS after trypsin digestion. It was anticipated that a majority of the adducts would originate from the abundant plant protein rubisco. This protein was also mentioned in the news article about the research of Lawrence Livermore National Laboratory.²⁷ However, the applied pronase digestion method is non-specific, and the monitored biomarkers can result from any plant protein containing tyrosine. Because of the lack of specific databases of nettle, laurel, and basil, only peptides that occur generically in plants could be identified. Consequently, this approach is generally applicable to a wider range of plant species.

Table 6.2 shows the identified peptides that were present in two nettle samples exposed to chlorine gas. No chlorinated peptides were found in the blank. As expected, mono and di-chlorinated rubisco peptides were found. Besides this protein, various peptides from other proteins were detected, such as chlorinated chloroplastic ATP synthase, which are involved in the CO₂ signalling pathway and control gas-exchange between plants and the atmosphere,⁴⁷ chlorophyll binding protein and serine-

glyoxylate aminotransferase. In one sample the peptide VGLTALTIAEY*FR was both mono chlorinated and dichlorinated.

After duplicate sulfur mustard exposure of laurel and basil, post-translational modifications were found as well (Table 6.2). Slightly different proteins were found in both samples of laurel and basil. The proteins calmodulin, cytochrome, photosystem II D2 and chloroplastic chlorophyll binding protein were modified. Of the latter protein, even two peptides were affected, which might indicate that this protein is an accessible target. Additionally, Table 6.2 shows the phosphorylated peptides that were formed after sarin exposure. Also, in this case different proteins were found in laurel compared to basil. Modifications in chloroplastic chlorophyll binding protein, chloroplastic transketolase, putative beta-D-xylosidase and rubisco were identified. The finding of rubisco was consistent with data obtained after chlorine exposure of nettle.

Table 6.2. Overview of peptides containing at least one chlorinated or phosphorylated tyrosine residue or histidine adduct of sulfur mustard, detected in duplicate samples of nettle, laurel or basil after exposure.

#	Peptide	Protein	Accession	Exposure	Species
1	GYPGY(Cl)LYTDLATIYER	ATP synthase	B0K8E7 VATB_THEP3	Cl	Nettle
2	EAQAVADDVFSLFISEEVDK-VELLY(Cl)TK	ATP synthase, chloroplastic	Q01908 ATPG1_ARATH	Cl	Nettle
3	VGLTALTIAEY(Cl)FR	ATP synthase, chloroplastic	O03081 ATPB_PSINU	Cl	Nettle
4	H*NLTDDQLSEFK	Calmodulin	Q39752 CALM_FAGSY	HD	Laurel
5	Y(Cl)AGVGAAIEYAVLHLK	Carbonic anhydrase, chloroplastic	P42737 BCA2_ARATH	Cl	Nettle
6	GPLENLADHLDAPVNNAWAY(Cl)ATKLCPGK	Chlorophyll binding protein, chloroplastic	P09755 CB22_SOYBN	Cl	Nettle
7	Y*GELLHGR	Chlorophyll binding protein, chloroplastic	Q07473 CB4A_ARATH	GB	Basil
8	EVPYLH*LQFDLSDLQNLAK	Chlorophyll binding protein, chloroplastic	Q9XF88 CB4B_ARATH	HD	Basil
9	EFLVLH*LQFELDSLDQGGLAK	Chlorophyll binding protein, chloroplastic	Q9XF88 CB4B_ARATH	HD	Basil
10	H*HLTPLLSPDPTTK	Cytochrome	A6MMV7 CYF_ILLOL	HD	Basil
11	WSFAAEH*HPENLLFPEEVLPK	Photosystem II D2	Q2MIA5 PSBD_SOLL	HD	Basil
12	Y*TLPGHKKAFLPR	Putative beta-D-xylosidase	P83344 XYNB_PRUPE	GB	Laurel
13	GHYNATAATC(Cl ₂)EEMLR	RuBisCO	Q1KVVO RBL_TETO	Cl	Nettle
14	LTYYTPEY(Cl)ETK	RuBisCO	P48706 RBL_LACSA	Cl	Nettle
15	VAY(Cl)PIDLFEEGSVTNLF-TSIVGNVFGFK	RuBisCO	P48711 RBL_PICAB	Cl	Nettle
16	WY*MVHSgtvvgqlewr	RuBisCO	P19163 RBL_NEUMU	GB	Basil
17	Y(Cl)NLSLGLGLNK	Serine-glyoxylate aminotransferase	P84187 SGAT_MAIZE	Cl	Nettle
18	KNQY*LEAEWNAK	Transketolase, chloroplastic	O20250 TKTC_SPIOL	GB	Laurel

In addition, similar chloroplastic chlorophyll binding proteins were targeted by all three chemical threat agents. An overview of all the detected plant-based peptides, including those that were only detected once, can be found in Table 6 of the Supporting Information. The comprehensive list of peptides showed that multiple proteins were modified by all studied chemicals, such as chloroplastic ATP synthase, ferredoxin-dependent glutamate synthase, oxygen-evolving enhancer protein 1, photosystem II CP47 reaction center protein, RuBisCO activase and RuBisCO. From these results, it can be concluded that many proteins are targeted by the various chemicals. Interestingly, some proteins showed modifications in all three plant species by all studied chemical threat agents. This indicates that a specific peptide biomarker approach as recently presented for human biological samples might also be feasible for plant-based evidence.

6.4. Conclusions

In this study a novel approach was developed for analyzing persistent biomarkers in vegetation for retrospective investigation of chemical warfare agent exposure. We demonstrate that these plant biomarkers are identical to the analytes that have been accepted as unequivocal biomarkers of exposure in biomedical samples of victims and that have been used by the designated laboratories of the OPCW to analyze samples associated with chemical weapons attacks. This finding was confirmed through the use of reference standards. The experience with complex matrices, protein isolation protocols and enzymatic digestion steps is a distinct advantage when implementing the method developed in this study in forensic investigations, guaranteeing rapid implementation of the technology. In addition, the focus on plant-based evidence can offer a number of distinct advantages. This work shows that CWA biomarkers formed in plants are very persistent and can be detected up to three months after exposure. It is also expected that these biomarkers will be formed generically in plants irrespective of the species and exposure conditions. Furthermore, plant-based evidence is relatively easy to sample, ship, store and process and typically is abundantly available at an incident scene. Finally, for perpetrators it will be difficult to remove or manipulate plant-based evidence after a CWA attack. Future research could focus on processing more plant material to further reduce the detection limit and thereby the minimum exposure concentration. The analysis of case-work samples is required to establish the applicability of the method for concentrations and conditions encountered after a CWA attack. Both in terms of verifying the presence of plant biomarkers after a confirmed CWA exposure and of showing the absence of these biomarkers in situations where no threat agent was released. In addition, the combination of various analytical techniques can provide complementary information or additional proof through the presence of

Verification of exposure through analysis of biomarkers in plants

specific biomarkers. In conclusion, the analysis of plant protein adducts can become a powerful tool to verify (or refute) the alleged use of chemical weapons.

6.5. Acknowledgements

This research is partially funded by the European Union, through a research contract awarded by the Organisation for the Prohibition of Chemical Weapons (OPCW), in support of the Plant Biomarker Challenge.

References

- (1) Organisation for the Prohibition of Chemical Weapons. *Compendium of correspondence shared by States Parties on Ukraine*. https://www.opcw.org/sites/default/files/documents/2022/Compendium_of_correspondence_shared_by_States_Parties_on_Ukraine.pdf (accessed 2022-11-30).
- (2) OPCW. Report Of The OPCW Fact-Finding Mission In Syria Regarding The Incidents Of The Alleged Use Of Chemicals As A Weapon In Marea, Syrian Arab Republic, On 1 And 3 September 2015. <https://www.opcw.org/sites/default/files/documents/2022/01/s-2017-2022%2B%28e%29.pdf> (accessed 2022-11-30).
- (3) OPCW. First Report by the OPCW Investigation and Identification Team (IIT) Pursuant to Paragraph 10 of Decision C-SS-4/Dec.3 "Addressing the Threat From Chemical Weapons Use" Ltamenah (Syrian Arab Republic) 24, 25, and 30 March 2017. <https://www.opcw.org/sites/default/files/documents/2020/04/s-1867-2020%28e%29.pdf> (accessed 2023-02-06).
- (4) John, H.; Schans, M. J. van der; Koller, M.; Spruit, H. E. T.; Worek, F.; Thiermann, H.; Noort, D.; John, H. Fatal Sarin Poisoning in Syria 2013: Forensic Verification within an International Laboratory Network. *Forensic Toxicol* **2018**, *36*, 61–71. <https://doi.org/10.1007/s11419-017-0376-7>.
- (5) OPCW Investigation and Identification Team (IIT). Second Report By The OPCW Investigation And Identification Team Pursuant To Paragraph 10 Of Decision C-Ss-4/Dec.3 "Addressing The Threat From Chemical Weapons Use" Saraqib (Syrian Arab Republic) – 4 February 2018. <https://www.opcw.org/sites/default/files/documents/2021/04/s-1943-2021%28e%29.pdf> (accessed 2022-11-30).
- (6) OPCW Fact-Finding Mission (FFM). Report of the OPCW Fact-Finding Mission in Syria Regarding the Incident of the Alleged Use of Chemicals as a Weapon in Kafr Zeita, Syrian Arab Republic 1 October 2016. <https://www.opcw.org/sites/default/files/documents/2022/02/s-2020-2022%28e%29.pdf> (accessed 2022-11-30).
- (7) OPCW. *Summary of the report on activities carried out in support of a request for technical assistance by Germany*. <https://www.opcw.org/sites/default/files/documents/2020/10/s-1906-2020%28e%29.pdf> (accessed 2023-02-06).
- (8) Castelvecchi, D. *Novichok nerve agents banned by chemical-weapons treaty*. Nature. <https://doi.org/10.1038/d41586-019-03686-y>.
- (9) Costanzi, S.; Koblentz, G. D. Controlling Novichoks after Salisbury: Revising the Chemical Weapons Convention Schedules. *Nonproliferation Review* **2019**, *26* (5–6), 599–612. <https://doi.org/10.1080/10736700.2019.1662618>.
- (10) Steindl, D.; Boehmerle, W.; Körner, R.; Praeger, D.; Haug, M.; Nee, J.; Schreiber, A.; Scheibe, F.; Demin, K.; Jacoby, P.; Tauber, R.; Hartwig, S.; Endres, M.; Eckardt, K. U. Novichok Nerve Agent Poisoning. *The Lancet* **2021**, *397* (10270), 249–252. [https://doi.org/10.1016/S0140-6736\(20\)32644-1](https://doi.org/10.1016/S0140-6736(20)32644-1).
- (11) Hooij schuur, E. W.; Kientz, C. E.; ATh Brinkman, U. Analytical Separation Techniques for the Determination of Chemical Warfare Agents. *J Chromatogr A* **2002**, *982*, 177–200. [https://doi.org/10.1016/S0021-9673\(02\)01426-7](https://doi.org/10.1016/S0021-9673(02)01426-7).
- (12) Kim, K.; Tsay, O. G.; Atwood, D. A.; Churchill, D. G. Destruction and Detection of Chemical Warfare Agents. *Chem Rev* **2011**, *111*, 5345–5403. <https://doi.org/dx.doi.org/10.1021/cr100193y>.
- (13) Pacsial-Ong, E. J.; Aguilar, Z. P. Chemical Warfare Agent Detection: A Review of Current Trends and Future Perspective. *Frontiers in Bioscience* **2013**, *5* (2), 516–543. <https://doi.org/https://doi.org/10.2741/S387>.
- (14) Popiel, S.; Sankowska, M. Determination of Chemical Warfare Agents and Related Compounds in Environmental Samples by Solid-Phase Microextraction with Gas Chromatography. *J Chromatogr A* **2011**, *1218* (47), 8457–8479. <https://doi.org/10.1016/j.chroma.2011.09.066>.
- (15) Terzic, O.; Gregg, H.; Voogt, P. De. Identification of Chemicals Relevant to the Chemical Weapons Convention Using the Novel Sample-Preparation Methods and Strategies of the Mobile Laboratory of the Organization for the Prohibition of Chemical Weapons. *Trends in Analytical Chemistry* **2015**, *65*, 151–166. <https://doi.org/10.1016/j.trac.2014.10.012>.

Verification of exposure through analysis of biomarkers in plants

6

- (16) Hernon-Kenny, L. A.; Behringer, D. L.; Crenshaw, M. D. Comparison of Latex Body Paint with Wetted Gauze Wipes for Sampling the Chemical Warfare Agents VX and Sulfur Mustard from Common Indoor Surfaces. *Forensic Sci Int* **2016**, *262*, 143–149. <https://doi.org/10.1016/j.forsciint.2016.02.036>.
- (17) Willison, S. A. Investigation of the Persistence of Nerve Agent Degradation Analytes on Surfaces through Wipe Sampling and Detection with Ultrahigh Performance Liquid Chromatography-Tandem Mass Spectrometry. *Anal Chem* **2015**, *87* (2), 1034–1041. <https://doi.org/10.1021/ac503777z>.
- (18) The Ministry for Foreign Affairs of Finland. *Recommended Operating Procedures For Analysis In The Verification Of Chemical Disarmament*; Vanninen, P., Ed.; University of Helsinki: Helsinki, 2017.
- (19) Enserink, M. U.N. Taps Special Labs to Investigate Syrian Attack. *Science (1979)* **2013**, *341* (6150). <https://doi.org/10.1126/science.341.6150.1050>.
- (20) Read, R. W. Verification of Exposure to Chemical Warfare Agents. *Issues in Toxicology* **2016**, No. 27, 179–218. <https://doi.org/10.1039/9781782628071-00179>.
- (21) de Bruin-Hoegée, M.; van Damme, I. M.; van Groningen, T.; van der Riet-van Oeveren, D.; Noort, D.; van Asten, A. C. Elucidation of in Vitro Chlorinated Tyrosine Adducts in Blood Plasma as Selective Biomarkers of Chlorine Exposure. *Chem Res Toxicol* **2022**, *35* (6), 1070–1079. <https://doi.org/10.1021/acs.chemrestox.2c00053>.
- (22) Gravett, M. R.; Hopkins, F. B.; Main, M. J.; Self, A. J.; Timperley, C. M.; Webb, A. J.; Baker, M. J. Detection of the Organophosphorus Nerve Agent VX and Its Hydrolysis Products in White Mustard Plants Grown in Contaminated Soil. *Analytical Methods* **2013**, *5* (1), 50–53. <https://doi.org/10.1039/c2ay25883h>.
- (23) Lian, X.; Yan, B. Trace Detection of Organophosphorus Chemical Warfare Agents in Wastewater and Plants by Luminescent UIO-67(Hf) and Evaluating the Bioaccumulation of Organophosphorus Chemical Warfare Agents. *ACS Appl Mater Interfaces* **2018**, *10*, 14869–14876. <https://doi.org/10.1021/acsami.8b00289>.
- (24) Kuska, M. T.; Behmann, J.; Mahlein, A. K. Potential of Hyperspectral Imaging to Detect and Identify the Impact of Chemical Warfare Compounds on Plant Tissue. *Pure and Applied Chemistry* **2018**, *90* (10), 1615–1624. <https://doi.org/10.1515/pac-2018-0102>.
- (25) Baygildiev, T.; Vokuev, M.; Braun, A.; Rybalchenko, I.; Rodin, I. Monitoring of Hydrolysis Products of Mustard Gas, Some Sesqui- and Oxy-Mustards and Other Chemical Warfare Agents in a Plant Material by HPLC-MS/MS. *Journal of Chromatography B* **2021**, *1162*, 122452. <https://doi.org/10.1016/j.jchromb.2020.122452>.
- (26) Vaezihir, A.; Pirkhezranian, A.; Sehati, N.; Hosseinzadeh, M. R.; Salehi-Lisar, S. Y.; Sanderson, H. Investigation of Long-Term Hazards of Chemical Weapon Agents in the Environment of Sardasht Area, Iran. *Environmental Science and Pollution Research* **2022**, *29*, 498–508. <https://doi.org/10.1007/s11356-021-15593-9>.
- (27) Celia Henry Arnaud. Biomarkers of Exposure to Chlorine Gas Identified in Plant Tissue. *Chemical & Engineering News*. 2021. <https://cen.acs.org/acs-news/acs-meeting-news/Biomarkers-exposure-chlorine-gas-identified/99/web/2021/04> (accessed 2022-09-10).
- (28) Fu, F.; Sun, F.; Lu, X.; Song, T.; Ding, J.; Gao, R.; Wang, H.; Pei, C. A Novel Potential Biomarker on Y263 Site in Human Serum Albumin Poisoned by Six Nerve Agents. *Journal of Chromatography B* **2019**, *1104*, 168–175. <https://doi.org/10.1016/j.jchromb.2018.11.011>.
- (29) Hemme, M.; Fidder, A.; van der Riet-van Oeveren, D.; van der Schans, M. J.; Noort, D. Mass Spectrometric Analysis of Adducts of Sulfur Mustard Analogues to Human Plasma Proteins: Approach towards Chemical Provenancing in Biomedical Samples. *Anal Bioanal Chem* **2021**, *413* (15), 4023–4036. <https://doi.org/10.1007/s00216-021-03354-z>.
- (30) Fidder, A.; Hulst, A. G.; Noort, D.; de Ruiter, R.; van der Schans, M. J.; Benschop, H. P.; Langenberg, J. P. Retrospective Detection of Exposure to Organophosphorus Anti-Cholinesterases: Mass Spectrometric Analysis of Phosphylated Human Butyrylcholinesterase. *Chem Res Toxicol* **2002**, *15* (4), 582–590. <https://doi.org/10.1021/tx0101806>.
- (31) John, H.; Thiermann, H. Poisoning by Organophosphorus Nerve Agents and Pesticides: An Overview of the Principle Strategies and Current Progress of Mass Spectrometry-Based Procedures for Verification. *Journal of Mass Spectrometry and Advances in the Clinical Lab* **2021**, *19*, 20–31. <https://doi.org/10.1016/j.jmsacl.2021.01.002>.

- (32) Noort, D.; Fidder, A.; Van Der Riet-Van Oeveren, D.; Busker, R.; Van Der Schans, M. J. Verification of Exposure to Novichok Nerve Agents Utilizing a Semitargeted Human Butyrylcholinesterase Nonapeptide Assay. *Chem Res Toxicol* **2021**, *34* (8), 1926–1932. <https://doi.org/10.1021/acs.chemrestox.1c00198>.
- (33) Sochaski, M. A.; Jarabek, A. M.; Murphy, J.; Andersen, M. E. 3-Chlorotyrosine and 3,5-Dichlorotyrosine as Biomarkers of Respiratory Tract Exposure to Chlorine Gas. *J Anal Toxicol* **2008**, *32*, 99–105. <https://doi.org/10.1093/jat/32.1.99>.
- (34) Nishio, T.; Toukairin, Y.; Hoshi, T.; Arai, T.; Nogami, M. Development of an LC–MS/MS Method for Quantification of 3-Chloro-L-Tyrosine as a Candidate Marker of Chlorine Poisoning. *Leg Med* **2021**, *53*, 101939. <https://doi.org/10.1016/j.legalmed.2021.101939>.
- (35) Bar-On, Y. M.; Milo, R. The Global Mass and Average Rate of Rubisco. *Proc Natl Acad Sci U S A* **2019**, *116* (10), 4738–4743. <https://doi.org/10.1073/pnas.1816654116>.
- (36) Adhikari, B. M.; Bajracharya, A.; Shrestha, A. K. Comparison of Nutritional Properties of Stinging Nettle (*Urtica Dioica*) Flour with Wheat and Barley Flours. *Food Sci Nutr* **2016**, *4* (1), 119–124. <https://doi.org/10.1002/fsn3.259>.
- (37) Jeannin, T.; Yung, L.; Evon, P.; Labonne, L.; Ouagne, P.; Lecourt, M.; Cazaux, D.; Chalot, M.; Placet, V. Native Stinging Nettle (*Urtica Dioica* L.) Growing Spontaneously under Short Rotation Coppice for Phytomanagement of Trace Element Contaminated Soils: Fibre Yield, Processability and Quality. *Ind Crops Prod* **2020**, *145*, 111997. <https://doi.org/10.1016/j.indcrop.2019.111997>.
- (38) Shahrajabian, M. H.; Sun, W.; Cheng, Q. Chemical Components and Pharmacological Benefits of Basil (*Ocimum Basilicum*): A Review. *Int J Food Prop* **2020**, *23* (1), 1961–1970. <https://doi.org/10.1080/10942912.2020.1828456>.
- (39) Batool, S.; Khera, R. A.; Hanif, M. A.; Ayub, M. A. Bay Leaf. In *Medicinal Plants of South Asia*; Elsevier, 2020; pp 63–74. <https://doi.org/10.1016/B978-0-08-102659-5.00005-7>.
- (40) Gandor, F.; Gawlik, M.; Thiermann, H.; John, H. Evidence of Sulfur Mustard Exposure in Human Plasma by LC-ESI-MS-MS Detection of the Albumin-Derived Alkylated HETE-CP Dipeptide and Chromatographic Investigation of Its Cis/Trans Isomerism. *J Anal Toxicol* **2015**, *39* (4), 270–279. <https://doi.org/10.1093/jat/bkv010>.
- (41) Singh, V. V.; Kumar, V.; Biswas, U.; Boopathi, M.; Ganesan, K.; Gupta, A. K. Luminol-Based Turn-On Fluorescent Sensor for Selective and Sensitive Detection of Sulfur Mustard at Ambient Temperature. *Anal Chem* **2021**, *93* (2), 1193–1199. <https://doi.org/10.1021/acs.analchem.0c04464>.
- (42) Mirbabaei, F.; Mohammad-Khah, A.; Naseri, M. T.; Babri, M.; Faraz, S. M.; Hosseini, S. E.; Ashrafi, D. Unambiguous Identification and Determination of A234-Novichok Nerve Agent Biomarkers in Biological Fluids Using GC-MS/MS and LC-MS/MS. *Anal Bioanal Chem* **2022**, *414*, 3429–3442. <https://doi.org/10.1007/s00216-022-03964-1>.
- (43) The National Institute for Occupational Safety and Health (NIOSH). *Sarin (GB): Nerve Agent*. https://www.cdc.gov/niosh/ershdb/emergencyresponsecard_29750001.html (accessed 2022-06-12).
- (44) The National Institute for Occupational Safety and Health (NIOSH). *Chlorine: Lung Damaging Agent*. https://www.cdc.gov/niosh/ershdb/emergencyresponsecard_29750024.html (accessed 2022-06-12).
- (45) The National Institute for Occupational Safety and Health (NIOSH). *Sulfur Mustard: Blister Agent*. https://www.cdc.gov/niosh/ershdb/emergencyresponsecard_29750008.html (accessed 2022-06-12).
- (46) Sporty, J. L. S.; Lemire, S. W.; Jakubowski, E. M.; Renner, J. A.; Evans, R. A.; Williams, R. F.; Schmidt, J. G.; Schans, M. J. van der; Noort, D.; Johnson, R. C. Immunomagnetic Separation and Quantification of Butyrylcholinesterase Nerve Agent Adducts in Human Serum. *Anal Chem* **2010**, *82* (15), 6593–6600. <https://doi.org/10.1021/ac101024z>.
- (47) Hu, H.; Boisson-dernier, A.; Israelsson-nordström, M.; Böhmer, M.; Xue, S.; Ries, A.; Godoski, J.; Kuhn, J. M.; Schroeder, J. I. Carbonic Anhydrases Are Upstream Regulators in Guard Cells of CO₂ -Controlled Stomatal Movements. *Nat Cell Biol* **2010**, *12* (1), 1–18. <https://doi.org/10.1038/ncb2009.Carbonic>.

Verification of exposure through analysis of biomarkers in plants

6



7

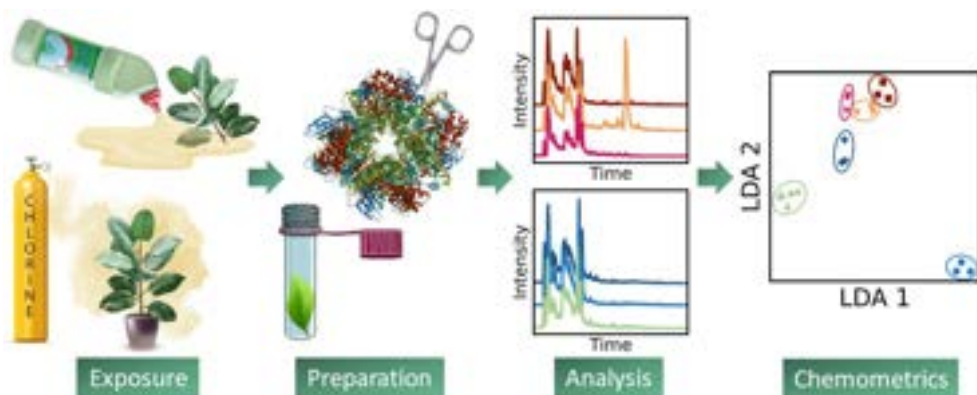
Biomarker profiling in plants to distinguish between exposure to chlorine gas and bleach using LC-HRMS/MS and chemometrics

Mirjam de Bruin-Hoegée, Marcel J. van der Schans, Jan P. Langenberg,
Arian C. van Asten, Biomarker profiling in plants to distinguish between
exposure to chlorine gas and bleach using LC-HRMS/MS and
chemometrics, *Forensic Science International* **2024**, 358, 112022.

DOI: 10.1016/j.forsciint.2024.112022.

Abstract

Since its first employment in World War I, chlorine gas has often been used as chemical warfare agent. Unfortunately, after suspected release, it is difficult to prove the use of chlorine as a chemical weapon and unambiguous verification is still challenging. Furthermore, similar evidence can be found for exposure to chlorine gas and other, less harmful chlorinating agents. Therefore, the current study aims to use untargeted high resolution mass spectrometric analysis of chlorinated biomarkers together with machine learning techniques to be able to differentiate between exposure of plants to various chlorinating agents. Green spire (*Euonymus japonicus*), stinging nettle (*Urtica dioica*), and feathergrass (*Stipa tenuifolia*) were exposed to 1000 and 7500 ppm chlorine gas and household bleach, pool bleach, and concentrated sodium hypochlorite. After sample preparation and digestion, the samples were analyzed by liquid chromatography high resolution tandem mass spectrometry (LC-HRMS/MS) and liquid chromatography tandem mass spectrometry (LC-MS/MS). More than 150 chlorinated compounds including plant fatty acids, proteins, and DNA adducts were tentatively identified. Principal component analysis (PCA) and linear discriminant analysis (LDA) showed clear discrimination between chlorine gas and bleach exposure and grouping of the samples according to chlorine concentration and type of bleach. The identity of a set of novel biomarkers was confirmed using commercially available or synthetic reference standards. Chlorodopamine, dichlorodopamine, and trichlorodopamine were identified as specific markers for chlorine gas exposure. Fenclonine (Cl-Phe), 3-chlorotyrosine (Cl-Tyr), 3,5-dichlorotyrosine (di-Cl-Tyr), and 5-chlorocytosine (Cl-Cyt) were more abundantly present in plants after chlorine contact. In contrast, the DNA adduct 2-amino-6-chloropurine (Cl-Ade) was identified in both types of samples at a similar level. The DNA adducts Cl-Cyt and Cl-Ade could clearly be identified even three months after the actual exposure. This study demonstrates the feasibility of forensic biomarker profiling in plants to distinguish between exposure to chlorine gas and bleach.



7.1. Introduction

Chlorine is a toxic dual-use chemical that was first employed as a chemical weapon during World War I.¹ More recently, it has been used multiple times as a weapon in the Syrian Arab Republic. The Fact-Finding Mission of the Organisation for the Prohibition of Chemical Weapons (OPCW) reported that chlorine gas was likely used in 14 instances,^{2–5} but it is expected that more than 300 chemical attacks with chlorine gas have occurred.⁶ Although chlorine is not scheduled in the Chemical Weapons Convention, any use of a chemical to cause intentional death or harm through its toxic properties on life processes is prohibited. Exposure to chlorine inflicts injury mainly in the respiratory tract.^{7,8} The acute exposure guideline level associated with mild irritation of mucous membranes (AEGL-1) for a 30-min exposure is 1.5 mg/m³.⁹ Exposure to a moderate concentration of 9 mg/m³ for 30 min (AEGL-2) leads to eye and throat irritation, vomiting, inflammation, and the formation of blisters. A severe 30-minute exposure at 81 mg/m³ (AEGL-3) can result in cell death, pulmonary edema, or a sudden death due to narrowing of the airways.⁹

Forensic research into the alleged use of chlorine gas as a chemical weapon is challenging. Several biomarkers have been found, mainly based on *in vivo* and *in vitro* studies, in the lungs,^{10–12} blood,^{13–17} nails,¹⁸ bronchoalveolar and nasal lavage fluid,^{19,20} and hair.^{21,22} The protein adducts 3-chlorotyrosine (Cl-Tyr) and 3,5-dichlorotyrosine (di-Cl-Tyr) have also been found in non-human biological samples.²³ In general, this type of evidence is abundant and easier to collect and transport. Other amino acids that might potentially become chlorinated are tryptophan,²⁴ lysine, and valine.²⁵ In addition, chlorination of the DNA-adducts adenine and cytosine might occur.^{26,27} Interestingly, the pH influences the formation of the specific isomer.²⁶

A disadvantage of the commonly used biomarkers, however, is their formation due to alternative, non-criminal reasons. The chlorinated tyrosine adducts were found in healthy people and at elevated levels in persons with inflammatory diseases.¹⁷ In addition, these biomarkers might be encountered as a result of exposure to other chlorinating agents. Even after exposure to a low concentration of household bleach, chlorinated tyrosine biomarkers were for instance discovered in hair.²² Also concentrated bleach is a likely candidate to encounter at the scene after a chemical weapons incident, since hypochlorite is often included in general CBRN decontamination procedures.^{28,29} Additionally, some rare cases of bleach poisoning were reported, however severe injuries and death only occurred after ingestion of huge amounts.³⁰ The staging of a chemical attack with household bleach was an alternative scenario proposed by the Syrian Arab Republic and the Russian Federation after a chlorine attack in Douma in 2018.³¹ Although bleach is known as a less reactive chlorinating agent than chlorine gas,^{32,33} it would be valuable to find novel

unambiguous biomarkers that are specific to the actual source of the chlorine, facilitating investigations of alleged use of chemical weapons.

Consequently, the aim of the current study is to explore whether bottom-up proteomics can be used to identify novel post-translational modifications in plants to distinguish between exposure to chlorine and other chlorinating agents. Three model vegetation species were selected, originating from various parts of the world. The low-nutrient feathergrass (*Stipa tenuifolia*) originally grows in South and North America.³⁴ Green spire (*Euonymus japonicus*) is an evergreen plant, native to Asia,³⁵ while the rapidly growing weed stinging nettle (*Urtica dioica*) is native to Europe.²³ The plants were exposed to three concentrations of chlorine gas and concentrated sodium hypochlorite (NaClO), pool bleach (<15% NaClO), and household bleach (<5% NaClO). After sample preparation, based on previous research,²³ the samples were analyzed by liquid chromatography-high resolution tandem mass spectrometry (LC-HRMS/MS). The compounds were tentatively identified with the software package Compound Discoverer and the data was processed by various machine learning methods to reduce data dimensionality and maximize discrimination between the different groups. The identity of a selection of markers was verified by using commercially available or synthetic reference standards and proton nuclear magnetic resonance (¹H-NMR). The present work demonstrates the potential of using untargeted high resolution mass spectrometric analysis of plant-based samples to discover new biomarkers that can differentiate between exposure to various chlorinating agents.

7.2. Experimental

7.2.1. Safety

The experiments, including chlorine gas exposure, were performed in a fume hood by trained personnel. The chemicals were handled in a leak-tight containment and personal protection measures, such as lab coats, gloves, and safety glasses were worn.

7.2.2. Chemicals and materials

Ammonium bicarbonate (ABC), calcium hypochlorite (Ca(ClO)₂), 3-chloro-L-tyrosine, formic acid, 5-chlorocytosine (Cl-Cyt), and protease from *Streptomyces griseus* (pronase, ≥3.5 units per mg solid) were obtained from Sigma-Aldrich (Zwijndrecht, The Netherlands). Acetonitrile (ACN) was purchased from Biosolve (Valkenswaard, The Netherlands). Hydrochloric acid (HCl), 2-amino-6-chloropurine (Cl-Ade), and 4-chloro-D-phenylalanine (Cl-Phe) were obtained from ThermoFisher Scientific (Landsmeer, The Netherlands) while 3,5-Di-chloro-L-tyrosine (di-Cl-Tyr) was purchased from BOC Sciences (London, UK). Dopamine was obtained from abcr GmbH (Karlsruhe, Germany). Additionally, MilliQ water (SimPak® 1) was used. The purities of the chemicals exceeded

95%. Feathergrass (*Stipa tenuifolia*) and green spire (*Euonymus japonicus*) were purchased from Intratuin and Nettle (local plant, Rijswijk) originated from the Netherlands. Concentrated sodium hypochlorite (10-20% NaOCl) with 60-185 g/L active chlorine was obtained from Boom (Meppel, The Netherlands). Three commercial household bleaches (< 5% NaOCl) were obtained from local grocery stores Albert Heijn (AH and Glorix) and Dirk (1deBeste). Pool chlorine containing 12.5 – 15% NaOCl was obtained from bol.com (B-care, Smartchim, and Huchem).

7.2.3. Exposure of the plants

A total of 78 plants were treated with either chlorine gas or bleach and 12 non-exposed plants were evaluated. First, leaves of each plant species were exposed to 7500 ppm chlorine gas ($n=3-6$, referred to as ‘chlorine, high’), which was generated by the reaction of 50 mg Ca(ClO)₂ and 1 mL of 12 M HCl, similar to the method applied by de Bruin-Hoegée et al.¹⁷ (Figure 7.1A). After reaction, the leaves were left in the closed 2L glass vial for 30 minutes. It should be noted that this concentration is calculated for a 100% reaction yield. Most likely a lower concentration was generated since some of the Ca(ClO)₂ was shielded by chlorine bubbles and remained in the vial after the reaction. In addition, each plant species was exposed to 1000 ppm chlorine gas ($n = 6$) generated from a cylinder for a long exposure duration of 1 hour at 1 L/min (referred to as ‘chlorine, long’) or a short exposure duration of 20 minutes at 0.5 L/min (referred to as ‘chlorine, short’) as depicted in Figure 7.1B. A total of four living plants exposed to chlorine gas (‘chlorine high’) were also sampled after three months. The samples were digested and stored at -20 °C for two years before analysis was conducted.

The plants were also exposed to three commercial household bleaches (< 5% NaOCl), three brands of pool chlorine (12.5-15% NaOCl), and concentrated NaOCl (10-20%, $n=3-6$). This was conducted by fully immersing a part of the living plant in the liquid for 30 minutes (Figure 7.1C). Afterwards the leaf was dried, and the pH of the slightly moist plants was measured before and after exposure.

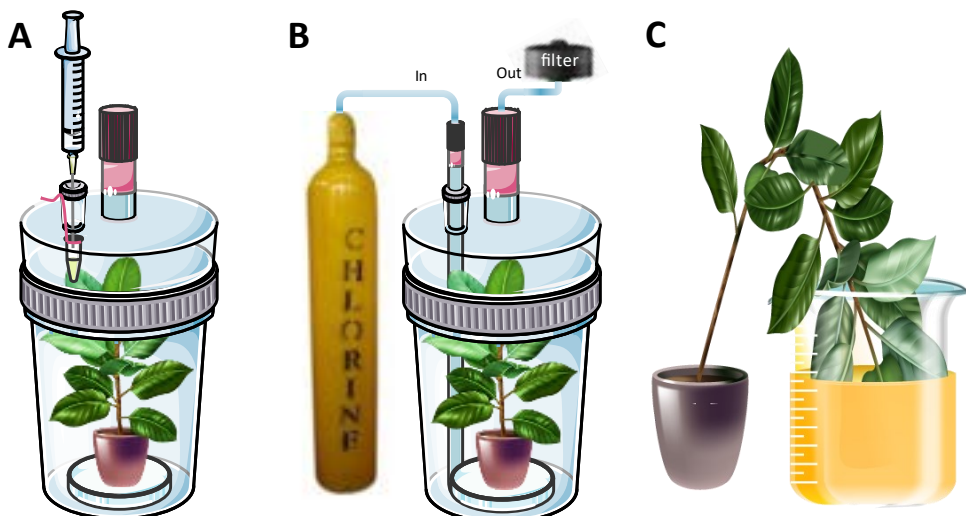


Figure 7.1. Schematic experimental set-up for controlled exposure of plants to A) A maximum of 7500 ppm chlorine gas formed by the reaction of 1 mL HCl injected into a vial with 50 mg $\text{Ca}(\text{ClO})_2$, B) 1000 ppm chlorine gas generated from a gas cylinder, and C) bleach.

7.2.4. Protein precipitation and digestion

After exposure, the sample preparation and pronase digestion were applied according to the method described by de Bruin-Hoegée et al.²³ The only exception was the exclusion of the washing step, to prevent the loss of potential biomarkers.

7.2.5. Chemical analysis

7.2.5.1. Data-dependent acquisition by LC-HRMS/MS

The samples were analyzed with a Thermo Ultimate 3000 UHPLC equipped with a Waters Acquity HSS T3 C18 column (1.8 μm , 2.1 \times 100 mm). The column temperature was maintained at 30 °C with a flow rate of 100 $\mu\text{L}/\text{min}$. Eluent A consisted of 0.2 v% formic acid in MilliQ water. Eluent B was composed of 0.2 v% formic acid in acetonitrile. Gradient elution started at 100% eluent A, ramping to 80% eluent B in 10 min and holding for 5 min. Then equilibrating at 100% eluent A for 1 min. The injection volume was 10 μL . The UHPLC was coupled to a Thermo Scientific Q Exactive Plus Orbitrap MS, which was set to a mass range of m/z 50–750 and operated in positive ESI mode. The capillary voltage was set to 3.5 kV, and the source temperature was maintained at 320 °C, the relative sheath gas (nitrogen) flow was 35. Data were first acquired with full scan MS mode. Based on the results obtained, an inclusion list was established using targeted MS/MS in parallel reaction monitoring (PRM) mode. The collision energy was 25 eV for all compounds.

7.2.5.2. Targeted analysis by LC-MS/MS

A selection of the samples was also analyzed with a Waters (Milford, MA, USA) Acquity ultra-high-pressure liquid chromatographic (UPLC) system equipped with a Waters Acquity HSS T3 C18 column (100 x 2.1 mm I.D., 1.8 µm). A volume of 5 µL was injected at 8 °C, after which the analysis was performed at room temperature with a gradient flow of 100 µL/min. Eluent A consisted of 0.2 v% formic acid in MilliQ water. The composition of eluent B was 0.2 v% formic acid in acetonitrile. Gradient elution started at 100% eluent A, holding for 2 min, then ramped to 80% eluent B in 8 min and held for 2 min. Finally, the system was equilibrated at 100% eluent A for 3 min in preparation for the next analysis. The UPLC system was coupled to a Waters Xevo TQ-S triple-quadrupole mass spectrometer, equipped with electrospray ionization operating in positive ionization mode. A capillary voltage of 3.5 kV was applied. The nitrogen cone gas flow was 150 L/h, and the argon collision gas flow was set to 0.19 mL/min. Data was acquired in selected reaction monitoring (SRM) mode and all compounds were analyzed with a single chromatographic method. Table S1 in the Supporting Information shows the chromatographic and mass spectrometric parameters for the biomarkers Cl-Tyr, di-Cl-Tyr, Cl-Phe, Cl-Cyt, chlorodopamine (Cl-dopamine), dichlorodopamine (di-Cl-dopamine), and trichlorodopamine (tri-Cl-dopamine). The identity of these compounds was verified with a synthetic reference standard. The identification was confirmed by comparing retention times, precursor ion, and characteristic fragment ion m/z values. Cone voltages of 10-30 V and optimized collision energies of 15-30 eV were used.

7

7.2.6. Data analysis

Data were first processed with Compound Discoverer 3.3 (Thermo Scientific). Peak areas were calculated by automatic integration of the extracted ion chromatogram of the identified compounds after subtraction of a negative control baseline signal as obtained for non-exposed plants. An inclusion table was established based on the first full-scan results. A large fraction of chlorinated chemicals did not match with a compound in the Chemspider database and only a formula was given. In contrast, for most non-chlorinated chemicals a match was found with the database. Consequently, the non-chlorinated chemicals in the blank were compared to the formulas of unidentified chlorinated chemicals in the treated samples. It was hypothesized that the -OH or -H would be replaced by a chlorine atom. For instance, dopamine ($C_8H_{11}NO_2$) was identified in the blank samples and a compound with formula $C_8H_{10}ClNO_2$ was found in the treated samples. This sample was preliminary identified as dopamine + Cl* and the mass was added to the inclusion table. Only chlorinated chemicals were included in the final selection. Ultimately, the markers are also visible in future research where samples might be exposed to even lower concentrations, therefore small peaks

(area < 1E7, <1% of maximum peak) were excluded. In addition, the chemical should have been identified in at least 3 repetitions of either the bleach or chlorine samples. By applying those criteria, the number of compounds was reduced from 13000 to 150. Finally, only compounds were considered that were either tentatively identified by MS/MS or present as non-chlorinated compound in the blank, resulting in 93 markers.

Python 3.9.12 with scikit-learn 1.0.2 and LIR 0.1.27 was used for the machine learning analysis. The code written for this research is published under a GNU General Public License.³⁶ PCA was applied to reduce the dimensionality of the data and identify discriminating markers. QuantileTransformer (quantiles=6) was used for normalizing the data. This method applies a non-linear transformation where the probability density function of each feature follows a uniform distribution and concurrently preserves the rank of the values along each feature. It reduces the impact of outliers, and it also provides results with similar standard deviations within classes for a given feature. The robustness was evaluated by leave-one-group-out validation. Subsequently, two LDA binary models were constructed from the data to distinguish between unexposed and exposed samples and to discriminate between samples treated with chlorine or bleach. In addition, an LDA score plot was used to classify the specific source of exposure. For all models, 3-fold cross-validation using Kernel density estimation (KDE) was applied. Two thirds of the data (containing two types of plant species) was used to train the model and one third (containing one group of plant species) was used to test the performance. After KDE construction, LR values were calculated for the classification of the exposure condition, in a similar way as described by de Bruin-Hoegée et al.³⁷ Because limited samples were evaluated, the issue of extrapolation was addressed by artificially reducing the empirical upper and lower bound (ELUB) for LR systems by a method based on the normalized Bayes error-rate as proposed by Vergeer et al.³⁸

7.3. Results & discussion

7.3.1. Visual examination of vegetation

After the exposure, the pH of the plants was assessed by bringing it into contact with pH-indicator paper (Merck, pH 1-10). The pH of the blank, chorine exposed, and bleach immersed leaf was approximately 6-8, 2, and 9, respectively. Because of this variation, it is likely that different chemical reactions will occur after chlorine and bleach exposure,²⁶ which can result in different biomarker profiles. Figure 7.2 shows the color change of the leaves over time. The leaf that was exposed to chlorine gas turned from green to brown to yellow. Small white spots were visible in the samples immersed in concentrated bleach and after one day the sodium hypochlorite crystallized on the surface of the leaf. It should be noted however, that household and pool bleach

resulted in similar discoloration as the leaves exposed to chlorine, which is likely due to other additives in the cleaning solution. Therefore, color change is not an unambiguous indicator of chlorine versus bleach exposure and cannot be used exclusively as a differentiating feature.



Figure 7.2 Blank nettle leaves (top row), leaves immersed in bleach (2nd row) and leaves exposed to 7500 ppm chlorine gas (3rd row). From left to right: after 0 min, 2 min, 5 min, 10 min, 30 min, 60 min, and 24 hours.

7.3.2. Classification of chlorinating agent

After data optimization, 93 chlorinated compounds were tentatively identified based on the exact mass, MS/MS spectra, and comparison with spectral libraries. An overview is presented in Table S2 in the Supporting Information. The compounds consist of chlorinated adducts of plant fatty acids, protein, and DNA adducts. All except five compounds were found in all species of treated investigated vegetation. In contrast, these specific markers were not found in all species of untreated plants. Most compounds were detected in both chlorinated and bleach exposed samples.

Subsequently, an unsupervised PCA model was constructed using the normalized peak area. Figure 7.3 shows the score plot of the two first principal components with grouping of the samples according to their exposure to either chlorine gas or bleach. There is full discrimination between samples treated with chlorine and bleach. However no clear trend with chlorine exposure level or exposure time is visible. This is not necessarily a disadvantage, because it means that similar markers were found for various chlorine concentrations and exposure times, making it better applicable to real-life situations where such variation is expected. The PCA model was found to be quite

robust for the given data set, since leaving out one type of exposure did not substantially reduce the explained variance (as indicated in Figure S1 in the Supporting Information).

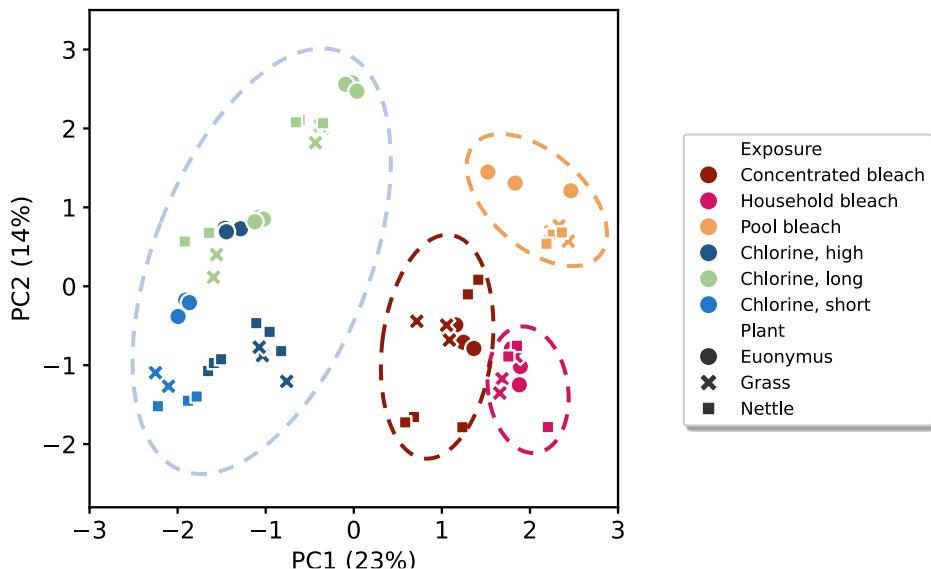


Figure 7.3. PCA-score plot based on 93 biomarkers detected by LC-HRMS/MS after chlorine gas or bleach exposure ($n=9-18$).

Additionally, the supervised machine learning method LDA was used for classification. First, a binary LDA model was computed to maximize discrimination between exposed (i.e., treated with bleach and chlorine) and unexposed samples. Figure S2 of the Supporting information shows clear discrimination between the unexposed and bleach or chlorine exposed plants. After indication of exposure, a second binary model was applied to distinguish between chlorine and bleach exposure. Figure 7.4 shows the distributions of the LDA test values. Based on the constructed Kernel density estimation, LRs were calculated. The following hypothesis pair was considered: H_1 : The plants were exposed to chlorine gas, and H_2 : The plants were exposed to bleach. The minimum and maximum LR values were assimilated to the size of the dataset, resulting in ELUB boundaries of 6.8×10^{-2} to 12 (Figure S3 of the Supporting Information). Due to the limited amount of data, the LR values were severely underestimated. False positive error rates were 0.7% and false negative error rates were 1.5%, as visualized in Tippett plots in Figure S4 in the Supporting Information. In addition to the binary model, LDA with 3-fold cross validation was performed to establish the specific source of exposure. Figure 7.5 shows the LDA-score plot of the test data with clear discrimination between the various groups. However, it should be noted that for the other two test sets, full separation of the classes was not achieved (Figure S5 of the Supporting Information).

Based on the PCA loadings, compounds can be discovered that contribute significantly to the separation of the classes (Figure S6 in the Supporting Information). In this study, discrimination was not dominated by one specific component. Rather a group of chemicals were found to be relevant markers. The chlorinated amino acid adducts dichlorinated valine, dichlorinated tyrosine, and chlorinated tryptophan are of importance. In addition, the chlorinated form of the natural product benzoic acid constitutes an important feature. Other interesting compounds that were detected are Cl-dopamine, di-Cl-dopamine, and tri-Cl-dopamine, which were only present in the chlorine-exposed samples and not in the bleach-treated samples. In addition, 4-chlorophenol (MCP) and 2,4-dichlorophenol (DCP) are relevant. Interestingly these compounds were also found in concrete samples during the investigation of alleged use of chemical weapons in Douma.³¹ It should be noted that no extensively chlorinated phenols, such as trichlorophenol (TCP) and tetrachlorophenol (TeCP), were found. However, the accessibility and reactivity in biological samples might be different compared to concrete and wooden objects, resulting in different degrees of chlorination. In the current research MCP was only detected in the chlorine-exposed samples while the amount of DCP (as indicated by the peak area) was found to be in a 100-fold excess in the chlorine-exposed samples. A selection of markers was further investigated as will be described in more detail in section 7.3.3.

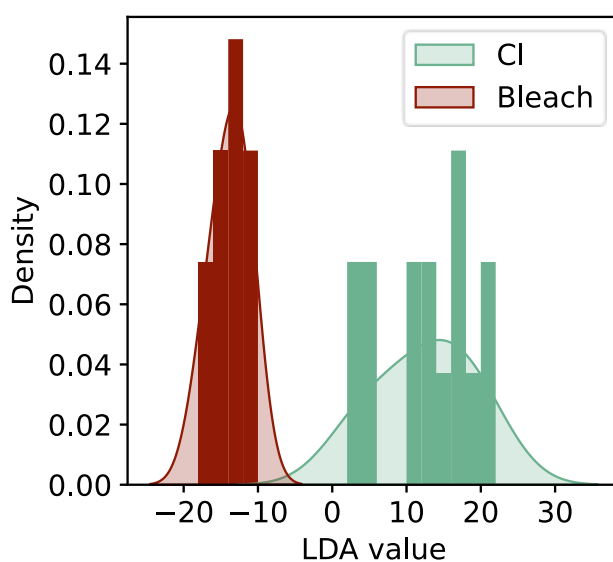


Figure 7.4. Distribution of LDA test scores after validation for plants exposed to chlorine gas (Cl) and bleach. The bars represent the frequency of the individual measurements for a given LDA value adding up to 1. The shaded curve is the kernel density estimation with a bandwidth of 0.8 (chlorine) and 1 (bleach).

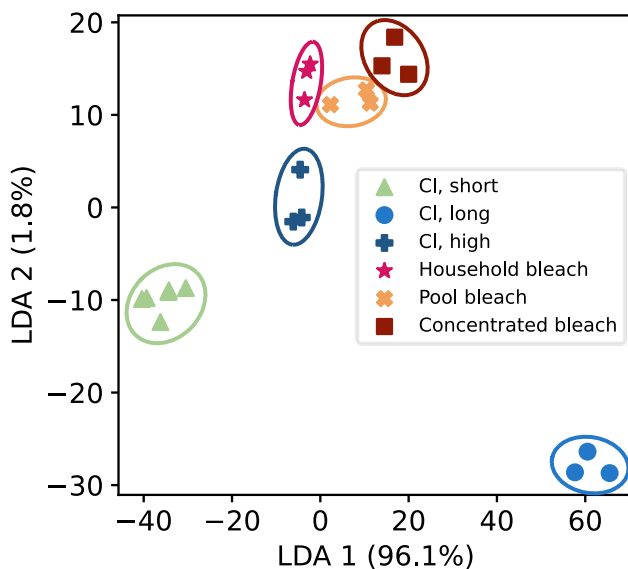


Figure 7.5. LDA-score plot after validation for classification of plants exposed to low, mid, or high chlorine gas and household, pool, or concentrated bleach. Corresponding LDA scores for the first and second discriminant function are shown.

7.3.3. Identification of novel biomarkers

7.3.3.1. Amino acid adducts

The tentative identification of selected novel biomarkers was verified by comparison with reference standards. Targeted LC-MS/MS analysis was performed of the exposed plants, commercially available reference standards for Cl-Tyr, di-Cl-Tyr, Cl-Phe, Cl-Cyt, and Cl-Ade, and synthetic reference standards for Cl-dopamine, di-Cl-dopamine, and tri-Cl-dopamine. The markers were not present in non-exposed vegetation. The amino acid adducts Cl-Phe, Cl-Tyr, and di-Cl-Tyr were present in all exposed samples, but a higher concentration was detected in the plants exposed to chlorine gas. Figure 7.6 shows the extracted ion chromatograms of the commercially available reference standard for Cl-Phe, nettle exposed to concentrated bleach, and nettle exposed to a high concentration of chlorine gas. The additional peak at a retention time of 6.4 min might be an isomer, such as ortho- or meta-chloro-phenylalanine.³⁹ The mass spectrum of the commercially available reference standard with at least two characteristic mass transitions matched the spectrum of the compound found in exposed plants. Additionally, the variation in retention time was within 0.2 min, as recommended in the work instruction for the reporting of the results of the OPCW biomedical proficiency tests.⁴⁰ An average area ratio of 3:1 was found for chlorine gas exposure compared to

bleach exposure. For Cl-Tyr and di-Cl-Tyr which were also identified in previous research,²³ the response was respectively 8 and 19 times higher for chlorine exposure (Figure S7 in the Supporting Information). Previous research demonstrated that Cl-Tyr and di-Cl-Tyr could still be detected in living plants and dried leaves three months after exposure.²³ This is invaluable in real-life scenarios where sampling can be delayed. In the current study, the marker Cl-Phe could not be detected anymore after three months. However, it is important to note that the samples were stored for a long period of time, so future research should be conducted to gain a better understanding of the stability of this marker. In the following sections, a ratio of markers will be introduced as a more robust statistic to compensate for varying exposure conditions.

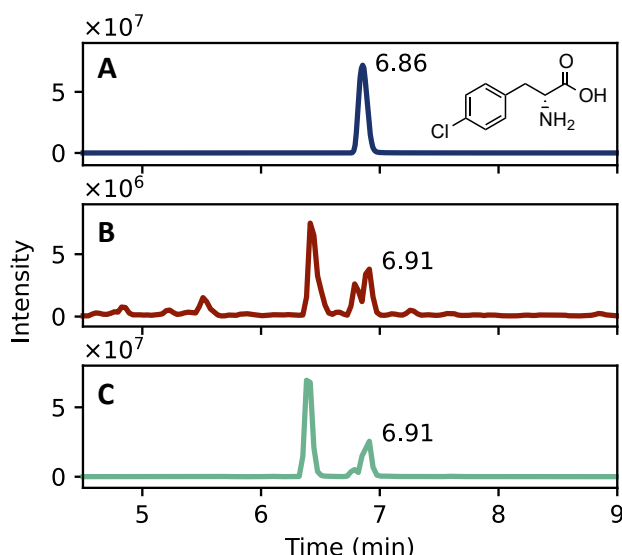


Figure 7.6. Extracted ion chromatograms (m/z 200.0 → 153.9) of 4-chloro-D-phenylalanine (Cl-Phe) at $t_R=6.86$ min. A) Commercially available reference standard, B) Nettle exposed to concentrated bleach, C) Nettle exposed to a high concentration chlorine.

7.3.3.2. DNA-adducts

In addition, two chlorinated DNA-adducts were identified. Figure 7.7 shows the extracted ion chromatograms of the DNA-adduct 2-amino-6-chloropurine (Cl-Ade). This biomarker was present in similar abundance in the bleach and chlorine exposed samples. The retention time was slightly shifted, although it is still within the allowed maximum variation. Interestingly, a compound at $t_r=7.43$ min was 300-fold more abundant in the bleach samples. This could be an isomer of 2-amino-6-chloropurine which is mainly formed after exposure to chlorinating agents with low pH. Also, an isomer with the same mass was preliminary identified at another $t_r=6.62$ min, which was more abundant in the chlorine samples. Future research could focus on isolation

of unknown markers and structural identification of these markers by NMR. Another DNA-adduct 5-chlorocytosine (Cl-Cyt) was identified (Figure S8 of the Supporting Information). Contrary to the former DNA-adduct, this compound was detected in a 10:1 ratio in chlorine samples compared to bleach-exposed plants. According to Xiang et al, chlorine substitution on the heterocyclic ring occurs at low pH, while chlorine substitution on the aliphatic amine is more likely at a higher pH.²⁶ Since they only report on chlorinated oxidation products, the results cannot directly be applied to the non-oxidized chemicals in the current study. Nonetheless, the authors demonstrated that the pH could have a significant effect on the formation of a specific isomer. Therefore, the lower pH could be a possible explanation for the fact that the other isomers were only detected in the bleach samples. Remarkably, these two DNA-adducts were still detected in living plants three months after the actual exposure to chlorine gas. The chromatograms analyzed three months after exposure are presented in Section S4 of the Supporting Information.

In forensic cases, the exposure concentration is often unknown, which makes it challenging to interpret the results. The utilization of one compound as internal standard could function as a normalizer and correct for varying sample conditions and analytical methods. A relatively sensitive parameter would be the ratio of Cl-Cyt/Cl-Ade which is 10 ± 8 ($n=5$, $\pm 95\%$ confidence interval) times higher for chlorine exposed samples compared to plants treated with bleach. Alternatively, the ratio of di-Cl-Tyr/Cl-Cyt is 3.8 ± 2.8 ($n=5$, $\pm 95\%$ confidence interval) fold higher for samples treated with bleach compared to plants exposed to chlorine gas. Together these results are promising for a robust and simple assessment of the source of Cl exposure.

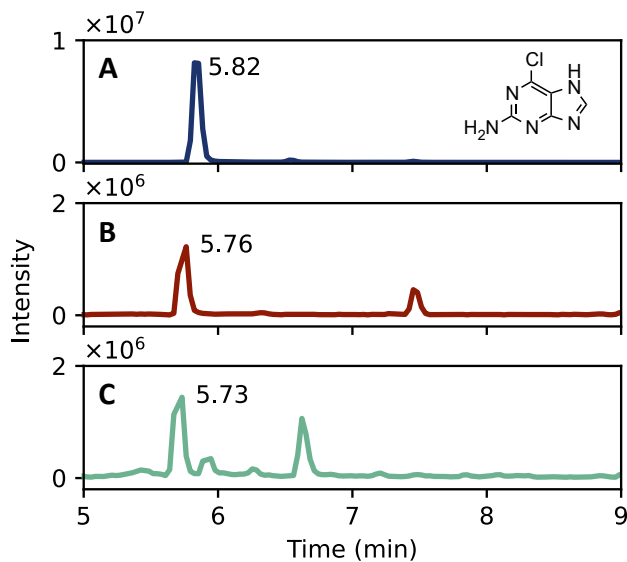


Figure 7.7. Extracted ion chromatograms (m/z 170.0 → 107.0) of 2-amino-6-chloropurine (Cl-Ade) at t_R =5.82 min. A) Commercially available reference standard, B) Nettle exposed to concentrated bleach, C) Nettle exposed to a high concentration chlorine.

7.3.3.3. Chlorinated dopamine

In contrast to the previously described compounds, chlorinated dopamine was only found in chlorine-exposed plants and is consequently a very promising biomarker for chlorine gas exposure. Dopamine promotes the growth of plants under stressful environmental conditions.⁴¹ During drought, salt stress, and nutrient deficiencies, the endogenous dopamine concentration increases.⁴¹ Its content varies amongst different species and its presence is most abundant in fully developed green leaves.⁴²

Since no commercially available standards exist, the plant samples were compared to dopamine (purity 95%) exposed to chlorine gas. The chlorinated products were separated and purified by LC-MS. Afterwards, the identification was confirmed with NMR and high-resolution mass spectrometric analysis of the exact mass, chlorine isotope patterns, and ion fragmentation. The NMR spectra are shown in Section S5 of the Supporting Information. Figure 7.8 displays a distinct chlorination pattern for Cl-dopamine, di-Cl-dopamine, and tri-Cl-dopamine in nettle plants and a single peak was visible for non-chlorinated dopamine as expected. The isotope pattern corresponds to the spectra of the synthetic reference standard for Cl-dopamine. Also, excellent correlation was found for the measured versus the theoretical monoisotopic masses and isotope ratios, with a maximum deviation of m/z 0.0011 (Section S6 of the Supporting Information).

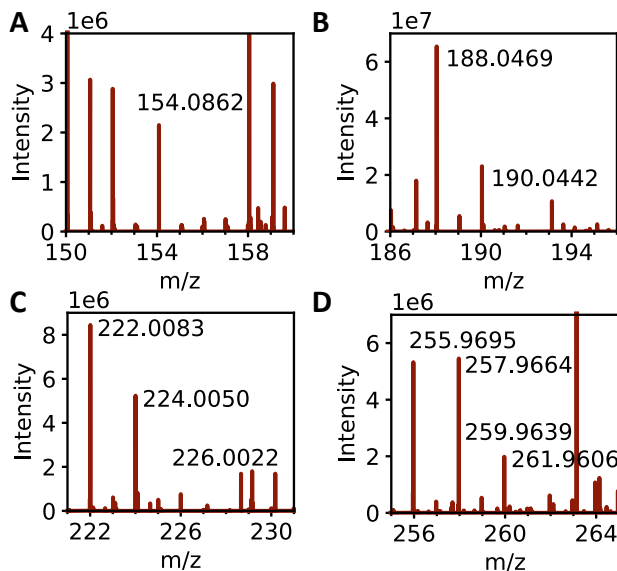


Figure 7.8. Full scan MS spectrum (LC-HRMS/MS) of singly charged chlorinated dopamine in nettle plants showing the chlorine isotope pattern. A) Dopamine, B) Cl-dopamine with an isotope ratio of 3:1, C) Di-Cl-dopamine with an isotope ratio of 9:6:1, and D) Tri-Cl-dopamine with an isotope ratio of 9:9:3:1.

Figure 7.9 shows the extracted ion chromatograms of di-Cl-dopamine. The chromatograms for Cl-dopamine and tri-Cl-dopamine are presented in Figure S9 and S10 in the Supporting Information. The retention time and mass spectrum of the compounds detected in nettle matches with the data of the synthetic reference standards. Tri-Cl-dopamine shows only one peak in the extracted ion chromatogram, while multiple peaks are present for both Cl-dopamine and di-Cl-dopamine. For both peaks comparable mass fragments are observed, which suggests the formation of two structurally similar isomers. Even three months after exposure di-Cl-dopamine and tri-Cl-dopamine were still identified in the plant samples exposed to chlorine gas and measured by LC-MS/MS (Section S4 of the Supporting Information). Only Cl-dopamine could not be detected anymore. However, these findings are limited since these markers could not unambiguously be identified in all analyzed samples because only one mass transition was found in some samples. Future research is required to gain a better understanding of the stability of chlorinated dopamine markers.

Based solely on the mass spectra no unambiguous identification of chlorinated dopamine could be accomplished (Section S7 of the Supporting Information). It was only revealed that chlorine did not react with the amine group, since for all variants the $-NH_3$ fragment was observed. Therefore, 1H -NMR analysis was performed to elucidate the chemical structure. The NMR spectra indicate that chlorination occurs in the aromatic ring. By comparison with reference spectra, Cl-dopamine is most likely

identified as 4-(2-aminoethyl)-5-chloro-1,2-benzenediol.^{43,44} In the present study, the NMR spectra from the different peaks could not be distinguished from each other, so additional research is recommended to determine the exact chemical structure. Since no reference spectra are available for di-Cl-dopamine and tri-Cl-dopamine, the results were compared with predicted spectra. The two peaks of di-Cl-dopamine were preliminary identified as 4-(2-aminoethyl)-3,6-dichlorobenzene-1,2-diol (t_r : 5.96 min) and 4-(2-aminoethyl)-3,5-dichlorobenzene-1,2-diol (t_r : 6.66 min). Presumably the small peak at t_r 5.4 min corresponds to the more sterically hindered 5-(2-aminoethyl)-3,4-dichlorobenzene-1,2-diol. The relatively low amount of synthesized marker limits the possibility to measure the sample with ^{13}C -NMR and obtain a detailed ^1H -NMR spectrum. Therefore, this study lays the groundwork for future research into the identification of a larger batch of chlorinated dopamines with a broader range of techniques.

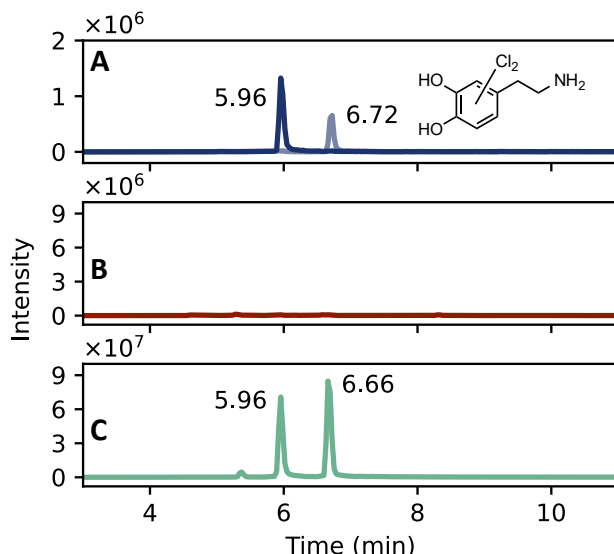


Figure 7.9. Extracted ion chromatograms (m/z 222.0 → 205.0) of dichlorodopamine (di-Cl-dopamine) at $t_{\text{R}}=5.99$ and 6.67 min. A) Synthetic reference standard, B) Nettle exposed to concentrated bleach, C) Nettle exposed to a high concentration chlorine.

7.4. Conclusions

In this study novel chlorine biomarkers were identified in vegetation using high resolution mass spectrometry with machine learning methods. The methodology proposed can be a valuable tool for the exploration of new biomarkers after contact with exogenous compounds and forms the basis for distinguishing between chlorine and hypochlorite exposure. Principal component analysis and linear discriminant analysis of tentatively identified compounds, such as chlorinated adducts of plant fatty

acids, proteins, and DNA adducts, enabled discrimination between chlorine gas exposure and various types of bleach. Distinctive markers that were discovered include dichlorinated valine, chlorinated tryptophan, chlorobenzoic acid, Cl-dopamine, di-Cl-dopamine, tri-Cl-dopamine, 4-chlorophenol, and 2,4-dichlorophenol. Since the chemometric analysis might be harder to implement in forensic laboratory practice, some biomarkers were also verified using commercially available or synthetic reference standards. Ultimately these biomarkers result in unambiguous identification. Unfortunately, most of the verified compounds were detected in both bleach and chlorine samples. Therefore, it remains important to compare case samples with control samples of locations where no threat agent was released. The amino acid adducts Cl-Phe, Cl-Tyr, and di-Cl-Tyr and the DNA-adduct Cl-Cyt were 3 to 19-fold more abundant in plants exposed to chlorine gas, compared to bleach exposed vegetation. Contrary to this, Cl-Ade was present at similar concentrations in both types of samples, and a preliminary identified isomer of Cl-Ade was even more than 300-fold more abundant in plants exposed to bleach. Consequently, the ratio of Cl-Cyt/ Cl-Ade is a promising parameter where a low value was found for bleach exposure, and a high number indicates chlorine exposed samples. By utilizing a compound ratio, absolute amounts are normalized making this parameter robust to actual exposure conditions. Interestingly, in addition, Cl-dopamine, di-Cl-dopamine, and tri-Cl-dopamine were solely detected in plants exposed to chlorine gas. To our knowledge, these biomarkers have not been reported as markers for chlorine gas exposure before. Lastly, this study demonstrated that biomarkers formed after chlorine exposure in plants are very persistent and can be identified up to three months after exposure. Future research could focus on confirming the identity of more biomarkers with reference standards, to provide extra tools for investigations of alleged use. In addition, lower exposure concentrations could be investigated with a combination of various analytical techniques. Also, the selection of the leaves could be improved by screening with portable detection techniques. In conclusion, promising biomarkers were identified by untargeted high resolution mass spectrometry facilitating incident reconstruction and differentiating between chlorine and bleach exposure.

7.5. Acknowledgements

This research is partially funded by the European Union, through a research contract awarded by the Organisation for the Prohibition of Chemical Weapons (OPCW), in support of the Plant Biomarker Challenge. We would like to thank René C. M. Olivier (TNO Rijswijk) for his assistance with the chlorine gas exposure experiments and Latifa Lamriti and Debora van der Riet-van Oeveren for their valuable LC-HRMS/MS analysis support. We are also grateful to Marco van Grol, Laura Rozing, and Martijn C. de Koning for their help with LC-MS purification and NMR analysis.

References

- (1) Sislin, J. D. Chemical Warfare in the Interwar Period: Insights for the Present? *Nonproliferation Review* **2018**, 25 (3–4), 185–202. <https://doi.org/10.1080/10736700.2018.1519343>.
- (2) OPCW. *Fact-Finding Mission*. <https://www.opcw.org/fact-finding-mission> (accessed 2023-04-25).
- (3) OPCW Fact-Finding Mission (FFM). *Report of the OPCW Fact-Finding Mission in Syria Regarding the Incident of the Alleged Use of Chemicals as a Weapon in Kafr Zeita, Syrian Arab Republic 1 October 2016*. <https://www.opcw.org/sites/default/files/documents/2022/02/s-2020-2022%28e%29.pdf> (accessed 2022-11-30).
- (4) OPCW Fact-Finding Mission (FFM). *Report of the Fact-Finding Mission Regarding the Incident of Alleged Use of Toxic Chemicals as a Weapon in Douma, Syrian Arab Republic, on 7 April 2018*. <https://www.opcw.org/fact-finding-mission> (accessed 2021-07-27).
- (5) OPCW. *First Report by the OPCW Investigation and Identification Team (IIT) Pursuant to Paragraph 10 of Decision C-SS-4/Dec.3 "Addressing the Threat From Chemical Weapons Use" Ltamenah (Syrian Arab Republic) 24, 25, and 30 March 2017*. <https://www.opcw.org/sites/default/files/documents/2020/04/s-1867-2020%28e%29.pdf> (accessed 2023-02-06).
- (6) Schneider, T.; Lütkefend, T. *Nowhere to Hide: The Logic of Chemical Weapons Use in Syria*. GPPi. <https://www.gppi.net/2019/02/17/the-logic-of-chemical-weapons-use-in-syria> (accessed 2023-04-24).
- (7) Squadrito, G. L.; Postlethwait, E. M.; Matalon, S. Elucidating Mechanisms of Chlorine Toxicity: Reaction Kinetics, Thermodynamics, and Physiological Implications. *Am J Physiol Lung Cell Mol Physiol* **2010**, 299, 289–300. <https://doi.org/10.1152/ajplung.00077.2010>.
- (8) Evans, R. B. Chlorine: State of the Art. *Lung* **2005**, 183 (3), 151–167. <https://doi.org/10.1007/s00408-004-2530-3>.
- (9) National Research Council. Chlorine: Acute Exposure Guideline Levels. In *Acute Exposure Guideline Levels for Selected Airborne Chemicals*; National Academies Press: Washington DC, 2004; Vol. 4, pp 13–76.
- (10) Ford, D. A.; Honavar, J.; Albert, C. J.; Duerr, M. A.; Oh, J. Y.; Doran, S.; Matalon, S.; Patel, R. P. Formation of Chlorinated Lipids Post-Chlorine Gas Exposure. *J Lipid Res* **2016**, 57, 1529–1540. <https://doi.org/10.1194/jlr.M069005>.
- (11) Elfsmark, L.; Ågren, L.; Akfur, C.; Bucht, A.; Jonasson, S. 8-Isoprostanate Is an Early Biomarker for Oxidative Stress in Chlorine-Induced Acute Lung Injury. *Toxicol Lett* **2018**, 282, 1–7. <https://doi.org/10.1016/j.toxlet.2017.10.007>.
- (12) Nishio, T.; Toukairin, Y.; Hoshi, T.; Arai, T.; Nogami, M. Development of an LC–MS/MS Method for Quantification of 3-Chloro-L-Tyrosine as a Candidate Marker of Chlorine Poisoning. *Leg Med* **2021**, 53, 101939. <https://doi.org/10.1016/j.legalmed.2021.101939>.
- (13) Sochaski, M. A.; Jarabek, A. M.; Murphy, J.; Andersen, M. E. 3-Chlorotyrosine and 3,5-Dichlorotyrosine as Biomarkers of Respiratory Tract Exposure to Chlorine Gas. *J Anal Toxicol* **2008**, 32, 99–105. <https://doi.org/10.1093/jat/32.1.99>.
- (14) Ahmad, S.; Ahmad, A.; Hendry-Hofer, T. B.; Loader, J. E.; Claycomb, W. C.; Mozziconacci, O.; Schöneich, C.; Reisdorph, N.; Powell, R. L.; Chandler, J. D.; Day, B. J.; Veress, L. A.; White, C. W. Sarcoendoplasmic Reticulum Ca21 ATPase A Critical Target in Chlorine Inhalation-Induced Cardiotoxicity. *Am J Respir Cell Mol Biol* **2015**, 52 (4), 492–502. <https://doi.org/10.1165/rcmb.2014-0005OC>.
- (15) Crow, B. S.; Quiñones-González, J.; Pantazides, B. G.; Perez, J. W.; Winkeljohn, W. R.; Garton, J. W.; Thomas, J. D.; Blake, T. A.; Johnson, R. C. Simultaneous Measurement of 3-Chlorotyrosine and 3,5-Dichlorotyrosine in Whole Blood, Serum and Plasma by Isotope Dilution HPLC-MS-MS. *J Anal Toxicol* **2016**, 40 (4), 264–271. <https://doi.org/10.1093/jat/bkw011>.
- (16) Nishio, T.; Toukairin, Y.; Hoshi, T.; Arai, T.; Nogami, M. Determination of 3-Chloro-L-Tyrosine as a Novel Indicator of Chlorine Poisoning Utilizing Gas Chromatography-Mass Spectrometric Analysis. *Leg Med* **2020**, 47, 101782. <https://doi.org/10.1016/j.legalmed.2020.101782>.
- (17) de Bruin-Hoegée, M.; van Damme, I. M.; van Groningen, T.; van Der Riet-Van Oeveren, D.; Noort, D.; van Asten, A. C. Elucidation of in Vitro Chlorinated Tyrosine Adducts in Blood Plasma as Selective Biomarkers of Chlorine Exposure. *Chem Res Toxicol* **2022**, 35 (6), 1070–1079. <https://doi.org/10.1021/acs.chemrestox.2c00053>.



Chapter 7

- (18) Toprak, S.; Kahriman, F.; Dogan, Z.; Gokhan Ersoy; Can, E. Y.; Akpolat, M.; Can, M. The Potential of Raman and FT-IR Spectroscopic Methods for the Detection of Chlorine in Human Nail Samples. *Forensic Sci Med Pathol* **2020**, *16*, 633–640. [https://doi.org/10.1007/s12024-020-00313-5/Published](https://doi.org/10.1007/s12024-020-00313-5).
- (19) Hemström, P.; Larsson, A.; Elfmark, L.; Åstot, C. L - α -Phosphatidylglycerol Chlorohydrins as Potential Biomarkers for Chlorine Gas Exposure. *Anal Chem* **2016**, *88* (20), 9972–9979. <https://doi.org/10.1021/acs.analchem.6b01896>.
- (20) Lindén, P.; Jonasson, S.; Hemström, P.; Ålander, L.; Larsson, A.; Ågren, L.; Elfmark, L.; Åstot, C. Nasal Lavage Fluid as a Biomedical Sample for Verification of Chlorine Exposure. *J Anal Toxicol* **2022**, *46*, 559–566. <https://doi.org/10.1093/jat/bkab069>.
- (21) Pantazides, B. G.; Crow, B. S.; Quiñones-González, J.; Perez, J. W.; Harvilchuck, J. A.; Wallery, J. J.; Hu, T. C.; Thomas, J. D.; Johnson, R. C.; Blake, T. A. Development of a Clinical Assay to Measure Chlorinated Tyrosine in Hair and Tissue Samples Using a Mouse Chlorine Inhalation Exposure Model. *Anal Bioanal Chem* **2021**, *413* (6), 1765–1776. <https://doi.org/10.1007/s00216-020-03146-x>.
- (22) Martz, S. V.; Wittwer, M.; Tan-Lin, C. W.; Bochet, C. G.; Brackmann, M.; Curty, C. Influence of Chlorinating Agents on the Formation of Stable Biomarkers in Hair for the Retrospective Verification of Exposure. *Anal Chem* **2022**, *94*, 16579–16586. <https://doi.org/10.1021/acs.analchem.2c01867>.
- (23) de Bruin-Hoegée, M.; Lamriti, L.; Langenberg, J. P.; Olivier, R. C. M.; Chau, L. F.; van der Schans, M. J.; Noort, D.; van Asten, A. C. Verification of Exposure to Chemical Warfare Agents through Analysis of Persistent Biomarkers in Plants. *Analytical Methods* **2023**, *15*, 142–153. <https://doi.org/10.1039/d2ay01650h>.
- (24) Karabencheva-Christova, T. G.; Torras, J.; Mulholland, A. J.; Lodola, A.; Christov, C. Z. Mechanistic Insights into the Reaction of Chlorination of Tryptophan Catalyzed by Tryptophan 7-Halogenase. *Sci Rep* **2017**, *7* (17395). <https://doi.org/10.1038/s41598-017-17789-x>.
- (25) How, Z. T.; Linge, K. L.; Busetti, F.; Joll, C. A. Chlorination of Amino Acids: Reaction Pathways and Reaction Rates. *Environ Sci Technol* **2017**, *51*, 4870–4876. <https://doi.org/10.1021/acs.est.6b04440>.
- (26) Xiang, Y.; Deng, Z.; Yang, X.; Shang, C.; Zhang, X. Transformation of Adenine and Cytosine in Chlorination — An ESI-TqMS Investigation. *Chemosphere* **2019**, *234*, 505–512. <https://doi.org/10.1016/j.chemosphere.2019.06.116>.
- (27) Masuda, M.; Suzuki, T.; Friesen, M. D.; Ravanat, J. L.; Cadet, J.; Pignatelli, B.; Nishino, H.; Ohshima, H. Chlorination of Guanosine and Other Nucleosides by Hypochlorous Acid and Myeloperoxidase of Activated Human Neutrophils: Catalysis by Nicotine and Trimethylamine. *Journal of Biological Chemistry* **2001**, *276* (44), 40486–40496. <https://doi.org/10.1074/jbc.M102700200>.
- (28) Zuidberg, M. C.; van Woerkom, T.; de Bruin, K. G.; Stoel, R. D.; de Puit, M. Effects of CBRN Decontaminants in Common Use by First Responders on the Recovery of Latent Fingerprints-Assessment of the Loss of Ridge Detail on Glass. *J Forensic Sci* **2014**, *59* (1), 61–69. <https://doi.org/10.1111/1556-4029.12281>.
- (29) Lepeytre, C.; Frances, F.; Charvolin, M. S.; Ludwig, A.; Le Toquin, E.; Comoy, E.; Grandjean, A.; Gossard, A. Colloidal Gel as an Efficient Process to Treat Chemical, Biological, Radiological (CBR) and Prion Contaminated Solid Surfaces. *Chem Eng Sci* **2021**, *246*, 116957. <https://doi.org/10.1016/j.ces.2021.116957>.
- (30) Ross, M. P.; Spiller, H. A. Fatal Ingestion of Sodium Hypochlorite Bleach with Associated Hypernatremia and Hyperchloremic Metabolic Acidosis. *Vet Hum Toxicol* **1999**, *41* (2), 82–86.
- (31) OPCW. *Third Report by the OPCW Investigation and Identification Team Pursuant to Paragraph 10 of Decision C-SS-4/DEC.3 “Addressing the Threat from Chemical Weapons Use” Douma (Syrian Arab Republic) – 7 APRIL 2018*. <https://www.opcw.org/sites/default/files/documents/2023/01/s-2125-2023%28e%29.pdf> (accessed 2023-04-28).
- (32) Núñez-Gaytán, A. M.; Vera-Avila, L. E.; De Llasera, M. G.; Covarrubias-Herrera, R. Speciation and Transformation Pathways of Chlorophenols Formed from Chlorination of Phenol at Trace Level Concentration. *Journal of Environmental Science and Health Part A* **2010**, *45* (10), 1217–1226. <https://doi.org/10.1080/10934529.2010.493785>.
- (33) Sivey, J. D.; Roberts, A. L. Assessing the Reactivity of Free Chlorine Constituents Cl₂, Cl₂O, and HOCl toward Aromatic Ethers. *Environ Sci Technol* **2012**, *46*, 2141–2147. <https://doi.org/10.1021/es203094z>.

- (34) Moretto, A. S.; Distel, R. A.; Didoné, N. G. Decomposition and Nutrient Dynamic of Leaf Litter and Roots from Palatable and Unpalatable Grasses in a Semi-Arid Grassland. *Applied Soil Ecology* **2001**, *18*, 31–37. <https://doi.org/10.1007/s11355-022-00527-5>.
- (35) Choi, K. S.; Park, S. The Complete Chloroplast Genome Sequence of Euonymus Japonicus (Celastraceae). *Mitochondrial DNA* **2016**, *27* (5), 3577–3578. <https://doi.org/10.3109/19401736.2015.1075127>.
- (36) de Bruin-Hoegée, M.; de Bruin, G. J. Python Code for Biomarker Profiling in Plants. 2023. <https://doi.org/10.5281/zenodo.10227405>.
- (37) de Bruin-Hoegée, M.; Kleiweg, D.; Noort, D.; Asten, A. C. Chemical Attribution of Fentanyl: The Effect of Human Metabolism. *Forensic Chemistry* **2021**, *24* (February). <https://doi.org/10.1016/j.forc.2021.100330>.
- (38) Vergeer, P.; van Es, A.; de Jongh, A.; Alberink, I.; Stoel, R. Numerical Likelihood Ratios Outputted by LR Systems Are Often Based on Extrapolation: When to Stop Extrapolating? *Science and Justice* **2016**, *56* (6), 482–491. <https://doi.org/10.1016/j.scijus.2016.06.003>.
- (39) Shin, J.-W. Extended Kinetic Method Study of the Effect of Ortho-, Meta-, and Para-Chlorination on the Proton Affinity of Phenylalanine with Full Entropy Analysis. *J Phys Org Chem* **2019**, *32* (9). <https://doi.org/10.1002/poc.3966>.
- (40) OPCW Technical Secretariat. *Work Instruction for the Reporting of the Results of the OPCW Biomedical Proficiency Tests*; 2021.
- (41) Liu, Q.; Gao, T.; Liu, W.; Liu, Y.; Zhao, Y.; Liu, Y.; Li, W.; Ding, K.; Ma, F.; Li, C. Functions of Dopamine in Plants: A Review. *Plant Signaling and Behavior*. Bellwether Publishing, Ltd. December 1, 2020. <https://doi.org/10.1080/15592324.2020.1827782>.
- (42) Świędrych, A.; Stachowiak, J.; Szopa, J. The Catecholamine Potentiates Starch Mobilization in Transgenic Potato Tubers. *Plant Physiology and Biochemistry* **2004**, *42* (2), 103–109. <https://doi.org/10.1016/j.plaphy.2003.11.002>.
- (43) García-Fernández, L.; Cui, J.; Serrano, C.; Shafiq, Z.; Gropeanu, R. A.; Miguel, V. S.; Ramos, J. I.; Wang, M.; Auernhammer, G. K.; Ritz, S.; Golriz, A. A.; Berger, R.; Wagner, M.; Del Campo, A. Antibacterial Strategies from the Sea: Polymer-Bound Cl-Catechols for Prevention of Biofilm Formation. *Advanced Materials* **2013**, *25* (4), 529–533. <https://doi.org/10.1002/adma.201203362>.
- (44) Maresh, J. J.; Ralko, A. A.; Speltz, T. E.; Burke, J. L.; Murphy, C. M.; Gaskell, Z.; Girel, J. K.; Terranova, E.; Richtscheidt, C.; Krzeszowiec, M. Chemoselective Zinc/HCl Reduction of Halogenated β-Nitrostyrenes: Synthesis of Halogenated Dopamine Analogues. *Synlett* **2014**, *25* (20), 2891–2894. <https://doi.org/10.1055/s-0034-1379481>.



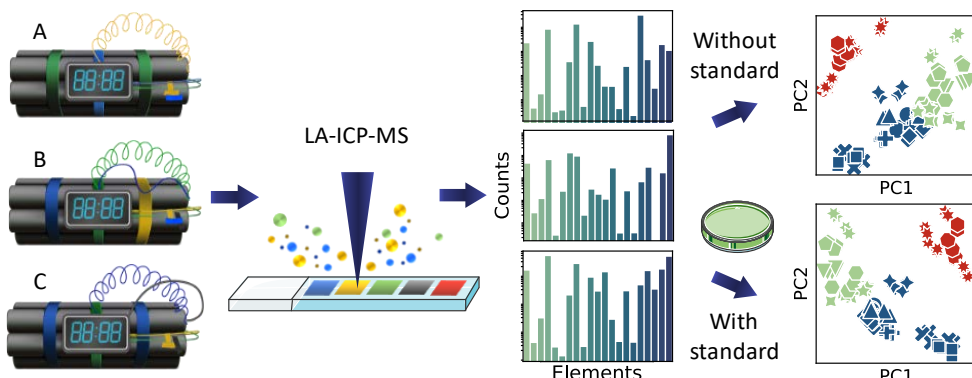
8

A novel standard for forensic elemental profiling of polymers by LA-ICP-TOF-MS

Mirjam de Bruin-Hoegée, Jorien Schoorl, Peter Zoon, Marcel J. van der Schans, Daan Noort, Arian C. van Asten, A Novel Standard for Forensic Elemental Profiling of Polymers by LA-ICP-TOF-MS. *Forensic Chemistry*
2023, 35, 100515. DOI: 10.1016/j.forc.2023.100515.

Abstract

Plastic materials are often found on crime scenes in improvised explosive devices. Determining the trace-elemental composition of polymer parts may yield discrimination between samples from different sources. Although quantitative laser ablation-inductively coupled plasma-mass spectrometry (LA-ICP-MS) is well established for forensic glass analysis, the lack of sufficiently reproducible and homogeneous reference standards hampers accurate quantification of trace elements in polymers. Therefore, the present study introduces a new standard for quantitative elemental profiling of polymers. A novel approach was developed for producing polyethylene (PE), polystyrene (PS), and polyvinyl chloride (PVC) standards containing 23 elements at three concentrations. The LA-ICP-TOF-MS measurements showed excellent linear response with $R^2 > 0.99$ for almost all elements and polymer matrices. Additionally, homogeneity was significantly improved to an average of 10% within-, and 17% between-sample variation. PVC and PE matrices presented the best homogeneity which was confirmed by line ablations. The added value of the standards was demonstrated by evaluating a set of realistic forensic polymer evidence items. The between-run variation was substantially reduced from 42% in absence of calibration to 30% when correcting with an elemental internal standard and even to 24% when applying the novel standards. In addition, its discriminating power between different classes was increased, as demonstrated by ANOVA and principal component analysis. In conclusion, this study shows the feasibility of using a novel standard for quantitative analysis of chemical attribution signatures of trace elements in polymers by LA-ICP-TOF-MS. The use of the polymer standards significantly improves classification and forensic comparison of polymer-based evidence.



8.1. Introduction

Polymers are used for many applications because of their material advantages, such as low weight, thermal isolation, and low manufacturing costs.¹ As a result of their widespread use, polymer objects are also often found on crime scenes and consequently submitted to forensic laboratories as physical evidence. Common traces include tapes, plastic bags, insulation of electrical wires, spray tanks, canisters, and storage drums. These polymeric materials may also be encountered during incidents involving chemical warfare agents. Both the chemicals and the dispersion devices designed for their release are prohibited in the Chemical Weapons Convention, which is implemented by the Organisation for the Prohibition of Chemical Weapons (OPCW).² This emphasizes the potential of not only investigating the toxic chemicals and their precursors but also additional traces that could originate from the delivery and dispersion system.

In addition to investigating which material was used, determining the trace-elemental composition of polymer parts may yield discrimination between samples from different sources and could provide leads for the criminal investigation. Matching elemental profiles of polymer parts may provide a link between fragments on a crime scene or can provide incriminating evidence when reference materials are confiscated from a suspect. Chemical attribution signatures, such as isotope ratio and impurity profiles can facilitate classification and forensic comparison. The analysis of elemental impurities by LA-ICP-MS has been used to obtain relevant intelligence information from various types of tapes^{3–7} and automotive paints.^{8,9} In addition, the analysis of plastic caps by visual examination, x-ray fluorescence (XRF), and laser ablation-inductively coupled plasma-mass spectrometry (LA-ICP-MS) provided characterization and differentiation of flash bangers in pre- and post- explosive casework.^{10,11} Stable isotope ratio analysis of the binder and plasticizer in plastic explosives discriminated two samples from different sources.¹² Additionally, elemental analyses, Fourier transform infrared spectroscopy (FT-IR), pyrolysis-gas chromatography-mass spectrometry (Py-GC-MS), and scanning electron microscopy/energy-dispersive spectroscopy (SEM/EDS) were used to distinguish backings of electrical tapes.¹³

In the manufacturing of polymers, many chemicals are introduced to aid the production process or optimize the performance of the end-product. Traditionally, almost half of all polymers is produced by catalytic polymerization reactions in the presence of transition metal compounds, such as $TiCl_4$, $ZrCl_4$, $TiCl_3$, $VOCl_3$, $AlEt_3$, and chromium-based catalysts.¹ These chemicals are applied at substantial levels and have to be removed from the product afterwards. Currently, low concentrations of the so-called leave-in catalysts are utilized, for which removal is not required thus simplifying plastic production. In addition, low-cost transition metal complexes, comprising of iron, cobalt,

chromium, nickel, manganese, copper, or zinc, have been developed and proved to be useful catalysts and initiators.^{14,15} Apart from this, common inorganic colorants such as iron oxide, aluminum oxide and titanium dioxide are applied to create the desired visual appearance.⁴ To reduce material ageing due to temperature, light, oxygen, water and microorganisms, and limit mechanical stress, the final product usually contains several additives.^{16,17} Another way of improving product properties is by replacing carbon with other elements like Si, Sn, Al and Ti, which is particularly useful for the development of heat-stable polymers. Overall, a wide range of chemicals are used to produce polymers, leading to the presence of many elements at variable levels. This provides excellent opportunities for elemental profiling of polymers for forensic attribution.

A suitable technique for the trace elemental analysis of a wide range of materials is LA-ICP-MS. This technique has numerous applications in recycling of plastics,¹⁸ food provenance and safety,¹⁹ archeology, anthropology, pharmaceuticals, and forensic sciences.²⁰ In forensic casework, glass comparison is most frequently requested, and based on robust quantitative analysis using well defined reference standards. Consequently, the evidential value of profile comparisons using reference glass databases can be accurately established.^{21–23} For instance, at the Netherlands Forensic Institute, an accredited LA-ICP-MS method is successfully applied to assist in criminal investigations where glass evidence has been secured. This contrasts with LA-ICP-MS analysis of polymers, where the lack of homogeneous reference standards hampers accurate quantification of trace elements and only qualitative or semi-quantitative analysis is applied.^{24,25} Without proper calibration, the elemental profile is affected by the polymer matrix and instrument settings, hampering database creation and forensic comparison. Nevertheless, LA-ICP-MS is ideally suited for forensic applications because of the limited sample preparation involved, the minimally invasive analysis, its ability to analyze microtraces, and the high specificity of the elemental profile. The alternative use of ICP-MS analysis combined with a suitable sample digestion process is less attractive from a forensic perspective because of the laborious and destructive sample preparation required and the need for a substantial amount of polymer material.

In forensic casework the application of a quadrupole MS is more common than a time-of-flight (TOF) MS, mainly due to the later development and the reduced sensitivity of TOF.²⁶ At the same time the TOF has many advantages, such as the high repetition rate and better resolution which can be used for precise isotope ratio measurements.^{27–29} The possibility of the fast analysis of the entire mass spectrum results in improved elemental profiling of small samples.³⁰ Therefore, the aim of the current study is to produce and to a certain degree validate new standards for quantitative elemental profiling of polymers with LA-ICP-TOF-MS and to assess their added value in forensic attribution of polymeric evidence materials. It should be noted that the added value is

not only determined by the features of the new standards but also by the elemental homogeneity in common polymer materials that can be encountered on a crime scene.

Consequently, a novel approach was developed for producing polyvinyl chloride (PVC), polystyrene (PS) and polyethylene (PE) standards with known elemental concentrations. These polymers were selected based on common occurrence and prevalence in forensic casework. More than twenty chemicals as well as the polymers were dissolved in various organic solvents and dried after mixing. The solid standards were then analyzed by LA-ICP-TOF-MS, FT-IR, and XRF and subsequently validated for a wide range of performance characteristics. The homogeneity was compared to existing glass and polymer standards. Lastly, a small set of forensic reference samples was analyzed using the new standard to study the feasibility of the developed method. The present work demonstrates the potential of quantitative analysis of elemental attribution signatures of polymers by using a novel standard, with the aim to improve forensic comparisons and to enable the development of databases for likelihood ratio estimations.

8.2. Experimental

8.2.1. Chemicals and materials

Linear low-density polyethylene (PE, melt index 1.0 g/10 min), polystyrene (PS, average Mw = 192,000), polyvinyl chloride (PVC, average Mw = 80,000 and Mn = 47,000), sodium ethanolate, magnesium chloride, aluminium triisopropylate, tetraethyl orthosilicate, potassium permanganate, calcium chloride dihydrate, titanium(IV)isopropoxide, chromium(III)chloride hexahydrate, potassium permanganate, iron(III)nitrate nonahydrate, cobalt(II)chloride hexahydrate, nickel(II)acetate tetrahydrate, copper(II)acetate, gallium(III)acetylacetone, arsenic(III)chloride, strontium tetramethylheptanedionate, zirconium(IV)butoxide solution (80 wt% in 1-butanol), tetrachlorobis(tetrahydrofuran)niobium, bis(triphenylphosphine)Pd(II)dichloride, tin(II) 2-ethylhexanoate (92.5-100.0%), antimony pentafluoride and barium bis(2-ethylhexanoate) were obtained from Sigma-Aldrich (Zwijndrecht, The Netherlands). Additionally, acetonitrile (ACN), tetrahydrofuran (THF), dichloromethane (DCM) and methanol (MeOH) were purchased from Biosolve (Valkenswaard, The Netherlands). Lead tetra acetate (95%) was obtained from Acros Organics (Geel, Belgium) and xylene was obtained from VWR chemicals (Amsterdam, The Netherlands). The purities of the chemicals exceeded 96% unless stated otherwise. Finally, expanded polystyrene (EPS 60) was purchased from local hardware store Praxis (Iso De Luxe, The Netherlands) and a set of forensically relevant objects was obtained from various sources as shown in Table S1 of the Supplementary Information.

8.2.2. Production of new polymer standards

Figure 8.1 illustrates the method for standard production. Stock solutions of the chemicals, as mentioned in section 8.2.1. dissolved into THF, ACN, MeOH or DCM were prepared. This resulted in a concentration of 0.05, 0.5 and 5 mg/mL for the 23 elements of interest: Na, Mg, Al, Si, K, Ca, Ti, Cr, Mn, Fe, Co, Ni, Cu, Ga, As, Sr, Zr, Nb, Pd, Sn, Sb, Ba, and Pb. A detailed overview is presented in section S2 of the Supplementary Information. The selection of the elements was based on the presence in polymer objects encountered in forensic casework and as analyzed by LA-ICP-MS in prior work including jerrycans, plastic bags, and PVC tapes. Although S, Cl and Zn were abundantly present, their background concentration in the blank polymer matrices was high and therefore these elements were excluded. Subsequently, volumes in the range of 20 µL to 2 mL of the dissolved chemicals, depending on the required concentration, as well as 10.0 g of PVC or (E)PS were added to 100 mL THF. For PE standards, the mixture was refluxed at 140 °C to dissolve 5.0 g of PE in 50 mL of xylene. Also, polymer blanks were included without the addition of the elemental reference solutions. After mixing, the solution was poured into a petri dish and dried at ambient temperature. When the mass did not decrease anymore, it was assumed that the solvent was fully evaporated. The produced polymer had a size of 700 cm² and a height of < 0.3 mm for PS and PVC. For PE a surface of approximately 230 cm² was covered with a height between 0.25 – 0.5 mm (n=3, for each concentration). Afterwards, the solid standards with elemental concentrations ranging from 0.02 – 2000 mg/kg were analyzed by LA-ICP-TOF-MS and XRF, as is described in more detail in section 8.2.3.

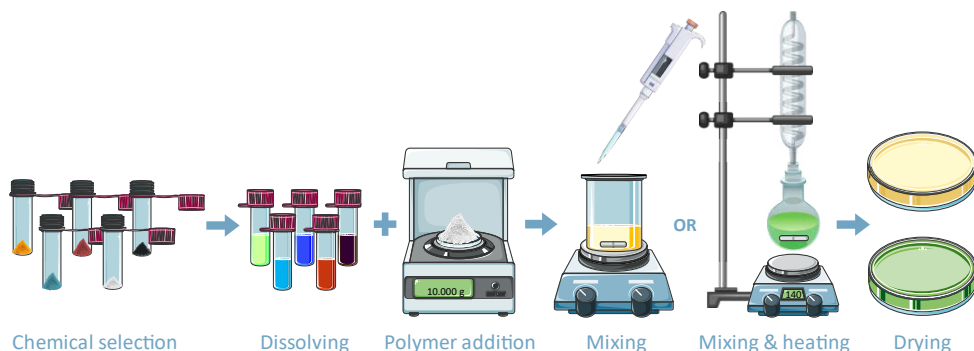


Figure 8.1. Schematic overview of the production of polymer reference standards. Figures adapted from www.smart.servier.com, CC BY 3.0.

The preparation method was optimized by evaluating the effect of mixing time, drying temperature, and polymer type on the homogeneity of the standard. A design of experiments (DOE) was created with Minitab® statistical software, to limit the number of measurements by combining the variables. Section S3 of the Supplementary

Information shows the $\frac{1}{2}$ fraction design with 18 runs, a Pareto Chart of the standardized effects, and line plots of the effect of the factors on the relative standard deviation (RSD). There was only a statistically significant association ($p < 0.05$) between the homogeneity, defined by the RSD of the concentrations analyzed by LA-ICP-MS, and the polymer type. The effect of mixing time and drying temperature was not significant. This trend was confirmed by visual and microscopic evaluation. Based on these results, 4, 20, or 30 hours of mixing time were selected for EPS, PVC, and PE, respectively, under ambient drying conditions for at least three days. Standards of all polymer types were created under optimized conditions, although PVC and PE presented better homogeneity than (E)PS. Section S4 of the Supplementary information shows pictures of the various produced standards after optimization. The experimental design with the number of measurements for the final optimized set of samples is shown in Table 8.1.

Table 8.1. Experimental design with the number of LA-ICP-MS measurements for the final set of standards.

Polymer	Level	Number of batches	Number of spot + line measurements per batch*	Repetitions over time
PVC	Blank	3	3 + 3	2
	Low	3	3 + 3	2
	Mid	3	3 + 3	2
	High	3	3 + 3	2
PE	Blank	3	3 + 3	2
	Low	3	3 + 3	2
	Mid	3	3 + 3	2
	High	3	3 + 3	2
PS	Blank	3	3 + 3	2
	Low	3	3 + 3	2
	Mid	3	3 + 3	2
	High	3	3 + 3	2

*Each line measurement consisted of three consecutive lines over a distance of 1 mm.

8.2.3. Instrumentation

A polymer fragment of approximately 5x5 mm was cut from the standards and measured by a New Wave Research 193 nm excimer laser ablation system (Elemental Scientific Lasers inc., Bozeman, MO, US) coupled to an inductively coupled plasma-time of flight-mass spectrometer (ICP-TOF-MS, type R, TOFWERK AG, Switzerland). The ICP-TOF-MS allows for acquisition of full mass spectra (6-280 m/z, with a resolution of 3000) of short transient signals. The data of 1650 waveforms of each 30 μ s is combined giving one datapoint. Collision cell technology (CCT) mode was applied, using 4% H₂ in helium as collision gas, to improve signal-to-noise ratio and remove polyatomic interferences. All samples were scanned for the presence of 52 elements. The notch filters were set to a mass of 40.3, 17.3 and 28.1 to suppress the signals of respectively argon, oxygen, and nitrogen (N₂) in the mass spectra. Other instrumental parameters for elemental analysis are listed in Table 8.2 and are based on ASTM2927-16e.³¹ Furthermore, the

data was mass-recalibrated, mass spectrum baseline-corrected, and re-integrated for each datapoint and the average of the entire spot or line using the data analysis package Tofware (TOFWERK AG, Switzerland; based on Igor Pro, WaveMetrics Inc., OR, USA). The data was further processed using Iolite v4 (Melbourne, Australia).

Table 8.2. LA-ICP-MS parameters for elemental analysis

Setting	Value
Argon flow	14 L/min
Argon nebulizer	0.8 L/min
Auxiliary flows	1.2 L/min
Helium flow	950 mL/min
ICP RF power	1550 W
Line sampling	1.0 – 1.5 mm
Line scan speed	100 µm/s
Spot dwell time	25 s
Spot energy	3.6 mJ/cm (50%)
Spot frequency	15 Hz
Spot size	150 µm

A circle with a diameter of 25 mm was cut from the standard, weighed, and analyzed by an energy dispersive x-ray fluorescence spectrometer (Xepos, Spectro) equipped with a Vitus silicon detector. Three batches with two replicate measurements (total 6 samples) of each high concentration polymer standard were measured. The concentrations of 54 elements were determined, at a limit of detection of 2000 mg/kg (Na), 300 mg/kg (Mg), 80 mg/kg (Mo, Ba), 70 mg/kg (Al), 60 mg/kg (Mn), 45 mg/kg (Ca, Sn), 40 mg/kg (K), 35 mg/kg (Cd), 30 mg/kg (S, Ti, Zn), 20 mg/kg (Si, Fe, Cu), 15 mg/kg (Cr, Ni, As, Pb), and 10 mg/kg (Cl, V).

A Bruker Alpha II compact FT-IR spectrometer with platinum ATR module was applied to characterize the polymer type of forensically relevant objects. Opus (Bruker) software was used, and the spectra were characterized using the Bruker optics ATR-polymer library.

8.2.4. Data analysis

Data analysis was performed with Python 3.9.12. The within-sample variation was calculated for three replicate spots within one batch of polymer concentration. Three batches were evaluated on day 1 and the same batches were measured two weeks later. The average RSDs of the three batches of day 1 were presented. For the between-sample variation, the average elemental concentrations of three spots within a batch was calculated. Subsequently, the RSD of the average for three batches was presented as the between-sample variation. The relative standard variation between two runs conducted over a period of two weeks was calculated for each batch separately after

which the average RSD of three batches was presented. For the XRF measurements the within-sample variation was calculated based on the average of three batches with two replicates of one batch. The between-sample variation was calculated based on the measurements of three batches. For the forensic objects the stability was calculated by using the formula for percent change: $(\text{new} - \text{old})/\text{old} * 100\%$. First, the uncorrected counts per seconds were used for comparison, then the elemental values were divided by the response of one element, or the values were divided by the response of the high concentration PVC or PE standards that were measured on the same day.

One-way analysis of variance (ANOVA) with F-test at a 99% confidence interval was applied according to the method described by Harris.³² The data was normalized ($\mu = 0$, $\sigma = \pm 1$) before analysis. The variance for each individual element was evaluated both within a set of samples from the same supplier as between different suppliers for jerrycans, wires and tubing separately. In addition, the variance was determined both within a set of samples of the same type of object with different suppliers and between the three groups of objects. The F-test at 99% confidence interval was performed to investigate the discrimination power of various elements for polymer type analysis. Scikit-learn 1.0.2 was used to perform principal component analysis (PCA) to reduce the dimensionality of the data and determine distinguishing elemental features. Data preprocessing was applied using normalization with QuantileTransformer. The robustness of this unsupervised multivariate data analysis technique was assessed by leave-one-out validation.

8.3. Results & discussion

8.3.1. Homogeneity of the new standard

To evaluate the homogeneity of the new standards, line ablation measurements were performed. Since a larger area of the standard is covered by using lines, these measurements are often applied to determine whether spot values are representative. Figure 8.2 shows the signals of four representative elements (Ca, Ti, Fe and Sb) for line ablation scans of polymer standards, prepared according to the optimized protocol described in section 8.2.2. Three consecutive line scans of 1 mm were applied over the same area to evaluate possible differences in homogeneity at the surface and inner part of the standard. Line scans of all added elements are shown in Section S5 of the Supplementary Information. A stable response is visible for the elements in the PE and PVC matrix. Surprisingly, the first line scan for the PS standard resulted in a higher abundance, suggesting the presence of surface contamination or an accumulation of the added chemicals at the surface during the production of the standard. The latter is more likely because all elements display the same effect. However, after the first line scan the signal seems to stabilize for subsequent scans.

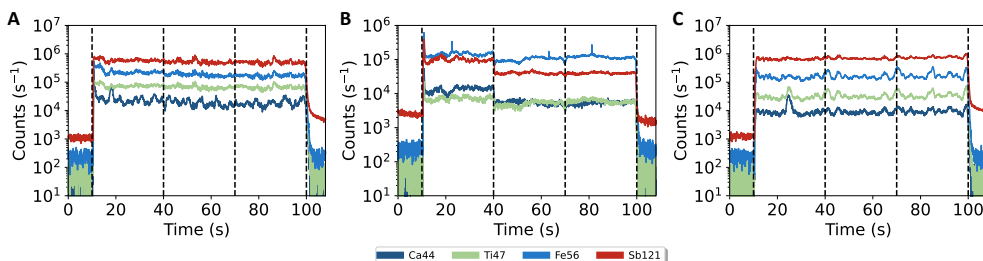


Figure 8.2. Three consecutive LA-ICP-TOF-MS line scans over a distance of 1 mm for A) PE, B) PS and C) PVC standards with four representative elements in the concentration range of 200 – 2000 mg/kg polymer. Dashed lines mark the start and end of a line scan.

Another approach to assess the homogeneity is by taking the relative standard deviation (RSD) of multiple spot ablations. Table 8.3 shows the within-sample (i.e., spot measurements on a single polymer standard) variation for low, middle, and high concentration of PE, PS, and PVC standards. In the current research K and Zr were excluded based on inhomogeneity and the lack of linearity as will be described in section 8.3.2. The average RSD values are shown in Table 8.4, with an overall average of 10%. The highest concentration standards showed the most consistent elemental abundance with an average RSD of 7% ($n=18$). The PS standards are the most inhomogeneous, probably partially due to air bubbles that were formed during production (Supplementary Information Section S4). Because there is no other polymer reference standard available that contains all the elements in the current standard at known concentrations, another method is required to correct for within- and between-run variation. A useful method is signal correction by selecting one element as internal standard. By dividing the elemental response by the Nickel abundance, the RSD was further reduced to 6%. For quadrupole LA-ICP-MS measurements, the abundant element ¹³C is often used for correction. However, the LA-ICP-TOF-MS shows reduced sensitivity for low-mass elements, which makes correction for lighter ions infeasible. In addition to Ni, similar results were obtained by selecting As, Mg, Ti, Cr, Fe, or Ga as internal standard. It should be noted that this procedure is more difficult for forensic objects because the concentrations of the elements, including the preferred internal standards, are unknown.

The novel standard showed an enhanced homogeneity compared to existing polymer reference standards, that were measured together in the same LA-ICP-MS run. For example, for PERM 680 and 681, consisting of 10 elements, an average RSD was established of 24% and 15%, respectively ($n=6$). Additionally, the NIST2855 standard containing 12 elements at three concentrations, yielded RSD values of 167%, 51%, and 44% ($n=6$) in order of increasing elemental levels. Although, the NIST612 glass standard has still better RSD values (< 5%), the non-matching matrix affects the elemental profile.

Therefore, the new polymer standards show a significant improvement compared to existing commercially available polyethylene standards.

Table 8.3. Relative standard deviation (RSD) for 21 elements as indicator for within-sample homogeneity for low, middle, and high concentration PE, PS and PVC standards (n=3 spots per polymer concentration, average value of 3 batches is given).

	Low (RSD, %)			Mid (RSD, %)			High (RSD, %)		
	PE	PS	PVC	PE	PS	PVC	PE	PS	PVC
Na23	212	LOD*	9	11	20	5	11	9	2.4
Mg24	5	10	6	1.3	12	1.9	3	9	2.1
Al27	13	LOD*	39	2.4	79	12	6	5	11
Si28	15	26	12	4	22	6	2.7	15	5
Ca44	31	21	7	32	10	1.9	4	7	1.4
Ti47	8	10	7	3	19	1.6	3	8	2.1
Cr53	2.4	9	10	4	17	3	2.5	7	2.3
Mn55	6	6	7	8	22	10	6	11	5
Fe56	8	7	9	4	15	6	2.9	7	3
Co59	10	7	7	1.8	20	4	4	6	2.2
Ni60	0	0	0	0	0	0	0	0	0
Cu63	5	9	10	5	10	5	4	8	2.3
Ga71	6	8	10	2.7	21	7	3	6	4
As75	6	13	8	3	19	0.8	2.3	10	4
Sr88	13	8	7	5	6	1.1	6	22	1.2
Nb93	10	10	8	8	20	1.8	3	13	2.4
Pd105	8	23	11	5	22	7	7	23	5
Sn118	LOD*	LOD*	30	11	36	4	3	13	5
Sb121	5	9	8	2.0	7	6	2.8	5	4
Ba137	7	11	7	7	14	4	4	65	3
Pb208	29	8	10	12	10	4	7	6	6

*The signal was below the limit of detection (LOD).

Table 8.4. Average relative standard deviation (RSD) for 21 elements as indicator for within-sample, between-sample and between-run variation, for low, middle, and high concentration PE, PS and PVC standards, analyzed by LA-ICP-TOF-MS (total of 18 spots per polymer concentration) and XRF (total of 6 spots per polymer). The signals are corrected by the nickel abundance.

	LA-ICP-MS (RSD, %)			XRF (RSD, %)	
	Within sample	Between sample	Between run*	Within sample	Between sample
PE low	20	24	9	n.a.	n.a.
PS low	11	11	23	n.a.	n.a.
PVC low	10	6	15	n.a.	n.a.
PE mid	6	17	10	n.a.	n.a.
PS mid	18	34	20	n.a.	n.a.
PVC mid	5	10	13	n.a.	n.a.
PE high	4	18	9	8	13
PS high	12	27	28	27	33
PVC high	3	5	9	21	25
Average	10	17	15	19	24

*Variation between two runs conducted over a period of two weeks.

Furthermore, the reproducibility was assessed by measuring standards produced from separate stock solutions. The average RSD was 17% as shown in Table 8.4. Especially, the PS and PE standards displayed increased variation between the different batches, while the variation for the PVC standards did not change significantly from the observed within-sample variation. All elements show comparable between-sample RSD values, with Al, Si and Pd showing the most variation and Mg, As and Sr amongst the most reproducible elements. In addition, the variation between two runs conducted over a period of two weeks was examined (Table 8.4). The elemental profile remained stable when the standards were stored at room temperature and no increase in variation was observed. The PS standards in general showed the most variation, which is likely due to an uneven distribution of the chemicals in the plastic or a higher background concentration. Lastly, it is important to characterize standards by at least two independent techniques. Therefore, XRF analyses were conducted to measure the homogeneity of the standards over a larger surface area. Because the XRF is less sensitive than LA-ICP-MS, only the high concentration standards were analyzed. The RSD values shown in Table 8.4 demonstrate that the within-sample variation is relatively high and comparable to the between-sample variation. One of the reasons for this variation is that some concentrations were near the detection limit and not detected in all cases, resulting in a threshold effect. Nevertheless, the average RSDs are only slightly higher than the values obtained with LA-ICP-MS and still below 25%.

8.3.2. Linear range

Overall, the new standards showed an excellent linear response with an average $R^2 > 0.99$ (Table 8.5). The calibration graphs are included in section S6 of the Supplementary Information. The y-intercept was in 94% of the linear graphs below 10% of the response of the target value of the analyte (\bar{y}). A likely reason for the reduced linearity of Ti in PS and PVC is the poor sensitivity, resulting in values below the detection limit for almost all measured concentrations. Consequently, this is accompanied by a relatively high LLOQ value. In addition, Ca and Al showed a relatively large within-sample variation, as was shown in Table 8.3, which seems to negatively affect linearity.

As was pointed out in the introduction to this paper, the elemental profile can be affected by the polymer matrix. Ideally one type of polymer standard is acceptable for measuring a wide range of plastic evidence materials. The appearance of the standards was slightly different. The colors varied from green for PE to yellow for PS and pale sand for the PVC standards. The PE standards were the most flexible and softest, while the PS standards show the highest brittleness. The calibration curves illustrate the effect of the polymer matrix on the response of the LA-ICP-TOF-MS. Interestingly, the intensities for most elements are quite comparable. The most variation is visible for Pd, Si, K, Ti, Mn, and Zr, which are also the elements that are the most inhomogeneous, probably

causing this variation. It could be considered to exclude these elements for a more robust method. Based on the linearity measurements, it can be assumed that one standard is applicable to at least PE, PS and PVC matrices.

Table 8.5. Linearity of elemental responses, y-intercept as percentage of mean response and lowest limit of quantification analyzed by LA-ICP-TOF-MS.

	PE			PS			PVC		
	R ²	y _{intercept} y (%)	LLOQ (mg/kg)	R ²	y _{intercept} y (%)	LLOQ (mg/kg)	R ²	y _{intercept} y (%)	LLOQ (mg/kg)
Na23	0.9999	-2.3	20	0.9965	-1.6	100	0.9991	-2.3	50
Mg24	0.9969	-2.3	40	0.9974	-5	50	0.9999	1.3	5
Al27	0.8612	-12	200	0.9933	-9	50	0.9927	-10	5
Si28	0.9992	-0.20	200	0.9986	22	1000	0.9985	-2.8	100
K39	0.9971	-6	2	0.9994	-1.2	10	0.9512	43	100
Ca44	0.8607	10	1000	0.9915	-4	200	1.0000	0.7	10
Ti47	0.9953	-303	2000	0.6219	24	500	0.8546	-66	1000
Cr53	0.9405	11	20	0.9885	-11	10	0.9998	-1.2	5
Mn55	0.9995	-1.8	2.8	0.9985	2.1	1.4	0.9941	-8	1.4
Fe56	0.9998	-1.0	2	0.9980	-5	5	0.9982	-4	2
Co59	0.9993	-2.0	1	0.9994	-2.9	0.1	0.9991	-2.7	0.2
Ni60	0.9999	1.0	1	0.9982	-5	0.5	0.9999	-0.18	0.2
Cu63	0.9997	-1.1	2	1.0000	-0.12	1	0.9961	-7	5
Ga71	0.9991	-2.9	2	0.9984	-5	1	0.9980	-4	1
As75	0.9989	-3	2	0.9983	-5	0.5	0.9990	-3	5
Sr88	0.9988	-3	4	0.9973	-6	1	0.9993	-2.7	1
Zr90	0.9983	4	0.04	1.0000	-0.8	0.2	0.9999	1.0	0.02
Nb93	0.9920	4	2	0.9957	-2.3	1	0.9929	4	1
Pd105	0.9935	-7	2	0.9992	2.9	1	0.9919	-9	1
Sn118	0.9992	-4	20	0.9994	-3	10	0.9971	3	200
Sb121	0.9982	-4	10	0.9996	-2.3	5	0.9946	-6	20
Ba137	0.9986	-4	10	0.9959	-7	5	0.9994	-2.7	5
Pb208	0.9980	-5	2	0.9976	-5	1	0.9995	-2.6	5

The novel standards were also quantified by XRF as a second independent method. This technique is often used for semi-quantitative analysis using element intensity ratios, since quantitative analysis requires more extensive sample preparation and well-defined sample shapes.^{11,33} Although in the current study the standard was corrected for the total mass, the shape and thickness still varied, therefore the absolute concentrations measured by XRF, as shown in Table S5 of the Supplementary Information, are of indicative nature only. Overall, the analyzed concentrations of the PE standard were the closest to the applied concentrations and deviated on average 23%. For Si, Ca, Cr, Fe, Ga, As, Nb, Pd, Ba, and Pb the difference was less than 20%. Most elemental concentrations for the PE and PVC standards were slightly lower than expected. This contrasted with the PS standard, where all concentrations were higher

than expected, which is likely due to the use of less purified expanded polystyrene material. In addition, the concentrations of the PVC standard deviated 35% on average compared to the applied concentrations, of which the elements Mg, Si, K, Nb, Pd and Ba deviated less than 20%.

8.3.3. Application to forensic samples

To demonstrate the potential of the new standard, a set of polymer objects with forensic relevance were analyzed and evaluated with and without the new standards on two days over a period of two weeks. First, the element selection was evaluated, because the new standards only contain a selection of the elements that are detected in forensic objects. Figure 8.3 shows typical line ablation results of four representative elements detected in electrical wires, PVC tubing, jerrycans, and tapes. The ten most abundant elements are also present in the standards. This contrasts with commercially available polyethylene standards, where not all those elements are present in known concentrations. Only scandium and sulfur were also abundantly present in jerrycans, and a high concentration of zinc was detected in tapes and tubing, but these latter two elements were not included in the standard, due to the high background of these elements in many polymeric objects. It should be noted that the most abundant elements are often not the most discriminating because such high levels indicate intentional addition to realize desired product properties. So where major elements could be useful for classification, trace elements can be more important for forensic comparison through elemental profiling.

As can be seen in the line scans of four representative elements in Figure 8.3, the objects show relatively poor homogeneity. Line scans with the ten most abundant elements are shown in Section S5 of the Supplementary Information. Based on triplicate spot measurements on three objects, the within-variation of the jerrycans is highest with 29%, while for the other objects it is less than 13%. The elements Cr and Ni show the highest variation which exceeds 30%, and the variation of Co, Cu, Ga and Nb is between 20-30%. To possibly mitigate measurement variation without applying a standard, one abundant element that is already present in the objects can be used as internal standard. For the within-variation however, this did not improve the homogeneity. Nevertheless, the between-sample variation is much larger with an average RSD of 99%, indicating that despite the observed inhomogeneity of typical low-cost polymeric products, elemental profiling is still feasible. However, larger datasets should be evaluated to verify this statement.

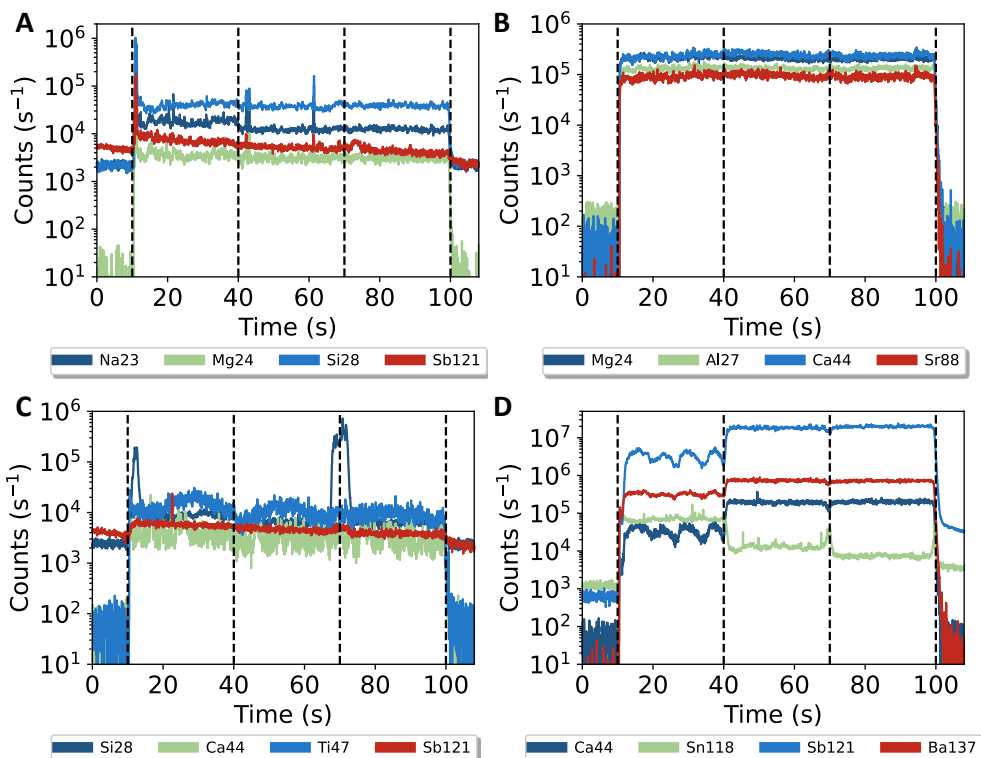


Figure 8.3. Three consecutive LA-ICP-TOF-MS line scans over a distance of 1 mm of four representative elements in A) an electrical wire, B) PVC tubing, C) jerrycan and D) tape backing. Dashed lines mark the start and end of a line scan.

8

Subsequently, the polymer types of forensic objects were determined by using FT-IR. All tubing, wires and tapes consisted of PVC and the jerrycans were made of low- and high-density PE (Table S1 of the Supplementary Information). Next, the forensic samples were measured together with the new PVC and PE standards by LA-ICP-TOF-MS. Both high concentration standards are in the concentration range of the forensic objects. The elemental profiles of the forensic samples, determined by using the PE and the PVC standard, are illustrated in Figure 8.4. The concentrations were calculated by applying the linear fit for each element using the blank, low, mid, and high concentration standards. The largest difference between the standards is for the low abundant elements, such as As, Co, Cr, Na, Nb, Pb, and Sr.

One of the advantages of having a standard is the possibility to correct for instrument response over time. The variation of uncorrected responses of the wires, PVC tubing, jerrycans and tape backings, were compared with the elemental values corrected by several methods. Correction by the high concentration PVC standard significantly improved the stability of the profile from 42% to 24% variation over two weeks. The

corrected value was calculated by dividing the elemental responses by the response of the standard corrected for the Nickel abundance. Also, for the PE jerrycans, correction for the PVC standard resulted in similar stability compared to using the PE standard. The same principle is applicable when applying the PE standard for PVC objects, which suggests that the standards can be used interchangeably. Since many polymer types exist, it would be very practical if one single reference standard could be used for all polymeric samples. Correction for the glass standard SRM612 also improves the stability to 29%. This is slightly worse compared to the new polymer samples. Another simpler approach to correct for variation, is using one element as internal standard. For most elements, this resulted in much worse homogeneity, except for Na, Mg, and Si where correction on the basis of Si abundance resulted in a variation of 30%. It can therefore be concluded that the application of an external polymer standard on forensic objects still gives the most consistent elemental concentration over time, although there is a minor difference with correction for the existing SRM612 glass standard and the relatively simple method of using internal element correction.

A common method for classification of forensic objects is by calculating whether the elemental concentrations of two samples overlap ($\text{mean} \pm 2 \times \text{standard deviation}$)⁷. In this case, only the individual variation of the forensic objects was considered. The forensic objects were evaluated without applying a standard, with application of one element as internal standard and by using the new standards. The elemental responses were corrected by the mean response of the polymer standards measured on the same day. It turned out that in all cases for all elements, at least two of the five to seven samples overlap (Supplementary Information Section S8). Although this method can be useful to compare a known and questioned sample, this method is less useful when comparing multiple profiles.

Another way to demonstrate the potential of the new standards is by applying ANOVA for comparison of the within- and between-group variation. Discrimination and significance testing using ANOVA has also been applied to elemental profiling of glass.^{33,34} Table 8.6 shows the average RSD, mean square and F-value for the 21 elements measured by LA-ICP-MS. Comparisons between the three different objects and within the 5-7 different types of jerrycans, PVC tubing, and electrical wires are shown. The within-sample RSD was generally lower than the between-sample RSD showing the potential for forensic discrimination between the various groups. In addition, for all elements the variances are sufficient (at the 99% confidence level) to differentiate between groups. Interestingly, the F-value was consistently higher for data corrected with the new standards compared to normalized data without correction for a standard. Although it would be forensically relevant to distinguish

between the different suppliers and brands, we will further focus on classifying the different objects due to the limited sample size.

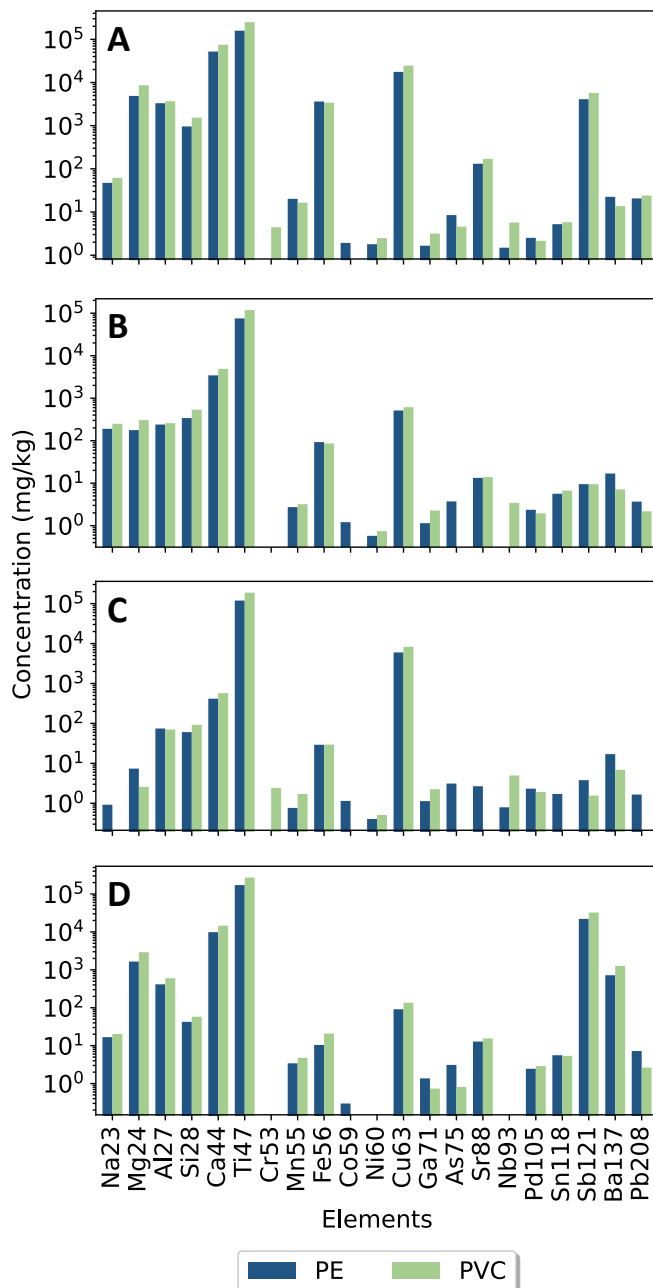


Figure 8.4. Average concentrations of 21 elements, analyzed by LA-ICP-MS using the new PE or PVC standards, from A) electrical wires, B) PVC tubing, C) jerrycans and D) tapes.

Table 8.6. Analysis of variance (ANOVA) to compare within- and between-group variation (h: number of groups, n: number of samples, MS: mean square, df: degrees of freedom). The average normalized values of all 21 elements measured by LA-ICP-MS are presented.

Type	h	n	Correction	Within group			Between groups			ANOVA	
				RSD (%)	MS	df	RSD (%)	MS	df	Mean F-value	Element with highest F-value
Objects	3	36	Normalizing	191	6.5 $\times 10^{-3}$	105	4 $\times 10^{18}$	9.11	2	1398	Na, Mg, Co
			Element correction	99	7.4 $\times 10^{-3}$	105	5 $\times 10^{17}$	7.57	2	1022	Na, Ca, Mn
			Standard	135	6.1 $\times 10^{-3}$	105	5 $\times 10^{17}$	10.4	2	1701	Si, Na, Mg
Jerry-cans	5	6	Normalizing	-20	1.7 $\times 10^{-2}$	25	-108	1.21	5	70	Si, Al, Cu
			Element correction	-105	2.9 $\times 10^{-1}$	25	110	5.66	5	19	As, Mg, Al
			Standard	-21	1.5 $\times 10^{-2}$	25	-7	1.31	5	90	Si, As, Ca
Tubing	7	6	Normalizing	-54	1.4 $\times 10^{-2}$	35	490	0.68	5	48	Al, As, Fe
			Element correction	-58	8.8 $\times 10^{-3}$	35	-67	0.87	5	99	Na, Al, Fe
			Standard	-43	1.1 $\times 10^{-2}$	35	216	0.80	5	75	Pb, Al, Sr
Wires	6	6	Normalizing	71	1.1 $\times 10^{-2}$	30	192	1.03	5	91	Mg, Fe, Ga
			Element correction	72	8.5 $\times 10^{-3}$	30	253	1.14	5	134	Mg, Ga, Al
			Standard	43	6.9 $\times 10^{-3}$	30	196	1.19	5	174	Ga, Fe, Al

The most significant elements for distinguishing between jerrycans, electrical wires, and PVC tubing are shown in Figure 8.5. The increased level of Si, Mg and Na can be explained through their use in halogen-free flame-retardant wires and cables.^{1,35,36} With ANOVA the individual variation of each element was assessed. However, it is expected that the elements will show some degree of correlation. Figure 8.6 illustrates the correlation coefficients of the elements detected in the jerrycans, wires and tubing. No highly negative correlation ($r < -0.7$) is present, while lead for example shows a strong positive correlation with As (0.89), Nb (0.82) and Sb (0.94).

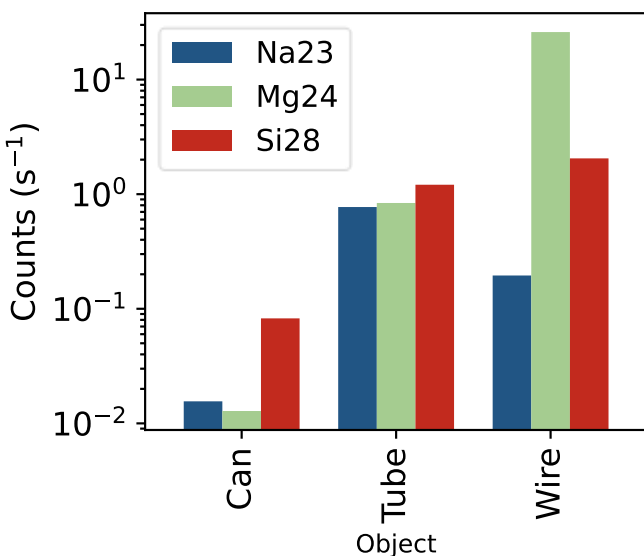


Figure 8.5. Bar chart of three most distinguishing elements measured by LA-ICP-MS for jerrycans, PVC tubing and electrical wires. The mean elemental responses are corrected using the new standard (n=36).

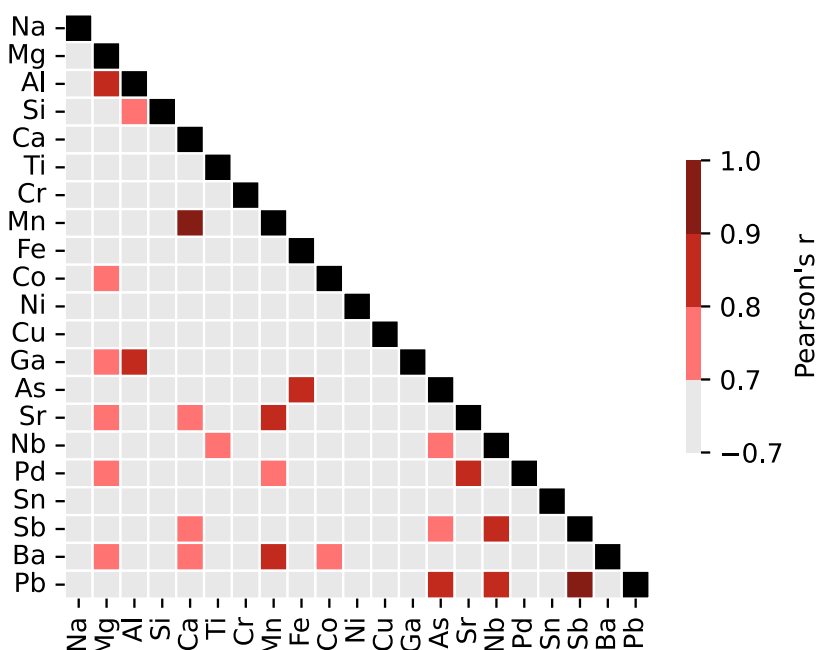


Figure 8.6. Pearson's correlation coefficients of the elements present in the jerrycans, electrical wires and PVC tubing based on the LA-ICP-MS results.

In addition, the dimensionality was reduced by applying PCA. Figure 8.7 shows the PCA-score plot with two principal components of normalized data. The data was evaluated without standard correction, using Si as the internal standard, and with correction for the new standards. The most important finding was the improved separation of the classes when using the new standard. The robustness of the PCA was checked by leave-one-out validation (Figure 8.8). The model showed sufficient robustness, since leaving out one sample did not affect the explained variance. In addition, Figure 8.8 shows the dimensionality of the elemental data. Due to the correlations as demonstrated in Figure 8.6, in total 99% of the variation is described by 14 principal components.

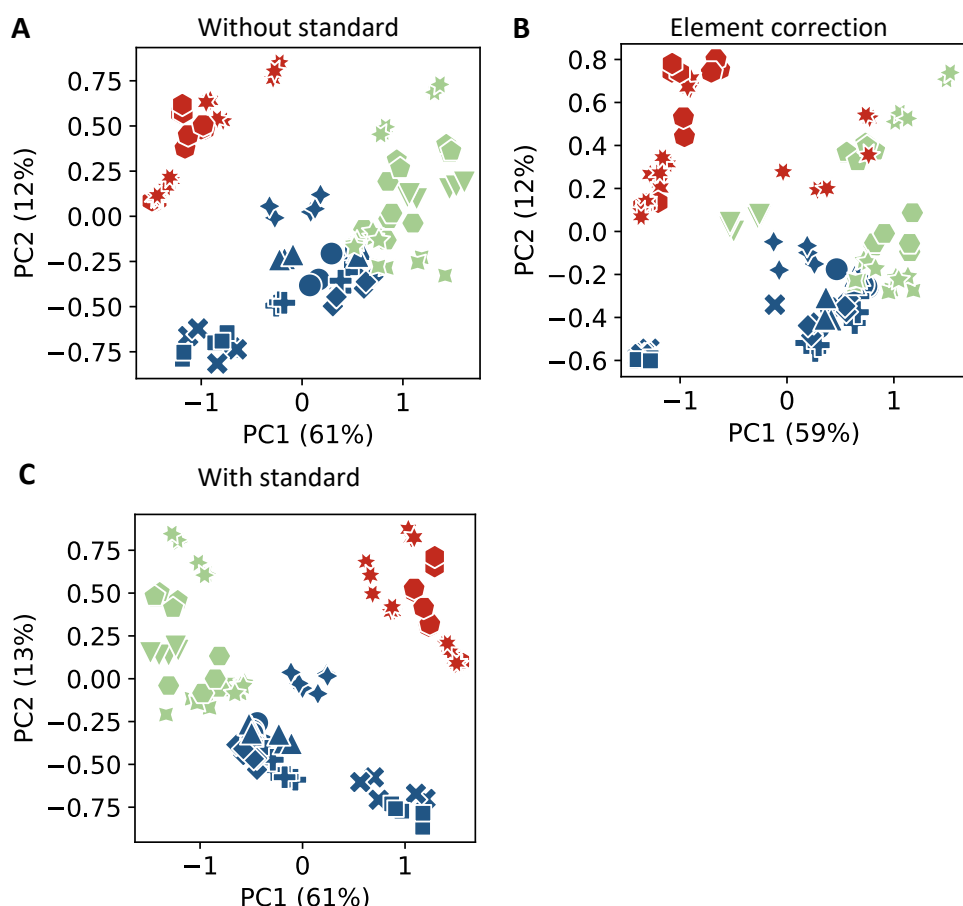


Figure 8.7. PCA-score plots for classification of PVC tubing (blue), electrical wires (green), and jerrycans (red) from different suppliers and brands (indicated by style), measured over a period of two weeks, based on 21 elements detected by LA-ICP-MS ($n = 36$). The PCA-scores for the first (PC1) and second (PC2) principal component are shown, using A) The elemental abundance, B) Applying Si correction, and C) Element quantification through application of novel standards.

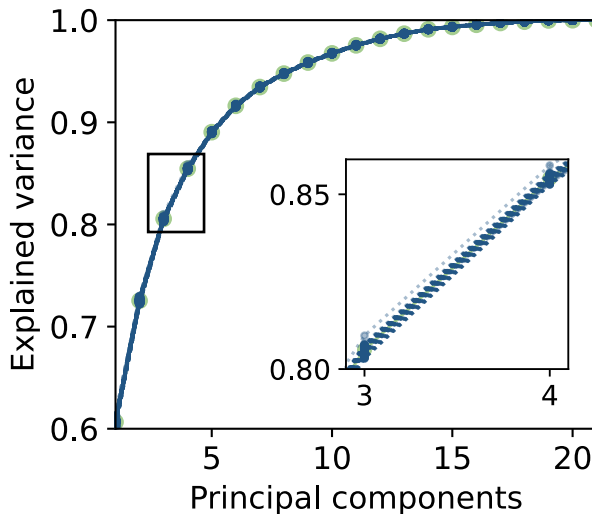


Figure 8.8. Explained variance of PCA with effect of leave-one-out validation on PCA robustness with zoom-in of plot. Blue line: PCA including all samples; dashed lines: PCAs with one sample left out.

Finally, PCA was used to evaluate which elements were relevant to discriminate the various objects. Figure 8.9 illustrates the PCA-loadings, with Mn, Ca, and Co as the most influential elements for PC1 and Na, Cr, and Nb as the most distinguishing variables for PC2. This is slightly different than the elements indicated by ANOVA (highlighted in red). The evaluation of larger datasets is required to indicate the distinguishing markers that discriminate the individual suppliers and brands within each group of materials.

8

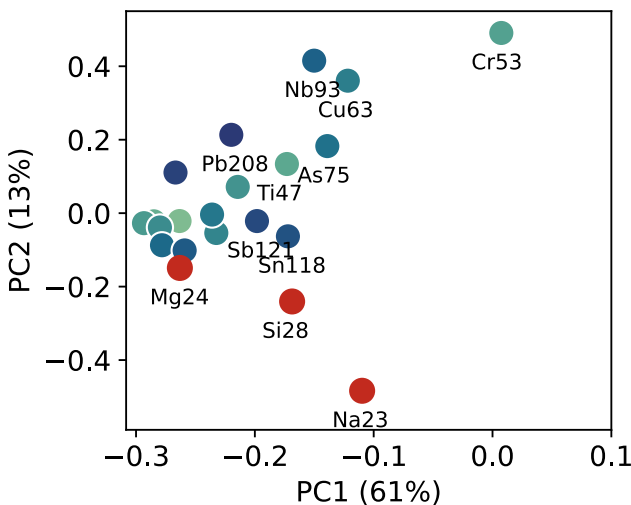


Figure 8.9. PCA-loading plot. PC1 represents 61% of the total variance and is affected by the elements Mn, Ca and Co. PC2 accounts for 13% of the variance and is mainly affected by the elements Na, Cr and Nb. Red points indicate the most significant elements determined by ANOVA.

8.4. Conclusions

In this study a promising method was developed for quantitative analysis of elemental attribution signatures of polymers by LA-ICP-TOF-MS using new standards. The standards showed enhanced homogeneity compared to existing polymer standards and facilitated forensic classifications. Furthermore, the application of an LA-ICP-MS method enables simple and fast analysis with little or no sample preparation, which makes this novel method easily applicable in forensic practice. The current study indicates that the PE and PVC standard could be used interchangeably for both types of forensic polymer objects, which could simplify the procedure for the construction of forensic elemental profiles. Furthermore, the experience of laboratories with LA-ICP-MS analysis of reference standards for glass comparisons is an advantage when implementing the developed method in forensic casework. In addition, a simpler approach was evaluated by using correction for one element in the forensic objects instead of using a standard material. However, the performance of an internal standard approach was found to be inferior compared to the method with the newly developed standards.

Future research will focus on verification of the standards by multiple laboratories with various complementary techniques. In addition, a larger dataset of forensic relevant plastic objects will be analyzed to further show the benefits and limitations of the approach. Especially the application of a single polymer standard (in terms of polymer matrix) to even more categories of polymer materials could be an advantage. Subsequently, a larger dataset could be constructed to enable the application of more sophisticated chemometric and machine learning methods for discrimination between different classes thus providing intelligence information on the type of material encountered. Additionally, with sufficient reference data, likelihood ratio models could be constructed that allow for forensic comparison in case work on the basis of elemental profiles of evidence items (e.g., comparing electrical wire insulators from a device with a wire stock found at the home of a suspect). Although the new standards showed excellent performance, the poor elemental homogeneity of polymer objects encountered in forensic casework could hamper practical application and will ultimately limit the added value. To that end, it is required that forensic polymer evidence material has significantly larger between-sample variation. As was shown in the current study with a limited dataset, such polymer materials do exist. In conclusion, the proposed standard could facilitate forensic elemental comparison studies of polymers.

8.5. Acknowledgements

We would like to thank Duurt P. W. Alkema for fruitful discussions on polymer synthesis and analysis. We are also grateful to Wim Wiarda and Marianne Schrader for performing initial measurements of the polymer standards with LA-ICP-MS.

References

- (1) Koltzenburg, S.; Maskos, M.; Nuyken, O. *Polymer Chemistry*; Springer: Berlin Heidelberg, 2017. <https://doi.org/10.1016/B978-1-84569-741-9.50002-1>.
- (2) Organisation for the Prohibition of Chemical Weapons. *Article II Definitions and Criteria*. Chemical Weapons Convention. <https://doi.org/10.1093/analys/22.5.109>.
- (3) Martinez-Lopez, C.; Trejos, T.; Sakayanagi, M.; Almirall, J. R. Elemental Analysis and Characterization of Electrical Tape Backings by LA-ICP-MS. *Forensic Chemistry* **2017**, *4*, 96–107. <https://doi.org/10.1016/j.forc.2017.03.003>.
- (4) Martinez-Lopez, C.; Sakayanagi, M.; Almirall, J. R. Elemental Analysis of Packaging Tapes by LA-ICP-MS and LIBS. *Forensic Chemistry* **2018**, *8*, 40–48. <https://doi.org/10.1016/j.forc.2018.01.004>.
- (5) Martinez-Lopez, C.; Trejos, T.; Coulson, S.; Goodpaster, J.; Igowsky, K.; Kuczelinis, F.; Mehlretter, A.; Pollock, E.; Simmross, U.; Weimer, R.; Weis, P.; Almirall, J. R. Interlaboratory Evaluations of the Performance of Elemental Analytical Methods for the Forensic Analysis and Comparisons of Electrical Tapes. *Forensic Chemistry* **2019**, *12*, 66–77. <https://doi.org/10.1016/j.forc.2019.01.001>.
- (6) Gupta, A.; Martinez-Lopez, C.; Curran, J. M.; Almirall, J. R. Multi-Element Comparisons of Tapes Evidence Using Dimensionality Reduction for Calculating Likelihood Ratios. *Forensic Sci Int* **2019**, *301*, 426–434. <https://doi.org/10.1016/j.forsciint.2019.06.002>.
- (7) Kuczelinis, F.; Weis, P.; Bings, N. H. Forensic Comparison of PVC Tape Backings Using Time Resolved LA-ICP-MS Analysis. *Forensic Chemistry* **2019**, *12*, 33–41. <https://doi.org/10.1016/j.forc.2018.11.004>.
- (8) Hobbs, A. L.; Almirall, J. R. Trace Elemental Analysis of Automotive Paints by Laser Ablation-Inductively Coupled Plasma-Mass Spectrometry (LA-ICP-MS). *Anal Bioanal Chem* **2003**, *376*, 1265–1271. <https://doi.org/10.1007/s00216-003-1918-x>.
- (9) Deconinck, I.; Latkoczy, C.; Günther, D.; Govaert, F.; Vanhaecke, F. Capabilities of Laser Ablation - Inductively Coupled Plasma Mass Spectrometry for (Trace) Element Analysis of Car Paints for Forensic Purposes. *J Anal At Spectrom* **2006**, *21*, 279–287. <https://doi.org/10.1039/b514007b>.
- (10) Bezemer, K.; Woortmeijer, R.; Koeberg, M.; Schoenmakers, P.; van Asten, A. Multicomponent Characterization and Differentiation of Flash Bangers — Part I: Sample Collection and Visual Examination. *Forensic Sci Int* **2018**, *290*, 327–335. <https://doi.org/10.1016/j.forsciint.2018.06.011>.
- (11) Bezemer, K.; Woortmeijer, R.; Koeberg, M.; Wiarda, W.; Schoenmakers, P.; van Asten, A. Multicomponent Characterization and Differentiation of Flash Bangers — Part II: Elemental Profiling of Plastic Caps. *Forensic Sci Int* **2018**, *290*, 336–348. <https://doi.org/10.1016/j.forsciint.2018.06.012>.
- (12) Howa, J. D.; Lott, M. J.; Chesson, L. A.; Ehleringer, J. R. Isolation of Components of Plastic Explosives for Isotope Ratio Mass Spectrometry. *Forensic Chemistry* **2016**, *1*, 6–12. <https://doi.org/10.1016/j.forc.2016.07.003>.
- (13) Mehlretter, A. H.; Bradley, M. J.; Wright, D. M. Analysis and Discrimination of Electrical Tapes: Part II. Backings. *J Forensic Sci* **2011**, *56* (6), 1493–1504. <https://doi.org/10.1111/j.1556-4029.2011.01873.x>.
- (14) Hofmann, R. J.; Vlatkovic, M.; Wiesbrock, F. Fifty Years of Hydrosilylation in Polymer Science: A Review of Current Trends of Low-Cost Transition-Metal and Metal-Free Catalysts, Non-Thermally Triggered Hydrosilylation Reactions, and Industrial Applications. *Polymers (Basel)* **2017**, *9* (534). <https://doi.org/10.3390/polym9100534>.
- (15) Maharana, T.; Nath, N.; Pradhan, H. C.; Mantri, S.; Routaray, A.; Sutar, A. K. Polymer-Supported First-Row Transition Metal Schiff Base Complexes: Efficient Catalysts for Epoxidation of Alkenes. *React Funct Polym* **2022**, *171* (105142). <https://doi.org/10.1016/j.reactfunctpolym.2021.105142>.
- (16) Paine, M. R. L.; Barker, P. J.; Blanksby, S. J. Ambient Ionisation Mass Spectrometry for the Characterisation of Polymers and Polymer Additives: A Review. *Analytica Chimica Acta*. January 15, 2014, pp 70–82. <https://doi.org/10.1016/j.aca.2013.10.001>.
- (17) Ligon, S. C.; Liska, R.; Stampfl, J.; Gurr, M.; Mühlaupt, R. Polymers for 3D Printing and Customized Additive Manufacturing. *Chem Rev* **2017**, *117* (15), 10212–10290. <https://doi.org/10.1021/acs.chemrev.7b00074>.
- (18) Bonta, M.; Limbeck, A. Metal Analysis in Polymers Using Tandem LA-ICP-MS/LIBS: Eliminating Matrix Effects Using Multivariate Calibration. *J Anal At Spectrom* **2018**, *33*, 1631–1637. <https://doi.org/10.1039/c8ja00161h>.

- (19) Voss, M.; Nunes, M. A. G.; Corazza, G.; Flores, E. M. M.; Müller, E. I.; Dressler, V. L. A New Approach to Calibration and Determination of Selected Trace Elements in Food Contact Polymers by LA-ICP-MS. *Talanta* **2017**, *170*, 488–495. <https://doi.org/10.1016/j.talanta.2017.04.048>.
- (20) Almirall, J. R.; Trejos, T. Applications of LA-ICP-MS to Forensic Science. *Elements* **2016**, *12* (5), 335–340. <https://doi.org/10.2113/gselements.12.5.335>.
- (21) Trejos, T.; Montero, S.; Almirall, J. R. Analysis and Comparison of Glass Fragments by Laser Ablation Inductively Coupled Plasma Mass Spectrometry (LA-ICP-MS) and ICP-MS. *Anal Bioanal Chem* **2003**, *376*, 1255–1264. <https://doi.org/10.1007/s00216-003-1968-0>.
- (22) Hoffman, T.; Corzo, R.; Weis, P.; Pollock, E.; van Es, A.; Wiarda, W.; Stryjnik, A.; Dorn, H.; Heydon, A.; Hoise, E.; le Franc, S.; Huifang, X.; Pena, B.; Scholz, T.; Gonzalez, J.; Almirall, J. An Inter-Laboratory Evaluation of LA-ICP-MS Analysis of Glass and the Use of a Database for the Interpretation of Glass Evidence. *Forensic Chemistry* **2018**, *11*, 65–76. <https://doi.org/10.1016/j.forc.2018.10.001>.
- (23) Lambert, K.; Montero, S.; Akmeemana, A.; Corzo, R.; Gordon, G.; Haase, E.; Jiang, P.; Ovide, O.; Prasch, K.; Redman, K.; Scholz, T.; Trejos, T.; Webb, J.; Weis, P.; Wiarda, W.; Wilczek, S.; Xie, H.; Zoon, P.; Almirall, J. An Interlaboratory Study to Evaluate the Forensic Analysis and Interpretation of Glass Evidence. *Forensic Chemistry* **2022**, *27*, 100378. <https://doi.org/10.1016/j.forc.2021.100378>.
- (24) Simons, C.; Hanning, S.; Wegner, A.; Mans, C.; Janßen, A.; Kreyenschmidt, M. Comparative Study on the Homogeneity of Polymeric Calibration Materials Using LA-ICP-MS. *J Anal At Spectrom* **2008**, *23*, 1038–1041. <https://doi.org/10.1039/b719145f>.
- (25) Limbeck, A.; Bonta, M.; Nischkauer, W. Improvements in the Direct Analysis of Advanced Materials Using ICP-Based Measurement Techniques. *J Anal At Spectrom* **2017**, *32*, 212–232. <https://doi.org/10.1039/c6ja00335d>.
- (26) Yip, Y.; Lam, J. C.; Tong, W. Applications of Lead Isotope Ratio Measurements. *TrAC - Trends in Analytical Chemistry* **2008**, *27* (5). <https://doi.org/10.1016/j.trac.2008.02.011>.
- (27) Ray, S. J.; Hieftje, G. M. Mass Analyzers for Inductively Coupled Plasma Time-of-Flight Mass Spectrometry. *Journal of Analytical Atomic Spectrometry*. 2001, pp 1206–1216. <https://doi.org/10.1039/b102857j>.
- (28) Solyom, D. A.; Hieftje, G. M. Simultaneous or Scanning Data Acquisition? A Theoretical Comparison Relevant to Inductively Coupled Plasma Sector-Field Mass Spectrometers. *J Am Soc Mass Spectrom* **2003**, *14*, 227–235. [https://doi.org/10.1016/S1044-0305\(02\)00910-8](https://doi.org/10.1016/S1044-0305(02)00910-8).
- (29) Vázquez Peláez, M.; Costa-Fernández, J. M.; Sanz-Medel, A. Critical Comparison between Quadrupole and Time-of-Flight Inductively Coupled Plasma Mass Spectrometers for Isotope Ratio Measurements in Elemental Speciation. *J Anal At Spectrom* **2002**, *17*, 950–957. <https://doi.org/10.1039/b202748h>.
- (30) Scadding, C. J.; Watling, R. J.; Thomas, A. G. The Potential of Using Laser Ablation Inductively Coupled Plasma Time of Flight Mass Spectrometry (LA-ICP-TOF-MS) in the Forensic Analysis of Micro Debris. *Talanta* **2005**, *67*, 414–424. <https://doi.org/10.1016/j.talanta.2005.05.015>.
- (31) American Society for Testing and Materials ASTM. Standard Test Method for the Determination of Trace Elements in Soda-Lime Glass Fragments Using Laser Ablation Inductively Coupled Plasma Mass Spectrometry for Forensic Comparisons; 2012. <https://doi.org/10.1520/E2927-16E01>.
- (32) Harris, D. C. *Quantitative Chemical Analysis*, 9th ed.; W. H. Freeman & Company: New York, 2016.
- (33) El-Deftar, M. M.; Speers, N.; Eggins, S.; Foster, S.; Robertson, J.; Lennard, C. Assessment and Forensic Application of Laser-Induced Breakdown Spectroscopy (LIBS) for the Discrimination of Australian Window Glass. *Forensic Sci Int* **2014**, *241*, 46–54. <https://doi.org/10.1016/j.forsciint.2014.04.040>.
- (34) von Wuthenau, K.; Segelke, T.; Kuschnerit, A.; Fischer, M. Glass Authentication: Laser Ablation-Inductively Coupled Plasma Mass Spectrometry (LA-ICP-MS) for Origin Discrimination of Glass Bottles. *Talanta* **2021**, *235*. <https://doi.org/10.1016/j.talanta.2021.122686>.
- (35) Morgan, A. B.; Cogen, J. M.; Opperman, R. S.; Harris, J. D. The Effectiveness of Magnesium Carbonate-Based Flame Retardants for Poly (Ethylene-Co-Vinyl Acetate) and Poly (Ethylene-Co-Ethyl Acrylate). *Fire Mater* **2007**, *31* (6), 387–410. <https://doi.org/10.1002/fam.950>.
- (36) Dhumal, P. S.; Lokhande, K. D.; Bondarde, M. P.; Bhakare, M. A.; Some, S. Heat Resistive, Binder-Free 3d-Dough Composite as a Highly Potent Flame-Retardant. *J Appl Polym Sci* **2022**, *139* (20). <https://doi.org/10.1002/app.52146>.



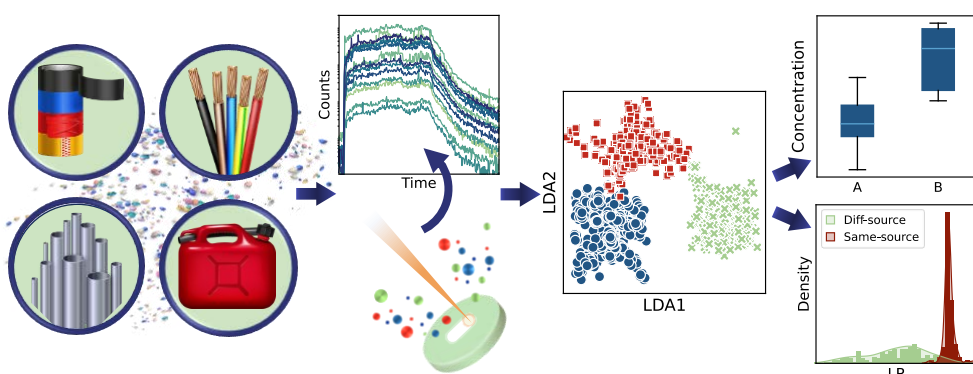
9

Evaluating the strength of evidence of elemental profiling of polymers with LA-ICP-MS

Mirjam de Bruin-Hoegée, Ruthmara Corzo, Peter Zoon, Peter Vergeer,
Jorien Schoorl, Marcel van der Schans, Daan Noort, Arian C. Van Asten,
Evaluating the strength of evidence of elemental profiling of polymers
with LA-ICP-MS. *Forensic Chemistry* **2024**, *38*, 100570.
DOI: [10.2139/ssrn.4748210](https://doi.org/10.2139/ssrn.4748210).

Abstract

Polymer evidence materials, such as tapes, are regularly recovered after violent crimes. LA-ICP-MS is a powerful technique for obtaining a forensic elemental profile. However, the lack of homogeneous polymer reference standards hampers database creation and reliably matching a sample to a specific source. Therefore, the current study aims to evaluate the strength of evidence of forensic polymer comparisons by applying a matrix-matched reference standard with known concentrations for elements of interest. Four datasets of tapes, electrical wires, tubing, and jerrycans were compiled using LA-ICP-MS. It was found that quantification with the new PVC standard or by simply using the response of one element as internal standard significantly reduced the between-run variation. For each class of polymeric materials, characteristic elements could be identified with PCA and LDA applied to data quantified with the PVC standard. Relatively high concentrations of Sb, Ba, Pb, and As were detected for tapes. Tubing contained elevated levels of Na, Si, and Ti, whereas wires were characterized by elevated levels of Ni, Sr, Mg, and Ca. To facilitate classification, elemental concentrations were found to be typical for specific colors. For forensic comparison, a score-based Bayesian likelihood ratio model and the t-test overlap method performed better than the feature-based model and 4-sigma criterion, in terms of rates of misleading evidence. Normalization to ^{13}C and quantification with the PVC standard with and without prior normalization to ^{13}C slightly reduced rates of misleading evidence. The t-test method showed an overall average false inclusion rate of only 0.45% and a false exclusion rate of 2.4%. For the score-based model, the average false inclusion and false exclusion rates were 3.4% and 3.0%, respectively. Finally, the feature-based model provided a false inclusion rate of 6.4% and a false exclusion rate of 6.5%. Maximum calibrated likelihood ratios of 0.014 to 1778 were found for the tape dataset. In conclusion, this study demonstrates that with the use of proper standards, quantitative elemental profiling with LA-ICP-MS is a promising and powerful tool for the forensic classification and comparison of polymer-based evidence materials.



9.1. Introduction

Establishing the origin of physical evidence found on a crime scene can provide valuable insights for forensic investigations. Elemental impurity profiling has the potential to provide a connection between (trace) materials discovered at separate locations that share a common origin. In addition, items from seemingly unrelated incidents can be matched through forensic databases.¹ The chemical analysis of trace materials, such as polymers, glass, and fibers, is frequently reported by forensic institutes in court cases.² Polymer-based evidence material is often created during violent crimes, including kidnapping (to restrain a victim) and the use of improvised explosive devices (as a container of the energetic material or as part of activation and timer devices).³ However, plastics can also constitute important evidence material when it is simply used to carry, join, or conceal items or when it is part of a tool, weapon, instrument, or transportation vehicle. This is simply the result of the abundant use of man-made and natural polymers in modern society. Global plastic production reached 368 million tons a year in 2019.⁴ Plastics are found everywhere and therefore also in crime scenes.

Electrical wires, tapes, and tubing often consist of polyvinyl chloride (PVC), while jerrycans and bags are primarily made from polyethylene (PE). The type of plastic is mainly determined by Fourier transform-infrared spectroscopy (FT-IR) or pyrolysis-gas chromatography-mass spectrometry (Py-GC-MS).⁵ In addition to the organic (polymeric) components, characteristic inorganic additives and impurities are present originating from the raw materials or production process. To produce PVC, substantial amounts of aluminum and titanium-based catalysts can be used.⁶ The most common non-toxic thermal stabilizer is a calcium-zinc additive.⁷ Additionally, pigments and dyes are added to give the final product a specific color. A typical pigment is titanium dioxide which induces opacity and whiteness.⁸ Other inorganic pigments are chrome green and copper blue. The organic pigment carbon black is most applied as UV-stabilizer and to induce a dark color.^{6,8} All these inorganic additives potentially provide characteristic information for forensic attribution studies when elemental analysis techniques are applied.

A powerful technique for chemical profiling of microtraces is laser ablation-inductively coupled plasma-mass spectrometry (LA-ICP-MS). This analytical method is sensitive, selective, minimally destructive, and it requires little sample preparation.³ The application of matrix-matched reference standards facilitates accurate quantitative measurements of elemental levels. This can be used to create a characteristic elemental fingerprint of evidence materials enabling source level comparisons in forensic investigations. This approach was successfully implemented for glass comparisons in casework by the Netherlands Forensic Institute.^{9,10} As part of the validation process,

interlaboratory comparison studies demonstrated good agreement with variation among laboratories below 10% relative standard deviation (RSD).^{11,12} Although an interlaboratory study of tapes correctly identified associated samples, further improvement of element quantitation in plastic matrices is needed to enable shared databases and profile comparisons from different laboratories using different instrumental settings and methods.⁵

There are various approaches to correct for instrument variation and improve quantification. First normalization to one element, such as Si is predominantly used in glass research.¹² In the same manner, normalization to the C response is often applied to polymers.^{13,14} However, other abundant elements like Ca, Ti, Pb, or a combination of element ratios can also be used for normalization.^{15–17} Furthermore, spectral overlay comparisons or correction for the total response accounted for variability within replicate measurements.^{5,14,18,19} Also, logarithmic transformations were applied to improve robustness.^{15,17,20–22} Recently, PVC, PE, and PS standards have been introduced that exhibit improved homogeneity and contain more elements than polymer standards available thus far.²³ Quantification using these standards reduced between run variation and increased the discrimination power between different classes of objects of forensic relevance.

Several approaches have been proposed to differentiate or associate unknown glass or polymer fragments with potential reference sources. Traditionally, match criteria have been used to compare elemental profiles of two or more traces. Examples of this are the standard deviation overlap method,^{5,10,24,25} Student's t-test with or without Bonferroni correction,^{14,24,26} Hotelling's T²-test,^{20,25} and Tukey's honestly significant difference (HSD) test.^{10,26} However, a drawback of these methods is the 'fall off the cliff' effect, where slight differences in the measured elemental profile can result in entirely opposing outcomes.²⁷ In addition, the rarity of the profile is not considered. For these reasons, forensic experts typically prefer the Bayesian approach which combines a measure of (dis)similarity and rarity in the form of a likelihood ratio (LR) to indicate the evidential strength.²⁸ Aitken and Lucy developed a feature-based method, often referred to as two-level model (TLM).^{15,20,27,29,30} If the between- source variability follows a Gaussian distribution, this is defined as a multivariate normal (MVN) model and when complex distributions need to be fitted with a kernel density estimate, the term multivariate kernel (MVK) model is used. Alternatively, robust score-based models have been applied to trace evidence.²⁹ An advantage is the robust application of this model to smaller reference datasets, but typically with the loss of information often resulting in lower LR values. However, in practice feature-based methods require feature selection, which results in some loss of information as well, whereas score-based models can often be based on all features.³¹ Finally, machine learning methods

that have been applied to glass evidence are principal component analysis (PCA),^{13,17,19} linear discriminant analysis (LDA), support vector machine (SVM), and random forest (RF).^{22,32}

In the present study several data pre-processing and statistical methods are explored to improve classification and comparison of polymer evidence materials of forensic relevance. Four datasets of tapes, electrical wires, tubing, and jerrycans with 220 forensically relevant polymer objects originating from 175 sources in total were analyzed by LA-ICP-MS. Robust quantitative elemental profiles were obtained through several methods: the application of one element as internal standard, the use of a certified glass reference standard, or the use of novel polymer standards.²³ The effect of these normalization and quantification methods was assessed in the subsequent classification and comparison studies. Additionally, the within-sample, within-batch, and between-run variability was assessed. Next, relationships between the elemental profiles of tapes, electrical wires, tubing, and jerrycans and polymer characteristics were investigated. Lastly, various comparison methods were evaluated. The performance of the 4-sigma overlap method and the t-test match criterion methods were compared to the feature-based MVK and score-based Bayesian models. The current study demonstrates the potential of measuring characteristic elemental profiles of polymer (trace) evidence materials with LA-ICP-MS to facilitate forensic classifications and comparisons in criminal investigations.

9.2. Experimental

9.2.1. Chemicals and materials

Polyvinyl chloride (PVC), low-density polyethylene (PE), and polystyrene (PS) standards, containing low, middle, or high elemental concentrations, were prepared at TNO (Rijswijk, The Netherlands). The production method is described in more detail by de Bruin-Hoegée et al.²³ An overview of the applied concentrations of the elements of interest, Na, Mg, Al, Si, K, Ca, Ti, Mn, Fe, Co, Ni, Cu, Ga, As, Sr, Nb, Pd, Sn, Sb, Ba, and Pb, is given in Section S1 in the Supplementary data. Standard Reference Material® (SRM) 612 was obtained from the National Institute of Standards and Technology (NIST, Gaithersburg).³³ A total of 220 forensically relevant polymer objects were obtained from 175 sources as shown in Section S2 of the Supplementary data. Tapes, tubing, and wires mainly consisted of unplasticized and plasticized PVC. In contrast, jerrycans were made from high-density PE (HDPE), low-density PE (LDPE), polypropylene (PP), or polyoxymethylene (POM).

9.2.2. Instrumentation

Plastic fragments of approximately 5x5 mm were analyzed by a 213 nm laser (Applied Spectra, J200) coupled to an inductively coupled plasma mass spectrometer (Thermo, iCAPQ). The torch alignment and flows were optimized based on the lowest amount of multiple charged elements and oxides. All samples were scanned for the presence of 23 elements: ^{13}C , ^{23}Na , ^{25}Mg , ^{27}Al , ^{29}Si , ^{37}Cl , ^{39}K , ^{44}Ca , ^{47}Ti , ^{55}Mn , ^{57}Fe , ^{59}Co , ^{60}Ni , ^{63}Cu , ^{65}Cu , ^{69}Ga , ^{75}As , ^{88}Sr , ^{93}Nb , ^{106}Pd , ^{118}Sn , ^{121}Sb , ^{138}Ba , ^{206}Pb , ^{207}Pb , and ^{208}Pb . The stable isotopes were selected based on minimal polyatomic interferences and maximum abundance. For Ca, Ti, Ni, Cu, Ga, Pd, Sb, Ba, and Pb, the best isotope was selected on the basis of the response, the relative standard deviation of three repetitions, and the relative standard deviation of the response of the three high concentration polymer standards. Each replicate consisted of a 45 s spot ablation followed by a 55 s gas blank. Prior to analysis, a daily performance check using NIST SRM 612 was performed. Also, a mid-concentration PVC standard was analyzed daily to monitor the quality of the system. For quantification of the forensic objects, NIST SRM 612 and three batches of the high concentration standards of PVC, PE, and PS were measured in triplicate before each analysis run. The polymer objects from different sources were analyzed in quadruplicate on two different days at least two weeks apart, resulting in a total of eight replicates for each part. The data was baseline and outlier-corrected by applying the Grubbs' test for outliers (significance, $\alpha=0.0005$) using R 4.3.0 with RStudio 2023.03.1.³⁴ The final LA-ICP-MS method used in this study is shown in Table 9.1.

Table 9.1. LA-ICP-MS parameters for elemental analysis of polymer materials.

Setting	Value
Helium carrier gas flow	0.9 L/min
Argon carrier gas flow	0.4 L/min
Argon nebulizer gas flow	0.2 L/min
Argon auxiliary gas flows	0.8 L/min
ICP RF power	1500 W
Line length	0.7 mm
Line scan speed	15 $\mu\text{m}/\text{s}$
Ablation time	45 s
Laser energy	2.82 J/cm ² (85%)
Laser frequency	10 Hz
Spot size	100 μm

To characterize the polymer type of forensically relevant objects, a Bruker Alpha II compact FT-IR spectrometer with platinum ATR module was applied. Opus (Bruker) software was used, and the spectra were characterized using the Bruker optics ATR-polymer library.

In addition, standard fragments, of approximately 5x5 mm, were analyzed with micro X-ray fluorescence (μ -XRF) using an M4 Tornado μ -XRF spectrometer (Bruker, Billerica, MA), equipped with two silicon drift detectors and a rhodium X-ray source. The following elements were measured: Al, Si, K, Ca, Ti, Cr, Mn, Fe, Co, Ni, Cu, Ga, As, Sr, Nb, Ba, and Pb. Due to the low response, K was excluded from all samples. For the same reason, Pb was not included in the measurements of the PS standards and Al in the PE and PVC standards. Additionally, Si, Ni, and Co showed a low response in the PVC standards and were removed, resulting in fifteen elements for the PE and PS standards and twelve elements for the PVC standard. Before analysis, the μ -XRF had to pass a daily performance check using the NIST SRM 1831. Also, a weekly energy calibration was conducted using Zr.³⁵ The method parameters used in this study are shown in Table 9.2.

Table 9.2. μ -XRF parameters for elemental analysis of polymer materials.

Setting	Value
X-Ray beam energy	50 kV
Current	200 μ A
Spot size	20 μ m
Vacuum	2000 Pa
Acquisition time	60 s live
Replicates	32

9.2.3. Data analysis

The data was further processed using Python 3.9.12 and LIR 0.1.27.³⁶ All LA-ICP-MS datasets of tapes, electrical wires, tubing, and jerrycans and python scripts are freely available and published under a GNU General Public License.³⁷ Table 9.3 gives an overview of the design of the experiments for each dataset of tapes, tubing, wires, and jerrycans. Since one source could contain multiple colors and batches, the number of parts are higher than the number of sources. It is important to note that the jerrycan parts were also evaluated separately in this study. It is possible that the individual parts were produced from the same polymer batch, but due to variation in the appearance and type of polymer measured with FT-IR it is assumed that these parts have different origins.

Table 9.3. Design of experiments with total number of measurements for tapes, tubing, wires, and jerrycans.

Object	Sources	Parts	N	Days	Measurements
Tapes	82	93	4	2	720*
Tubing	36	39	4	2	312
Wires	44	49	4	2	360†
Jerrycans	13	39	4	2	312

*The within-batch evaluation was only performed on one day, so 6 parts were measured 4 times in total. †Eight parts were measured on one day only.

9.2.3.1. *Data pre-processing*

The four datasets shown in Table 9.3 were further evaluated, including the data of either nine or eighteen elements (features). Highly correlated elements and elements present at levels below 1000 counts/s were excluded, which will be discussed in more detail in Section 3.2.1. The response was normalized by the elemental response of ^{13}C , ^{27}Al , or ^{44}Ca . In addition, the (normalized) response was quantified and converted to mg/kg values by using the NIST SRM 612, PVC, or PE standard. It should be noted that if the standards have C, Al, or Ca levels that are significantly different from that of the samples the quantitation with prior normalization will have a large systematic error. Afterwards, a logarithmic transformation (\log_{10}) was applied to bring the data closer to normality and reduce stochastic measurement fluctuations.³⁸ Before applying PCA, LDA, and the score-based model, the data was standardized using the Standardscaler function, which subtracts the mean and scales the data to unit variance.³⁹

9.2.3.2. *Variability*

The within-sample variation was measured based on four replicates of a forensic object analyzed at the same day. Subsequently, the between-run variation was calculated by $|(\text{new} - \text{old})/\text{old}| * 100\%$ of the responses on two separate days, in a similar way as previously reported.²³ Only for the tapes, three batches of the same supplier and production type were measured to assess the within-batch variability.

9.2.3.3. *Classification*

PCA and LDA were applied to reduce the dimensionality of the data and visually identify characteristic elements which can potentially discriminate between various types of forensic objects. The robustness of PCA was assessed by leave-one-out validation. In addition, LDA was applied to maximize discrimination between the groups and highlight characterizing elements. The quality of LDA was evaluated by leave-one-out cross validation.

9.2.3.4. Comparison

To evaluate whether a sample originates from a known source or from an arbitrary background source, four comparison models were evaluated. These models were performed separately on each dataset of tapes, tubing, wires, and jerrycans. First, ASTM E2927 suggests a modified match criterion of four standard deviations (stdv) for glass analysis.⁴⁰ This criterion for glass was also applied to polymers in this study, since no guidelines for LA-ICP-MS comparisons of polymers exist yet. The modified confidence interval of the known sample is defined as the average ± 4 stdv for each element. If the standard deviation is less than 3% of the mean, then 3% of the mean is used instead of the standard deviation. Subsequently, the average of the questioned sample is calculated and compared to the comparison interval of the known sample. If there is an overlap for all measured elements, the known and questioned sample are assumed to originate from the same source. If at least one element does not match, the samples are distinguishable and it is concluded that they are from different sources. Second, a similar approach was tested by applying a t-test with Bonferroni correction.²⁴ A Welch's t-test was utilized in this study which considers the variance of both the known and questioned sample.

Additionally, two likelihood ratio models were constructed, based on the two-level MVK feature-based method,^{20,38} and a score-based method.²⁹ The LR is defined as the probability of the evidence given H_1 divided by the probability of the evidence given H_2 . The prosecutor's hypothesis (H_1) for comparison problems is the proposition that two samples originate from the same source, while the defense hypothesis (H_2) is expressed as two samples having different sources. Section S3 of the Supplementary data elaborates on the equations used for the MVK feature-based model that was applied as the third comparison method. Due to deviations of the data from the modelling assumptions underpinning the two-level model, the output cannot be interpreted as an LR. In order to convert the output to LR values, the output was calibrated with the Pool Adjacent Violators (PAV) algorithm.¹⁵ Bounds were imposed by applying Laplace-rule, to prevent extrapolation problems. A double 10-fold cross validation method was applied to obtain calibrated LR values, in a similar way as described by Corzo et al.¹⁵ Lastly, the score-based model was calculated based on a python notebook published by Leegwater et al.⁴¹ For this model the mean of four random replicates was calculated, which resulted in two means for each sample. The data was split into a training, test, and validation set, which consisted of 60%, 20%, and 20% of the data, respectively. Subsequently, a score was assigned to each comparison using the dissimilarity measure Manhattan distance or the machine learning model SVM. Based on the H_1 and H_2 histograms of the scores, two continuous functions were generated that convert scores to LR values. A generative approach with KDE or a discriminative approach with logistic regression were fitted to the score sets.⁴¹ The obtained LR values were also calibrated

with the PAV algorithm. Additionally, to prevent extrapolation problems, the LR range was limited by using empirical lower and upper bounds (ELUB).⁴²

The performance of the four models was characterized by the rates of misleading evidence. A same-source comparison was applied by comparing four random replicates of a source to four other replicates of the same source (ground truth: samples originate from the same source). For the 4-sigma method, t-test, and score-based model, the mean of four replicates was used for the comparison calculations. In contrast, the feature-based approach evaluated the repetitions separately, by comparing the first 3 replicates of each sample to the last 3 replicates of the same sample. The calculation was performed for the validation dataset, to evaluate the false exclusion rate (false negatives). In addition, the false inclusion (false positives) rate was assessed by applying a different-source comparison. Eight replicates of a source were compared to eight replicates of another source (assumption: samples originate from different sources). Again, the mean was used for the 4-sigma method, t-test, and score-based model, while the feature-based model compared the first three replicates of each sample to the last three replicates of all different samples. For the 4-sigma criterion and t-test, each element was evaluated separately, increasing the number of comparisons by multiplication with the number of elements.

9.3. Results & discussion

9.3.1. LA-ICP-MS method optimization

Ideally, the settings of the LA-ICP-MS are selected to yield the highest response and the lowest relative standard deviation within a sample and within batches. Section S4 of the Supplementary data visualizes the effect of the laser energy and spot size on the sensitivity and measurement variation of mid concentration standards of PVC, PE, and PS. The optimum results for spot measurements were obtained for a combination of 2.4 J/cm² laser energy with 100 µm spot size, or 2.8 J/cm² laser energy with 80 µm or 100 µm spot size. The same settings were varied for line ablations with various lengths and laser speeds. Overall, a relatively low speed of 0.015 mm/s with a line length of 0.7 mm gave better performance compared to a speed of 0.1 mm/s with 3-line ablations over a length of 1.4 mm. The best performance was found for 0.7 mm (0.015 mm/s) line ablations with 100 µm spot size and 2.82 J/cm² laser energy.

The homogeneity of the PVC, PE, and PS standards determined by LA-ICP-MS and µ-XRF was similar to the results obtained by LA-ICP-TOF-MS measurements in previous research.²³ PVC and PE standards show the most stable elemental response with a maximum relative variation of 17%. The PS standard shows poor homogeneity; therefore this standard was not used for quantification in this study. It is common

practice for forensic LA-ICP-MS glass analysis to use a single point external calibration standard.⁴³ Since the polymer standards show a linear response for various concentrations, the forensic objects were only quantified with the high concentration standards to limit the total number of measurements. Finally, the signal drift was in the same order of magnitude as the within-sample and within-batch variation, so no correction for drift was taken into account when analyzing the data, and the mean values were used as reference for the remaining part of this paper. More details on the applied method and the performance of the polymer standards are available in Section S5 of the Supplementary data.

9.3.2. Data pre-processing

9.3.2.1. Element selection

In tubing and jerrycan samples, ⁵⁹Co, and ¹⁰⁶Pd were present at levels below 200 counts/s. Because of the low responses, these elements were not included in the elemental profile. Multiple isotopes were analyzed for Cu and Pb. The isotopes ⁶³Cu and ²⁰⁸Pb were selected based on a high response, low relative standard deviation of three repetitions, and low relative standard deviation of the response. Additionally, the elements ⁶⁹Ga/¹³⁸Ba showed high within and between correlation in all cases, as illustrated for tubing in Figure 9.1. This is likely due to doubly charged ¹³⁸Ba. Since BaSO₄ is a common filler in polymers and ¹³⁸Ba was more homogenously distributed, ⁶⁹Ga was removed, which resulted in a profile of a total of 18 elements (²³Na, ²⁵Mg, ²⁷Al, ²⁹Si, ³⁹K, ⁴⁴Ca, ⁴⁷Ti, ⁵⁵Mn, ⁵⁷Fe, ⁶⁰Ni, ⁶³Cu, ⁷⁵As, ⁸⁸Sr, ⁹³Nb, ¹¹⁸Sn, ¹²¹Sb, ¹³⁸Ba, ²⁰⁸Pb). The correlation plots for the other objects are shown in Section S6 of the Supplementary data. Some correlation was object specific, which is expected based on the incorporation of different raw materials. For example, for the jerrycans a high correlation was found for ²⁹Si and ²⁵Mg, which may originate from magnesium silicate (talc), which is widely used as a polymer filler. For wires an increased correlation was visible between ⁵⁵Mn and ⁸⁸Sr. It was decided to keep the same group of elements for all types of objects, but in further research these correlated elements could be discarded for the data of jerrycans and wires, respectively. Additionally, a smaller dataset was constructed consisting of elements with the highest ratio of between/within RSD. The following nine isotopes were included: ²⁵Mg, ²⁷Al, ²⁹Si, ⁴⁴Ca, ⁵⁷Fe, ⁶³Cu, ⁷⁵As, ¹¹⁸Sn, and ²⁰⁸Pb.

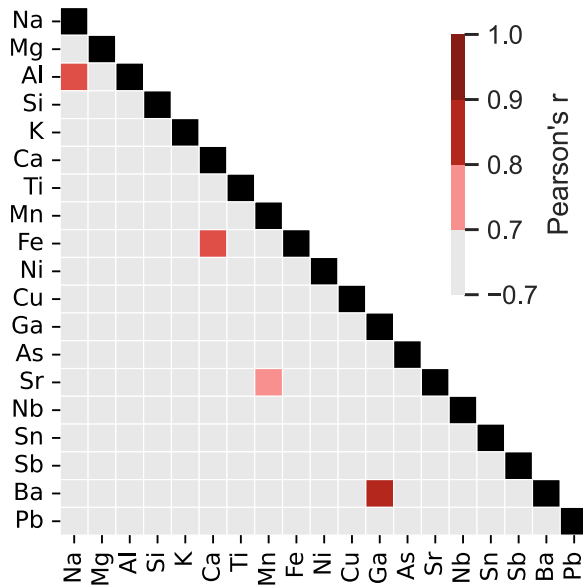


Figure 9.1. Pearson's correlation coefficients of the elements detected by LA-ICP-MS in the PVC tubing.

9.3.2.2. Variability

Various normalization methods were evaluated to reduce variation between runs and improve elemental quantification of tapes, wires, jerrycans, and tubing. The data was processed without normalization, with quantification using the NIST SRM 612 glass, and with quantification using the PVC and PE standards. In addition, the effect of normalization by using abundantly present elements, such as C, Ca, and Al, as internal standard (IS) was investigated. Calcium and aluminum likely originate from commonly applied thermal stabilizers and catalysts.⁶ Correction using the summed responses for all elements was not included since the selection of elements and isotopes often varies between measurements and laboratories. It is worth mentioning that if normalization to ¹³C is applied, comparison with other instruments, such as time-of-flight mass spectrometers, would be hampered by its reduced sensitivity for low-mass elements.²³

The within-sample variation averaged over all samples and elements and without normalization and quantification with a standard was 12%, 19%, 21%, and 34% for tape, wire, tubing, and jerrycan parts, respectively. Overall, Ca, Sr, Mg, Fe, Mn, Al, and Si were most homogeneously distributed (on average 11% - 15% variation). Quantification with reference standards or normalization to C, Ca, and Al did not substantially reduce the within-sample variation. Decreasing the number of elements to 9 elements with the lowest within-variation for each object, however, did reduce the variation, with a significant improvement to 23% for jerrycans (²⁵Mg, ²⁷Al, ²⁹Si, ³⁹K, ⁴⁴Ca, ⁴⁷Ti, ⁵⁵Mn, ⁵⁷Fe,

and ^{88}Sr were included). For three suppliers of tapes, three batches of the same type were evaluated to assess the within-batch variation. Without correction, an average RSD of 15% was found. Prior normalization by using Al as an internal standard resulted in a slightly lower RSD of 12%. Table 9.4 shows the between-run variation for tapes, wires, jerrycans, and tubing with various normalization and quantification methods. Overall, normalization to one element improved the repeatability, with significant improvement for wires and jerrycans. Quantification with the PVC standard resulted in slightly better reproducibility than quantification with the NIST SRM 612 glass and PE standard. Only for tapes, the lowest between-run variation was obtained either without quantification or with quantification using NIST SRM 612. Since the results indicate that normalization is beneficial for reproducible responses, normalization to carbon, and quantification with NIST SRM 612 and PVC standard will be evaluated in the subsequent sections.

Table 9.4. Mean between-run variation of 18 elements: Na, Mg, Al, Si, K, Ca, Ti, Mn, Fe, Ni, Cu, As, Sr, Nb, Sn, Sb, Ba, and Pb, measured in tapes, wires, jerrycans, and tubing by LA-ICP-MS. Data was processed as such or by quantification with the NIST SRM 612 glass or PVC standard, with or without normalization to C, Ca, or Al.

Quantification	IS	Tapes	Wires	Jerrycans	Tubing
Without	-	11	123	118	12
	C	9	25	30	12
	Ca	15	26	22	12
	Al	10	17	18	13
NIST SRM 612	-	24	43	37	12*
	C	20	32	48	14*
	Ca	10	37	31	11*
	Al	9	22	33	12*
PVC standard	-	26	36	27	16
	C	22	19	26	12
	Ca	21	19	27	12
	Al	59	21	34	12
PE standard	-	61	36	46	20
	C	9	38	30	15
	Ca	10	21	23	13
	Al	14	42	53	12

*A limited sample set was evaluated, because the NIST SRM 612 was not measured for all samples.

9.3.3. Classification

9.3.3.1. Forensic objects

If an unknown type of polymer evidence material is secured from a crime scene, it is important to classify the kind of product. Especially, when dealing with small traces or heavily damaged materials, such classification may visually be laborious. Unsupervised and supervised multivariate techniques can provide information and some simple rules of thumb can be derived from this information. Figure 9.2 shows the PCA score plot,

with the two first principal components (PCs), based on the elemental concentrations of the forensic objects. The jerrycans were not included, because they could be distinguished from the other objects based on their polymer type. In addition, the jerrycans were characterized by a general absence (low response) of elements. Therefore, only the tapes, tubing, and wires made from PVC were included in the PCA model. The plot shows grouping of the samples according to their type. The first PC accounts for 35% of the variance and the second PC for 15% of the variance. Similar discrimination was obtained when applying other normalization methods. Section S7 of the Supplementary data elaborates on the evaluation of the robustness of the PCA by leave-one-out validation. The model showed excellent robustness, since leaving out one sample resulted in comparable variance. Figure 9.2B shows that multiple elements contribute to the grouping of the objects. The tapes contain a remarkably high concentration of Sb and Ba. Also, the level of Pb and As was higher in tapes compared to other objects, but it is important to note that this concentration was still relatively low. The tubing exhibits elevated levels of Na, Si, and Ti. Lastly, the wires are characterized by the significant presence of Ni, Fe, Sr, and Mn.

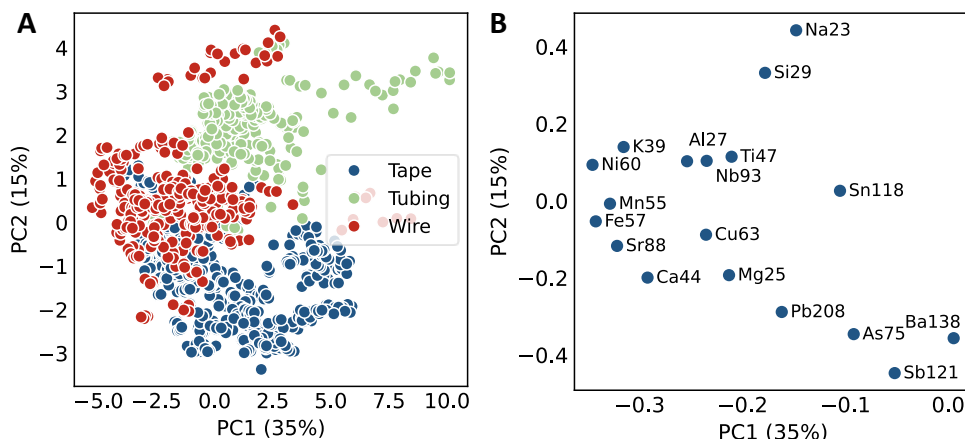


Figure 9.2. A) PCA-score plot based on the elemental concentrations of tapes, tubing, and wires measured by LA-ICP-MS. Responses are quantified with the PVC standard and log10 transformed. B) Corresponding PCA loadings with characterizing elements.

In addition, LDA was applied to maximize discrimination between tapes, tubing, and wires (Figure 9.3A). As expected, grouping of the objects was more distinct compared to PCA but some partial overlap between the tapes and wires remained. Section S8 of the Supplementary data elaborates on the evaluation of the quality of the LDA by leave-one-out cross validation. The predicted observations deviated on average 23% RSD (median 2.6% RSD) for the first dimension and 34% (median 5.2% RSD) for the second dimension and similar grouping of the samples was observed in the training and test data. The difference was mainly attributed to misclassification of a transparent wire.

Figure 9.3B shows the LDA loadings with characterizing elements. Similar elements contribute to discrimination of objects as visible in the PCA plot, although the significance of several elements was more clearly highlighted. For example, the tapes were distinctly characterized by the presence of Ba, the wires by elevated levels of Ni and Sr, and the tubing by a high concentration of Na. Boxplots with the median concentrations grouped by each object are shown in Section S9 of the Supplementary data. In summary, PCA is a powerful tool for exploring the features that are most important in explaining the variance in a dataset, while LDA provides the opportunity to understand the features that maximize discrimination between objects.

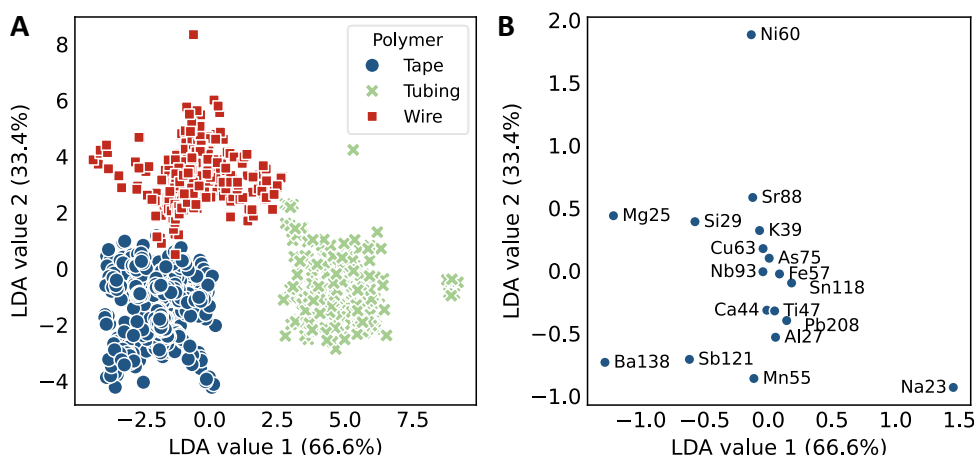


Figure 9.3. A) LDA-score plot based on the elemental concentrations of tapes, tubing, and wires measured by LA-ICP-MS. Responses are quantified with the PVC standard and log₁₀ transformed. B) Corresponding LDA loadings with characterizing elements.

9.3.3.2. Colors

In some forensic investigations, such as post-explosion cases, it could be difficult to establish the color of an object.¹³ In this case, LA-ICP-MS analysis might provide information about the inorganic pigments that are present, to give an indication of the original appearance of the sample. At the same time, different colors can provide variability in a product class. So, to classify the object type (existing in different colors), it could be useful to remove elements that strongly correlate to color. Figure 9.4 shows the median elemental concentrations in forensic objects grouped by each color. The dimensions of the box indicate the first and the third quartile of the data. The whiskers are presented for the furthest data points lying within 1.5 times the inter-quartile range. Interestingly, grey and yellow objects contained a high concentration of Na. Although this effect was visible for all types of objects, it was particularly visible in tubing, which were mostly yellow and grey. Therefore, it could also be an additive specifically used in the production process of PVC tubing. As expected, white polymer

materials contain relatively high levels of Ti, which likely originates from titanium dioxide, a typical pigment that induces opacity and whiteness.⁸ In addition, brown products were characterized by the presence of Fe. A plausible source of this element is the pigment Fe₂O₃. Finally, it is highly probable that the pigment copper phthalocyanine is present in blue and green samples, since high levels of Cu were observed. Boxplots with the concentrations of all analyzed elements grouped by color are presented in Section S9 of the Supplementary data.

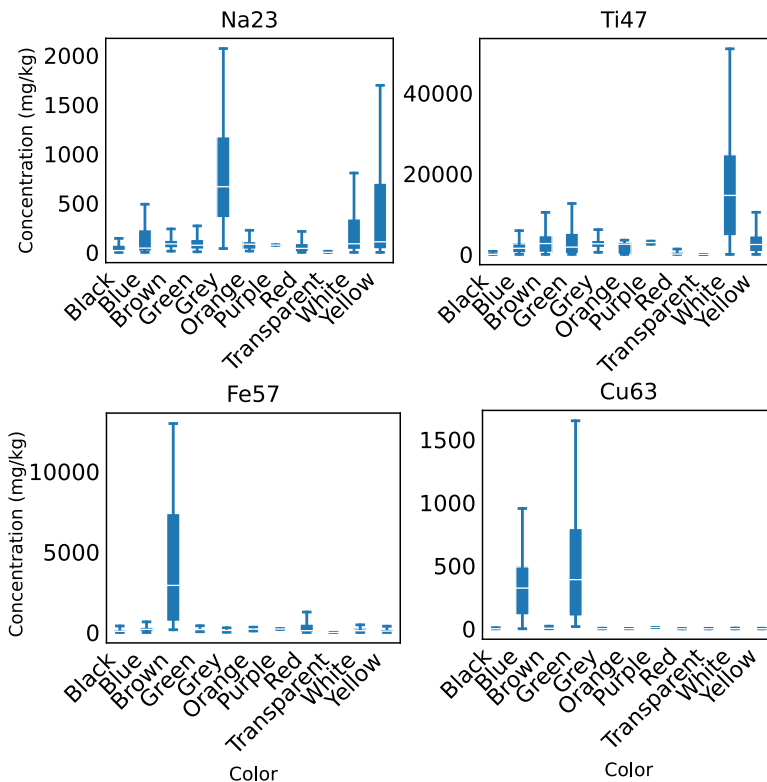


Figure 9.4. Boxplot of concentrations of Na, Ti, Fe, and Cu in forensic objects grouped by color. Elemental concentrations are shown based on quantification with the PVC standard.

9.3.4. Comparison

After classification it is important to establish the origin of a piece of evidence. Various statistical comparison methods that can be used to associate a sample to a specific source were evaluated in this study. A measure of the performance of the models is the rate of misleading evidence. Ideally, no false inclusions or exclusions occur although it is not expected that these rates reduce to zero due to the measurement and modelling uncertainties associated with LA-ICP-MS elemental profiling. Table 9.5 shows the error rates for the tapes, tubing, wires, and jerrycans database using the 4-sigma criterion, t-

test, MVK feature-based model, and SVM score-based model. The rates were evaluated for the validation data, including 18 elements. For the score-based model, the results are shown for the machine learning model SVM with KDE. This LR system was selected based on the test data with the maximum LR values for known matches and lowest rates of misleading evidence. As can be seen from the table, the match criteria models resulted in very low false inclusion rates. The false exclusion rates were considerably higher for the 4s-model, especially for the wires and jerrycans. The low rate of false inclusions is likely due to the strict ASTM criterion which requires that all elements are matching. From a forensic point of view, a false inclusion can ultimately lead to the conviction of an innocent person. Therefore, false inclusions should especially be avoided. The false inclusion rates were dominated by profiles including elements with a relatively high within-sample variation and a low between-sample variation, such as As, K, Sb, Sn, Si, and Ni. The false exclusions for the feature-based model were in the same range as the values for the t-test, except for the tubing where higher false exclusion rates were observed. Overall, the t-test and score-based model provided the lowest rates of misleading evidence. The t-test match criterion model showed an overall average false inclusion rate of only 0.45% and a false exclusion rate of 2.4%. Quantification with the PVC standard slightly improved the performance. The rates for the score-based likelihood ratio model were somewhat higher, with an overall average false inclusion rate of 3.4% and a false exclusion rate of 3.0%. It is important to bear in mind that the random sample selection slightly influences the performance of the models. This is mainly due to the variation between measurements performed on two different days. If the mean of two samples from day 1 and two samples of day 2 was compared with two other samples from day 1 and two other samples from day 2, the performance was improved. For example, the percentage of false exclusion and false inclusion of the tubing, quantified with the PVC standard, would reduce from 13% and 16% to 5.7% and 14%, respectively. Interestingly, the various normalization and quantification methods provided very similar results. In most cases, quantification with the glass standard resulted in slightly worse performance and normalization to ^{13}C with or without subsequent quantification with the PVC standard showed the best performance. For datasets with only 9 elements, the rates of false exclusions slightly decreased, and the rates of false inclusions increased (Section S10 of the Supplementary data).

Table 9.5. Rates of misleading evidence for tapes, tubing, wires, and jerrycans validation data including 18 elements, calculated using the modified 4-sigma criterion, the t-test with Bonferroni correction, MKV feature-based model, and SVM score-based model.

Database	Normalization and quantification	False exclusion (%)				False inclusion (%)			
		4s	t-test	Feature	Score	4s	t-test	Feature	Score
Tapes	Without	1.1	4.6	4.6	0	1.2	0.080	1.8	0.65
	¹³ C	5.7	2.3	2.3	0	0.16	0.094	4.8	0.65
	Glass standard	40	2.3	4.6	0	0.040	0.027	5.4	0.65
	PVC standard	2.3	3.4	4.6	0	0.24	0.013	6.0	0.65
	¹³ C, PVC standard	2.3	1.1	3.4	0	0.24	0	5.1	0.65
Tubing	Without	5.1	0	17	13	11	0.17	14	7.1
	¹³ C	5.1	5.1	15	0	1.9	0.20	5.3	11
	Glass standard*	41	2.6	16	0	0.20	0.60	30	7.1
	PVC standard	2.6	2.6	13	13	8.1	0.34	16	3.6
	¹³ C, PVC standard	2.6	2.6	18	0	2.3	0.20	5.2	11
Wires	Without	2.0	0	6.1	10	0.60	0.17	4.2	0
	¹³ C	16	2.0	2.0	0	0.13	0	2.1	0
	Glass standard	20	2.0	6.1	0	0.17	0.13	5.2	0
	PVC standard	6.1	0	4.1	10	2.5	0.085	4.2	0
	¹³ C, PVC standard	10	2.0	2.0	0	0.26	0	2.1	0
Jerrycans	Without	21	2.6	3.2	0	2.0	1.3	4.4	0
	¹³ C	13	5.1	0	0	1.4	2.0	2.2	7.1
	Glass standard	13	2.6	2.9	0	14	0.88	2.0	3.6
	PVC standard	15	2.6	3.7	0	1.2	0.61	2.6	7.1
	¹³ C, PVC standard	18	2.6	6.5	13	1.6	2.2	4.4	7.1
Overall average		12	2.4	6.8	3.0	2.5	0.45	6.4	3.4

*Limited number of repetitions for tubing data quantified with the glass standard.

Figure 9.5 shows the likelihood ratios obtained by the feature-based MVK model for different-source and same-source comparisons. Both uncalibrated and calibrated likelihood ratios are displayed. The responses were normalized to ¹³C and subsequently quantified with the PVC standard. Since the database size was limited, unreasonably large likelihood ratios were found for the uncalibrated LRs. Similar ranges were found for models with other normalization procedures or without quantification. Calibration with the PAV algorithm, including Laplace-rule, limited the LR output on the basis of the available elemental profile data. The calibrated and validated LRs for various normalization and quantification methods are shown in Table 9.6. Two performance measures are provided as an indicator of the validity and reliability of the likelihood-ratio system. The log-likelihood-ratio cost (Clrr) is a measure of the accuracy of the model, where a lower value indicates better performance. If the rate of misleading evidence is limited, the cost will be reduced, and with that the Clrr.⁴⁴ Additionally, the minimum log-likelihood-ratio cost (Clrr_{min}) is shown, where also a low result is favored. This metric is dependent on the discrimination performance of the LR output. Additionally, section S11 of the Supplementary data shows Tippett plots that provide

information on the number and extend of misclassifications.⁴⁵ Normalization to ^{13}C provided the best (lowest) Cllr and Cllr_{min} values and widest LR range, although the performance of the various normalization and quantification methods is very similar. The highest computed PAV-calibrated likelihood ratio values are obtained for the tape database with a range of 0.013 to 229 (log10 LR of -1.89 to 2.36). Similar results were obtained for the dataset with 9 elements, as presented in Section S12 of the Supplementary data.

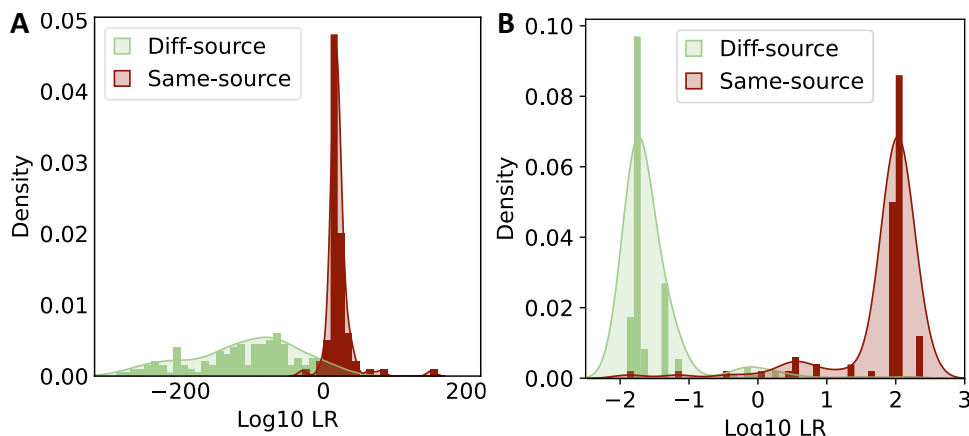


Figure 9.5. A) Uncalibrated and B) PAV-calibrated log10 LR values for the tapes dataset, obtained with the feature-based MVK model for elemental concentrations normalized to C and quantified with the PVC standard. Different-source and same-source distributions are illustrated.

Figure 9.6 shows the likelihood ratios obtained by the score-based SVM model for different-source and same-source comparisons. The dissimilarity score before calibration and the validated LR distributions are displayed. The responses were normalized to ^{13}C and subsequently quantified with the PVC standard. The distributions are similar to the feature-based data, although a slightly better separation is visible. The calibrated and validated LRs, Cllr, and Cllr_{min} measures of the score-based system are shown in Table 9.7. Additionally, Tippett plots that provide information on the number and extend of misclassifications are presented in S13 of the Supplementary data. Overall, normalization to ^{13}C with or without subsequent quantification with the PVC standard showed the best performance. Also, for this model, the performance of the various normalization and quantification methods is very similar. The highest computed ELUB likelihood ratios are for the tape dataset with a range of 0.014 to 1778 (log10 LR of -1.84 to 3.25). The performance measures for the dataset with 9 elements and other models based on the Manhattan distance scoring function are shown in Section S14 of the Supplementary data.

Table 9.6. Performance measures of the feature-based LR model after calibration and validation, for the tapes, tubing, wires, and jerrycans datasets with 18 elements: log-likelihood-ratio cost (Cllr), Cllr_{min}, minimum, and maximum log₁₀ PAV-calibrated LR value.

Database	Normalization and quantification	Cllr	Cllr _{min}	Min log ₁₀ LR	Max log ₁₀ LR
Tapes	Without	0.19	0.17	-1.83	2.31
	¹³ C	0.18	0.14	-1.89	2.36
	Glass standard	0.17	0.14	-1.88	2.33
	PVC standard	0.20	0.16	-1.89	2.33
	¹³ C, PVC standard	0.17	0.14	-1.87	2.34
Tubing	Without	0.50	0.39	-1.41	1.43
	¹³ C	0.40	0.35	-1.44	1.57
	Glass standard	0.58	0.46	-1.43	1.48
	PVC standard	0.42	0.38	-1.46	1.55
	¹³ C, PVC standard	0.51	0.42	-1.37	1.43
Wires	Without	0.32	0.28	-1.63	1.87
	¹³ C	0.17	0.14	-1.63	1.89
	Glass standard	0.27	0.23	-1.63	1.87
	PVC standard	0.26	0.21	-1.63	1.88
	¹³ C, PVC standard	0.12	0.092	-1.64	1.89
Jerrycans	Without	0.21	0.18	-1.55	1.65
	¹³ C	0.059	0.000	-1.56	1.68
	Glass standard	0.17	0.094	-1.56	1.68
	PVC standard	0.15	0.12	-1.54	1.67
	¹³ C, PVC standard	0.23	0.17	-1.55	1.67

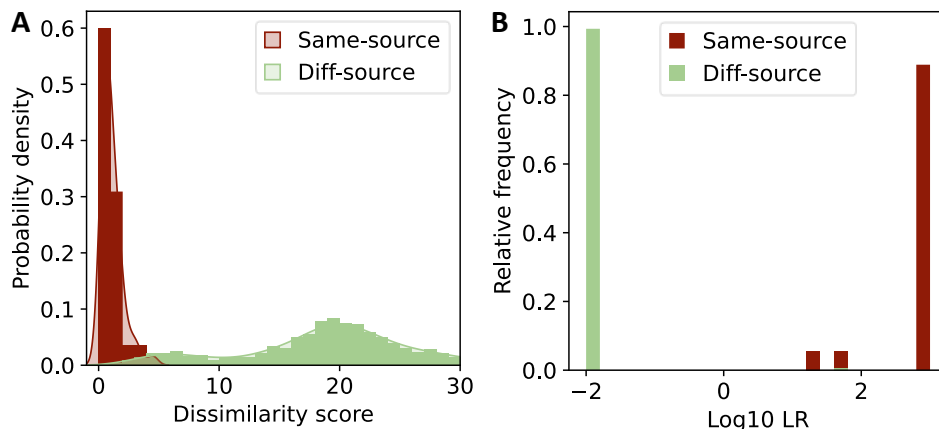


Figure 9.6. A) Histogram with KDE fit of the H₁-true scores (same source) and H₂-true scores (different-source) and B) validated distribution of log₁₀ LRs with ELUB bounds for the tapes dataset, obtained by the score-based model with SVM scoring system, for elemental concentrations normalized to ¹³C and quantified with the PVC standard.

Table 9.7. Performance measures of score-based LR model after calibration and validation, for the tapes, tubing, wires, and jerrycans datasets with 18 elements: log-likelihood-ratio cost (Cllr), Cllr_{min}, minimum, and maximum log₁₀ LR with ELUB.

Database	Normalization and quantification	Cllr	Cllr _{min}	Min log ₁₀ LR	Max log ₁₀ LR
Tapes	Without	0.048	0.022	-1.74	3.23
	¹³ C	0.032	0.015	-1.84	2.86
	Glass standard	0.035	0.020	-1.84	3.03
	PVC standard	0.036	0.020	-1.84	3.25
	¹³ C, PVC standard	0.032	0.018	-1.84	2.92
Tubing	Without	0.46	0.20	-1.36	2.24
	¹³ C	0.25	0.17	-1.48	2.09
	Glass standard	0.19	0.088	-1.23	1.95
	PVC standard	0.34	0.22	-1.36	2.30
	¹³ C, PVC standard	0.24	0.061	-1.42	2.09
Wires	Without	0.27	0.15	-1.45	2.73
	¹³ C	0.038	0	-1.47	2.71
	Glass standard	0.064	0	-1.48	2.73
	PVC standard	0.086	0	-1.49	2.73
	¹³ C, PVC standard	0.052	0	-1.50	2.71
Jerrycans	Without	0.090	0	-1.36	2.61
	¹³ C	0.19	0.093	-1.13	2.62
	Glass standard	0.065	0	-1.38	2.56
	PVC standard	0.12	0	-1.11	2.59
	¹³ C, PVC standard	0.31	0.093	-1.36	2.62

A possible explanation for a false inclusion could be that objects from different suppliers were actually made in the same production facility. Also, tapes, tubing, wires, and jerrycans from the same manufacturer with different sizes were considered as different sources, although the raw material could be highly similar. This could also explain the relatively high Cllr values for the tubing and jerrycan datasets. From a forensic point of view, it is valuable to combine multiple detection techniques for individualization. Particularly, for the jerrycan dataset, the polymer type determined by FT-IR is very specific for each part. Ultimately, separate databases should be built for each type of polymer and object. However, due to the existence of numerous natural and synthetic polymers, it is difficult to build large enough databases for each type. Nevertheless, most forensic objects in this study were made from PVC and PE, and for these polymer types, elemental profile data can readily be gathered and included in databases for comparison studies.

9.4. Conclusion

In the present study, four sample sets of forensic polymer evidence materials were analyzed with LA-ICP-MS and evaluated using match criteria and Bayesian likelihood ratio models. Matrix-matched reference standards with known concentrations were

used to improve the repeatability and advance forensic classifications and comparisons. Characteristic elements were identified with PCA and LDA for each type of dataset. Tapes were found to contain relatively high concentrations of Sb, Ba, Pb, and As, whereas tubing was characterized by the presence of Na, Si, and Ti. It is important to note that Pb and As were present in low concentrations in all objects, but these levels were the most abundant in the tapes. Particularly, grey and yellow objects contained elevated levels of Na and white polymers showed high levels of Ti. Additionally, wires showed high levels of Ni, Sr, Mg, and Ca. In contrast, polyethylene jerrycans contained fewer inorganic raw materials and were defined by the lack of elemental response. In general, the concentration of Cu was clearly elevated for blue and green objects. Also, high concentrations of Fe were detected in brown polymer materials and elevated Ti levels were observed in objects with a white color.

The t-test with Bonferroni correction provided the lowest false inclusion and false exclusion rates. An average false inclusion rate of only 0.45% and a false exclusion rate of 2.4% were obtained. Quantification with the PVC standard slightly improved the performance. However, an advantage of the feature- and score-based approaches is that it provides a continuous approach to evidence interpretation and that the likelihood ratio provides an indication of the strength of evidence. For the score-based model, an average false inclusion rate of 3.4% and a false exclusion rate of 3.0% were calculated. Normalization to ^{13}C with or without quantification with the PVC standard showed the best performance for the feature and score-based models. In addition, the low Cllr and Cllr_{min} indicated good calibration, validation, and discrimination. PAV calibrated likelihood ratios were in the range of 0.013 to 229 for the tape dataset normalized to ^{13}C as obtained by the feature-based MVK model. Analysis with the score-based model resulted in ELUB likelihood ratios of 0.014 to 1778 for the tape dataset normalized to ^{13}C and subsequent quantification with the PVC standard.

Future research could focus on interlaboratory comparisons of elemental profiles obtained with LA-ICP-MS. The effect of the normalization and quantification was marginal in this study. However, the benefit can be increased significantly when results from different instruments in multiple laboratories are compared and shared for reference database creation. In addition, it would be informative to investigate the specific production processes of each object to gain more understanding about the expected elemental impurities and to prevent classification of objects from the same manufacturer as different sources. Also, more samples could be analyzed for the jerrycans dataset to improve forensic comparison. Although it is expected that the elemental impurity profile remains relatively stable, the influence of polymer degradation due to explosions, ageing, light, or water, should be further investigated. Ultimately, the datasets could be used to provide intelligence information regarding

the type and origin of plastic material encountered in forensic casework. Additionally, well-validated likelihood ratio models could facilitate forensic comparisons in a similar way as is currently being done for forensic glass evidence in case work. Ultimately, this could lead to the accredited use of the elemental profiling of polymers with LA-ICP-MS in forensic practice.

Acknowledgements

We would like to thank Dr. Donald Windover (NIST, Gaithersburg) for his assistance with the μ -XRF measurements and Dr. Tatiana Trejos (West Virginia University, Morgantown) for providing additional tape samples.

Disclaimer

Certain commercial equipment, instruments, or materials are identified in this paper in order to specify the experimental procedure adequately. Such identification is not intended to imply recommendation or endorsement by the National Institute of Standards and Technology, nor is it intended to imply that the materials or equipment identified are necessarily the best available for the purpose.

References

- (1) Zoon, P. D.; Janssen, M. H. Crystal Clear Connections - Database Matching Unknown Glass Fragments to Reference Glass from ATM Explosions. *Forensic Sci Int* **2024**, Submitted.
- (2) Woodman, P. A.; Spiranovic, C.; Julian, R.; Ballantyne, K. N.; Kelty, S. F. The Impact of Chemical Trace Evidence on Justice Outcomes: Exploring the Additive Value of Forensic Science Disciplines. *Forensic Sci Int* **2020**, 307. <https://doi.org/10.1016/j.forsciint.2019.110121>.
- (3) Almirall, J. R.; Trejos, T. Applications of LA-ICP-MS to Forensic Science. *Elements* **2016**, 12 (5), 335–340. <https://doi.org/10.2113/gselements.12.5.335>.
- (4) PlasticsEurope. *Plastics - The Facts 2020 an Analysis of European Plastics Production, Demand and Waste Data*; Brussels, 2020. <https://plasticseurope.org/knowledge-hub/plastics-the-facts-2020/> (accessed 2024-01-09).
- (5) Martinez-Lopez, C.; Trejos, T.; Coulson, S.; Goodpaster, J.; Igowsky, K.; Kuczelinis, F.; Mehlretter, A.; Pollock, E.; Simmross, U.; Weimer, R.; Weis, P.; Almirall, J. R. Interlaboratory Evaluations of the Performance of Elemental Analytical Methods for the Forensic Analysis and Comparisons of Electrical Tapes. *Forensic Chemistry* **2019**, 12, 66–77. <https://doi.org/10.1016/j.forc.2019.01.001>.
- (6) Koltzenburg, S.; Maskos, M.; Nuyken, O. *Polymer Chemistry*; Springer: Berlin Heidelberg, 2017. <https://doi.org/10.1016/B978-1-84569-741-9.50002-1>.
- (7) Wang, M.; Xu, J.; Wu, H.; Guo, S. Effect of Pentaerythritol and Organic Tin with Calcium/Zinc Stearates on the Stabilization of Poly(Vinyl Chloride). *Polym Degrad Stab* **2006**, 91 (9), 2101–2109. <https://doi.org/10.1016/j.polymdegradstab.2006.01.011>.
- (8) Allen, N. S.; Edge, M. Perspectives on Additives for Polymers. Part 2. Aspects of Photostabilization and Role of Fillers and Pigments. *Journal of Vinyl and Additive Technology* **2021**, 27 (2), 211–239. <https://doi.org/10.1002/vnl.21810>.
- (9) van Asten, A. *Chemical Analysis for Forensic Evidence*, 1st ed.; Elsevier: Amsterdam, 2022.
- (10) Berends-Montero, S.; Wiarda, W.; De Joode, P.; Van Der Peijl, G. Forensic Analysis of Float Glass Using Laser Ablation Inductively Coupled Plasma Mass Spectrometry (LA-ICP-MS): Validation of a Method. *J Anal At Spectrom* **2006**, 21 (11), 1185–1193. <https://doi.org/10.1039/b606109e>.
- (11) Trejos, T.; Koons, R.; Becker, S.; Berman, T.; Buscaglia, J.; Duecking, M.; Eckert-Lumsdon, T.; Ernst, T.; Hanlon, C.; Heydon, A.; Mooney, K.; Nelson, R.; Olsson, K.; Palenik, C.; Pollock, E. C.; Rudell, D.; Ryland, S.; Tarifa, A.; Valadez, M.; Weis, P.; Almirall, J. Cross-Validation and Evaluation of the Performance of Methods for the Elemental Analysis of Forensic Glass by μ -XRF, ICP-MS, and LA-ICP-MS. *Anal Bioanal Chem* **2013**, 405 (16), 5393–5409. <https://doi.org/10.1007/s00216-013-6978-y>.
- (12) Lambert, K.; Montero, S.; Akmeemana, A.; Corzo, R.; Gordon, G.; Haase, E.; Jiang, P.; Ovide, O.; Prasch, K.; Redman, K.; Scholz, T.; Trejos, T.; Webb, J.; Weis, P.; Wiarda, W.; Wilczek, S.; Xie, H.; Zoon, P.; Almirall, J. An Interlaboratory Study to Evaluate the Forensic Analysis and Interpretation of Glass Evidence. *Forensic Chemistry* **2022**, 27, 100378. <https://doi.org/10.1016/j.forc.2021.100378>.
- (13) Bezemer, K.; Woortmeijer, R.; Koeberg, M.; Wiarda, W.; Schoenmakers, P.; van Asten, A. Multicomponent Characterization and Differentiation of Flash Bangers — Part II: Elemental Profiling of Plastic Caps. *Forensic Sci Int* **2018**, 290, 336–348. <https://doi.org/10.1016/j.forsciint.2018.06.012>.
- (14) Kuczelinis, F.; Weis, P.; Bings, N. H. Forensic Comparison of PVC Tape Backings Using Time Resolved LA-ICP-MS Analysis. *Forensic Chemistry* **2019**, 12, 33–41. <https://doi.org/10.1016/j.forc.2018.11.004>.
- (15) Corzo, R.; Hoffman, T.; Weis, P.; Franco-Pedroso, J.; Ramos, D.; Almirall, J. The Use of LA-ICP-MS Databases to Calculate Likelihood Ratios for the Forensic Analysis of Glass Evidence. *Talanta* **2018**, 186, 655–661. <https://doi.org/10.1016/j.talanta.2018.02.027>.
- (16) Deconinck, I.; Latkoczy, C.; Günther, D.; Govaert, F.; Vanhaecke, F. Capabilities of Laser Ablation - Inductively Coupled Plasma Mass Spectrometry for (Trace) Element Analysis of Car Paints for Forensic Purposes. *J Anal At Spectrom* **2006**, 21, 279–287. <https://doi.org/10.1039/b514007b>.
- (17) Gupta, A.; Martinez-Lopez, C.; Curran, J. M.; Almirall, J. R. Multi-Element Comparisons of Tapes Evidence Using Dimensionality Reduction for Calculating Likelihood Ratios. *Forensic Sci Int* **2019**, 301, 426–434. <https://doi.org/10.1016/j.forsciint.2019.06.002>.

Evaluating the strength of evidence of elemental profiling

9

- (18) Martinez-Lopez, C.; Sakayanagi, M.; Almirall, J. R. Elemental Analysis of Packaging Tapes by LA-ICP-MS and LIBS. *Forensic Chemistry* **2018**, *8*, 40–48. <https://doi.org/10.1016/j.forc.2018.01.004>.
- (19) Martinez-Lopez, C.; Trejos, T.; Sakayanagi, M.; Almirall, J. R. Elemental Analysis and Characterization of Electrical Tape Backings by LA-ICP-MS. *Forensic Chemistry* **2017**, *4*, 96–107. <https://doi.org/10.1016/j.forc.2017.03.003>.
- (20) Aitken, C. G. G.; Lucy, D. *Evaluation of Trace Evidence in the Form of Multivariate Data*; 2004; Vol. 53. <http://www.blackwellpublishing.com/rss>.
- (21) Ramos, D.; Maroñas, J.; Almirall, J. Improving Calibration of Forensic Glass Comparisons by Considering Uncertainty in Feature-Based Elemental Data. *Chemometrics and Intelligent Laboratory Systems* **2021**, *217*. <https://doi.org/10.1016/j.chemolab.2021.104399>.
- (22) von Wuthenau, K.; Segelke, T.; Kuschnereit, A.; Fischer, M. Glass Authentication: Laser Ablation-Inductively Coupled Plasma Mass Spectrometry (LA-ICP-MS) for Origin Discrimination of Glass Bottles. *Talanta* **2021**, *235*. <https://doi.org/10.1016/j.talanta.2021.122686>.
- (23) de Bruin-Hoegée, M.; Schoorl, J.; Zoon, P.; van der Schans, M. J.; Noort, D.; van Asten, A. C. A Novel Standard for Forensic Elemental Profiling of Polymers by LA-ICP-TOF-MS. *Forensic Chemistry* **2023**, *35*. <https://doi.org/10.1016/j.forc.2023.100515>.
- (24) Weis, P.; Dücking, M.; Watzke, P.; Menges, S.; Becker, S. Establishing a Match Criterion in Forensic Comparison Analysis of Float Glass Using Laser Ablation Inductively Coupled Plasma Mass Spectrometry. In *Journal of Analytical Atomic Spectrometry*; 2011; Vol. 26, pp 1273–1284. <https://doi.org/10.1039/c0ja00168f>.
- (25) Trejos, T.; Koons, R.; Weis, P.; Becker, S.; Berman, T.; Dalpe, C.; Duecking, M.; Buscaglia, J.; Eckert-Lumsdon, T.; Ernst, T.; Hanlon, C.; Heydon, A.; Mooney, K.; Nelson, R.; Olsson, K.; Schenk, E.; Palenik, C.; Pollock, E. C.; Rudell, D.; Ryland, S.; Tarifa, A.; Valadez, M.; Van Es, A.; Zdanowicz, V.; Almirall, J. Forensic Analysis of Glass by μ -XRF, SN-ICP-MS, LA-ICP-MS and LA-ICP-OES: Evaluation of the Performance of Different Criteria for Comparing Elemental Composition. *J Anal At Spectrom* **2013**, *28* (8), 1270–1282. <https://doi.org/10.1039/c3ja50128k>.
- (26) Trejos, T.; Almirall, J. R. Sampling Strategies for the Analysis of Glass Fragments by LA-ICP-MS: Part I. Micro-Homogeneity Study of Glass and Its Application to the Interpretation of Forensic Evidence. *Talanta* **2005**, *67* (2), 388–395. <https://doi.org/10.1016/j.talanta.2005.01.042>.
- (27) van Es, A.; Wiarda, W.; Hordijk, M.; Alberink, I.; Vergeer, P. Implementation and Assessment of a Likelihood Ratio Approach for the Evaluation of LA-ICP-MS Evidence in Forensic Glass Analysis. *Science and Justice* **2017**, *57* (3), 181–192. <https://doi.org/10.1016/j.scijus.2017.03.002>.
- (28) Lindley, D. V. *A Problem in Forensic Science*; 1977; Vol. 64. <https://www.jstor.org/stable/2335686>.
- (29) Bolck, A.; Ni, H.; Lopatka, M. Evaluating Score-and Feature-Based Likelihood Ratio Models for Multivariate Continuous Data: Applied to Forensic MDMA Comparison. *Law, Probability and Risk* **2014**, *14* (3), 243–266. <https://doi.org/10.1093/lpr/mgv009>.
- (30) Ramirez-Hereza, P.; Ramos, D.; Maroñas, J.; Balanya, S. A.; Almirall, J. Gaussianization of LA-ICP-MS Features to Improve Calibration in Forensic Glass Comparison. *Forensic Sci Int* **2023**, *349*. <https://doi.org/10.1016/j.forsciint.2023.111735>.
- (31) Vergeer, P. From Specific-Source Feature-Based to Common-Source Score-Based Likelihood-Ratio Systems: Ranking the Stars. *Law, Probability and Risk* **2023**, *22* (1). <https://doi.org/10.1093/lpr/mgad005>.
- (32) Kaspi, O.; Israelsohn-Azulay, O.; Yigal, Z.; Rosengarten, H.; Krmpotić, M.; Gouasmia, S.; Bogdanović Radović, I.; Jalkanen, P.; Liski, A.; Mizohata, K.; Räisänen, J.; Kasztovszky, Z.; Harsányi, I.; Acharya, R.; Pujari, P. K.; Mihály, M.; Braun, M.; Shabi, N.; Girshevitz, O.; Senderowitz, H. Toward Developing Techniques—Agnostic Machine Learning Classification Models for Forensically Relevant Glass Fragments. *J Chem Inf Model* **2023**, *63* (1), 87–100. <https://doi.org/10.1021/acs.jcim.2c01362>.
- (33) National Institute of Standards and Technology. *Certificate of Analysis of Standard Reference Material 612*; Gaithersburg, MD, 2012.
- (34) Martinez Lopez, C.; Carter, J. A.; Corzo, R.; Todorov, T. I. Method Development for the Quantitative Analysis of Multivitamin Supplements by Laser Ablation–Inductively Coupled Plasma–Mass Spectrometry (LA-ICP-MS). *Food Anal Methods* **2022**, *15*, 3079–3091. <https://doi.org/10.1007/s12161-022-02351-x>.



Chapter 9

- (35) Ovide, O.; Corzo, R.; Trejos, T. The Analysis of Glass from Portable Electronic Devices and Glass Accessories Using M-XRF for Forensic Investigations. *Forensic Sci Int* **2023**, *343*, 111550. <https://doi.org/10.1016/j.forsciint.2022.111550>.
- (36) Netherlands Forensic Institute. LIR Python Likelihood Ratio Library. 2024. <https://github.com/NetherlandsForensicInstitute/lir> (accessed 2024-01-09).
- (37) de Bruin-Hoegée, M.; de Bruin, G. J. Python Code for Chemical Profiling of Polymers with LA-ICP-MS. 2024. <https://doi.org/10.5281/zenodo.10668714>.
- (38) Zadora, G.; Martyna, A.; Ramos, D.; Aitken, C. *Statistical Analysis in Forensic Science: Evidential Value of Multivariate Physicochemical Data*; Wiley, 2014.
- (39) Pedregosa, F.; Varoquaux, G.; Gramfort, A.; Michel, V.; Thirion, B.; Grisel, O.; Blondel, M.; Prettenhofer, P.; Weiss, R.; Dubourg, V.; Vanderplas, J.; Passos, A.; Cournapeau, D.; Brucher, M.; Perrot, M.; Duchesnay, E. Scikit-Learn: Machine Learning in Python. *Journal of Machine Learning Research* **2011**, *12*, 2825–2830. <https://doi.org/10.48550/arXiv.1201.0490>.
- (40) ASTM International. *ASTM E2927-16e1, Standard Test Method for Determination of Trace Elements in Soda-Lime Glass Samples Using Laser Ablation Inductively Coupled Plasma Mass Spectrometry for Forensic Comparisons*; West Conshohocken, PA, 2016.
- (41) Leegwater, J.; Vergeer, P.; Alberink, I.; van de Wetering, J.; El Harchauoui, R.; Bosma, W.; Ypma, R.; Sjerps, M. From Data to a Validated Score-Based LR System: A Practitioner's Guide. *Forensic Sci Int* **2024**, Under Review.
- (42) Vergeer, P.; van Es, A.; de Jongh, A.; Alberink, I.; Stoel, R. Numerical Likelihood Ratios Outputted by LR Systems Are Often Based on Extrapolation: When to Stop Extrapolating? *Science and Justice* **2016**, *56* (6), 482–491. <https://doi.org/10.1016/j.scijus.2016.06.003>.
- (43) Trejos, T.; Montero, S.; Almirall, J. R. Analysis and Comparison of Glass Fragments by Laser Ablation Inductively Coupled Plasma Mass Spectrometry (LA-ICP-MS) and ICP-MS. *Anal Bioanal Chem* **2003**, *376*, 1255–1264. <https://doi.org/10.1007/s00216-003-1968-0>.
- (44) Meuwly, D.; Ramos, D.; Haraksim, R. A Guideline for the Validation of Likelihood Ratio Methods Used for Forensic Evidence Evaluation. *Forensic Sci Int* **2017**, *276*, 142–153. <https://doi.org/10.1016/j.forsciint.2016.03.048>.
- (45) de Bruin-Hoegée, M.; Kleiweg, D.; Noort, D.; van Asten, A. C. Chemical Attribution of Fentanyl: The Effect of Human Metabolism. *Forensic Chemistry* **2021**, *24*, 100330. <https://doi.org/10.1016/j.forc.2021.100330>.



10

Conclusions and future
perspectives

10.1 Concluding remarks

Forensic intelligence is of key importance to obtain crucial information to accelerate solving a crime, with the ultimate goal to prevent criminal acts before they are executed. This thesis contributes to that goal by revealing the origin of chemical weapons to support forensic intelligence purposes. Various multi-analytical profiling strategies for chemical warfare agents are recommended to advance the field of chemical forensics. Important knowledge gaps were addressed: 1) Forensic CWA intelligence, 2) CWA profiling in biological samples, and 3) Characterization of CWA dispersion devices.

Chapters 2 and 3 demonstrate the potential of chemical profiling in biomedical samples as a valuable addition to the more classical approach of analyzing bulk samples. Characteristic markers of synthetic opioids were identified in pre- and post-metabolism samples by GC-MS and LC-HRMS/MS. Although not all markers were stable during metabolism, their discriminating potential was transferred to the metabolic products. In addition to a match criterion approach, the chemometric PCA and LDA models were applied to distinguish between different synthesis routes. The obtained insights can provide valuable tactical information on the production method to assist forensic investigations.

The emerging field of proteomics in combination with advanced data science makes it possible to search for new biomarkers of CWA exposure. Chapter 4 describes the identification of site-specific chlorinated peptides by high-resolution mass spectrometric analysis as a more selective indicator of chlorine gas exposure. Several promising protein adducts with multiple chlorination sites were found in haptoglobin and albumin, which are abundantly present in human whole blood. An interesting feature is that such biomarkers may be used to discriminate between endogenous processes and exogenous exposure, which is particularly relevant for investigations of alleged use of chlorine gas as a chemical weapon.

Chapter 5 reports the capabilities of a mobile test kit for fast and reliable diagnosis of nerve agent intoxications. Remarkably, the exposure signature was preserved for at least one month by using dried blood spots stored under ambient conditions. This facilitated confirmatory laboratory analysis with complementary analytical techniques, which is generally required for forensic verification. Both LC-MS/MS and GC-MS/MS were successfully used for sensitive and selective analysis of biomarkers of sarin and Novichock nerve agents.

After a suspected chemical attack in a conflict area, it can be difficult for forensic investigators to get immediate access to the crime scene due to safety and security

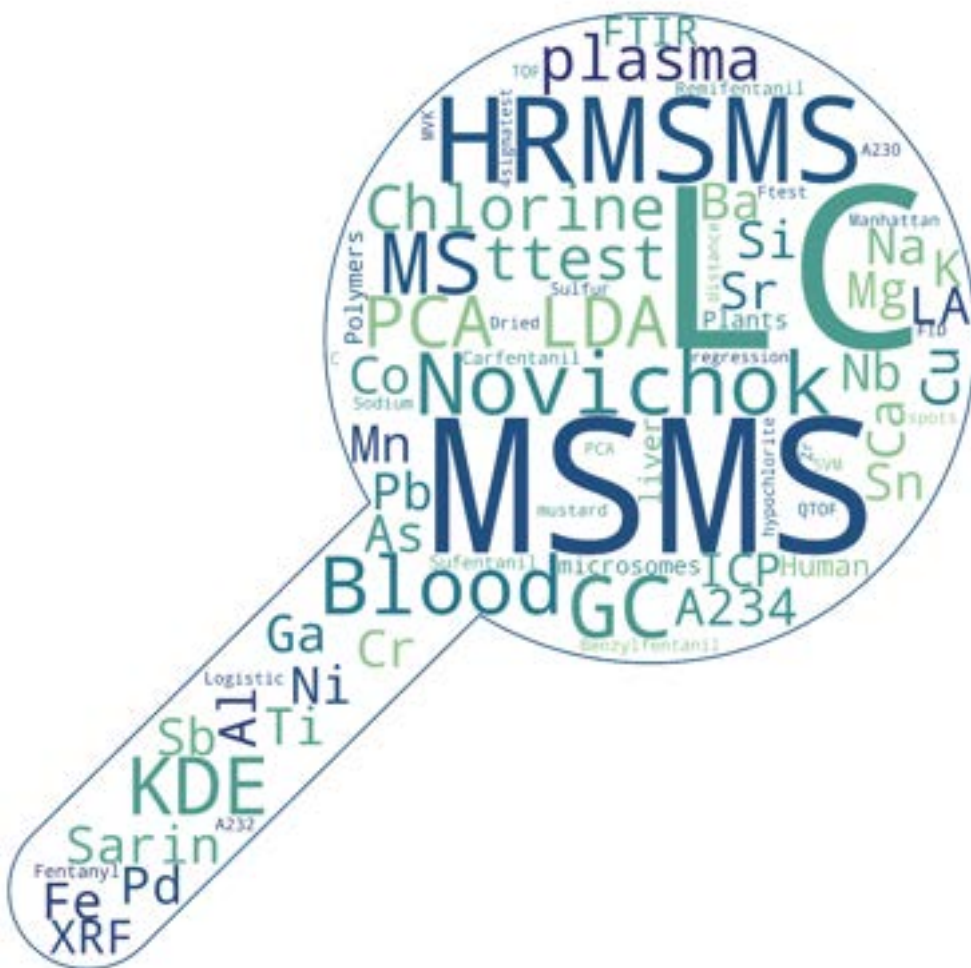
concerns. Since chemical warfare agents are highly reactive chemicals, the intact agent is often not detectable anymore. Chapter 6 offers an alternative source of evidence, which can be utilized for retrospective investigations of chemical weapons use. A novel approach was developed for analyzing persistent biomarkers of sarin, Novichok nerve agent, sulfur mustard, and chlorine in plants. Even three months after exposure, protein adducts were still detectable with LC-MS/MS. In addition, proteomic analysis with high-resolution mass spectrometry revealed chlorination of the highly abundant protein rubisco, as well as other plant proteins. Consequently, the inclusion of vegetation as a valuable source of biological evidence material at the alleged scene of the incident offers forensic scientists new possibilities for accurate reconstruction.

Chapter 7 extends the research on CWA-induced plant metabolomics by providing characteristic chemical fingerprints for various chlorinating agents. A large number of post-translational modifications were identified by untargeted high resolution mass spectrometry. These include plant fatty acids, amino acids, and DNA adducts. Chemometric PCA and LDA models showed clear differentiation between exposure to chlorine gas and the frequently used bleaching agent hypochlorite. Furthermore, the identity of characteristic markers was confirmed using reference standards. Consequently, the presented profiling methodology can be valuable for the discovery of new biomarkers which differentiate between various chemical threat agents and commonly used chemical products.

Plastic is found everywhere and therefore also on the crime scene as part of chemical dispersion devices. Chapters 8 and 9 introduce LA-ICP-(TOF-)MS as a powerful technique to obtain forensic elemental profiles of polymers. A novel matrix-matched standard was developed to facilitate accurate quantification of trace elements in polymers. The within-sample and between-run variation were significantly reduced when correcting for one element as internal standard or when applying the novel standards. The accomplished reproducibility promoted forensic classification and comparison approaches. Several Bayesian models were applied to a relatively large dataset in which the degree of similarity between two plastic samples was expressed through likelihood ratios to indicate the evidential strength. This statistical method, that is currently accepted in court for glass comparison, could ultimately be validated for polymer samples as well, to assist elemental profile comparisons of plastic evidence materials in criminal investigations.

Key topics discussed in this thesis are schematically visualized in Figure 10.1. A wide range of analytes, instruments, matrices, and chemometric models were investigated. This includes fourteen chemicals belonging to the group of nerve agents, blister agents, pharmaceutical-based agents, and toxic industrial chemicals. In total 23

elements were measured by LA-ICP-(TOF)MS. The most applied analytical technique was LC-MS/MS, followed by LC-HRMS/MS. More than 200 known analytes, peptides, and tentatively identified impurities were analyzed. In addition, gas chromatographic methods, XRF, FT-IR, and NMR were employed. The main biological sample matrices included (blood)plasma, human liver microsomes, plants, polymers, and dried blood spots. Finally, multiple types of chemometric models were applied and evaluated. Match criterion approaches, PCA, and LDA with KDE were the most performed statistical analyses.



10

Figure 10.1. Word cloud with key words of the research topics covered in this thesis. This includes the analytes of interest, applied analytical techniques, matrices, and data analysis tools.

10.2 Future research directions

The following subsections provide insights into important challenges for chemical attribution research. The first section discusses the translation of in-vitro studies to realistic case scenarios. The second section shows the potential of investigating a broader range of chemicals and applying different analytical techniques. The third section deals with the implementation in forensic practice. The last section focusses on the possible use of chemical profiling strategies as important evidence in the (international) court of justice.

10.2.1 Translation to realistic case scenarios

The human CWA biomarker results presented in this work are exclusively based on in-vitro studies. In Chapters 2 and 3 human liver microsomes were used to mimic in-vivo human metabolism. Although this system has been proven to be a realistic model to study drug metabolism,¹ it obviously represents a simplified version of real human metabolic fates. In Chapters 4 and 5 human plasma was incubated in-vitro by various chemical warfare agents. Interestingly, for sarin the presence of most biomarkers have been verified in authentic cases.² Additionally, the less-specific chlorotyrosine biomarkers were detected in both blood of an unexposed population and at elevated levels after acute chlorine exposure in individuals.^{3–5} However, site-specific biomarkers for chlorine gas exposure have not yet been investigated after intoxication. In addition, Novichok nerve agents have been scarcely studied and to date only results of in-vitro analyses have been published. Further research should indicate whether these in-vitro experiments are representative for real-world cases. In particular, intra-person and intra-population variation, in vivo stability, as well as in vivo persistency of the impurities and biomarkers might affect their applicability. Other factors that play a pivotal role are instrument precision because of the low levels observed in casework samples. To further advance the field of toxicology, innovations directed towards more sensitive analytical techniques remain essential.

Another interesting research direction worthwhile to explore is the effect of external factors, such as storage and weather conditions on the stability of chemical attribution signatures. As discussed in the introduction, chemical threat agents are highly reactive chemicals which rapidly decompose in the environment or metabolize in biological matrices. Several methods were proposed to retain the metabolic profile in biological samples. Dried blood spots were fixated on filter paper to slow down degradation and preserve the signature after nerve agent exposure. A similar method can potentially be applied to fentanyl samples to maintain the metabolic profile.⁶ Nevertheless, it is worth mentioning that the fentanyl profiling studies presented in this thesis indicate that a substantial proportion of the original pharmaceutical-based

agent persists in the metabolized sample. In contrast, nerve agents easily hydrolyze in environmental and biological samples, eventually losing chemical information that is specific for the type of nerve agent. This characteristic chemical information can be retrieved for a longer period of time by using vegetation as a source of information. Chemical attribution signatures were also retained in some other matrices as described in literature. For instance, nerve agent markers were stable in food for at least three weeks.⁷ Also it has previously been observed that VX is not always completely destroyed by fire or liquid decontamination, although the chemical attribution signature significantly changed.⁸ Contrary to chemical threat agents, plastics exhibit remarkable persistence. It is this problematic feature that causes major environmental concerns (e.g. microplastics). To limit long-term ecological effects, the biodegradability of plastics should be drastically improved. However, from a forensic point of view the stability of plastics has many advantages for retrieving and securing the chemical profile. Nonetheless, it is likely that future material improvements will lead to new challenges for criminal investigations. If so, understanding of the degradation mechanism can become crucial for this type of evidence.

Although the synthesis impurities were reproducible and small changes were observed when carfentanil and remifentanil were produced by different organic chemists, differences are expected in products synthesized in other laboratories. It would be valuable to profile many samples from different sources to correct for batch and laboratory variation. Interestingly, the profiling of a large volume of data generated as part of regular drug screening is envisioned in a new project at the University of Amsterdam.⁹ An advantage of observing small synthesis variations is the opportunity to connect a confiscated fentanyl sample to a specific laboratory or production protocol. The prospect of matching a chemical attribution signature obtained from the blood of a victim to a specific batch of material discovered at the residence of a suspect could be highly valuable in a forensic context.

10.2.2 Expanding the forensic toolbox

This thesis mainly focuses on laboratory techniques for multi-analytical profiling of chemical warfare agents. Chapter 5 describes the use of portable techniques for nerve agent identification. Several methods for determining the type of chemical released can directly be deployed at the site of an incident. However, chemical profiling with portable detectors remains extremely challenging. Attribution signatures are typically present at trace levels, that cannot sensitively be detected by conventional on-site methods. Interestingly, studies exist in other research areas that explore the possibility of impurity profiling by on-scene detectors. For instance, in the field of illicit drug analysis, innovative research has emerged concerning the portable analysis

of adulterants in forensic drug samples by near-infrared spectroscopy.¹⁰ A similar approach may be applied to street samples containing high levels of fentanyl, because these opioids are also consumed as pill or tablet. Extrapolation to other chemical warfare agents can be more difficult since these compounds are often dispersed as a gas or vapor. When civilians or military personnel encounter an attack, it is strongly advised to leave the incident scene for safety purposes. By the time first responders and forensic investigators enter the incident scene, the acute threat has normally dissipated, and thus CWA concentrations have been significantly reduced. Therefore, remote detectors, robots, or drones can possibly be employed for reaching inaccessible areas and increasing the profiling capabilities directly after a CBRN incident. Alternative applications of these portable detectors are initial screening to support sampling of forensic evidence. Materials with high chemical warfare agent concentrations can be collected and highlighted to facilitate forensic reconstruction. Also, indirect changes in the environment can be indicative of exposure, such as discoloration of the surrounding soil or vegetation. Therefore, portable screening can advance investigations of alleged use, but it is expected that laboratory analysis will remain essential for chemical attribution research.

Many analytical techniques can potentially be used for chemical profiling. The choice of analytical technique is mainly dependent on the matrix, with GC-(HRMS/)MS predominantly applied to environmental samples and LC-(HRMS/)MS most often applied to biomedical samples. Despite this, other options may be suitable. In this thesis LA-ICP-MS was introduced for profiling of chemical weapons and associated devices. However, the combination of laser technology and high-end mass spectrometry makes it an expensive technique which is not available to all laboratories investigating alleged chemical weapons use. In addition, Chapter 7 describes the use of NMR for structural identification of markers. Other studies also apply this technique for source attribution. Characteristic intramolecular isotopic distributions were measured in soman synthesized from three distinctive starting materials.¹¹ Another analytical technique, that has been applied in the field of CWA analysis, is two-dimensional gas chromatography-mass spectrometry. Trace amounts of VX were detected in complex accelerant-containing fire debris.⁸ Additionally, isotope ratio mass spectrometry was used as a fingerprinting tool. The natural isotopic variability in nerve-agent precursors was used to distinguish between various stocks.¹² Remarkably, the isotopic signature was also inherited into the next intermediate compound of sarin synthesis. There are three other promising analytical methods that have not been applied to profiling of chemical warfare agents yet. First, two-dimensional liquid chromatography is an excellent technique for the analysis of highly complex non-volatile samples. It has been applied to proteomic profiling and chemical characterization of smokeless powders and complex mixtures of traditional

Chinese medicine.^{13,14} Second, capillary electrophoresis (CE) is widely used for impurity profiling of drugs.¹⁵ It is a sensitive analytical method which provides high resolution and fast results. Third, direct analysis in real time (DART) MS is a powerful and very rapid tool to analyze a wide range of forensic samples.¹⁶ It is a fast technique which requires minimal sample preparation. In the field of explosive research, DART-MS was for instance successfully used for profiling nitrate ester explosives.¹⁶ Future research should indicate whether these suggested analytical methods provide better, or complementary information compared to the more commonly used techniques of chromatography coupled to mass spectrometry. One remaining challenge is further reducing analytical detection limits to find impurities present at even lower levels. In this respect, ongoing improvements in the sensitivity and resolution of mass spectrometry are promising for future CWA-related research.

Another crucial element in expanding the forensic toolbox involves the examination of a wider range of chemicals. Novel techniques proposed in this thesis have been applied to a selection of chemicals. Chapters 2 and 3 presented the attribution of fentanyl and fentanyl analogs in biomedical samples. It is important to extend this research to other chemical threat agents. Until now the focus in literature has mainly been on obtaining a metabolic profile, while no studies report on attribution using biomedical samples. As a follow-up research direction, chemical profiling in different biological matrices can be explored. Chapter 5 describes the identification of nerve agents in dried blood spots. This can potentially be combined with chemical attribution research into a novel concept of chemical profiling in dried blood spots. The methodology proposed in Chapter 4 is applied to chlorine gas as a chemical weapon. A similar analytical approach was described for several other chemicals in literature. Site-specific protein adducts were identified for sarin, tabun, soman, and VX.¹⁷ This research can further be extended to blister agents and toxic industrial chemicals to find new biomarkers. Subsequently, detection of plant protein adducts was investigated for distinct chemical threat agents. It is hypothesized that this approach can be applied to other chemical warfare agents as well, specifically when validated methods exists for biomarker detection in human biological samples. In addition to studying well-characterized chemical warfare agents, it is important to examine structurally related chemicals, metabolites, and impurities. Development of chemical databases would advance identification. In conclusion, to further improve chemical forensic research, the expansion to a more extensive array of chemicals and matrices would be valuable to extend the set of available biomarkers and understand their origin and selectivity.

10.2.3 Implementation in forensic practice

A very recent report emphasizes the importance of chemical attribution research for obtaining key insights into the origin of an unknown sample.¹⁸ The detailed analysis of impurities in sulfur mustard samples obtained in the Syrian Arab Republic and Iraq revealed the specific synthesis method that was employed and the technical skills of the manufacturers. Characteristic impurities for crude sulfur mustard produced by the Levinstein route were identified. The precursors of the improvised production method were most likely chemicals that are commonly available and that are not subject to trade restrictions. Since the sulfur mustard declared by State actors, and confirmed with analytical data, was produced via a Meyer production route, it is extremely unlikely that the samples originated from a State's stockpile. Therefore, the evidence indicates that it is more likely that the sulfur mustard at the site of the incident was deployed by a non-State actor operating in the area and possessing the means and expertise to employ weapons with a chemical payload than that the sulfur mustard was deployed by a State actor engaged in hostilities in the Syrian Arab Republic. This research is in line with the mandate of the OPCW to identify the perpetrators of chemical weapons, with the aim of holding them accountable.

Because chemical attribution investigations can have significant impact, the use of robust and reproducible analytical methods and procedures is crucial. To test the technical capability of laboratories, the OPCW organizes yearly biomedical and environmental proficiency tests. Laboratories should qualitatively investigate the possible presence of chemical warfare agents or related chemicals in complex matrices. Similar interlaboratory testing protocols would also be very beneficial for the analysis of chemical attribution signatures. Recently, a first interlaboratory comparison study of a nerve agent precursor was initiated by Holmgren et al.¹⁹ It was followed up by a second round-robin test, where a new quality control was evaluated by various designated laboratories.²⁰ It is expected that more confidence building exercises will follow to ensure competence of designated laboratories in chemical attribution research. Methods developed in this thesis may be included in the interlaboratory comparison tests. Experience with the current biomedical proficiency test is a distinct advantage when implementing new practices, because of the knowledge required with respect to complex matrices, protein isolation protocols, and enzymatic digestion steps. Ultimately, it would be valuable if more evidence, like vegetation, dried blood spots, and polymers were included in forensic CWA investigations. However, this would require more laboratories to adopt the novel methodologies introduced in this thesis.

To ensure preparedness for a chemical weapons attack, sharing information on chemical detection techniques is essential. It is recognized that there is a lack of

scientific data on the newly scheduled Novichok and carbamate nerve agents.²¹ Information about their chemical properties, suitable protective equipment, and medical countermeasures would enhance national security. This also applies to other types of chemical warfare agents, where more information can be shared about the synthesis impurities to advance chemical attribution studies. International partnerships with scientific experts, policy, and law enforcement organizations could effectively address these knowledge gaps.

10.2.4 Evidential value in court

It would be desirable to use chemical profiling strategies to support forensic intelligence and provide important evidence in a court of law. Chemical attribution signatures can be used to link the evidence to its original source. The findings can then support or refute the hypothesis that a connection between materials exists. However, to assess the evidential value and to be able to assess random match probabilities, a substantial background database is required. For obvious reasons this is very challenging when considering chemical weapons. Chapter 9 demonstrates the application of a polymer database which can be used to assess the probability of evidence under different hypotheses in line with the Bayesian framework for evidence interpretation. Ideally, this is also constructed for impurity profiles of chemical warfare agents. However, due to safety and security reasons and complex synthesis methods, this is incredibly labor intensive. Consequently, there is limited literature available on the construction of likelihood ratios for CWA evidence. It is worth mentioning that the judge must be aware of the prior probabilities given the fact that incidents with chemical weapons are rare. In the absence of sufficient data and calibration, as discussed in Chapter 2, likelihood ratios are of an indicative nature only. Semi-quantitative methods need to be developed that allow forensic experts to make qualitative but nonetheless robust statements on the probability of the evidence under different hypotheses. This approach was utilized in the investigation of sulfur mustard samples obtained after the chemical attack in the Syrian Arab Republic as described in Section 10.2.3.¹⁸ As such, attribution studies that were initially used for forensic intelligence can also bring added value to court proceedings.

Recently, more attention is paid to the application of chemometrics in chemical weapons research. A completely new chapter on this topic was added to the recommended operating procedures for analysis in the verification of chemical disarmament as was recently published.²² Much focus is directed on data preprocessing and normalization. It is recommended to apply multivariate methods that are explainable and validated. Future research can show the potential of integrating artificial intelligence models in chemical attribution analyses. Increasingly powerful models will enhance the speed and efficiency of forensic science. However,

three drawbacks are briefly emphasized to conclude this section. First, a substantial number of methods require large datasets. Second, artificial intelligence models are prone towards bias (especially in the absence of sufficient reference data). Third, complex machine learning models lack explainability. These obstacles are acknowledged in machine learning research, so advancements are anticipated in this regard. Simultaneously, the application of chemometrics can be improved by making data open access and creating infrastructure that makes code easy to run by others. This in turn can be hampered by the sensitive nature of information regarding incidents involving CWAs. Despite these challenges, advanced data science can play a key role in innovating forensic attribution research.

References

- (1) Asha, S.; Vidyavathi, M. Role of Human Liver Microsomes in in Vitro Metabolism of Drugs-A Review. *Appl Biochem Biotechnol* **2010**, *160*, 1699–1722. <https://doi.org/10.1007/s12010-009-8689-6>.
- (2) John, H.; Schans, M. J. van der; Koller, M.; Spruit, H. E. T.; Worek, F.; Thiermann, H.; Noort, D.; John, H. Fatal Sarin Poisoning in Syria 2013: Forensic Verification within an International Laboratory Network. *Forensic Toxicol* **2018**, *36*, 61–71. <https://doi.org/10.1007/s11419-017-0376-7>.
- (3) Boles, S. L.; Pantazides, B. G.; Perez, J. W.; Sternberg, M. R.; Crow, B. S.; Blake, T. A. Establishing Population Values for Chlorine Exposure in the United States (2015–2016) Using 2 Chlorine Biomarkers, 3-Chlorotyrosine and 3,5-Dichlorotyrosine. *J Appl Lab Med* **2024**. <https://doi.org/10.1093/jalm/jfad114>.
- (4) Nishio, T.; Toukairin, Y.; Hoshi, T.; Arai, T.; Nogami, M. Development of an LC–MS/MS Method for Quantification of 3-Chloro-L-Tyrosine as a Candidate Marker of Chlorine Poisoning. *Leg Med* **2021**, *53*, 101939. <https://doi.org/10.1016/j.legalmed.2021.101939>.
- (5) Nishio, T.; Toukairin, Y.; Hoshi, T.; Arai, T.; Nogami, M. Determination of 3-Chloro-L-Tyrosine as a Novel Indicator of Chlorine Poisoning Utilizing Gas Chromatography-Mass Spectrometric Analysis. *Leg Med* **2020**, *47*, 101782. <https://doi.org/10.1016/j.legalmed.2020.101782>.
- (6) Massano, M.; Incardona, C.; Gerace, E.; Negri, P.; Alladio, E.; Salomone, A.; Vincenti, M. Development and Validation of a UHPLC-HRMS-QTOF Method for the Detection of 132 New Psychoactive Substances and Synthetic Opioids , Including Fentanyl, in Dried Blood Spots. *Talanta* **2022**, *241*, 123265. <https://doi.org/https://doi.org/10.1016/j.talanta.2022.123265>.
- (7) Jansson, D.; Lindström, S. W.; Norlin, R.; Hok, S.; Valdez, C. A.; Williams, A. M.; Alcaraz, A.; Nilsson, C.; Åstot, C. Part 2: Forensic Attribution Profiling of Russian VX in Food Using Liquid Chromatography-Mass Spectrometry. *Talanta* **2018**, *186*, 597–606. <https://doi.org/10.1016/j.talanta.2018.02.103>.
- (8) Gravett, M. R.; Hopkins, F. B.; Self, A. J.; Webb, A. J.; Timperley, C. M.; Riches, J. R. Fate of the Chemical Warfare Agent O-Ethyl S-2-Diisopropylaminoethyl Methylphosphonothiolate (VX) on Soil Following Accelerant-Based Fire and Liquid Decontamination. *Anal Bioanal Chem* **2014**, *406*, 5121–5135. <https://doi.org/10.1007/s00216-014-7963-9>.
- (9) NWO. *New Research Will Launch for the Intervention and Prevention of Subversive Crime*. <https://www.nwo.nl/en/news/new-research-will-launch-intervention-and-prevention-subversive-crime-kic> (accessed 2024-01-31).
- (10) Kranenburg, R. F.; Ramaker, H. J.; Sap, S.; van Asten, A. C. A Calibration Friendly Approach to Identify Drugs of Abuse Mixtures with a Portable Near-Infrared Analyzer. *Drug Test Anal* **2022**, *14* (6), 1089–1101. <https://doi.org/10.1002/dta.3231>.
- (11) Lindberg, S.; Engqvist, M.; Mörén, L.; Åstot, C.; Norlin, R. Source Attribution of the Chemical Warfare Agent Soman Using Position-Specific Isotope Analysis by ^2H NMR Spectroscopy: From Precursor to Degradation Product. *Anal Chem* **2021**, *93*, 12230–12236. <https://doi.org/10.1021/acs.analchem.1c01271>.
- (12) Moran, J. J.; Fraga, C. G.; Nims, M. K. Stable-Carbon Isotope Ratios for Sourcing the Nerve-Agent Precursor Methylphosphonic Dichloride and Its Products. *Talanta* **2018**, *186*, 678–683. <https://doi.org/https://doi.org/10.1016/j.talanta.2018.04.021>.
- (13) van den Hurk, R. S.; Pursch, M.; Stoll, D. R.; Pirok, B. W. J. Recent Trends in Two-Dimensional Liquid Chromatography. *TrAC - Trends in Analytical Chemistry* **2023**, *166*, 117166. <https://doi.org/10.1016/j.trac.2023.117166>.
- (14) van den Hurk, R. S.; Abdulhussain, N.; van Beurden, A. S. A.; Dekker, M. E.; Hulsbergen, A.; Peters, R. A. H.; Pirok, B. W. J.; van Asten, A. C. Characterization and Comparison of Smokeless Powders by On-Line Two-Dimensional Liquid Chromatography. *J Chromatogr A* **2022**, *1672*, 463072. <https://doi.org/10.1016/j.chroma.2022.463072>.
- (15) Shah, M.; Patel, N.; Tripathi, N.; Vyas, V. K. Capillary Electrophoresis Methods for Impurity Profiling of Drugs: A Review of the Past Decade. *J Pharm Anal* **2022**, *12*, 15–28. <https://doi.org/10.1016/j.jpha.2021.06.009>.

- (16) Sisco, E.; Forbes, T. P. Direct Analysis in Real Time Mass Spectrometry of Potential By-Products from Homemade Nitrate Ester Explosive Synthesis. *Talanta* **2016**, *150*, 177–183. <https://doi.org/10.1016/j.talanta.2015.12.013>.
- (17) Fu, F.; Sun, F.; Lu, X.; Song, T.; Ding, J.; Gao, R.; Wang, H.; Pei, C. A Novel Potential Biomarker on Y263 Site in Human Serum Albumin Poisoned by Six Nerve Agents. *Journal of Chromatography B* **2019**, *1104*, 168–175. <https://doi.org/10.1016/j.jchromb.2018.11.011>.
- (18) OPCW. *Fourth Report by the OPCW Investigation and Identification Team Pursuant to Paragraph 10 of Decision C-SS-4/DEC.3 “Addressing the Threat from Chemical Weapons Use” Marea (Syrian Arab Republic) - 1 September 2015*; 2024. <https://www.opcw.org/sites/default/files/documents/2024/02/s-2255-2024%28e%29.pdf> (accessed 2024-03-04).
- (19) Holmgren, K. H.; Hakulinen, H.; Norlin, R.; de Bruin-Hoegée, M.; Spiandore, M.; See, S. Q. S.; Webster, R.; Jacques, K. L.; Mauravaara, L.; Ang, L. H.; Evans, C. P.; Ovenden, S.; Noort, D.; Delaporte, G.; Dahlén, J.; Fraga, C. G.; Vanninen, P.; Åstot, C. Interlaboratory Comparison Study of a Chemical Profiling Method for Methylphosphonic Dichloride, a Nerve Agent Precursor. *Forensic Chemistry* **2023**, *33*, 100473. <https://doi.org/10.1016/j.forc.2023.100473>.
- (20) Säde, S.; Delaporte, G.; Fraga, C. G.; Hakulinen, H.; Höjer Holmgren, K.; Spiandore, M.; Åstot, C.; Akmeemana, A.; de Bruin-Hoegée, M.; Doward, J.; Jacques, K.; Kesah, S. A.; See, S.; Thomson, S.; Flinck, J.; Kalliovirta, L.; Vanninen, P. Interlaboratory Development and Proposition for a New Quality Control Sample for Chemical Forensics Analysis of Chemical Warfare Agents. *Talanta Open* **2023**, *8*, 100249. <https://doi.org/10.1016/j.talo.2023.100249>.
- (21) Hotchkiss, P. J. The World’s Chemical-Weapons Stockpiles Are Gone — but a New Challenge Looms. *Nature* **2023**, *623*, 459. <https://doi.org/10.1038/d41586-023-03509-1>.
- (22) Vanninen, P. *Recommended Operating Procedures for Analysis in the Verification of Chemical Disarmament*; University of Helsinki, 2023.





Summary & Samenvatting

Summary

Continuing threats of military conflicts and terrorism may involve the misuse of toxic chemicals as weapons. Recent concerns of chemical attacks in Ukraine and the poisoning of Sergei Skripal and Alexei Navalny emphasize the continued risk of chemical weapons use. In case of an alleged use of chemical weapons, forensic investigations are conducted to investigate whether a chemical attack has happened and if so, to establish the nature of the utilized agent. This is essential for providing suitable care for victims and maintaining the safety of first responders. In addition to chemical identification, it is important to determine the origin of chemical threat agents, to accurately reconstruct events and identify the perpetrators or exonerate innocent suspects. The ultimate goal is to prevent criminal acts before they are executed. Chemical attribution research aims to establish methods that can indicate whether a link exists between a material found at a crime scene and a person, location, or other evidence. Chemical attribution signatures are usually based on impurities related to the production, processing, and storage of chemicals. Unfortunately, the unambiguous identification of these chemicals is complicated due to their presence at extremely low concentrations. It is also challenging to detect intact chemical warfare agents, since they are highly reactive and rapidly degrade in the environment or metabolize in the human body. Sensitive analytical techniques are required for their detection at trace levels in complex matrices. The obtained characteristic chemical fingerprint can support law enforcement in tactical investigations and ultimately provide important evidence in a court of law. Therefore, the primary goal of this thesis is to develop multi-analytical profiling strategies for chemical warfare agents and associated dispersion devices to provide valuable forensic intelligence information.

Chapter 2 focusses on chemical impurity profiling of fentanyl to gather forensic intelligence. Fentanyl is a potent synthetic opioid with a lethal dose of only a few milligrams. It is used as illicit drug and is related to a dramatic number of overdose fatalities in the United States. The aim of the study is to identify markers for a specific fentanyl synthesis method that could be detected after intoxication. This would allow the use of biomedical samples for chemical provenance purposes. The approach is as follows, two fentanyl batches were synthesized and subsequently incubated with human liver microsomes to mimic human metabolism. Gas chromatography-mass spectrometry (GC-MS) and liquid chromatography-high resolution tandem mass spectrometry (LC-HRMS/MS) were able to detect impurities in amounts low enough to be realistic for forensic casework. Subsequently, multivariate data analysis was used to identify discriminating markers. The results were implemented in a forensic framework by establishing likelihood ratios. Low false positive and negative error rates were found. Future work should substantiate the initial findings by enlarging the data set size and



Summary

by demonstrating the viability of the approach in biomedical samples from real exposure victims. Nonetheless, the current study demonstrates the possibility of chemical attribution of drugs in biomedical samples for the first time.

Chapter 3 continues to explore chemical profiling of synthetic opioids in biomedical samples. The potential use of fentanyl analogues as a chemical weapon is an increasing concern. For instance, carfentanil is a powerful analgesic which is expected to be 10,000 more potent than morphine. Therefore, the effect of human metabolism on the chemical impurity profiles of carfentanil, remifentanil, sufentanil, and benzylfentanyl was examined to advance forensic investigations. Various batches of fentanyl analogues were synthesized and subsequently incubated with human liver microsomes. Afterwards, chemical impurity profiles were established by LC-HRMS/MS in pre- and post-metabolism samples. The detected impurities were in the same concentration range as found in real overdose cases. Principal component analysis (PCA) was performed to reduce the dimensionality of the data and visually identify characteristic markers. Additionally, PCA was used in combination with linear discriminant analysis (LDA) to maximize discrimination of the various synthesis routes. Kernel density estimations were constructed and used to express likelihood ratios for the assignment of the production method of unknown samples. This study supports the findings introduced in Chapter 2 and expands the potential of using biomedical samples for retrieving information about the synthesis route after exposure.

Chapter 4 addresses another challenge in chemical forensic research. Chlorine has been used as a chemical warfare agent in numerous military conflicts and is involved in a substantial number of accidental exposures. However, unambiguous verification of exposure is hampered by lack of specific biomarkers for chlorine gas. Chlorinated peptides were found in healthy individuals who have not been exposed to chlorine gas and biomarker concentrations can be elevated for people with inflammatory diseases. Therefore, more reliable biomarkers need to be elucidated for discrimination between endogenous formation and exogenous exposure. The latest developments in proteomics and data science enables the exploration of novel biomarkers of exposure. Human blood plasma was exposed to various levels of chlorine gas and analyzed by liquid chromatography tandem mass spectrometry (LC-MS/MS) and LC-HRMS/MS. Several site-specific chlorinated tyrosine adducts were identified. Promising peptides with multiple chlorination sites, were found in haptoglobin and albumin, proteins which are abundantly present in human whole blood. These biomarkers were only present in exposed samples and not in untreated blood samples of healthy people. Additionally, other studies reported that this part of human serum albumin is nitrated rather than chlorinated under physiological conditions. In summary, the developed method allows for robust and specific analysis of chlorinated biomarkers, which may be used to verify

chlorine gas intoxication and distinguish between endogenous formation and exogeneous exposure.

There is a growing demand for analytical methods ready to deploy directly at the crime scene. Fast identification and characterization is likely to be crucial for the health of first responders and military personnel. **Chapter 5** investigated whether portable detection in combination with confirmatory laboratory analysis could be used for fast and reliable diagnosis of nerve agent intoxications. Human whole blood was exposed to sarin and three types of Novichok nerve agents. Subsequently, blood samples were spotted on a protein saver card, dried, and stored under ambient conditions. Remarkably, this slowed down degradation of nerve agent biomarkers and the chemical signature was preserved for more than one month. Various biomarkers were detected in liquid whole blood and dried blood spots by a variety of analytical techniques. This chapter demonstrates the feasibility of using a combination of on-site detection and state-of-the-art laboratory analysis of dried blood spots for unambiguous verification of nerve agent exposure.

After a chemical attack in a conflict zone, forensic investigators may face challenges in reaching the crime scene directly after an incident due to safety and security considerations, resulting in the inability to measure intact chemical warfare agents. This obstructs a thorough crime scene investigation and an accurate reconstruction of events. To tackle this issue, **Chapter 6** introduces a novel method to use plants as an alternative source of evidence of the release of chemical weapons. Plants are often abundantly present at incident sites. This study explores whether persistent biomarkers could be detected in exposed plants after a simulated attack with sarin, Novichok nerve agent, sulfur mustard, and chlorine. This study convincingly demonstrates that even three months after actual exposure, adducts of chemical warfare agents can still be detected in plants by LC-MS/MS. An additional benefit of the current method is that these plant biomarkers are identical to the protein adducts that have been accepted as unequivocal biomarkers of exposure in humans. In addition, proteomic analysis by LC-HRMS/MS elucidated which proteins were most frequently modified. The most abundant protein on earth, rubisco and several other plant proteins, were targeted by all types of chemical warfare agents and could be used as a novel source of biochemical evidence. In conclusion, the analysis of long-lasting plant biomarkers is a powerful tool for retrospective investigation of a suspected attack with chemical weapons.

Similar to the biomedical samples discussed in Chapter 4, chlorinated protein adducts in plants can also form due to non-criminal activities. This led to the exploration of novel specific chlorine biomarkers in plants as discussed in **Chapter 7**. Untargeted high resolution mass spectrometric analysis and machine learning techniques were applied to differentiate between exposure of plants to various chlorinating agents. Distinctive



Summary

chlorinated markers were found in plant fatty acids, proteins, and DNA. A selection of promising biomarkers were verified by synthetic reference standards, including multiple chlorinated dopamine, which was solely identified in plants exposed to chlorine gas. This marker, which is also a hormone present in humans, promotes the growth of plants under stressful conditions. In addition, it was possible to distinguish between chlorine gas and distinct types of bleach by applying multivariate data analysis using PCA and LDA. This chapter expands the application of forensic profiling in plants to facilitate incident reconstruction and to differentiate between the alleged use of chlorine versus regular cleaning bleach.

Another rather uncommon source of evidence is munition, improvised explosive devices, and other equipment which could be used for the release of toxic chemicals. These materials often contain plastics, which can be analyzed to reveal their origin. The trace-elemental composition of polymer parts may yield discrimination between samples from various sources and could provide leads for the criminal investigation. However, lack of reproducible and homogeneous reference standards hampers accurate quantification of the elemental profile. For this reason, **Chapters 8 and 9** introduce a novel standard for elemental profiling of polymers by laser ablation-inductively coupled plasma-mass spectrometry (LA-ICP-MS). The specific objective of Chapter 8 is to evaluate the added value of a new class of polyethylene (PE), polystyrene (PS), and polyvinyl chloride (PVC) standards. The homogeneity was substantially improved compared to existing reference materials. In addition, the discriminating power between different classes of forensic objects was improved when using these novel polymer standards. Drawing upon this research, Chapter 9 evaluates the strength of evidence of elemental profiling of tapes, electrical wires, PVC tubing, and jerrycans. For forensic comparisons, the score-based Bayesian likelihood ratio model and the t-test overlap method performed better than the feature-based model and traditional 4-sigma match criterion approach. For example, lower percentages of false inclusion and false exclusion rates were found. In conclusion, these studies demonstrate that with the use of proper standards, elemental profiling with LA-ICP-MS is a promising and powerful tool for establishing the origin of plastic evidence found on a crime scene.

Chapter 10 concludes this thesis and highlights future perspectives. The most important challenge concerns the translation of in-vitro studies to realistic in-vivo case scenarios. To broaden the impact of the current work, more chemicals, batches, and analytical techniques should be studied. Moreover, continued efforts are needed to use chemical profiling strategies as evidence with a high forensic value in a court of law. Finally, international collaborations and interlaboratory comparison studies are required to ensure competence and enhance national security. Addressing these

challenges will bring chemical attribution research a step closer to the actual use in international investigations and court cases.

Samenvatting

De voortdurende dreiging van militaire conflicten en terrorisme kan gepaard gaan met misbruik van giftige stoffen voor het maken van wapens. Recente zorgen over chemische aanvallen in Oekraïne en de vergiftiging van Sergej Skripal en Aleksej Navalny benadrukken het aanhoudende risico van het gebruik van chemische wapens. Als er een vermoeden is van inzet van chemische wapens, wordt er forensisch onderzoek verricht om te bepalen of er een chemische aanval heeft plaatsgevonden en als dit het geval is, welke chemische stof gebruikt is. Dit is essentieel voor het bieden van passende zorg aan slachtoffers en het beschermen van de veiligheid van hulpverleners. Naast chemische identificatie is het belangrijk om de oorsprong van giftige stoffen te achterhalen, zodat gebeurtenissen nauwkeurig worden gereconstrueerd en de daders worden geïdentificeerd of onschuldige verdachten worden vrijgesproken. Het doel van chemisch attributie onderzoek is het ontwikkelen van methodes die kunnen aangeven of er een verband is tussen materiaal dat gevonden wordt op een plaats delict, en een persoon, locatie of ander bewijsmateriaal. Kenmerken van chemische attributies zijn meestal gebaseerd op onzuiverheden die verband houden met productie, verwerking en opslag van chemicaliën. Helaas is de ondubbelzinnige identificatie van deze chemicaliën gecompliceerd vanwege de aanwezigheid in extreem lage concentraties. Het is ook een uitdaging om intacte chemische strijdmiddelen te detecteren, omdat ze zeer reactief zijn en snel worden afgebroken in het milieu of metaboliseren in het menselijk lichaam. Gevoelige analytische technieken zijn vereist voor de detectie van minimale niveaus in complexe matrices. De verkregen kenmerkende chemische vingerafdruk kan vervolgens de rechtshandhaving ondersteunen bij tactische onderzoeken en uiteindelijk belangrijk bewijsmateriaal opleveren in de rechtkamer. Daarom is het hoofddoel van dit proefschrift het ontwikkelen van meerdere analytische profileringssstrategieën voor middelen en materialen van chemische oorlogsvoering zodat forensische inlichtingen het gerechtelijk onderzoek bevorderen in een vroeg stadium.

Hoofdstuk 2 richt zich op de profiling van chemische onzuiverheden in fentanyl om forensische inlichtingen te verzamelen. Fentanyl is een sterke synthetische opioïde met een dodelijke dosis van slechts enkele milligrammen. Het wordt gebruikt als illegale drug en houdt verband met een dramatisch aantal sterfgevallen door een overdosis in de Verenigde Staten. Het doel van de studie is om na vergiftiging markers te identificeren die horen bij een specifieke syntheseroute van fentanyl. Hierdoor zou het mogelijk zijn om biomedische monsters te gebruiken voor het bepalen van de herkomst van een chemische stof. De aanpak is als volgt, fentanyl werd gesynthetiseerd op twee verschillende manieren en vervolgens werden menselijke levermicrosomen toegevoegd om het menselijke metabolisme na te bootsen. Gaschromatografie-



massaspectrometrie (GC-MS) en vloeistofchromatografie-hoge resolutie gekoppelde massaspectrometrie (LC-HRMS/MS) waren in staat om onzuiverheden te detecteren in realistische lage hoeveelheden die vergelijkbaar zijn met concentraties die gevonden worden in forensische zaakonderzoeken. Vervolgens werd multivariate data-analyse gebruikt om onderscheidende markers te identificeren. De resultaten werden forensisch geïnterpreteerd door de likelihood ratio te bepalen. Zeer lage foutpositieve en foutnegatieve percentages werden gevonden. Toekomstig werk zou de bevindingen moeten onderbouwen door de dataset te vergroten en de haalbaarheid van de aanpak aan te tonen in toxicologische monsters van slachtoffers in echte forensische zaken. Ten slotte laat deze studie voor het eerst de mogelijkheid zien van chemische attributie van drugs in biomedische samples.

Hoofdstuk 3 gaat verder met onderzoek naar de chemische profilering van synthetische opioïden in biomedische monsters. Het potentiële gebruik van fentanyl-achtige stoffen als chemisch wapen is een toenemende zorg. Ter illustratie, carfentanil is een krachtig middel dat naar verwachting 10.000 sterker is dan morfine. Daarom werd onderzocht wat het effect is van het menselijk metabolisme op het profiel van chemische onzuiverheden in carfentanil, remifentanil, sufentanil en benzylfentanyl. Het doel is om hiermee het forensische onderzoek te bevorderen. Fentanyl analogen werden op verschillende manieren gesynthetiseerd en vervolgens werden menselijke levermicrosomen toegevoegd. Daarna werden profielen van chemische onzuiverheden gemeten met LC-HRMS/MS in monsters voor en na metabolisme. De concentraties waren vergelijkbaar met levels gemeten in echte gevallen van een overdosis. Principale-componentenanalyse (PCA) werd uitgevoerd om de dimensionaliteit te verminderen en karakteristieke markers te identificeren. Bovendien werd PCA gebruikt in combinatie met lineaire discriminantanalyse (LDA) om het onderscheidend vermogen tussen verschillende syntheseroutes te maximaliseren. Er werden schattingen van de kerneldichtheid (KDE) gemaakt en gebruikt om likelihood ratio's uit te drukken die gebruikt kunnen worden voor de toewijzing van de productiemethode van onbekende monsters. Deze studie ondersteunt de bevindingen die geïntroduceerd zijn in Hoofdstuk 2 en verruimt het potentieel van het gebruik van biomedische monsters voor het verkrijgen van informatie over de syntheseroute na blootstelling.

Hoofdstuk 4 behandelt een andere uitdaging op het gebied van chemisch forensisch onderzoek. Chloor is gebruikt als chemisch strijdmiddel in talloze militaire conflicten en is betrokken bij een aanzienlijk aantal onopzettelijke blootstellingen. De ondubbelzinnige verificatie van een blootstelling wordt echter belemmerd door het ontbreken van specifieke biomarkers voor chloorgas. Gechloreerde peptiden werden aangetroffen bij gezonde personen die niet zijn blootgesteld aan chloorgas en de concentraties waren verhoogd bij mensen met ontstekingsziekten. Daarom moeten

betrouwbaardere biomarkers worden opgehelderd om onderscheid te maken tussen lichaamseigen stoffen en externe blootstelling. De nieuwste ontwikkelingen op het gebied van proteomics en data science maken het mogelijk om nieuwe biomarkers te ontdekken. Menselijk bloedplasma werd blootgesteld aan verschillende hoeveelheden chloorgas en geanalyseerd met vloeistofchromatografie-gekoppelde massaspectrometrie (LC-MS/MS) en LC-HRMS/MS. Op verschillende specifieke plekken werden gechloreerde tyrosine-adducten geïdentificeerd. Veelbelovende peptiden met chlorering op meerdere plekken werden gevonden in haptoglobine en albumine. Deze eiwitten zijn overvloedig aanwezig in het bloed. Een belangrijke vinding is dat de gechloreerde biomarkers alleen aanwezig waren in blootgestelde monsters en niet in onbehandeld bloed van gezonden mensen. Daarbij meldden andere onderzoekers dat dit deel van albumine genitreerd wordt in plaats van gechloreerd onder fysiologische omstandigheden. Samengevat maakt de ontwikkelde methode een robuuste en specifieke analyse van gechloreerde biomarkers mogelijk, die gebruikt kan worden om een vergiftiging met chloorgas te verifiëren en onderscheid te maken tussen endogene vorming en exogene blootstelling.

Er is een groeiende vraag naar analysemethoden die direct op de plaats delict kunnen worden ingezet. Snelle identificatie en karakterisering kan cruciaal zijn voor de gezondheid van hulpverleners en militair personeel. **Hoofdstuk 5** onderzocht of draagbare detectie in combinatie met laboratoriumanalyse gebruikt kon worden voor een snelle en betrouwbare diagnose van zenuwgasintoxicaties. Bloed werd blootgesteld aan sarin en drie soorten Novichok-zenuwgassen. Vervolgens werden de bloedmonsters gedruppeld op filterkaartjes die zorgen dat eiwitten bewaard blijven. De kaartjes werden gedroogd en bewaard bij kamertemperatuur. Opmerkelijk genoeg vertraagde dit de afbraak van zenuwgas biomarkers en bleef het chemische profiel langer dan een maand behouden. Met behulp van een heel scala aan analytische technieken werden verschillende biomarkers gedetecteerd in vloeibaar bloed en gedroogde bloedvlekken. Dit hoofdstuk laat zien dat een combinatie van detectie ter plaatse en geavanceerde laboratoriumanalyse van opgedroogde bloedvlekken gebruikt kan worden voor ondubbelzinnige verificatie van een zenuwgas blootstelling.

Na een chemische aanval in een conflictgebied kan het lastig zijn voor forensische onderzoekers om de plaats delict op tijd te bereiken vanwege veiligheidsoverwegingen. Hierdoor zijn de intacte chemische wapens mogelijk niet meer detecteerbaar. Dit belemmert het forensische onderzoek en een nauwkeurige reconstructie van de gebeurtenissen. Daarom introduceert **Hoofdstuk 6** een methode om planten te gebruiken als alternatieve bron van bewijs voor een aanval met chemische wapens. Planten zijn vaak overvloedig aanwezig op de plekken waar de incidenten plaatsvinden. Deze studie onderzoekt of stabiele biomarkers konden worden gedetecteerd in



blootgestelde planten na een gesimuleerde aanval met sarin, Novichok-zenuwgas, mosterdgas en chloor. Deze studie liet overtuigend zien dat zelfs drie maanden na feitelijke blootstelling van planten, er eiwitadducten van chemische strijdmiddelen gedetecteerd konden worden met LC-MS/MS. Een bijkomend voordeel van de huidige methode is dat deze biomarkers in planten identiek zijn aan de eiwitadducten die geaccepteerd zijn als ondubbelzinnige biomarkers voor blootstelling bij mensen. Daarnaast maakte proteomic analyse met LC-HRMS/MS duidelijk welke eiwitten het meeste worden gemodificeerd. Het meest voorkomende eiwit op aarde rubisco en verschillende andere plantaardige eiwitten, reageerden met de verschillende soorten chemische strijdmiddelen en konden worden gebruikt als nieuw bewijsmateriaal. Tot slot, de analyse van stabiele biomarkers in planten is een krachtig instrument voor retrospectief onderzoek naar een mogelijke aanval met chemische wapens.

Net als bij de biomedische monsters die in Hoofdstuk 4 werden besproken, kunnen adducten van gechloreerde eiwitten in planten ook ontstaan door niet-criminele handelingen. Dit leidde tot het opsporen van nieuwe chloorbiomarkers in planten, zoals behandeld in **Hoofdstuk 7**. Hoge resolutie massaspectrometrie en data analysetechnieken werden toegepast om onderscheid te kunnen maken tussen de blootstelling van planten aan verschillende chloreringsmiddelen. Onderscheidende gechloreerde markers werden gevonden in plantaardige vetzuren, eiwitten en DNA. Een selectie van veelbelovende biomarkers werd geverifieerd door het toepassen van synthetische referentiestandaarden, waaronder meervoudig gechloreerd dopamine, dat uitsluitend werd geïdentificeerd in planten die waren blootgesteld aan chloorgas. Deze marker, die ook als hormoon aanwezig is in mensen, bevordert de groei van planten onder stressvolle omstandigheden. Bovendien was het mogelijk om onderscheid te maken tussen chloorgas en verschillende soorten bleek door het toepassen van de multivariate technieken PCA en LDA. Dit hoofdstuk verruimt de toepassing van forensische profilering in planten om de reconstructie van incidenten te vergemakkelijken en om onderscheid te maken tussen een vermoedelijke aanval met chloor of het gebruik van bleek als schoonmaakmiddel.

Een andere ongebruikelijke bron van bewijsmateriaal is munitie, geïmproviseerde explosieven en andere apparatuur die gebruikt kunnen worden bij een aanval met giftige chemicaliën. Deze materialen bevatten vaak plastics, die kunnen worden geanalyseerd om de herkomst ervan te achterhalen. De aanwezigheid van kleine hoeveelheden elementen in polymeren, kunnen zorgen voor onderscheid tussen monsters met een verschillende oorsprong. Dit kan aanknopingspunten bieden voor het strafrechtelijk onderzoek. Helaas belemmert gebrek aan reproduceerbare en homogene referentiestandaarden een nauwkeurige kwantificering van het elementprofiel. Om deze reden introduceren **Hoofdstukken 8 en 9** een nieuwe

standaard voor elementprofielering van polymeren door middel van laserablatie-inductief gekoppelde plasma-massaspectrometrie (LA-ICP-MS). Het specifieke doel van hoofdstuk 8 is het evalueren van de toegevoegde waarde van een nieuwe klasse polyethyleen (PE), polystyreen (PS) en polyvinylchloride (PVC) standaarden. De homogeniteit was substantieel verbeterd ten opzichte van bestaande referentie materialen. Bovendien werd het onderscheidend vermogen tussen verschillende soorten forensische objecten verbeterd wanneer de vernieuwende standaarden werden toegepast. Op basis van dit onderzoek evalueert Hoofdstuk 9 de kracht van het bewijsmateriaal van elementprofielering van tapes, elektriciteitsdraden, PVC buizen en jerrycans. Voor forensische vergelijkingen presteerden het op scores gebaseerde Bayesiaanse likelihood ratio-model en de t-test overlap methode beter dan het op kenmerken gebaseerde Bayesiaanse model en de traditionele 4-sigma matchcriterium benadering. Er werden bijvoorbeeld lagere percentages van foutnegatieve en foutpositieve resultaten gevonden. Samengevat tonen deze onderzoeken aan dat, met het gebruik van de juiste standaarden, elementprofielering met LA-ICP-MS een veelbelovend en krachtig hulpmiddel is voor het vaststellen van de oorsprong van plastic bewijsmateriaal dat gevonden is op een plaats delict.

Hoofdstuk 10 sluit dit proefschrift af en belicht toekomstperspectieven. De belangrijkste uitdaging betreft de vertaling van in-vitrostudies naar realistische scenario's. Om de impact van het huidige werk te vergroten zouden meer chemicaliën en analytische technieken bestudeerd moeten worden. Bovendien zijn voortdurende inspanningen nodig om chemische profileringstrategieën als belangrijk bewijsmateriaal in de rechtkant te gebruiken. Ten slotte zijn internationale samenwerkingen en vergelijkende onderzoeken tussen verschillende laboratoria essentieel om de competentie te waarborgen en de nationale veiligheid te vergroten. Het adresseren van deze uitdagingen zal de implementatie van chemische attributie onderzoek bevorderen voor daadwerkelijk gebruik in internationale onderzoeken en rechtszaken.



The background of the slide features a dark navy blue gradient. On the left side, there are three distinct, vibrant ink splatters. The top-most splatter is a bright cyan color, appearing wispy and ethereal. Below it is a large, expressive orange-yellow blob. At the bottom left is a large, textured cluster of pink and red ink, with some translucent white areas revealing the dark background underneath.

Additional information

Supplemental information

The supplementary data for the chapters in this thesis are available online, accompanying the publications in the scientific journals. An overview of all supplementary data is provided on the website forensicscientist.nl and can be found via this DOI: 10.5281/zenodo.10723923.





List of abbreviations

¹ H-NMR	Proton nuclear magnetic resonance
4-ANBP	4-anilino-1-benzylpiperidine
4-ANPP	4-anilino-N-phenethyl-piperidine
ABC	Ammonium bicarbonate
ACh	Acetylcholine
AChE	Acetylcholinesterase
ACN	Acetonitrile
AEGL	Acute exposure guideline level
AMDIS	Automatic mass spectral deconvolution and identification system
ANOVA	Analysis of variance
ATR	Attenuated total reflection
BChE	Butyrylcholinesterase
CAS	Chemical attribution signature
CBRN	Chemical, biological, radiological, and nuclear
CCT	Collision cell technology
CE	Capillary electrophoresis
ChE	Cholinesterase
Cl ₂	Chlorine
Cl-Ade	2-amino-6-chloropurine
Cl-Cyt	5-chlorocytosine
Cl-Phe	Fenclonine
Cl-Tyr	3-chlorotyrosine
ClIr	Log-likelihood-ratio cost
CNS	Central nervous system
CWA	Chemical warfare agent
CWC	Chemical Weapons Convention
CYP	Cytochrome-P450
DART	Direct analysis in real time
DBS	Dried blood spot
DC	Methylphosphonic dichloride
DCP	2,4-dichlorophenol
DCM	Dichloromethane

df	Degrees of freedom
Di-Cl-Tyr	3,5-dichlorotyrosine
DMP	Dimethyl pimelidate
DIMP	Diisopropylmethylphosphonate
DMMP	Dimethyl methylphosphonate
DMPADC	N,N-dimethylphosphoramidic dichloride
DNA	Deoxyribose nucleic acid
DOE	Design of experiments
DTT	Dithiothreitol
EA-IRMS	Elemental analyzer-isotope ratio mass spectrometry
ED ₅₀	Median effective dose
EI	Electron ionization
EIC	Extracted ion chromatogram
ELUB	Empirical lower and upper bounds
EMPA	Ethyl methylphosphonic acid
EPS	Expanded polystyrene
ESI	Electrospray ionization
FT-IR	Fourier-transform infrared spectroscopy
Py-GC-MS	Pyrolysis-gas chromatography-mass spectrometry
G6P	Glucose-6-phosphate sodium salt
GA	Tabun
GB	Sarin
GC	Gas chromatography
GC-FID	Gas chromatography with flame ionization detector
GC x GC-MS	Comprehensive two-dimensional gas chromatography-mass spectrometry
GC-HRMS	Gas chromatography-high resolution mass spectrometry
GC-MS	Gas chromatography-mass spectrometry
GC-MS/MS	Gas chromatography tandem mass spectrometry
GD	Soman
HCA	Hierarchical cluster analysis
HD	Sulfur mustard
HILIC	Hydrophilic interaction liquid chromatography
HLM	Human liver microsomes
HSD	Tukey's honestly significant difference test



List of abbreviations

ICP-MS	Induced coupled plasma-mass spectrometry
IMPA	Isopropyl methylphosphonic acid
IPA	Isopropanol
IS	Internal standard
KDE	Kernel density estimation
LA-ICP-MS	Laser ablation-inductively coupled plasma-mass spectrometry
LA-ICP-TOF-MS	Laser ablation-inductively coupled plasma time-of-flight mass spectrometry
LC	Liquid chromatography
LC-HRMS/MS	Liquid chromatography-high resolution tandem mass spectrometry
LC-MS	Liquid chromatography-mass spectrometry
LC-MS/MS	Liquid chromatography tandem mass spectrometry
LC-QTOF-MS	Liquid chromatography quadrupole-time of flight mass spectrometry
LC _{t₅₀}	Median lethal concentration
LD ₅₀	Median lethal dose
LDA	Linear discriminant analysis
LOQ	Limit of quantification
LR	Likelihood ratio
M	Molar concentration (mol/m ³)
MCP	4-chlorophenol
MDMA	3,4-methylenedioxymethamphetamine
MPA	Methylphosphonic acid
MS	Mass spectrometry
MRM	Multiple reaction monitoring
MSMTESE	Methylsulfinyl-2-[2-(methylthio)ethylsulfonyl]ethane
MVN	Multivariate normal model
MVK	Multivariate kernel model
N7-HETE-G	N7-(2-hydroxyethylthioethyl)-2'-guanine
NADP	β-nicotinamide adenine dinucleotide phosphate hydrate
NIST	National Institute of Standards and Technology
NMR	Nuclear magnetic resonance
NPP	N-Phenethyl-Piperidone

NV	Novichok
OP	Organophosphate
OPCW	Organisation for the Prohibition of Chemical Weapons
PAV	Pool Adjacent Violators
PBA	Pharmaceutical based agents
PBS	Phosphate buffered saline
PC	Principal component
PCA	Principal component analysis
PE	Polyethylene
PLS-DA	Partial least squares-discriminant analysis
PMPA	Pinacolyl methylphosphonic acid
ppm	Parts per million
PRM	Parallel reaction monitoring
PS	Polystyrene
PS-MS	Paper spray mass spectrometry
PTM	Post-translational modification
PVC	Polyvinyl chloride
Py-GC-MS	Pyrolysis-gas chromatography-mass spectrometry
Q	Sesquimustard
RF	Random forest
RNA	Ribonucleic acid
rpm	Rates per minute
RSD	Relative standard deviation
RT	Room temperature
SBMSE	1,1-sulfonylbis-[2-(methylsulfinyl)ethane]
SEM/EDS	Scanning electron microscopy/energy-dispersive spectroscopy
S/N	Signal-to-noise
SPE	Solid phase extraction
SRM	Selected reaction monitoring
Std	Standard deviation
SVM	Support vector machine
TCP	Trichlorophenol
TDG	Thiodiglycol
TeCP	Tetrachlorophenol



List of abbreviations

THF	Tetrahydrofuran
TIC	Toxic industrial chemical
TLM	Two-level feature-based model
t_r	Retention time
UDPGA	Uridine 5'-diphosphoglucuronic acid trisodium salt
U(H)PLC	Ultra-high pressure liquid chromatography
VR	Russian VX
WWI	First World War
WWII	Second World War
XRF	X-ray fluorescence
μ -XRF	micro X-ray fluorescence

List of publications

- 1. Contact transfer risk from fentanyl-contaminated RSDL® Kit.**

Mirjam de Bruin-Hoegée, Martijn C. de Koning, Laura Cochrane, Marloes J.A. Joosen
Toxicology Letters **2020**, 319, 237-241. DOI: 10.1016/j.toxlet.2019.11.013.
- 2. Decontamination of Toxic Industrial Chemicals and Fentanyl by Application of the RSDL® Kit.**

Elwin R. Verheij, Marloes J. A. Joosen, Laura Cochrane, Mirjam de Bruin-Hoegée, Martijn C. de Koning
Journal of special operations medicine **2020**, 20 (1), 55-59. DOI: 10.55460/COFJ-WMPA.
- 3. Chemical attribution of fentanyl: The effect of human metabolism**

Mirjam de Bruin-Hoegée, Djarah Kleiweg, Daan Noort, Arian C. van Asten
Forensic Chemistry **2021**, 24, 100330. DOI: 10.1016/j.forc.2021.100330.
This publication is covered by **Chapter 2**
- 4. Elucidation of in Vitro Chlorinated Tyrosine Adducts in Blood Plasma as Selective Biomarkers of Chlorine Exposure**

Mirjam de Bruin-Hoegée, Irene M. van Damme, Tomas van Groningen, Debora van der Riet-van Oeveren, Daan Noort, Arian C. van Asten
Chemical research in toxicology **2022**, 35 (6), 1070–1079.
DOI: 10.1021/acs.chemrestox.2c00053.
This publication is covered by **Chapter 4**
- 5. Verification of exposure to chemical warfare agents through analysis of persistent biomarkers in plants**

Mirjam de Bruin-Hoegée, Latifa Lamriti, Jan P. Langenberg, René C. M. Olivier, Lai Fun Chau, Marcel J. van der Schans, Daan Noort, Arian C. van Asten
Analytical Methods **2022**, 15, 142-153. DOI: 10.1039/D2AY01650H.
This publication is covered by **Chapter 6**



- 6. Real-time characterization of chemical threat agent aerosols for improvement of inhalation studies**
Mirjam de Bruin-Hoegée, Duurt P. W. Alkema, Ruud W. Busker, Marloes J. A. Joosen, Arjan L. van Wuijckhuijse
Inhalation Toxicology **2023**, 35 (9-10), 254–265.
DOI: 10.1080/08958378.2023.2254323.
- 7. Interlaboratory comparison study of a chemical profiling method for methylphosphonic dichloride, a nerve agent precursor**
Karin Höjer Holmgren, Hanna Hakulinen, Rikard Norlin, Mirjam de Bruin-Hoegée, Marie Spiandore, Samantha Qi Shu See, Renee Webster, Karen L. Jacques, Lauri Mauravaara, Lee Hwi Ang, Christopher P. Evans, Simon Ovenden, Daan Noort, Grégoire Delaporte, Johan Dahlén, Carlos G. Fraga, Paula Vanninen, Crister Åstot
Forensic Chemistry **2023**, 33, 100473. DOI: 10.1016/j.forc.2023.100473.
- 8. A novel standard for forensic elemental profiling of polymers by LA-ICP-TOF-MS**
Mirjam de Bruin-Hoegée, Jorien Schoorl, Peter Zoon, Marcel J. van der Schans, Daan Noort, Arian C. van Asten
Forensic Chemistry **2023**, 35, 100515. DOI: 10.1016/j.forc.2023.100515.
This publication is covered by **Chapter 8**
- 9. On-site detection and laboratory verification of the presence of nerve agent biomarkers using dried blood spots**
Mirjam de Bruin-Hoegée, Alex Fidder, Tomas van Groningen, Marcel J. van der Schans, Daan Noort, Arian C. van Asten
Forensic Chemistry **2023**, 35, 100526. DOI: 10.1016/j.forc.2023.100526.
This publication is covered by **Chapter 5**
- 10. Interlaboratory development and proposition for a new quality control sample for chemical forensics analysis of chemical warfare agents**
Solja Säde, Grégoire Delaporte, Carlos G. Fraga, Hanna Hakulinen, Karin Höjer Holmgren, Marie Spiandore, Crister Åstot, Anuradha Akmeemana, Mirjam de Bruin-Hoegée, Justin Doward, Karen Jacques, Saiful Anuar Kesah, Samantha See, Stuart Thomson, Jens Flinck, Leena Kalliovirta, Paula Vanninen
Talanta Open **2023**, 8, 100249. DOI: 10.1016/j.talo.2023.100249.

- 11. CHART: a novel system for detector evaluation against toxic chemical aerosols**
Dinesh Durán Jiménez, Tom Venema, Mirjam de Bruin-Hoegée, Duurt P. W. Alkema, Ruud W. Busker, Arjan L. van Wuijckhuijse
Scientific Reports **2024**, *14*, 1050. DOI: 10.1038/s41598-023-50718-9.
- 12. Biomarker profiling in plants to distinguish between exposure to chlorine gas and bleach using LC-HRMS/MS and chemometrics**
Mirjam de Bruin-Hoegée, Marcel J. van der Schans, Jan P. Langenberg, Arian C. van Asten
Forensic Science International **2024**, *358*, 112022.
DOI: 10.1016/j.forsciint.2024.112022.
This publication is covered by **Chapter 7**
- 13. Evaluating the strength of evidence of elemental profiling of polymers with LA-ICP-MS**
Mirjam de Bruin-Hoegée, Ruthmara Corzo, Peter D. Zoon, Peter Vergeer, Jorien Schoorl, Marcel J. van der Schans, Daan Noort, Arian C. van Asten
Forensic Chemistry **2024**, *38*, 100570. DOI: 10.2139/ssrn.4748210.
This publication is covered by **Chapter 9**
- 14. Post-metabolism impurity profiling of carfentanil, remifentanil, sufentanil, and benzylfentanyl**
Daan Vangerven*, Mirjam de Bruin-Hoegée*, Fleur Kerstens, Meike Kerklaan, Rowdy P. T. Bross, Alex Fidder, Marcel van der Schans, Daan Noort, Arian C. Van Asten
*Equal contribution
Forensic Chemistry **2024**, Under review. DOI: 10.2139/ssrn.4796215.
This publication is covered by **Chapter 3**
- 15. Nerve agents**
Mirjam de Bruin-Hoegée, Daan Noort
In Christopher Timperley et al., **The chemistry of chemical forensics and attribution of chemical weapons**
Chemical Reviews, Manuscript in preparation.
Part of this publication is covered by **Chapter 1**



Overview of co-authors' contributions

Chapter 1. Introduction

Mirjam de Bruin-Hoegée:	Conceptualization, Visualization, Writing - original draft
Daan Noort:	Writing - review & editing, Supervision
Arian C. van Asten:	Writing - review & editing, Supervision

Chapter 2. Chemical attribution of fentanyl: The effect of human metabolism

Mirjam de Bruin-Hoegée:	Conceptualization, Methodology, Software, Validation, Formal analysis, Investigation, Writing – original draft, Visualization
Djaria Kleiweg:	Methodology, Validation, Formal analysis, Investigation
Daan Noort:	Conceptualization, Writing - review & editing, Supervision
Arian C. Van Asten:	Writing - review & editing, Supervision

Chapter 3. Post-metabolism impurity profiling of carfentanil, remifentanil, sufentanil, and benzylfentanyl

Daan Vangerven:	Methodology, Software, Validation, Formal analysis, Investigation, Writing – original draft
Mirjam de Bruin-Hoegée:	Conceptualization, Methodology, Software, Validation, Formal analysis, Investigation, Writing – original draft, Visualization
Fleur Kerstens:	Methodology, Validation, Formal analysis, Investigation
Meike Kerklaan:	Methodology, Validation, Formal analysis, Investigation
Rowdy P. T. Bross:	Methodology, Investigation
Alex Fidder:	Methodology, Investigation
Marcel J. van der Schans:	Writing - review & editing, Supervision
Daan Noort:	Conceptualization, Writing - review & editing, Supervision
Arian C. van Asten:	Writing - review & editing, Supervision

Chapter 4. Elucidation of in vitro chlorinated tyrosine adducts in blood plasma as selective biomarkers of chlorine exposure

Mirjam de Bruin-Hoegée:	Conceptualization, Methodology, Software, Validation, Formal analysis, Investigation, Writing – original draft, Visualization
Irene M. van Damme:	Methodology, Validation, Formal analysis, Investigation
Tomas van Groningen:	Methodology, Validation
Debora van der Riet-van Oeveren:	Methodology, Validation
Daan Noort:	Conceptualization, Writing - review & editing, Supervision
Arian C. van Asten:	Writing - review & editing, Supervision

Chapter 5. On-Site Detection and Laboratory Verification of the Presence of Nerve Agent Biomarkers Using Dried Blood Spots

Mirjam de Bruin-Hoegée:	Conceptualization, Methodology, Validation, Formal analysis, Investigation, Writing – original draft, Visualization
Alex Fidder:	Methodology, Validation, Investigation
Tomas van Groningen:	Methodology, Validation
Marcel J. van der Schans:	Writing – review & editing, Supervision
Daan Noort:	Conceptualization, Methodology, Writing – review & editing, Supervision
Arian C. van Asten:	Writing – review & editing, Supervision

Chapter 6. Verification of exposure to chemical warfare agents through analysis of persistent biomarkers in plants

Mirjam de Bruin-Hoegée:	Conceptualization, Methodology, Software, Validation, Formal analysis, Investigating, Writing – original draft, Visualization
Latifa Lamriti:	Methodology, Validation, Investigation
Jan Langenberg:	Conceptualization, Funding acquisition
René C. M. Olivier:	Methodology, Investigation
Lai Fun Chau:	Methodology, Investigation
Marcel van der Schans:	Conceptualization, Methodology, Writing – review & editing, Supervision, Project administration
Daan Noort:	Conceptualization, Methodology, Writing – review & editing, Supervision
Arian C. van Asten:	Writing – review & editing, Supervision



Overview of co-authors' contributions

Chapter 7. Biomarker profiling in plants to distinguish between exposure to chlorine gas and bleach using LC-HRMS/MS and chemometrics

Mirjam de Bruin-Hoegée:	Conceptualization, Methodology, Validation, Formal analysis, Investigation, Writing – original draft, Visualization, Funding acquisition
Marcel J. van der Schans:	Writing - review & editing, Supervision, Project administration
Jan P. Langenberg:	Writing - review & editing, Funding acquisition
Arian C. van Asten:	Writing - review & editing, Supervision

Chapter 8. A novel standard for forensic elemental profiling of polymers by LA-ICP-TOF-MS

Mirjam de Bruin-Hoegée:	Conceptualization, Methodology, Software, Validation, Formal analysis, Investigating, Writing – original draft, Visualization
Jorien Schoorl:	Methodology, Validation, Investigation, Writing – review & editing
Peter Zoon:	Conceptualization, Methodology, Writing – review & editing
Marcel J. van der Schans:	Writing – review & editing, Supervision
Daan Noort:	Writing – review & editing, Supervision
Arian C. van Asten:	Conceptualization, Writing – review & editing, Supervision

Chapter 9. Evaluating the strength of evidence of elemental profiling of polymers with LA-ICP-MS

Mirjam de Bruin-Hoegée:	Conceptualization, Methodology, Software, Validation, Formal analysis, Investigating, Writing – original draft, Visualization
Ruthmara Corzo:	Methodology, Software, Validation, Formal analysis, Writing – review & editing
Peter D. Zoon:	Writing – review & editing
Peter Vergeer:	Writing – review & editing
Jorien Schoorl:	Writing – review & editing
Marcel J. van der Schans:	Writing - review & editing, Supervision
Daan Noort:	Writing - review & editing, Supervision
Arian C. van Asten:	Writing - review & editing, Supervision

Chapter 10. Conclusions and future perspectives

Mirjam de Bruin-Hoegée: Conceptualization, Visualization, Writing - original draft

Daan Noort: Writing - review & editing, Supervision

Arian C. van Asten: Writing - review & editing, Supervision

Summary & Samenvatting

Mirjam de Bruin-Hoegée: Conceptualization, Writing - original draft

Daan Noort: Writing - review & editing, Supervision

Arian C. van Asten: Writing - review & editing, Supervision



Acknowledgements

During my Ph.D., there were many opportunities to collaborate with wonderful people. I am grateful for their contributions and the support of people around me.

The idea of pursuing a Ph.D. started during the master Forensic Science. The enthusiasm of various scientists ignited my own excitement. This was amplified during my internship at TNO, when I observed that people were conducting fascinating research. I would like to thank my supervisor at that time, **Marloes Joosen**, for sharing honest and captivating insights about science. I am also grateful for the opportunities provided by **Arjan van Wuijckhuijse** to explore various research directions in the field of CBRN protection during my work as a scientist at TNO. Regarding the preparation for my Ph.D. research, I would like to express my gratitude towards **Arian van Asten**, **Ruud Busker**, **Frans van Gemerden**, and **Daan Noort** for the discussions about relevant and scientifically challenging topics and their support in writing a proposal for this Ph.D. project. After approval, I was happy to start investigating the topic ‘Forensic Attribution for CWA IntelliGence (FACING)’ at the University of Amsterdam (UvA) in collaboration with TNO.

In particular, I would like to thank my promotor and co-promotor who were very supportive during these years. **Arian**, I am inspired by your enthusiasm and out-of-the-box ideas. Thank you for always finding time to discuss research, reading manuscripts, and for having interesting conversations about all kinds of topics, varying from movies to winter sports. Even when I sent multiple manuscripts in a short time-frame your responses were detailed and fast, as always. **Daan**, thank you for being a mentor for me. I will never forget your insightful advice regarding work, emphasizing the importance of recognizing that: “Better is the enemy of good.” I am grateful that you shared many novel scientific ideas and introduced me to a lot of people. **Peter Schoenmakers**, it was always enjoyable when we had a talk at Science Park. You shared interesting ideas about science communication, teaching, and academic life. This added an extra dimension to research. **Marcel van der Schans**, I appreciate your support and valuable insights. You were always available for a discussion and were giving me the freedom to explore many topics. In my opinion, the best talks about life and work took place during the weekly fitness class at TNO.

Life as a Ph.D. candidate would not have been complete without my amazing UvA colleagues. **Irene van Damme**, our collaboration started already at TNO, where your research project resulted in a nice publication which is part of this thesis. Although we did not see each other often at work, I was always happy if we were together at the UvA or the Netherlands Forensic Institute (NFI). Thank you for the personal talks and the support during the more difficult parts of the Ph.D. project, for example when

collaborations took more effort than expected. **Jennifer Bonetti, Rick van den Hurk, Ruben Kranenburg, and Irene**, we had a great time together in Stockholm at the EAES conference, sharing our passion for sports, food, and science. **Bob Pirok, Lotte Schreuders, Mimi den Uijl, and Peter**, I have pleasant memories of having a drink together sitting in the sun in Chicago. After the scientific part of the ACS conference, I enjoyed the relaxing attitude and nice conversations. **Rianne Hofstraat**, we often travelled together since we live so close to each other. I loved the intense and passionate train discussions we ended up with every time. **Jelle de Koning**, I appreciate your kindness as a colleague, both at the UvA and TNO. I look forward to the opportunity to work together again in the future. **Tom Aalbers, Noor Abdulhussain, Jim Boelrijk, Sanne Boot, Tijmen Bos, Pascal Camoiras, Aleksandra Chojnacka, Maria Hayder, Gerben van Henten, Denice van Herwerden, Wouter Knol, Nino Milani, Stef Molenaar, Leon Niezen, Masashi Serizawa, Viktoria Turkina, Luca Tutiš, Joshka Verduin-Weijers, Ziran Zhai, and Annika van der Zon**, thank you for cheering up the office and having good moments together at group meetings and Friday afternoon drinks.

Over the years, there were many students that joined the group for a while. It was always inspiring and delightful to supervise students during their projects. **Djolah Kleiweg**, thank you for your hard work which resulted in the first publication of my thesis. It was nice to get to know each other and it felt like we were really working as a team. **Fleur Kerstens**, you were very enthusiastic, and you quickly got to know every TNO colleague. Thank you for your contribution to the last paper of this thesis. **Latifa Lamriti**, you are a great team player, and I loved our conversations about life and religion. Your project also resulted in a publication which is covered in this thesis. I am happy that you are now my colleague at TNO and that we can prolong our lively discussions. **Meike Kerklaan**, you continued the project of Fleur, and it was very nice working together on this topic. Thank you for your contribution. **Daan Vangerven**, you had the difficult task of finishing the project of Fleur and Meike which was started already three years before. Still, you managed to get great results. The collaboration felt very smooth, and it resulted in a publication with you as joint first author. **Bence Dallos**, I appreciated your eagerness and creativity. You managed to carry on despite administrative and technical difficulties. I hope we will publish your work in the future. **Esra Akturan, Lida Angelou-Koutsoumpeli, Isairah Baptiste, Sofie Lazeroms, Ids Lemmink, Mee Loke Lim, Giulia Palermo, Ludovica Scutumella, Ioanna Skara, Brian van 't Veer, and Selma Wagemakers**, thank you for your interesting literature theses and contributions to the field of forensic science and chemical warfare agent analysis.

I also would like to thank all my TNO colleagues. In particular, **Duurt Alkema, Rowdy Bross, Alex Fidder, Lai Fun Chau, Marco van Grol, Tomas van Groningen, Ad de Jong, Martijn de Koning, Jan Langenberg, René Olivier, Debora van der Riet-van Oeveren**,



Acknowledgements

and **Laura Rozing**, for their contributions to the research covered in this thesis. **Roland van den Berg, Alex Cornelissen, Jiska Kentrop, Jelle, and Laura**, thank you for being always so helpful and I loved the conferences we visited together. The department of CBRN protection is the most engaged group I know. I look forward to continuing to work in this positive atmosphere. This research was not possible without the support of the Netherlands Forensic Institute (NFI). **Jorien Schoorl, Marianne Schrader, Peter Vergeer, Wim Wiarda, and Peter Zoon**, thank you for your technical advice and providing me the opportunity to learn new techniques. Furthermore, I had an amazing time at the National Institute of Standards and Technology (NIST) in the U.S.A. **Ruthmara Corzo**, I am grateful for your willingness to share your knowledge with me and for always being available to help and answer questions.

To all my **family and friends**, thank you for your support and helping me recharging after work. **Joëlle and Arco van Doleweerd, Leanne and Coen Heger, Roelien and Gerben van den Hudding, Rhodé and Mark de Jong**, thank you for being friends for such a long time. I love our personal conversations and your curious questions about work. **Hannah and Daniël Hoekstra, Deliana and Johan Rozendaal**, I am always inspired by the topics we discuss and energized by the activities we undertake together. Thank you for your understanding regarding the demands that work can often entail. **Andrea and Corné Blokland, Margreet and David Cronie**, I love that we can talk about everything and that you are helping me get a broader view of the world. **Rob and Linda Hoegée**, thank you for making the Covid period more bearable by spending a lot of evenings together, by having dinner and playing board games. Additionally, my **volleyball** team, the winter sports volleyball group, the technical committee, and all the other people from UVV-Sphynx, thank you for helping me maintain a healthy work-life balance. I cherished the shared dedication to sports and the moments of relaxation we had after the training and matches.

Most of all, I want to thank **Gerrit-Jan de Bruin**, for always standing by my side and enjoying life together. Thank you for your encouragement and understanding. You thought along or helped me to nuance my work when necessary.

Finally, I thank **God** who gave me the opportunities, skills, and perseverance to complete this Ph.D. research. I feel blessed and grateful that I was able to enjoy my work.

“Turn away from evil and do good.

Search for peace,

and work to maintain it.”

David – New Living Translation Bible 1996, Psalm 34:14

